Załącznik nr 1
do Zarządzenia Rektora PG nr 30/2022 z 14 kwietnia 2022 r.

GDAŃSK UNIVERSITY OF TECHNOLOGY

The author of the doctoral dissertation: Agnieszka Kurdyn, MSc Eng.
Scientific discipline: Chemical Sciences

DOCTORAL DISSERTATION

Title of doctoral dissertation:

Cellular response induced by unsymmetrical bisacridines in pancreatic cancer cells cultured in 2D and 3D conditions

Title of doctoral dissertation (in Polish):

Odpowiedź komórkowa indukowana przez niesymetryczne bisakrydyny w komórkach raka trzustki hodowanych w warunkach 2D i 3D

Supervisor *signature*
Ewa Augustin, PhD, DSc, Gdańsk Tech Professor

Gdańsk, year 2026

Załącznik nr 2

do Zarządzenia Rektora PG nr 30/2022 z 14 kwietnia 2022 r.

POLITECHNIKA GDAŃSKA

STATEMENT

The author of the doctoral dissertation: Agnieszka Kurdyn, MSc Eng.

I, the undersigned, declare that I am aware that in accordance with the provisions of Art. 27 (1) and (2) of the Act of 4th February 1994 on Copyright and Related Rights (Journal of Laws of 2021, item 1062), the university may use my doctoral dissertation entitled:

Cellular response induced by unsymmetrical bisacridines in pancreatic cancer cells cultured in 2D and 3D conditions

for scientific or didactic purposes.[1]

Gdańsk,..... .....

signature of the PhD student

Aware of criminal liability for violations of the Act of 4th February 1994 on Copyright and Related Rights and disciplinary actions set out in the Law on Higher Education and Science(Journal of Laws 2021, item 478), as well as civil liability, I declare that the submitted doctoral dissertation is my own work.

I declare that the submitted doctoral dissertation is my own work performed under and in cooperation with the supervision of Ewa Augustin, PhD, DSc, Gdańsk Tech Professor.

This submitted doctoral dissertation has never before been the basis of an official procedure associated with the awarding of a PhD degree.

All the information contained in the above thesis, which is derived from written and electronic sources, is documented in a list of relevant literature in accordance with Art. 34 of the Copyright and Related Rights Act.

I confirm that this doctoral dissertation is identical to the attached electronic version.

Gdańsk,..... .....

signature of the PhD student

I, the undersigned, agree to include an electronic version of the above doctoral dissertation in the open, institutional, digital repository of Gdańsk University of Technology.

Gdańsk,..... .....

signature of the PhD student

[1] Art 27. 1. Educational institutions and entities referred to in art. 7 sec. 1 points 1, 2 and 4–8 of the Act of 20 July 2018 – Law on Higher Education and Science, may use the disseminated works in the original and in translation for the purposes of illustrating the content provided for didactic purposes or in order to conduct research activities, and to reproduce for this purpose disseminated minor works or fragments of larger works.

2. If the works are made available to the public in such a way that everyone can have access to them at the place and time selected by them, as referred to in para. 1, is allowed only for a limited group of people learning, teaching or conducting research, identified by the entities listed in paragraph 1.

GDAŃSK UNIVERSITY OF TECHNOLOGY

DESCRIPTION OF DOCTORAL DISSERTATION

The Author of the doctoral dissertation: Agnieszka Kurdyn, MSc Eng.

Title of doctoral dissertation: *Cellular response induced by unsymmetrical bisacridines in pancreatic cancer cells cultured in 2D and 3D conditions*

Title of doctoral dissertation in Polish: *Odpowiedź komórkowa indukowana przez niesymetryczne bisakrydyny w komórkach raka trzustki hodowanych w warunkach 2D i 3D*

Language of doctoral dissertation: English

Supervisor: Ewa Augustin, PhD, DSc, Gdańsk Tech Professor

Date of doctoral defense:

Keywords of doctoral dissertation in Polish: niesymetryczne bisakrydyny; rak trzustki; aktywność przeciwnowotworowa; hodowle komórkowe 2D i 3D; wielokomórkowe sferoidy nowotworowe; apoptoza; senescencja; autofagia; migracja

Keywords of doctoral dissertation in English: unsymmetrical bisacridines; pancreatic cancer; anticancer activity; 2D and 3D cell cultures; multicellular tumor spheroids; apoptosis; senescence, autophagy; migration

Summary of doctoral dissertation in Polish:

Rak trzustki jest wysoce złośliwym nowotworem o znacznej oporności na chemioterapię i szybkim tempie progresji. Celem niniejszej pracy było scharakteryzowanie aktywności biologicznej trzech nowych niesymetrycznych pochodnych bisakrydyny (UAs; C-2028, C-2045 i C-2053) wobec ludzkich komórek raka trzustki hodowanych w postaci monowarstw i sferoidów. UAs wykazywały większą cytotoksyczność wobec komórek nowotworowych w porównaniu z normalnymi komórkami nabłonka trzustki. Jako główny mechanizm śmierci komórkowej zidentyfikowano apoptozę, a indukcja SMAD4 ułatwiała ten proces. Kluczowym odkryciem było obniżenie ekspresji onkoproteiny c-Myc, która pośredniczyła w śmierci komórkowej w sposób niezależny od p53. Ponadto UAs indukowały zależne od dawki przyspieszone starzenie komórkowe poprzez zwiększenie ekspresji p21, a starzejące się komórki ostatecznie przechodziły w stan apoptozy. W sferoidach UAs utrzymywały aktywność proapoptotyczną. Badania wykazały również, że UAs wyzwalały niezależny

GDAŃSK UNIVERSITY OF TECHNOLOGY

od Bekliny1 przepływ autofagiczny o charakterze głównie prośmierciowym. Autofagia indukowana przez UAs hamowała potencjał migracyjny poprzez niekanoniczną modulację markerów przejścia nabłonkowo-mezenchymalnego. Wyniki te wskazują UAs, jako silne, wielofunkcyjne związki zdolne do pokonania oporności genetycznej i ograniczenia migracji komórek raka trzustki.

Summary of doctoral dissertation in English:

Pancreatic cancer is a highly aggressive malignancy characterized by profound chemoresistance and rapid progression. This doctoral dissertation aimed to characterize the biological activity of three novel unsymmetrical bisacridine derivatives (UAs; C-2028, C-2045, and C-2053) against human pancreatic cancer cells cultured as monolayers and spheroids. UAs exhibited markedly greater cytotoxicity toward cancer cells compared to normal pancreatic epithelial cells. Apoptosis was identified as the primary cell death mechanism, and the induction of SMAD4 facilitated this process. A crucial finding was the profound downregulation of the c-Myc oncoprotein, which mediated cell death in a p53-independent manner. Furthermore, UAs induced dose-dependent accelerated senescence via p21 upregulation, with senescent cells ultimately transitioning into apoptosis. In spheroids, UAs maintained pro-apoptotic activity. Studies also demonstrated that UAs triggered Beclin1-independent autophagic flux of a predominantly pro-death nature. UA-induced autophagy was found to suppress migratory potential through the non-canonical modulation of epithelial-mesenchymal transition markers. These findings identify UAs as potent, multifunctional candidates capable of overcoming genetic resistance and inhibiting the migration of pancreatic cancer cells.

Rodzicom –
z wdzięcznością za miłość, która zawsze dodawała mi sił,
za wsparcie, które prowadziło mnie przez najtrudniejsze chwile,
i za wiarę we mnie – nawet wtedy, gdy sama jej nie miałam.

Powstanie tej pracy nie byłoby możliwe bez obecności i wsparcia wielu wyjątkowych osób, które miałam szczęście spotkać na swojej drodze. To dzięki Nim ten czas, pełen wyzwań i wysiłku, stał się również doświadczeniem niezwykle wartościowym.

Szczególne wyrazy wdzięczności kieruję do mojej Pani Promotor, Profesor Ewy Augustin – za opiekę naukową, zaufanie oraz cenne wskazówki, które pozwalały mi rozwijać się i wytrwale podążać wybraną ścieżką. Jest Pani dla mnie przykładem siły i konsekwencji w dążeniu do celu.

Z całego serca dziękuję Pani Profesor Zofii Mazerskiej, która towarzyszyła mi, jako Promotor na wcześniejszych etapach kształcenia i pozostała dla mnie wsparciem również w trakcie doktoratu. Dziękuję za życzliwość, liczne rozmowy oraz za to, że zawsze mogłam liczyć na Pani doświadczenie i dobre słowo.

Serdeczne podziękowania kieruję do Moniki Pawłowskiej za nieocenioną pomoc merytoryczną i praktyczną w laboratorium, cierpliwość oraz otwartość w przekazywaniu wiedzy. Ale jeszcze bardziej za Twoje ciepło i dobroć – to dzięki nim nasza znajomość ma dla mnie szczególną wartość – nie tylko naukową.

Dziękuję Pani Doktor Agnieszce Potędze za obecność i nieustanną wiarę we mnie. Pani postawa była dla mnie nie tylko wsparciem, lecz także ważnym źródłem motywacji i przypomnieniem, jak istotna jest wytrwałość.

Wyrazy wdzięczności składam Pani Doktor Ewie Paluszkiewicz za syntezę związków stanowiących podstawę moich badań – Pani wkład miał kluczowe znaczenie dla realizacji tej pracy.

Dziękuję moim Koleżankom z laboratorium – Joli Kuleszy, Bożenie Pezała i Marcie Ryś – za codzienną życzliwość, wsparcie, rozmowy i śmiech. To dzięki Wam praca nabierała lżejszego wymiaru, a trudniejsze chwile stawały się łatwiejsze do pokonania.

Rodzicom dziękuję za bezgraniczną wiarę we mnie i zaufanie, gdy droga nie była oczywista. Wasza obecność – zarówno w chwilach sukcesów, jak i zwątpienia – jest dla mnie największą siłą i oparciem.

Moim Braciom – Michałowi, Wojtkowi i Maciejowi – dziękuję za obecność i niezliczone rozmowy, które niejednokrotnie pozwalały mi zachować równowagę. Świadomość, że zawsze mogę na Was liczyć, jest dla mnie bezcenna.

Szymonowi dziękuję za spokój, który wnosił w najtrudniejszych momentach, za cierpliwość i nieustające wsparcie na każdym etapie tej drogi. Dziękuję, że jesteś przy mnie, gdy najbardziej tego potrzebuję.

Na koniec kieruję ogromną wdzięczność do mojej Rodziny i Przyjaciół – za obecność i wsparcie, którego nie sposób przecenić.

TABLE OF CONTENTS

ABBREVIATIONS

2D	Two-dimensional
3D	Three-dimensional
5-FU	5-Fluorouracil
ABC	ATP-binding cassette
AMP	Adenosine monophosphate
AMPK	Adenosine monophosphate-activated protein kinase
APAF-1	Apoptotic protease-activating factor-1
ATRA	All-trans retinoic acid
AUC	Area under the curve
Bcl-2	B-cell lymphoma 2
BH3	Bcl-2-homology-3
BMI	Body mass index
BRPC	Borderline resectable PC
C-2028	9'-{N-[(imidazo[4,5,1-de]-acridin-6-on-5-yl)aminopropyl]-N-methylamino-propyl-amino}-1'- nitroacridine×1.5HCl
C-2045	9'-{N-[(8-hydroxyimidazo[4,5,1-de]-acridin-6-on-5-yl)aminopropyl]-N-methyl-aminopropylamino}-4'-methyl-1'-nitroacridine×3HCl
C-2053	9'-{N-[(imidazo[4,5,1-de]-acridin-6-on-5-yl)aminopropyl]-N-methylamino-propylamino}-4'-methyl-1'-nitroacridine×3HCl
CA 19-9	Carbohydrate antigen 19-9
CAFs	Cancer-associated fibroblasts
CAM-DR	Cell adhesion-mediated drug resistance
CCAT1	Colon cancer-associated transcript 1
CDA	Cytidine deaminase
CDKN2A	Cyclin-dependent kinase inhibitor 2A
CDKs	Cyclin-dependent kinases
CP	Chronic pancreatitis
CSC	Cancer stem cell
CT	Computed tomography
ctDNA	Circulating tumor DNA
CYP	Cytochrome P450 isoenzymes
DAP	Death-associated protein kinase
dCK	Deoxycytidine kinase
DDR	DNA damage response
dFdC	Difluorodeoxycytidine
DIABLO	Direct IAP-binding protein with low pI
DISC	Death-inducing signaling complex
DM	Diabetes mellitus
ECM	Extracellular matrix

ECOG	Eastern Cooperative Oncology Group
EC-MS	Electrochemical mass spectrometry
EI24	Etoposide-induced 2.4 kb transcript
EMP	Epithelial-mesenchymal plasticity
EMT	Epithelial-mesenchymal transition
EVs	Extracellular vesicles
FADD	Fas-associated death domain
FAK	Focal adhesion kinase
FAP	Familial adenomatous polyposis
FASN	Fatty acid synthase
FMOs	Flavin monooxygenases
FOLFIRINOX	Folinic acid (leucovorin), fluorouracil, irinotecan, and oxaliplatin
G4	G-quadruplex
GDP	Guanosine diphosphate
GEM	Gemcitabine
GLUD1	Glutamate dehydrogenase 1
GnP	Gemcitabine and nab-paclitaxel
GOF	Gain-of-function
GOT1	Aspartate transaminase
GSH	Glutathione
GSTs	Glutathione S-transferases
GTP	Guanosine triphosphate
HA	Hyaluronic acid
HBOC	Hereditary breast and ovarian cancer syndrome
HDAC	Histone deacetylase
HIF-1α	Hypoxia-inducible transcription factor
HNPCC	Hereditary non-polyposis colorectal cancer (Lynch syndrome)
HP	Hereditary pancreatitis
HRD	Homologous recombination deficiency
HREs	Hypoxia response elements
HTS	High-throughput screening
IARC	International Agency for Research on Cancer
iCAFs	Inflammatory CAFs (cancer-associated fibroblasts)
ICIs	Immune checkpoint inhibitors
ICT	Immune checkpoint therapy
IFP	Interstitial fluid pressure
IGF-1	Insulin-like growth factor-1
IRI	Irinotecan
JNK1	c-Jun N-terminal kinase 1
KRAS	Kirsten rat sarcoma viral oncogene homolog

LDH	Lactate dehydrogenase
LV	Leucovorin
MAPK	Mitogen-activated protein kinase
MCR	Multicellular resistance
MCTS	Multicellular tumor spheroids
MD	Molecular dynamics
MDR	Multidrug resistance
MDSCs	Myeloid-derived suppressor cells
mFOLFIRINOX	Modified FOLFIRINOX (folinic acid (leucovorin), fluorouracil, irinotecan, and oxaliplatin)
miRNAs	MicroRNAs
MiT/TFE	Microphthalmia/transcription factor E
MOMP	Mitochondrial outer membrane permeabilization
mOS	Median overall survival
mPFS	Median progression-free survival
MSI-H/dMMR	Microsatellite instability-high/mismatch repair deficient
mTOR	Mechanistic target of rapamycin
myCAFs	Myofibroblastic CAFs (cancer-associated fibroblasts)
NADPH	Nicotinamide adenine dinucleotide phosphate hydrogen
nal-IRI	Nanoliposomal irinotecan
NALIRIFOX	Nanoliposomal irinotecan, 5-fluorouracil, folinic acid, and oxaliplatin
NHE III1	Nuclease hypersensitive element III1
NK	Natural killer (cells)
NMR	Nuclear magnetic resonance
OIS	Oncogene-induced senescence
ORR	Objective response rate
OS	Overall survival
OXA	Oxaliplatin
PanINs	Pancreatic intraepithelial neoplasia
PAR	Protease-activated receptors
PARP	Poly(ADP-ribose) polymerase
PC	Pancreatic cancer
PDAC	Pancreatic ductal adenocarcinomas
PDOs	Patient-derived organoids
PDX	Patient-derived xenografts
PE	Phosphatidylethanolamine
PEGPH20	PEGylated human hyaluronidase
PFS	Progression-free survival
PI3K	Phosphatidylinositol 3-kinase
PIP3	Phosphatidylinositol-3,4,5-trisphosphate

PJS	Peutz-Jeghers syndrome
PLGA	Poly(lactic-co-glycolic) acid
PP	Pancreatic polypeptide
PPP	Pentose phosphate pathway
PSCs	Pancreatic stellate cells
PTEN	Phosphatase and tensin homolog
qPSCs	Quiescent PSCs (pancreatic stellate cells)
QDs	Quantum dots
ROS	Reactive oxygen species
RR	Ribonucleotide reductase
RTKs	Receptor tyrosine kinases
SA-β-gal	Senescence-associated β-galactosidase
SAHF	Senescence-associated heterochromatin foci
SASP	Senescence-associated secretory phenotype
SIPS	Stress-induced premature senescence
Smac	Second mitochondria-derived activator of caspase
SMAD4	Mothers against decapentaplegic homolog 4
SNARE	Soluble N-ethylmaleimide-sensitive factor attachment protein receptors
T2DM	Type 2 diabetes mellitus
TAMs	Tumor-associated macrophages
TCA	Tricarboxylic acid cycle
TGF-β	Transforming growth factor β
TGI	Tumor growth inhibition
TIGAR	TP53-inducible glycolysis and apoptosis regulator
TIS	Therapy-induced senescence
TME	Tumor microenvironment
TNF	Tumor necrosis factor
Topo I	Topoisomerase I
TRAIL	TNF-related apoptosis-inducing ligand
Tregs	Regulatory T cells
TS	Thymidylate synthase
TSC2	Tuberous sclerosis complex 2
UAs	Unsymmetrical bisacridines
UGTs	UDP-glucuronosyltransferases
ULK1	Unc-51-like kinase 1
VMP1	Vacuole membrane protein 1
WHO	World Health Organization
XIAP	X-linked inhibitor of apoptosis protein
α-SMA	α-smooth muscle actin

INTRODUCTION

1. The Pancreatic Cancer Burden: Epidemiology, Prognosis, and Etiology

Pancreatic cancer (PC) remains one of the most lethal malignancies, posing a persistent challenge to modern oncology due to its high propensity for early metastasis, intrinsic resistance to treatment, and complex tumor microenvironment (TME). Therefore, understanding the underlying genetic factors, molecular pathology of the characteristic aggressive phenotype, and mechanisms underlying therapeutic failure is critical for the development of effective therapeutic strategies. This chapter provides a comprehensive overview of the burden of pancreatic cancer, detailing its growing epidemiological significance, explaining the molecular pathogenesis caused by underlying genetic alterations and unique features of the desmoplastic niche, and finally exploring the current therapeutic landscape, mechanisms of resistance, and prospects for innovative interventions.

1.1. Pancreatic Cancer: A Global Health Crisis

Affecting millions of people worldwide, cancer is a complex disease characterized by uncontrolled cell growth and resistance to cell death. It remains a key global challenge for modern medicine due to the persistent high mortality rate. According to the International Agency for Research on Cancer (IARC), a part of the World Health Organization (WHO), there were nearly 20 million new cases in 2022, with 9.7 million deaths. Lung cancer was the most common cancer worldwide (12.4%), followed by female breast cancer (12.5%), colorectal cancer (9.6%), prostate cancer (7.3%), and stomach cancer (4.8%). Lung cancer was also characterized by the highest mortality rate, accounting for 18.7% of the total cancer deaths. The subsequent highest death rates were attributable to colorectal cancer (9.3%), liver cancer (7.8%), breast cancer (6.8%), stomach cancer (6.8%), and pancreatic cancer (4.8%) [1]. It is projected that new cancer cases in 2045 will reach 32.6 million, a 63% increase from 2022 [2]. The scale of this global challenge is visualized in **Figure 1.1**.

Pancreatic cancer poses a constant and serious challenge to global health. The vast majority of pancreatic neoplasms, constituting over 90% of cases, are classified as pancreatic ductal adenocarcinomas (PDAC), originating from exocrine ductal cells. PDAC is a highly aggressive cancer, characterized by rapid progression, complex molecular pathology, and late diagnosis [3].

The incidence of PC has been steadily rising across many countries, including the United States, China, and also Europe [3, 4]. This trend is partially due to demographic changes, such as longer life expectancies and the rise in major risk factors, including the global obesity epidemic [5, 6]. PC is predicted to become the second leading cause of cancer-related deaths in the United States by 2030, further highlighting the urgent need for improved therapeutic strategies [7].

The prognosis for PC patients is exceptionally poor, primarily due to the clinically silent nature of the disease in its early stages, which usually leads to diagnosis at an advanced, non resectable, or metastatic stage [8]. Approximately 80% to 90% of patients have distant

metastases or locally advanced disease at the time of diagnosis. Consequently, the five-year overall survival (OS) rate remains very low, fluctuating around 9% for all stages combined [9]. Even for the minority of patients (15–20%) eligible for curative surgical resection, the recurrence rate is high (up to 85%), demanding stringent post-operative chemotherapy [10, 11].

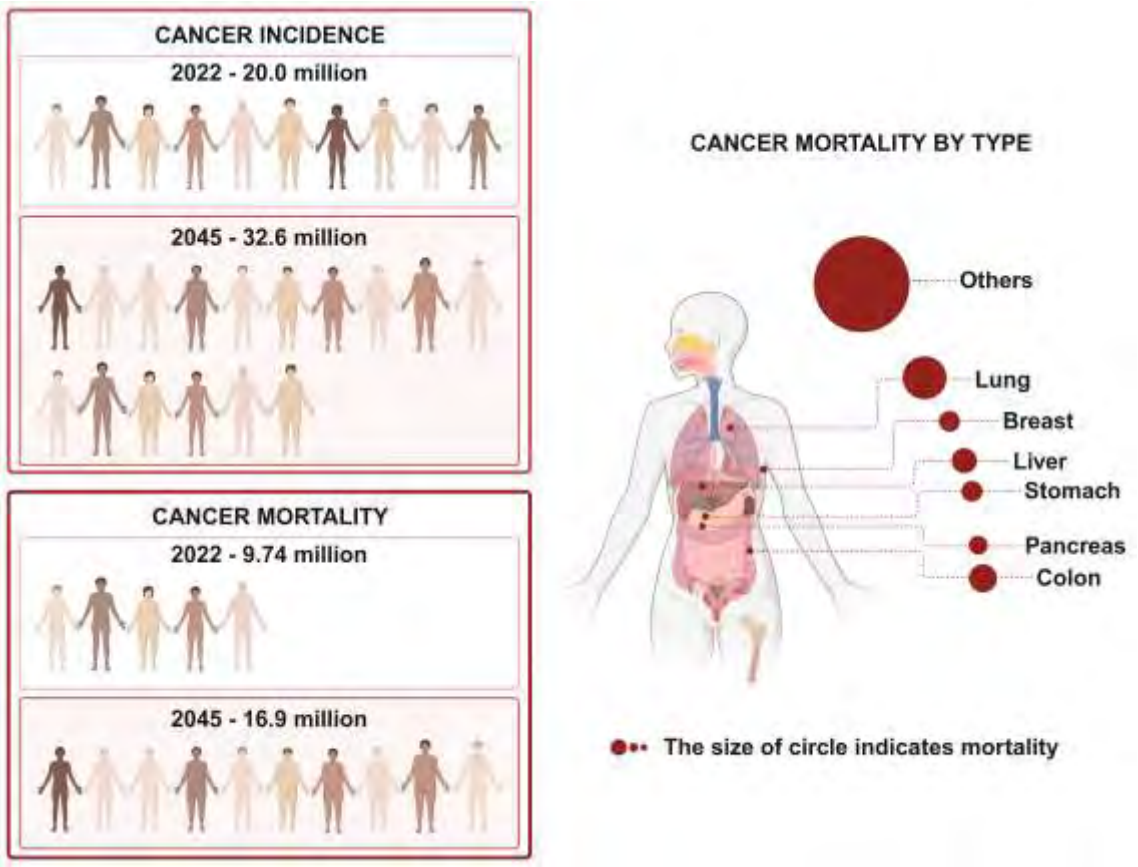

Figure 1.1. Global cancer incidence and mortality in both sexes in 2022 with projections for 2045, based on [2].

1.2. Anatomy and Functional Histology of the Pancreas

The pancreas is a unique organ with dual functions, combining the endocrine and exocrine systems to maintain metabolic homeostasis and digestive efficiency. The exocrine portion, which accounts for approximately 90% of the pancreas's mass, consists mainly of acinar cells and duct cells. Acinar cells are the main executors of the exocrine system, specializing in the synthesis and secretion of digestive enzymes, including amylase, lipase, and proteases, such as trypsin, which are essential for the breakdown of carbohydrates, fats, and proteins. These enzymes are transported through a branched network of ducts lined with duct cells, which secrete a bicarbonate-rich fluid that neutralizes stomach acid and provides an optimal pH for enzymatic activity in the duodenum [12].

The endocrine portion, on the other hand, is organized into specialized clusters known as Langerhans islets, which are scattered throughout the exocrine parenchyma. Hormonal regulation within these islets is controlled by at least five cell types: β cells that produce insulin to lower blood glucose levels, α cells that secrete glucagon to induce hyperglycemia during fasting, and δ cells

that produce somatostatin, which exerts a paracrine inhibitory effect on both insulin and glucagon secretion. In addition, PP cells secrete pancreatic polypeptide, which regulates gastrointestinal motility and energy expenditure. Beyond their independent functions, endocrine and exocrine elements exhibit profound “endocrine-exocrine crosstalk”, facilitated by their shared embryonic origin and specialized “insulo-acinar” port system. This anatomical arrangement ensures that high concentrations of endocrine hormones can directly influence the function and growth of surrounding acinar and ductal tissues, forming a communication axis that is often disrupted in pathological conditions such as pancreatic cancer and diabetes [12]. The spatial distribution of the specialized cell populations and their integration into the pancreatic parenchyma are illustrated in **Figure 1.2**.

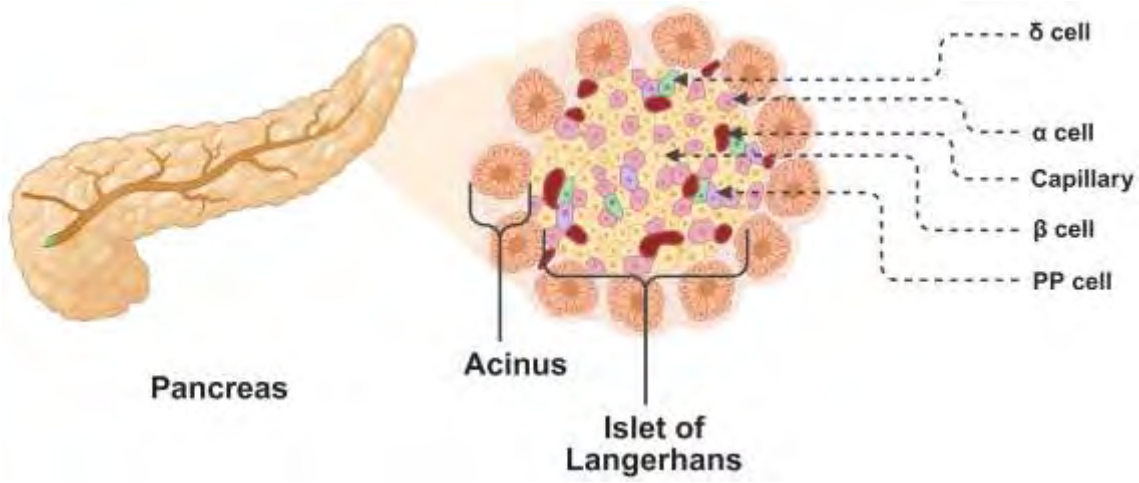

Figure 1.2. Structural organization and cellular diversity of the human pancreas, based on [12].

1.3. Molecular Pathogenesis and Hallmarks of Pancreatic Cancer

The development of pancreatic cancer is a complex, multifactorial process influenced by both non-modifiable (genetic) and modifiable (environmental or lifestyle) factors. Understanding these risk factors is crucial for prevention and targeted surveillance in high-risk groups [13].

Smoking and tobacco use are clearly recognized as the main lifestyle risk factors, contributing to an estimated 20% to 35% of all pancreatic cancer cases. This risk is directly related to the duration and intensity of smoking [10]. The carcinogenic mechanism involves the induction of mutations in genes such as *KRAS* and *TP53*, as well as the promotion of chronic inflammation. Nicotine and carcinogens in tobacco smoke promote tumor growth, alter the tumor microenvironment crosstalk, and enhance the infiltration of myeloid-derived suppressor cells (MDSCs) [6].

Obesity is a significant independent risk factor for PC, linked to an elevated risk by approximately 10% for every 5 kg/m^2 increase in body mass index (BMI), and obese individuals may be diagnosed one year earlier than those of normal weight. Pathogenesis is associated with adiposopathy and chronic inflammation in adipose tissue, resulting in elevated circulating levels of pro-inflammatory cytokines such as TNF-α (tumor necrosis factor), IL-6, and leptin [3, 14].

The relationship between diabetes mellitus (DM), especially Type 2 DM (T2DM), and PC is clear but complex. While long-standing T2DM increases the risk by 1.5- to 2.0-fold, often preceding cancer diagnosis by several years, newly diagnosed diabetes is often considered a paraneoplastic symptom or a consequence of the malignancy itself [3, 10]. Hence, mechanisms involve hyperinsulinemia and high levels of Insulin-like growth factor-1 (IGF-1), which stimulate pancreatic glandular proliferation and activate pancreatic stellate cells (PSCs), contributing to fibrosis [3, 6].

Chronic pancreatitis (CP), often caused by alcohol abuse, smoking, or hereditary factors, is a major high-risk factor, with approximately 5% of CP patients developing PC within 20 years [10]. Consequently, chronic inflammation stimulates pathogenic mechanisms, including the production of pro-inflammatory cytokines (TNF-α, IL-6, IL-8) and reactive oxygen species (ROS), promoting cell proliferation and ultimately malignant transformation. Excessive alcohol consumption (more than three drinks per day) increases the relative risk, mainly through induced chronic inflammation [3].

Inherited risk factors account for approximately 10% of PC cases. High-risk syndromes include hereditary breast and ovarian cancer syndrome (HBOC, involving *BRCA1* and especially *BRCA2* mutations), familial adenomatous polyposis (FAP), Lynch syndrome (HNPCC), Peutz-Jeghers syndrome (PJS; involving *STK11* mutations), and hereditary pancreatitis (HP, often caused by *PRSS1* mutation) [3]. Patients with a mutation in *PRSS1*, the gene encoding cationic trypsinogen, which is the best-characterized gene for hereditary pancreatitis, have an astonishing cumulative risk of PC of approximately 50% at age 75 [15]. In turn, PJS, linked to the *STK11* gene, carries the highest genetic risk, increasing the relative risk of PC by up to 132 times [14].

1.3.1. The Genetic Blueprint of Pancreatic Cancer

As previously mentioned, the pancreas is anatomically composed of distinct exocrine and endocrine compartments, with PDAC arising primarily from the exocrine lineage. The exocrine parenchyma consists of acinar cells, which synthesize and secrete digestive enzymes, and ductal epithelial cells that line the complex network of pancreatic ducts. These epithelial components are intimately embedded within a stromal microenvironment comprising resident fibroblasts, including PSC, immune cells, and a structural extracellular matrix (ECM) [16]. The development of pancreatic cancer follows a multistep carcinogenesis model, progressing through noninvasive epithelial proliferations known as pancreatic intraepithelial neoplasia (PanINs). This sequence progresses from low-grade (PanIN-1A/1B) to intermediate-grade (PanIN-2) lesions, culminating in high-grade (PanIN-3 or *carcinoma in situ*) lesions before transforming into invasive adenocarcinoma. The time required for the gradual accumulation of genetic and epigenetic alterations that lead from the initial oncogenic mutation to metastatic disease spans many years, suggesting a critical window for intervention [5]. This evolutionary trajectory from precursor lesions to invasive pancreatic cancer, alongside the complex cellular composition of the surrounding stroma, is depicted in **Figure 1.3**.

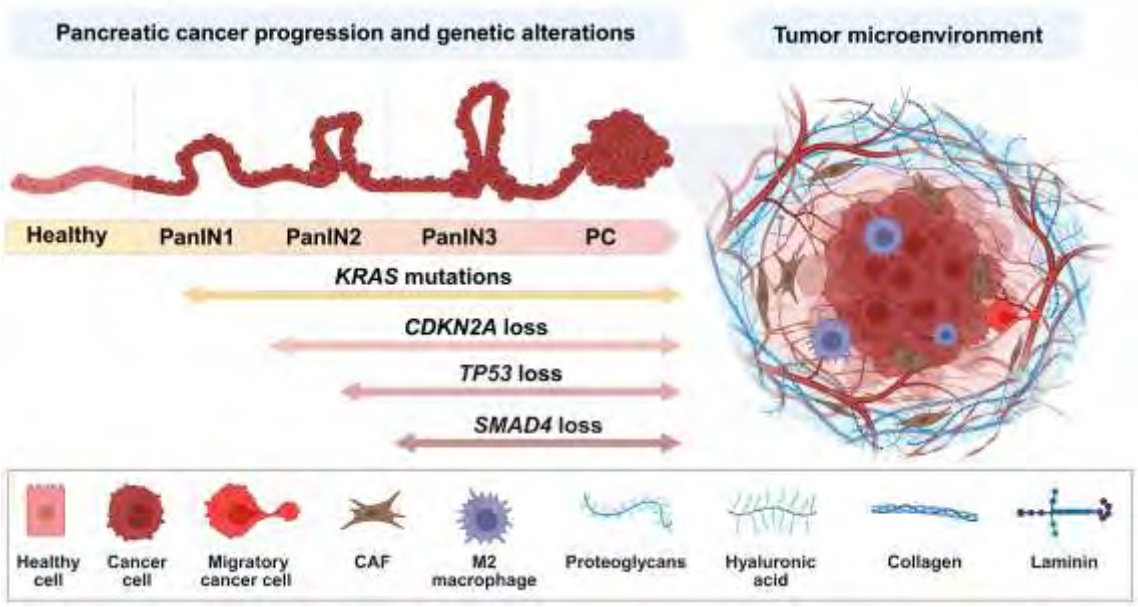

Figure 1.3. Pancreatic cancer progression, genetic alterations, and the tumor microenvironment, based on [15].

The genomic landscape of PC is characterized by high complexity, typically involving 60 or more genetic alterations across 12 core signaling pathways, and is dominated by four major, recurrent driver genes: *KRAS*, *CDKN2A*, *TP53*, and *SMAD4* [5].

The first core genetic determinant is *KRAS* (Kirsten Rat Sarcoma Viral Oncogene Homolog). Mutational activation of the *KRAS* oncogene is the earliest and most frequent event, occurring in over 90% of all PC cases. These activating mutations (most commonly G12D, G12V, G12R, and G12C) impair the protein's intrinsic GTPase activity, locking it in a constitutively active state. Consequently, activated *KRAS* continuously stimulates downstream signaling pathways, particularly the RAF/MEK/ERK and PI3K/AKT axes, promoting cell proliferation and transformation. In addition to its autonomous effects, mutant *KRAS* coordinates the development of a favorable TME and stimulates extensive metabolic reprogramming, such as increased glucose uptake and constitutive macropinocytosis, enabling PC cells to grow under nutrient-deprived conditions [17, 18]. The molecular cycling of *KRAS* and the primary signaling axes it activates are summarized in **Figure 1.4**.

The tumor suppressor gene *CDKN2A* (cyclin-dependent kinase inhibitor 2A) is frequently inactivated in over 95% of PC cases, typically through homozygous deletions. The loss of *CDKN2A* removes a key regulator (p16INK4a) that normally enforces the G1 cell cycle checkpoint, thereby driving the proliferation of cancer cells. Furthermore, deletion of the *CDKN2A* locus at 9p21 is often associated with co-deletion of adjacent interferon clusters, resulting in TME “immune coldness” and strongly correlating with primary resistance to immune checkpoint therapy (ICT) [19, 20].

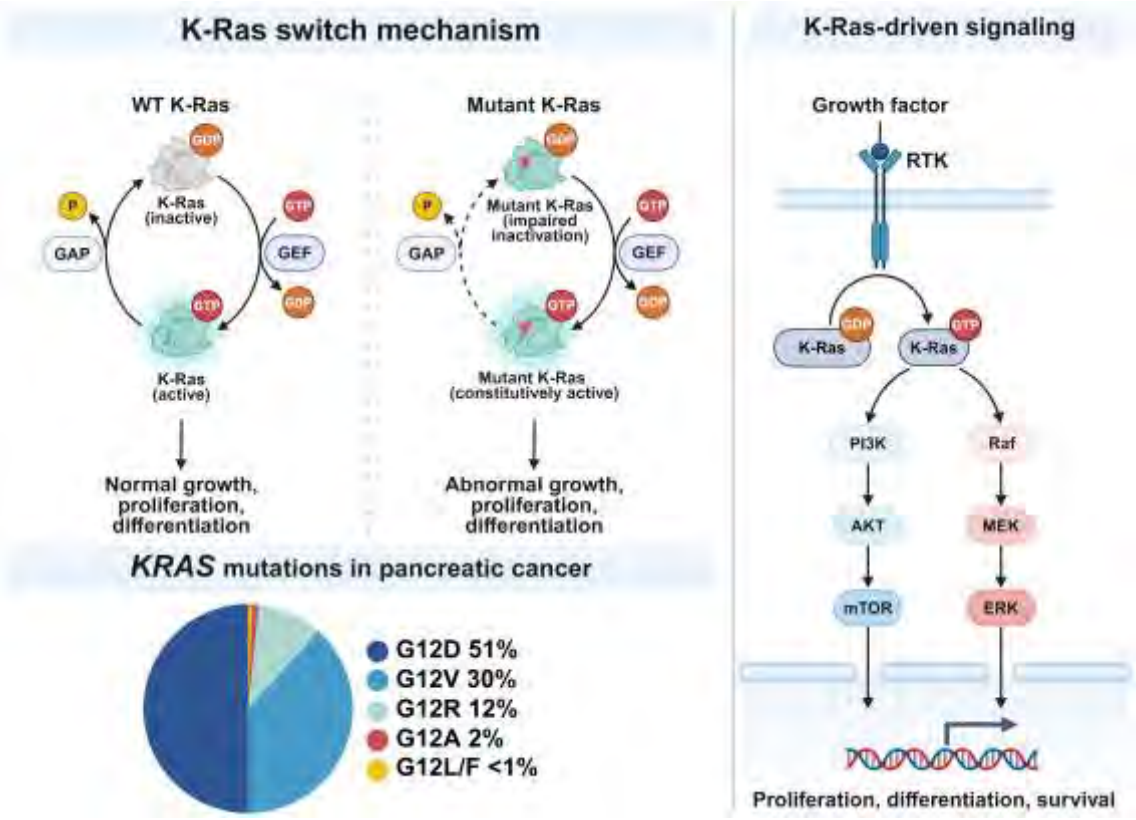

Figure 1.4. *KRAS* mutation dynamics and downstream signaling pathways, based on [18, 21].

Mutations in the *TP53* tumor suppressor gene, which encodes the p53 protein, occur in 50–75% of cases (often at a later stage of tumor development). Unlike many tumor suppressors, *TP53* mutations are often missense mutations that confer gain-of-function (GOF) properties. Predominantly, missense mutations occur at the hotspots R175H, R248Q, R273H, and R282W, while some nonsense or frameshift variants result in truncations. These compromise the protein's role in regulating DNA repair and inducing apoptosis. Loss of p53 function promotes genomic instability and increases the propensity for metastasis, while facilitating evasion of the immune response through an altered secretory phenotype associated with aging (SASP) and reduced antigen presentation [22, 23].

In turn, inactivation or loss of *SMAD4* (mothers against decapentaplegic homolog 4) occurs in approximately 55% of PC cases, a key step in the progression of aggressive disease. As a central mediator in the TGF-β signaling pathway, SMAD4 protein normally exerts tumor-suppressive effects, such as growth arrest and apoptosis, by forming a heteromeric complex with SMAD2/3 to regulate transcription of target genes. However, its disruption by missense mutations that cause partial inactivation or by homozygous deletions that lead to complete loss shifts TGF-β toward pro-tumorigenic functions that promote EMT (epithelial-mesenchymal transition), local invasion, and genomic instability. Complete loss of *SMAD4* correlates with distant metastases to sites such as the liver and lungs, evasion of the immune response, and a significantly worse prognosis [21, 24]. The signaling cascades of the TGF-β/SMAD and p53 pathways, which are frequently dysregulated in PC, are illustrated in **Figure 1.5**.

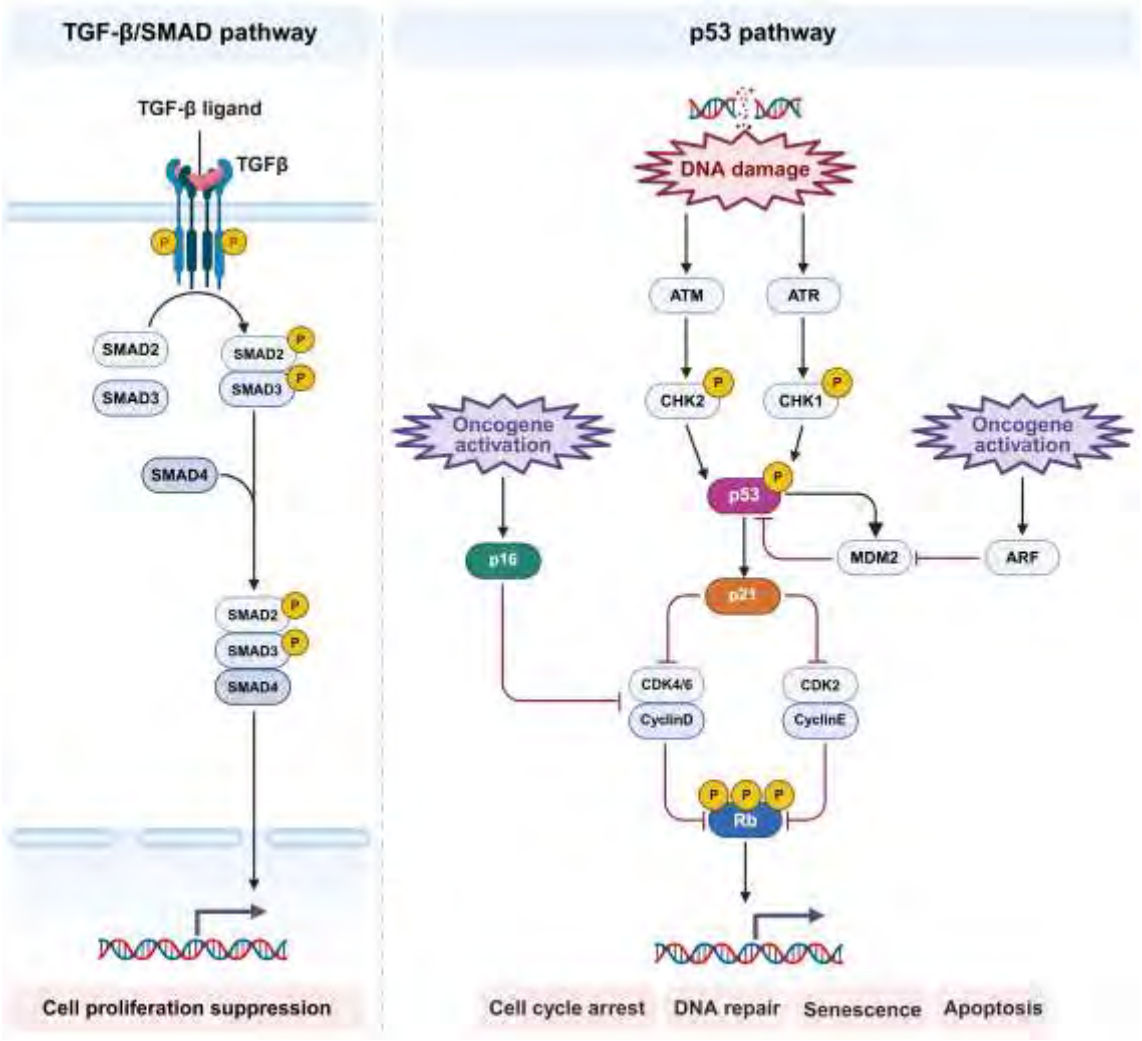

Figure 1.5. The TGF-β/SMAD and p53 tumor suppressor pathways, based on [25, 26].

1.3.2. The Desmoplastic Niche and Cellular Heterogeneity

A defining pathological hallmark of PC is its unique TME, dominated by extensive, dense, and fibrotic stroma (desmoplasia), which can account for up to 90% of the total tumor mass (**Figure 1.3)**. This TME exerts a strong immunosuppressive effect, contributing to treatment resistance [27, 28].

The dense stroma is composed primarily of various acellular components, including abundant fibrillar collagens (e.g., type I and III), fibronectin, laminin, high molecular weight hyaluronic acid (HA), and proteoglycans [29]. Excessive deposition and cross-linking of these ECM proteins lead to elevated interstitial fluid pressure (IFP), which compresses vessels, reduces blood flow, and causes widespread hypoxia [28–30]. This hostile environment acts as a physical barrier, severely restricting the perfusion and homogeneous distribution of systemic chemotherapeutic agents.

The primary producers of the ECM proteins are cancer-associated fibroblasts (CAFs), which are predominantly derived from activated pancreatic stellate cells (PSCs) [29]. Quiescent PSCs (qPSCs) normally store vitamin A and become activated (aPSCs, α-SMA^{+}) in response to

inflammatory signals, oxidative stress, and, particularly, KRAS oncogenic signaling from cancer cells, leading to extensive ECM secretion. Upon activation, PSCs acquire a myofibroblast-like phenotype, characterized by the expression of α-smooth muscle actin (α-SMA) [28, 29, 31].

CAFs do not constitute a uniform population but rather exhibit significant functional and spatial heterogeneity. Two main subtypes have been described: myofibroblastic CAFs (myCAFs) and inflammatory CAFs (iCAFs). MyCAFs, located adjacent to cancer cells and expressing high levels of α-SMA, are largely responsible for generating and contracting dense ECM (fibrosis). In contrast, iCAFs are located farther from the tumor mass, exhibit lower α-SMA expression, and secrete large amounts of pro-inflammatory cytokines, such as IL-6 [32].

The overall characteristics of the TME can vary among patients, and mutations can influence its features in PC cells. Although CAFs are generally perceived as promoting resistance, studies suggest that CAF-induced fibrosis and matrix deposition may initially hinder tumor growth. Therefore, the observed depletion of α-SMA$^+$ myCAFs and fibrosis in mouse models may paradoxically induce immunosuppression, accelerate tumor progression, and shorten survival [33, 34].

1.4. Therapeutic Challenges, Standard Regimens, and Emerging Strategies

1.4.1. Fundamental Mechanisms of Therapy Resistance in PC

Therapeutic resistance in PC is highly complex and results from both intrinsic tumor factors and extrinsic factors provided by the TME.

The TME is characterized by multiple mechanisms that contribute to drug resistance. One of the barriers associated with the TME is the aforementioned physical barrier, which causes poor drug delivery. The dense ECM, driven by CAF/PSC, and the resulting high interstitial fluid pressure compress blood vessels, causing poor blood supply. This physical barrier significantly limits the penetration and distribution of systemic cytotoxic agents, thereby reducing their effectiveness [35].

The hypovascular environment, deprived of nutrients, leads to widespread tissue hypoxia. In response, the hypoxia-inducible transcription factor (HIF-1α) is stabilized. This leads to the formation of the HIF-α/ARNT heterodimer, which, together with transcription coactivators, binds to hypoxia response elements (HREs) in gene promoters, thereby enhancing transcription of genes that facilitate glycolysis, neoplasia, and metastasis [36].

Furthermore, oncogenic *KRAS* drives metabolic reprogramming to cope with nutrient deprivation, relying on clearance pathways such as macropinocytosis and constitutive autophagy. Notably, PC cells engage in a symbiotic metabolic interaction in which they stimulate CAF/PSCs to undergo autophagy and secrete intermediate metabolic products, such as alanine and glutamate, which PC cells then utilize as an energy source, thereby bypassing their dependence on glucose and glutamine [28].

The TME fosters an immunosuppressive environment characterized by high infiltration of MDSCs, M2-polarized tumor-associated macrophages (TAMs), and regulatory T cells (Tregs), while cytotoxic T cells (CD8$^+$ T cells) are excluded or inactivated. CAFs contribute directly to this

process by secreting chemokines such as CXCL12, which sequester $CD8^+$ T cells in the surrounding stroma, preventing effective antitumor immunity [27].

1.4.2. Cytotoxic Chemotherapy Regimens

Systemic chemotherapy is the backbone of PC management, employed in neoadjuvant, adjuvant, and advanced (metastatic) settings.

Gemcitabine (GEM; difluorodeoxycytidine, dFdC), a deoxycytidine analog, has been the first-line reference drug since 1997. GEM requires intracellular activation via sequential phosphorylation by deoxycytidine kinase (dCK) to the active form of triphosphate (dFdCTP). Thereafter, dFdCTP incorporates into DNA, causing immediate termination or "masked chain termination," inhibiting DNA synthesis. However, resistance is common, mediated by reduced cellular uptake, often due to low levels of nucleoside transporters like hENT1, and by rapid inactivation by catabolic enzymes such as cytidine deaminase (CDA). Elevated expression of ribonucleotide reductase (RR) subunits RRM1 and RRM2 is also a recognized mechanism of gemcitabine resistance [37, 38].

Gemcitabine remained the drug of choice until the introduction of the multidrug regimen FOLFIRINOX (fluorouracil, leucovorin, irinotecan, and oxaliplatin). FOLFIRINOX is a potent cytotoxic combination regimen, generally reserved for patients with good performance status (Eastern Cooperative Oncology Group [ECOG] 0-1) due to its significant toxicity profile. This regimen combines four agents. 5-Fluorouracil (5-FU) is a pyrimidine analog that inhibits thymidylate synthase (TS), disrupting DNA synthesis, and which metabolites are incorporated into DNA and RNA, ultimately inducing apoptosis. Leucovorin (LV, folinic acid) is used to enhance the cytotoxic effect of 5-FU. Irinotecan (IRI), on the other hand, is a topoisomerase I (Topo I) inhibitor that stabilizes the DNA-Topo I complex, preventing religation of single-strand DNA breaks and causing lethal double-strand breaks during replication. Oxaliplatin (OXA), a platinum-based alkylating agent, forms irreversible DNA cross-links (intra- and inter-strand), which inhibit DNA replication and induce apoptosis [39, 40]. The PRODIGE trial established that the median overall survival (mOS) for FOLFIRINOX is 11.1 months, which is significantly better than for GEM monotherapy (6.8 months) [41]. For resected PC, modified FOLFIRINOX (mFOLFIRINOX, 75% of standard-dose) is more effective than GEM monotherapy, providing an impressive mOS of 54.4 months versus 35.0 months, respectively [39, 40].

The combination of nanoparticle albumin-bound paclitaxel (nab-paclitaxel) with GEM (GnP) was established as first-line therapy for metastatic PC based on the phase III MPACT trial published in 2013. It showed an mOS of 8.5 months compared to 6.7 months for GEM alone in metastatic disease, progression-free survival - PFS (5.5 vs 3.7 months), and objective response rate - ORR (23% vs 7%). The mechanism of action of paclitaxel involves binding to the β-subunit of tubulin, promoting microtubule polymerization, causing mitotic arrest (G2/M phase), and inducing apoptosis. In turn, nab-paclitaxel is hypothesized to modulate the dense tumor stroma, potentially improving the intra-tumoral penetration of GEM [42–44].

NALIRIFOX (nanoliposomal irinotecan, 5-FU, leucovorin, and oxaliplatin) is an emerging standard-of-care approach for metastatic PC. This modified regimen replaces standard irinotecan with nanoliposomal irinotecan (nal-IRI), an encapsulated formulation (ONIVYDE/MM-398) in combination with 5-FU/LV/OXA. IRI encapsulation in a lipid bilayer vesicle extends circulation time and allows higher, sustained levels of the active metabolite SN-38 in the tumor compared to free irinotecan. The NAPOLI-3 trial demonstrated that NALIRIFOX was superior to gemcitabine/nab-paclitaxel, achieving a mOS of 11.1 months compared to 9.2 months. Importantly, meta-analyses suggest that NALIRIFOX and FOLFIRINOX have similar efficacy for PFS and OS. Moreover, NALIRIFOX is associated with a lower incidence of severe hematological toxic effects (e.g., neutropenia, thrombocytopenia) and peripheral neuropathy compared with FOLFIRINOX, potentially due to a lower cumulative OXA dose and the use of nal-IRI. However, NALIRIFOX may cause a higher incidence of severe diarrhea [44, 45].

Despite the emerging new chemotherapeutic approaches, resection remains the only potentially curative option for PC. However, due to the late stage of the disease at the time of diagnosis, only 15%−20% of patients are eligible for immediate surgery. Furthermore, even for patients undergoing curative resection, the recurrence rate reaches 85%, requiring stringent adjuvant therapy [5, 7]. Application of postoperative chemotherapy (adjuvant) with mFOLFIRINOX significantly reduces the risk of recurrence and improves survival [40]. While preoperative therapy (neoadjuvant) with FOLFIRINOX or GnP is increasingly utilized, especially for borderline resectable PC (BRPC), to increase the likelihood of R0 resection (complete surgical margin clearance), which strongly correlates with improved survival. A phase II trial of neoadjuvant GnP (GnP-NAT) in BRPC patients achieved a 64% R0 resection rate [5].

1.4.3. Targeted Therapies and Emerging Approaches

The growing understanding of PC's molecular landscape and TME has prompted researchers to seek targeted approaches beyond conventional chemotherapy, though their clinical application remains challenging.

The recent development of specific inhibitors for $KRAS^{G12C}$ (sotorasib, adagrasib) and $KRAS^{G12D}$ (MRTX1133) represents a major shift. Nevertheless, the main challenge remains primary and acquired resistance, often driven by bypass mechanisms such as amplification of receptor tyrosine kinases (RTKs; e.g., EGFR, MET, ERBB2) or compensatory activation of the PI3K/AKT/mTOR signaling pathway. Although sotorasib shows activity in G12C-mutated *KRAS* (mOS of 6.9 months), it often requires combination therapy (e.g., with chemotherapy or other pathway inhibitors) to maintain efficacy [46].

Targeting DNA damage repair (DDR) defects also gained attention. Patients carrying germline mutations in DDR genes, particularly *BRCA1/2* and *PALB2* (occurring in 5-10% of cases), exhibit homologous recombination deficiency (HRD). Therefore, tumors with HRD exhibit a "synthetic lethality" dependence on poly(ADP-ribose) polymerase (PARP) function. The PARP inhibitor olaparib has shown substantial efficacy as maintenance therapy after platinum-based

chemotherapy in metastatic *BRCA*-mutated PC (POLO trial), improving median progression-free survival (mPFS) to 7.4 months compared with 3.8 months for placebo [47].

Given the profound role of the stroma in resistance, targeted modulation is a highly active area of research. Strategies focus on modulating the desmoplasia rather than complete removal, as stromal ablation can accelerate metastasis. One approach is to target HA (PEGPH20, PEGylated human hyaluronidase), although clinical results have been mixed, with toxicity and poorer survival reported in some trials [29]. Inhibition of the TGF-β pathway with agents such as galunisertib modulates fibrosis and the immune response. In turn, losartan (angiotensin II receptor antagonist), reduces TGF-β activation and normalizes dysfunctional tumor vasculature by decreasing vascular permeability, potentially enhancing chemotherapy delivery [48, 49]. In addition, agents that reprogram CAFs by employing vitamin D agonists (paricalcitol) or all-trans retinoic acid (ATRA) to induce quiescence are being used [29].

As already mentioned, PC is generally considered "immunologically cold" due to its immunosuppressive TME, which limits the effectiveness of immune checkpoint inhibitors (ICIs) used as monotherapy. However, ICIs (e.g., pembrolizumab) show efficacy in the rare subset of PC characterized by tumors with microsatellite instability-high/mismatch repair deficient (MSI-H/dMMR) [44]. Novel strategies focus on combining ICIs with chemotherapy, vaccines (e.g., GVAX), or TME-modulating agents [50–52].

The landscape of pancreatic cancer therapy has changed significantly with recent breakthroughs that bridge the gap between innovative physical methods and multi-point molecular targeting. The Phase III PANOVA-3 clinical trial demonstrated that combining electric field therapy (TTFields), a non-invasive, variable-intensity electric field, with standard gemcitabine and nab-paclitaxel therapy significantly extends median survival (16.2 months compared to 14.2 months) and doubles pain-free survival in patients with inoperable, locally advanced pancreatic adenocarcinoma. This is the first Phase III trial in this specific population to show a significant survival benefit without additional systemic toxicity [53]. Concurrently, advanced preclinical research led by Prof. Mariano Barbacid has provided a potential solution to the chronic challenge of K-Ras inhibitor resistance. Recent findings indicate that triple-targeted therapy, simultaneously inhibiting K-Ras (using Ras(ON) inhibitors such as daraxonrasib), EGFR (afatinib), and the orthogonal STAT3 signaling node (using the SD36 degradator), can achieve complete and durable tumor regression in orthotopic and patient-derived xenograft models. Most importantly, this multi-node approach has been shown to prevent tumor recurrence for more than 200 days after treatment by systematically blocking compensatory signaling axes that typically cause therapy evasion in *KRAS*-mutated cancers [54].

1.5. Diagnostic Methods for Pancreatic Cancer

Early detection of PC remains the paramount challenge due to the pancreas's deep anatomical location and the lack of symptoms in its early stages. While nearly 70% of pancreatic cancers are located in the head of the pancreas, frequently resulting in biliary obstruction and jaundice, PC is seldom detected early. Notably, the majority of patients experience mild and

nonspecific symptoms that develop primarily in advanced stages, including abdominal pain, weight loss, anorexia, nausea, and vomiting [10].

In terms of tissue acquisition and imaging techniques, endoscopic ultrasound is the most sensitive method for detecting cystic lesions. Advanced imaging also gains attention. This AI-assisted image analysis (radiomics, deep learning) shows promise for increasing diagnostic sensitivity in computed tomography (CT) scans by identifying subtle changes invisible to the human eye [4, 55].

However, the inability to conduct reliable screening tests among the general population necessitates the discovery of easily measurable, non-invasive biomarkers. Carbohydrate antigen 19-9 (CA 19-9) is the only tumor marker approved by the FDA. Unfortunately, due to its low sensitivity for early detection, it is mainly used for monitoring rather than early diagnosis. CA 19−9 is not produced by approximately 5%−10% of the population, who are Lewis antigen-negative. An interesting approach is the detection of novel biomarkers using liquid biopsy. Liquid biopsy assays detect circulating biomarkers, such as circulating tumor DNA (ctDNA), microRNAs (miRNAs), and proteins, which may offer higher sensitivity and specificity for early detection. MicroRNAs show strong promise, with a recent meta-analysis in early-stage (stage I/II) PC reporting high pooled diagnostic accuracy (sensitivity 0.88, specificity 0.91, and area under the curve (AUC) 0.95). They are highly stable in biofluids and may reflect early molecular changes. Meanwhile, ctDNA typically exhibits high specificity (0.94) but moderate sensitivity (0.65) for early detection. Detection of mutated *KRAS* sequences in ctDNA is also a valuable tool. Combining ctDNA analysis with CA 19−9 significantly improves diagnostic performance. Multiplex protein panels (e.g., detecting MIC-1/GDF15, THBS2) can achieve strong diagnostic performance (AUC 0.90). Extracellular vesicles (EVs), including exosomes, that contain tumor-specific cargo (e.g., the Glypican-1 protein and specific miRNAs) are under investigation as potential early detection markers [10, 55, 56].

The integration of multiple non-invasive biomarkers (e.g., molecular signatures and proteins) significantly improves diagnostic accuracy compared to using a single marker. In addition, for high-risk groups, monitoring fasting blood glucose/HbA1c is recommended to detect newly diagnosed diabetes, as newly diagnosed diabetes often precedes the diagnosis of PC [56].

2. Key Cellular Processes in Pancreatic Cancer Biology

The pathogenesis of PC is primarily defined by the sequential accumulation of mutations in four main driver genes, starting with the activating mutation of the *KRAS* oncogene (K-Ras), followed by the functional inactivation of tumor suppressors such as *CDKN2A* (p16), *TP53* (p53), and DPC4/*SMAD4*. Collectively, these genetic events facilitate cell cycle deregulation, evasion of programmed cell death, and acquisition of a highly invasive phenotype [57].

2.1. Molecular and Genetic Characteristics of Selected PDAC Cell Line Models

The selection of cell lines as experimental models is a critical prerequisite for investigating the molecular pathophysiology of PC and evaluating the efficacy of novel anticancer agents. Since PC is characterized by extreme genetic heterogeneity, using a panel of cell lines that recapitulate the most frequent clinical mutations is essential for achieving robust, translatable results. The pathogenesis of PC involves a systematic accumulation of genetic alterations, dominated by the activating mutation of the *KRAS* oncogene and the functional inactivation of tumor suppressors such as *CDKN2A*/p16, *TP53*, and *SMAD4*. To accurately reflect these diverse molecular backgrounds, four well-established human PC cell lines were employed in this dissertation: Panc-1, MIA PaCa-2, AsPC-1, and BxPC-3 [58]. The detailed mutational status and clinical origin of these experimental models are summarized in **Table 2.1**.

Table 2.1. Molecular and genetic characteristics of selected human pancreatic cancer (PC) cell line models, based on [58].

Cell Line	Origin	*KRAS* Status	*TP53* Status	*CDKN2A* Status	*SMAD4* Status	Differentiation Grade
Panc-1	Primary tumor	Mutated (G12D)	Mutated (R273H)	Homozygous Deletion	Wild-type	Poor
MIA PaCa-2	Primary tumor	Mutated (G12C)	Mutated (R248W)	Homozygous Deletion	Wild-type	Poor
AsPC-1	Metastasis (Ascites)	Mutated (G12D)	Deletion (Exon 5)	Homozygous Deletion	Wild-type / Variable	Moderate to High
BxPC-3	Primary tumor	Wild-type	Mutated (Y220C)	Homozygous Deletion	Homozygous Deletion	Moderate

The Panc-1 and MIA PaCa-2 cell lines serve as representative models of primary, poorly differentiated, and highly aggressive pancreatic ductal adenocarcinomas [59]. Both lines exhibit constitutive activation of the K-Ras signaling axis through point mutations at codon 12, specifically the G12D variant in Panc-1 and the G12C variant in MIA PaCa-2. Moreover, these models are characterized by missense mutations in *TP53*, namely R273H in Panc-1 and R248W in MIA PaCa-2, which collectively contribute to the evasion of apoptosis-inducing factors and increased genomic instability. Both Panc-1 and MIA PaCa-2 carry homozygous deletions of the *CDKN2A*/p16 gene, leading to the loss of a critical G1/S cell cycle checkpoint regulator. Interestingly, these cell lines retain wild-type *SMAD4* status, allowing analysis of TGF-β-dependent pathways in the context of proliferation and invasion [60].

The AsPC-1 cell line was established from a patient's ascites and represents a metastatic model of the disease [59]. Genotypically, AsPC-1 carries the G12D *KRAS* mutation and a complex *TP53* deletion, specifically a homozygous deletion of exon 5, resulting in a null p53 phenotype. Similar to the primary tumor models, AsPC-1 has lost p16 function through homozygous deletions of exons 2 and 3 [61]. The *SMAD4* status in AsPC-1 is often reported as wild-type, although its expression levels can vary due to the cell line's heterogeneous origin [58].

The BxPC-3 cell line is an indispensable control in PC research, as it is one of the few malignant models with wild-type *KRAS* [61]. Despite the absence of *KRAS* mutations, BxPC-3 cells display high malignancy due to a constitutively active *BRAF* deletion mutant and significant tumor suppressor loss [62]. These cells carry other alterations, including the Y220C *TP53* mutation and the simultaneous homozygous deletion of *CDKN2A* and *SMAD4* [61]. The loss of *SMAD4* in BxPC-3, which occurs in the later stages of human PC progression, makes this line a pivotal model for studying the transition from an epithelial to a mesenchymal state and the regulation of non-canonical TGF-β signaling [63].

Using these four models, this study covers the full spectrum of genetic mutations found in clinical PC, ensuring that observations on apoptosis, senescence, and autophagy induced by anticancer compounds are validated across diverse oncogenic contexts.

2.2. Apoptosis: Mechanisms and Role in Cancer Therapy

Apoptosis is a systematically coordinated mechanism of programmed cell death, essential for maintaining tissue homeostasis and eliminating pre-malignant cells [64]. This process is executed by caspases, a family of cysteine-aspartic acid proteases that are synthesized as inactive zymogens and activated through proteolytic cleavage [65]. The extrinsic pathway uses extracellular signals to induce apoptosis. It is triggered by the binding of death ligands to surface receptors of the TNF superfamily, such as TNF-related apoptosis-inducing ligand (TRAIL) or Fas, which recruit the adaptor protein Fas-associated death domain (FADD) and initiator caspase-8 to form the death-inducing signaling complex (DISC). Conversely, the intrinsic pathway utilizes the mitochondria and mitochondrial proteins and is regulated by the Bcl-2 family proteins, which act as arbiters of mitochondrial outer membrane permeabilization (MOMP). This family includes pro-apoptotic effectors such as Bax and Bak, BH3-only sensitizers like Bim, Bad, and Puma, and anti-apoptotic members such as Bcl-2 and Bcl-xL. Upon activation, MOMP allows the release of cytochrome c and Smac (second mitochondria-derived activator of caspase)/DIABLO (direct IAP binding protein with low pI) into the cytoplasm. Cytochrome c then associates with apoptotic protease-activating factor-1 (APAF-1) and pro-caspase-9 to form an apoptosome, which subsequently activates executioner caspases 3 and 7, leading to the cleavage of structural and functional proteins such as protease-activated receptors (PAR) [65, 66].

In pancreatic cancer, these life-and-death mechanisms are systematically disrupted by excessive survival signals. The primary driver of this evasion is the *KRAS* gene, which encodes a 21 kDa small GTPase that serves as a binary molecular switch, cyclically switching between an

active state, associated with guanosine triphosphate (GTP), and an inactive state associated with guanosine diphosphate (GDP). In PC, point mutations at codons 12, 13, or 61 impair the intrinsic GTPase activity, maintaining K-Ras in a constitutively active state that persistently stimulates downstream signaling cascades. Since *KRAS* mutations are found in nearly all PC cases, this cancer is arguably the most RAS-addicted of all human malignancies [67].

The hyperactivation of K-Ras drives two major survival pathways: the Raf/MEK/ERK and PI3K/AKT/mTOR pathways [67]. The Raf/MEK/ERK cascade, a member of the mitogen-activated protein kinase (MAPK) family, is initiated when active K-Ras recruits RAF kinases to the plasma membrane, leading to the sequential phosphorylation of MEK and ERK, which then translocate to the nucleus to regulate the expression of proliferation-related genes [40]. Simultaneously, K-Ras activates the PI3K/AKT/mTOR axis, where phosphatidylinositol 3-kinase (PI3K) phosphorylates lipids to produce phosphatidylinositol-3,4,5-trisphosphate (PIP3), which recruits and activates the serine-threonine kinase Akt. Once activated, Akt phosphorylates numerous downstream targets. Among these, mechanistic target of rapamycin (mTOR) is a key effector of Akt, coordinating the activity of multiple proteins to drive cancer progression. This pathway is further amplified by the loss of PTEN, a phosphatase and tensin homolog that normally acts as a negative regulator by dephosphorylating PIP3 [68].

Beyond cell signaling, K-Ras hyperactivation also induces metabolic reprogramming, such as increased glutamine metabolism and protein synthesis, to support rapid cancer cell growth. A central feature of this reprogramming is the Warburg effect, in which K-Ras enhances glucose uptake and glycolysis by upregulating the transcription of glucose transporters (GLUT1, GLUT4) and rate-limiting enzymes like HK1, ENO1, and LDHA. This glycolytic flux is redirected to anabolic pathways, such as the nonoxidative pentose phosphate pathway (PPP), which generates ribose 5-phosphate for nucleotide synthesis and nicotinamide adenine dinucleotide phosphate hydrogen (NADPH) for reactive oxygen species detoxification. K-Ras shifts glutamine utilization from the canonical tricarboxylic acid cycle (TCA; Györgyi–Krebs cycle) to a non-canonical pathway by upregulating aspartate transaminase (GOT1) and downregulating glutamate dehydrogenase 1 (GLUD1). This shift is essential for maintaining the redox balance required for cell proliferation. K-Ras also significantly alters lipid metabolism by upregulating fatty acid synthase (FASN) and promoting lipid droplet accumulation. By inhibiting hormone-sensitive lipase (HSL) activity, K-Ras attenuates fatty acid oxidation and stores lipids that are later utilized to fuel tumor cell invasion and metastasis. These metabolic changes are often accompanied by the loss of tumor suppressors like *TP53*, which further enhances glycolytic flux by eliminating glucose transporter arrest and inhibiting the glycolysis regulator *TP53*-inducible glycolysis and apoptosis regulator (TIGAR). Mechanistically, sustained K-Ras signaling drives these alterations by activating the MAPK pathway and stabilizing transcription factors such as c-Myc and HIF1α, which in turn regulate the necessary metabolic enzymes. [69]

In pancreatic cancer, the myelocytomatosis oncogene *MYC* plays a pivotal role as a dual regulator of cell fate, capable of promoting both rapid proliferation and programmed cell death. c-Myc is a major oncogenic transcription factor overexpressed in approximately 43% to 75% of

primary and metastatic pancreatic cancers, where it serves as a primary driver of neoplastic progression and chemoresistance [70]. c-Myc functions as a critical downstream convergence point for the most prevalent oncogenic drivers and tumor suppressors, including *KRAS*, *TP53*, *SMAD4*, and *CDKN2A*. Deregulation of c-Myc is associated with gene amplification but also stems from alterations in these upstream regulators. The primary driver of this network is oncogenic *KRAS*, whose signaling is essential for the stabilization and accumulation of c-Myc protein [71]. Specifically, K-Ras activates the MAPK/ERK pathway, which phosphorylates and inhibits the tumor suppressor FBW7. Since FBW7 is the E3 ubiquitin ligase responsible for targeting c-Myc for proteasomal degradation, its inhibition by K-Ras leads to sustained c-Myc stability and accumulation, thereby fueling metabolic reprogramming and cell survival [72].

Furthermore, K-Ras promotes *MYC* mRNA translation via the eIF5A-PEAK1 signaling axis and the PI3K/AKT/mTOR pathway, thereby ensuring high levels of the oncoprotein [71]. The loss of key tumor suppressors potentiates this oncogenic impulse. In normal physiology, the TGF-β signaling pathway, mediated by SMAD4, acts as a repressor of *MYC* transcription. However, SMAD4 is frequently deleted or mutated in PC, thereby abolishing this inhibitory signal and allowing uncontrolled *MYC* expression. Concurrently, the progression of PC from intraepithelial neoplasia to invasive carcinoma is marked by the cooperative loss of *CDKN2A* (p16) and *TP53*, along with c-Myc activation [71]. p53 normally functions to restrain tumorigenesis by inducing the expression of the long non-coding RNA *Pvt1*, which suppresses *MYC* transcription. Consequently, the loss of p53 function in PC removes this brake, facilitating c-Myc overexpression. In the context of cell cycle regulation, c-Myc acts as a potent accelerator of the G1/S phase transition, interacting with cyclin-dependent kinases (CDKs) and cyclins. Notably, c-Myc promotes the expression of Cyclin D1 and Cyclin D2, often through the upregulation of the long non-coding RNA *CCAT1*, which stabilizes the transcriptional machinery necessary for Cyclin D1 expression. By enhancing Cyclin D activity and simultaneously repressing CDK inhibitors such as p21, c-Myc forces cancer cells into rapid, uncontrolled proliferation [73]. The pleiotropic roles of c-Myc in regulating diverse cellular processes, from metabolism to DNA repair, are highlighted in **Figure 2.1**.

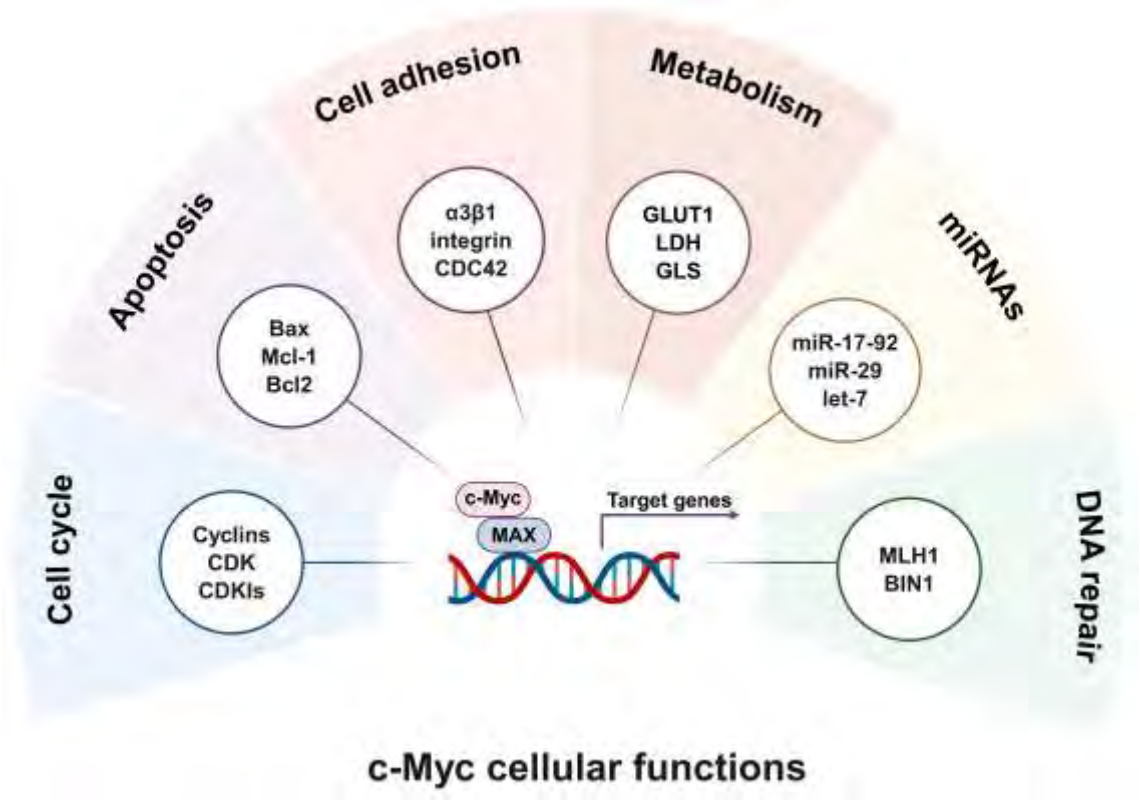

Figure 2.1. Cellular functions of the c-Myc transcription factor, based on [74].

Antitumor compounds aim to reinstate apoptotic pathways, often by inhibiting anti-apoptotic regulators such as XIAP or by modulating the c-Myc transcription factor. XIAP (X-linked inhibitor of apoptosis protein), which is frequently overexpressed in PC, binds and inhibits initiator caspase-9 and executioner caspases-3 and -7, thereby blocking both mitochondrial-dependent and independent death pathways. To restore functional apoptotic pathways, therapeutic strategies use XIAP inhibitors, such as Smac mimetics or small-molecule compounds like embelin, a benzoquinone derived from the herb *Ardisia* [75]. Based on current therapeutic strategies, innovative approaches like the 3'UTRMYC1-18 mRNA drug have been developed to address the critical challenge of c-Myc-driven chemoresistance. This mRNA-based therapeutic remodels stable poly (U) sequences in the 3' UTR of the c-Myc gene into destabilized forms. Mechanistically, the drug specifically recognizes and binds to endogenous c-Myc mRNA exons, causing ribosomes to stall as they attempt to translate the transcript. The EXOSC4-PELO-RPL3 complex detects this arrest. This specialized cellular machinery subsequently triggers the degradation of the target c-Myc transcript, leading to a dose-dependent reduction in oncogenic protein levels [70]. Interestingly, stabilizing G-quadruplexes (G4s) in the *MYC* promoter region offers a promising strategy to inhibit c-Myc transcription at the DNA level directly. The *MYC* gene contains a guanine-rich sequence, the nuclease hypersensitive element III1 (NHE III1), which can naturally fold into a four-stranded G4 structure that physically blocks the transcriptional machinery from accessing the gene. Small-molecule ligands designed to bind and stabilize these structures prevent the unwinding of DNA necessary for transcription, effectively silencing *MYC* expression. Prominent compounds in this class include QN1 and TMPyP4, the latter of which has shown the

ability to inhibit c-Myc with reduced toxicity toward normal cells. In addition, the novel G4 stabilizer CM03 has demonstrated high selectivity for pancreatic ductal adenocarcinoma, proving effective even in gemcitabine-resistant models. Studies indicate that CM03 aggravates DNA damage, inducing cancer cell arrest, and is particularly potent when combined with histone deacetylase (HDAC) inhibitors like SAHA [71].

2.3. Cellular Senescence: Tumor Suppression and Therapy-Induced Senescence

Cellular senescence is a state of cell cycle arrest in the G1 phase, which constitutes a critical barrier against malignant transformation. It is characterized by specific morphological changes, including an enlarged and flattened cell body, increased cytoplasmic granularity, and the formation of senescence-associated heterochromatin foci (SAHF), which suppress the expression of growth-related genes, such as E2F targets. The hallmark of senescent cells is the increased activity of the lysosomal enzyme senescence-associated β-galactosidase (SA-β-gal), which is detectable at a suboptimal pH of 6.0 [76, 77]. Additionally, senescent cells exhibit loss of nuclear membrane integrity, often manifested by a significant decrease in Lamin B1 protein levels and increased expression of CDK inhibitors, such as $p16^{INK4A}$ and $p21^{Cip1/Waf1}$ [78]. Cellular senescence is typically initiated through three main triggers: telomere attrition (replicative senescence), hyperactivation of oncogenes (oncogene-induced senescence, OIS), and exposure to subcytotoxic doses of chemotherapeutic agents or radiation (therapy-induced senescence, TIS). Furthermore, various external factors, such as DNA-damaging agents, oxidative stress, nutrient depletion, and others, cause aging, a process known as stress-induced premature senescence (SIPS) [79, 80].

The molecular process of senescence primarily depends on the activation of two tumor suppressor pathways: the p53-p21 and p16-Rb pathways. DNA damage response signaling, mediated by the ATM and ATR kinases, stabilizes the p53 transcription factor, which transactivates its downstream target p21 (*CDKN1A*) to inhibit CDK2 activity [81]. Notably, research has demonstrated that p21-dependent senescence can be induced in cancer cells regardless of their p53 status, which is particularly relevant in PC, where *TP53* is frequently mutated [82]. In addition, the transcription factor c-Myc is an important regulator of this program, as its inhibition has been shown to relieve the repression of the p21 promoter, thereby facilitating the onset of senescence and coordinating it with apoptotic pathways [83, 84]. In turn, p16 (*CDKN2A*), a member of the INK4 family, specifically inhibits CDK4 and CDK6, thereby maintaining the retinoblastoma protein (Rb) in a hypophosphorylated, active state that prevents the transition from G1 to S phase [85].

In the complex landscape of the PC tumor microenvironment, senescent cells exert profound non-cell-autonomous effects through the secretion of a diverse array of molecules collectively termed the senescence-associated secretory phenotype. SASP consists of proinflammatory cytokines such as IL-6 and IL-8, growth factors like VEGF and TGF-β, and matrix metalloproteinases (MMPs), which modulate the surrounding tissue in a context-dependent manner [86]. In the early stages of tumorigenesis, SASP can be beneficial by recruiting immune

cells, such as natural killer (NK) cells and macrophages, to clear precancerous senescent cells, a process known as senescence surveillance [76]. However, in established PC, the chronic presence of senescent cells and their secretome becomes primarily pro-tumorigenic. For instance, senescent cancer-associated fibroblasts and pancreatic stellate cells produce SASP factors that promote tumor cell proliferation, invasiveness, and the EMT [76, 87]. Moreover, the SASP can foster an immunosuppressive microenvironment by recruiting MDSCs and Tregs, which inhibit cytotoxic T-cell function and allow the tumor to evade immune detection [78].

A necessary condition for PC progression is the ability of transformed cells to escape or bypass senescence [81]. The sequential accumulation of genetic alterations in key genes drives this escape. Activating mutations in the *KRAS* oncogene are the earliest events, typically found in PanIN-1 lesions. While oncogenic *KRAS* initially triggers OIS, subsequent loss-of-function mutations in *CDKN2A* and *TP53* allow cells to re-enter the cell cycle and proliferate indefinitely [22]. Inactivation of the *SMAD4* gene, which occurs in the later stages of invasive PC, further enhances this escape by promoting cell survival and metastasis [40]. Beyond genetic mutations, chronic inflammation associated with pancreatitis has been shown to disrupt the OIS barrier in PanIN lesions, facilitating their rapid transition to malignant adenocarcinoma. Recent evidence also suggests that senescent cancer cells may regain proliferative capacity through telomerase reactivation or upregulation of mitotic regulators such as Cdc2/Cdk1, posing a serious risk of cancer recurrence [78, 81].

2.4. Autophagy: Dual Role in Tumor Survival and Death

Autophagy (type II cell death) is an evolutionarily conserved catabolic process that involves the lysosomal degradation and recycling of damaged proteins and organelles [88]. The complete autophagic process, often referred to as autophagic flux, proceeds through five distinct stages: (1) initiation, (2) elongation, (3) maturation, (4) fusion, and (5) degradation. Autophagy is governed by the mTOR1 kinase, which binds and phosphorylates Unc-51-like kinase 1 (ULK1). When a cell experiences amino acid deprivation, autophagy is initiated by the ULK1 dephosphorylation complex, which consists of the serine/threonine kinase ULK1, the scaffold protein FIP200, and the regulatory subunits ATG13 and ATG101. Following initiation, the nucleation stage involves the recruitment of the class III PI3K complex I, which contains VPS34 (a lipid kinase), Beclin1 (a central scaffold protein), and ATG14L, to generate phosphatidylinositol 3 phosphate (PI3P) on the omegasome, a precursor structure associated with the endoplasmic reticulum [89, 90]. The sequential stages of the autophagic process and the key protein complexes involved are detailed in **Figure 2.2**.

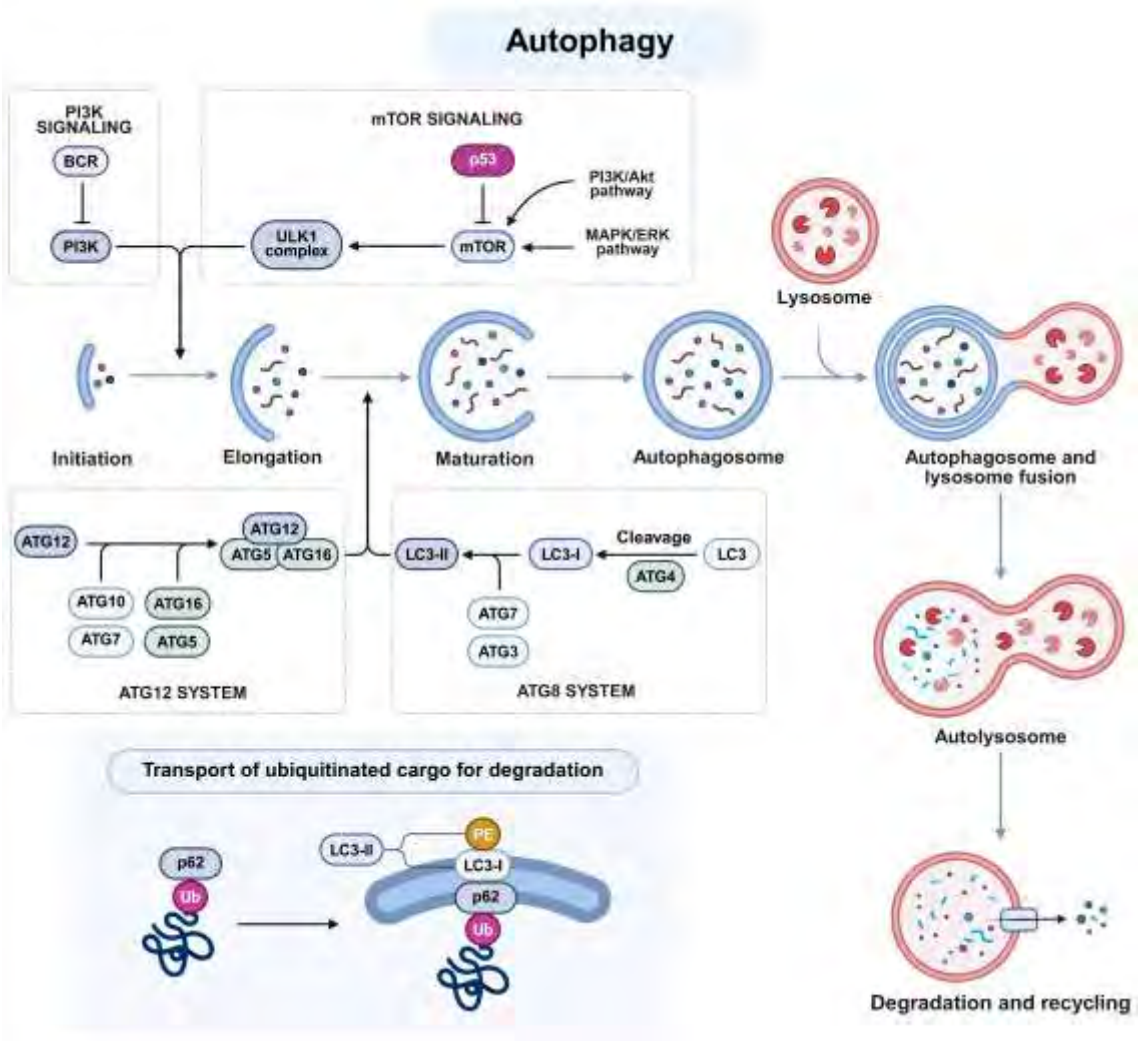

Figure 2.2. The molecular machinery of autophagy, based on [90].

Two ubiquitin-like conjugation systems mediate the elongation of the nascent phagophore into a double-membrane autophagosome. The first system involves the covalent conjugation of ATG12 to ATG5, catalyzed by the E1-like enzyme ATG7 and the E2-like enzyme ATG10, forming a stable complex with ATG16L1. The second system involves the processing of LC3 (the mammalian homolog of yeast Atg8) by the cysteine protease ATG4 to form LC3 I, which is then ligated to phosphatidylethanolamine (PE) by ATG7 and ATG3 to form LC3 II. LC3 II is incorporated into the phagophore membrane and serves as a marker for autophagosome formation. Selective cargo recognition is achieved by the receptor p62/SQSTM1, which binds both ubiquitinated proteins and membrane-associated LC3 II to sequester targets for degradation. During fusion, the autophagosome moves along microtubules. It fuses its outer membrane with a lysosome to form an autolysosome, a process that requires the GTPase Rab7 and SNARE proteins (soluble N-ethylmaleimide-sensitive factor attachment protein receptors). Finally, at the degradation stage, lysosomal hydrolases digest the sequestered cargo and the inner membrane, releasing nutrients back into the cytoplasm. Consequently, the degradation of membrane-associated LC3-II and p62 reflects active autophagic flux [89, 91, 92].

The regulation of autophagy is mainly controlled by two major nutrient-sensing nodes: mTORC1 and AMPK. Under nutrient-rich conditions, mTORC1 (a member of the PI3K-related kinase family) inhibits autophagy by phosphorylating ULK1 at Ser757 to prevent its interaction with AMPK (an adenosine monophosphate-activated protein kinase). In contrast, under conditions of energy stress, AMPK is activated by elevated AMP/ATP ratios and stimulates autophagy by directly phosphorylating ULK1 at Ser317 and Ser777, while simultaneously inhibiting mTORC1 activity. Autophagy is also suppressed by the PI3K/AKT/mTORC1 signaling axis, where AKT phosphorylates TSC2 (tuberous sclerosis complex 2) to activate mTORC1 [89, 93]. Interestingly, non-classical regulations have been observed in which c-Myc inhibition or the use of stapled peptides can strongly disrupt autophagic flux, effectively transforming the survival mechanism into a cell death program [94]. Interestingly, c-Myc levels are significantly reduced via autophagic-lysosomal degradation, a process driven by the tumor suppressor protein EI24 (etoposide-induced 2.4 kb transcript). In pancreatic cancer cells, restoring EI24 expression activates the autophagy machinery, targeting c-Myc for lysosomal degradation, thereby reversing its oncogenic effects. Consequently, this autophagic clearance of c-Myc suppresses tumor proliferation and induces S-phase cell cycle arrest, demonstrating a critical crosstalk between autophagy and cell growth regulation [95].

While autophagy typically functions as a transient, stress-inducible response in normal tissues, in PC it acts as a critical, autonomous cellular mechanism essential for tumor maintenance and metabolic adaptation [96]. The high degree of basal autophagy in PC results from higher ATG expression levels. The constitutive activation is driven by a unique transcriptional program in which the microphthalmia/transcription factor E (MiT/TFE) is released from cytoplasmic sequestration via mTORC1. This allows them to constitutively translocate to the nucleus and stimulate the expression of genes involved in autophagy initiation, extension, substrate capture, autophagosome transport, and lysosomal fusion. Furthermore, oncogenic K-Ras sustains this elevated autophagy through the upregulation of VMP1 (vacuole membrane protein 1), which interacts with Beclin-1 to initiate the phagophore formation [89].

In the hypovascular, nutrient-deprived PC microenvironment, this elevated autophagic flux serves two fundamental metabolic functions. It mitigates the accumulation of cytotoxic reactive oxygen species (ROS), thereby preventing DNA damage and genomic instability, and it recycles intracellular components to provide bioenergetic intermediates [96]. Specifically, autophagy generates amino acids such as glutamine, which are essential for fueling the TCA cycle and sustaining mitochondrial oxidative phosphorylation [88]. PSCs' autophagy contributes to this metabolic support in the tumor stroma by secreting non-essential amino acids, particularly alanine, which are taken up by PC cells to support their central carbon metabolism [90]. Consequently, pharmacological or genetic inhibition of autophagy in PC leads to an energy crisis, accumulation of damaged mitochondria, and tumor regression [96].

The functional outcome of autophagy in PC is highly context-dependent. In the early stages of tumor development, autophagy acts as a tumor suppressor by maintaining homeostasis and preventing inflammation [97]. However, in established invasive tumors, it switches to a

pro-tumorigenic role. This duality is further influenced by p53 status, where in models with p53 loss, autophagy inhibition may accelerate tumor onset. In contrast, in the presence of functional or mutant p53, autophagy is generally essential for tumor progression [98]. Additionally, autophagy contributes significantly to chemoresistance, acting as a cytoprotective mechanism against agents such as gemcitabine and 5-fluorouracil, and its inhibition can sensitize cells to caspase-dependent apoptosis [99].

2.5. Crosstalk Between Apoptosis and Autophagy

The cellular decision between survival and death relies on a complex, molecular interplay between the autophagic and apoptotic machineries, which do not operate in isolation but are regulated by a shared network of proteins. At the center of this crosstalk lies the interaction between Beclin1, an essential autophagy effector protein belonging to the BH3-only protein subfamily, and the anti-apoptotic members of the Bcl-2 family (B-cell lymphoma 2), specifically Bcl-2 and Bcl-xL. Structurally, Beclin-1 contains a Bcl-2-homology-3 (BH3) domain at its N-terminus, which mediates its binding to the hydrophobic groove of Bcl-2 or Bcl-xL. Under basal conditions, Bcl-2 sequesters Beclin-1, preventing its assembly with the PI3K complex and thereby inhibiting the nucleation of the phagophore. This inhibition can be relieved by phosphorylation of Bcl-2 by JNK1 (c-Jun N-terminal kinase 1) or of Beclin-1 by DAPK (death-associated protein kinase), which disrupts the complex, releasing Beclin-1 to initiate autophagy [100].

The critical molecular switch involves caspase-mediated proteolytic cleavage of Beclin-1. Upon induction of apoptosis, activated caspases-3 and -8 cleave Beclin-1 at specific aspartate residues (e.g., D149), thereby destroying its pro-autophagic activity. Importantly, the resulting C-terminal fragment of Beclin-1 is transported to the mitochondria, where it sensitizes the organelle to permeabilization and promotes the release of pro-apoptotic factors, such as cytochrome *c*, thereby creating a positive feedback loop that amplifies apoptosis [100].

Notably, the tumor suppressor p53 acts as a dual regulator within this network. Nuclear p53 acts as a transcription factor that upregulates pro-apoptotic genes (e.g., PUMA, NOXA) and autophagy-related genes (e.g., DRAM), whereas cytoplasmic p53 inhibits autophagy by interacting with the mTOR pathway [101, 102]. In the context of PC treatment, certain compounds induce a form of apoptosis-promoting autophagy, also described as autophagic cell death. In this non-classical scenario, rather than acting as a survival mechanism, excessive autophagic flux degrades essential survival factors, such as the inhibitor of apoptosis proteins and catalase, leading to ROS accumulation and subsequent mitochondrial dysfunction [103]. For instance, treatment with compounds like phycocyanin has been shown to block the Akt/mTOR signaling pathway while stimulating the NF-κB pathway, leading to a synergistic induction of both autophagy and apoptosis that overwhelms the adaptive capacity of cancer cells [104]. Consequently, therapeutic strategies that simultaneously trigger extensive autophagy and apoptosis can overcome the intrinsic chemoresistance of PC cells by turning their recycling machinery into a mechanism of self-destruction.

2.6. Cell Migration and Invasion: Mechanisms of Metastasis

The lethal nature of PC is largely attributed to its early metastatic spread, a process driven by the acquisition of a migratory phenotype through epithelial-mesenchymal transition. EMT is a biological program in which epithelial cells lose their apical-basal polarity and cell-cell adhesion structures, such as adherens junctions and tight junctions, to acquire a mesenchymal, spindle-shaped morphology [105]. At the molecular level, this transformation is coordinated by the "cadherin switch," characterized by the repression of *CDH1* transcription encoding E-cadherin and the *de novo* expression of N-cadherin, Vimentin, and fibronectin [106]. This reprogramming is driven by key transcription factors, including Snail, Slug, ZEB1, and TWIST1, which bind to E-box consensus sequences in the *CDH1* promoter to silence its expression [105]. These transcription factors are often upregulated in PC in response to signals from the TME, including TGF-β, hypoxia, and inflammatory cytokines such as IL-6 [107].

Invasion requires ECM degradation, a process facilitated by specialized actin-rich membrane protrusions called invadopodia. These structures recruit MMPs, particularly MMP-2 and MMP-9, which are zinc-dependent endopeptidases that degrade collagen and other ECM components. The formation of invadopodia and the turnover of focal adhesions, multi-protein structures linking the actin cytoskeleton to the ECM via integrins, are regulated by signaling kinases such as FAK (focal adhesion kinase) and Src [105]. In particular, the phosphorylation of the adaptor protein paxillin by FAK and Src is essential for the disassembly of focal adhesions at the trailing edge of the migrating cell, allowing for net forward movement [88].

In PC, the EMT program is closely linked to the activation of oncogenic signaling pathways, particularly K-Ras and TGF-β. Oncogenic K-Ras drives invasion through the Raf/MEK/ERK and PI3K/AKT pathways, which modulate cytoskeletal dynamics and stabilize EMT-inducing transcription factors. Moreover, TGF-β signaling plays a pivotal role in promoting invasion by activating Smad-dependent and Smad-independent pathways (such as p38 MAPK and JNK), which cooperate to upregulate the expression of Snail and ZEB family transcription factors [108]. While classical EMT involves a complete phenotypic switch, recent evidence suggests that PC cells often exist in intermediate states of epithelial-mesenchymal plasticity (EMP) or "partial EMT", expressing both epithelial and mesenchymal markers simultaneously. These hybrid phenotypes are associated with the highest tumorigenic potential and chemoresistance, allowing cells to migrate collectively as cohesive clusters rather than solely as individual mesenchymal cells [105, 109].

2.7. Interplay Between Apoptosis, Autophagy, Senescence, and Migration

The therapeutic response of PC is regulated by a dynamic and integrated decision-making network in which the balance between apoptosis, autophagy, and cellular senescence determines whether the tumor is eliminated or remains in a resistant, potentially metastatic state. The p21 protein acts as a key molecular switch in this network, as its nuclear accumulation is primarily required for cell cycle arrest and the maintenance of senescence. In comparison, its cytoplasmic localization or proteolytic cleavage by caspases can promote

apoptosis or paradoxically induce cell proliferation [84]. Although TIS initially acts as a tumor-suppressive mechanism by halting proliferation via the p53-p21 and p16-Rb pathways, senescent PC cells frequently acquire resistance to apoptosis by upregulating anti-apoptotic Bcl-2 family proteins, such as Bcl-xL, requiring the subsequent use of senolytic agents to trigger apoptosis [110]. Autophagy serves as a critical metabolic support system for these senescent cells, providing the recycled bioenergetic intermediates and amino acids necessary to meet the high metabolic demands of the SASP [111]. SASP creates a pro-tumorigenic microenvironment that can paradoxically stimulate EMT and migration in neighboring non-senescent cancer cells, thereby facilitating metastasis [87].

Furthermore, autophagy plays a complex, multifaceted role in regulating cell migration and invasion. Although it supports the dynamic turnover of focal adhesions by degrading paxillin to enable cell motility, autophagy inhibition in *RAS*-mutated cells can lead to the accumulation of the cargo receptor p62/SQSTM1 and subsequent NF-κB activation, which surprisingly drives EMT and invasion [88]. Inhibition of the K-Ras/ERK signaling axis has been shown to result in a compensatory increase in autophagic flux, making cells highly dependent on lysosomal degradation for survival [112]. Consequently, a "one-two punch" therapeutic strategy is proposed, in which senescence is first induced by chemotherapeutic agents or pathway inhibitors, followed by the blockade of autophagy or Bcl-2 family proteins to deprive senescent cells of metabolic support and survival signals, forcing them into apoptosis [110]. The goal of targeting the interactions between these pathways is to shift the cellular response from cytoprotective autophagy and stable aging toward irreversible apoptosis, while simultaneously weakening the invasion drive induced by SASP [107].

3. Acridine Derivatives as Anticancer Agents

3.1. Overview of Acridines and Bisacridines

Investigation of acridine derivatives as potential chemotherapeutic agents has a rich history, deeply rooted in the need to develop compounds that can interact with DNA to disrupt the proliferation of cancer cells. This research direction has been particularly prominent at the Gdańsk University of Technology, where decades of synthetic and biological studies have led to the development of several generations of agents with anticancer properties. The fundamental success in this field was the synthesis and subsequent introduction into medicine of nitracrine, known as 1-nitro-9-(3',3'-dimethylaminopropylamino)acridine. Registered in Poland in 1970 under the trade name Ledakrin (code C-283), this compound emerged as a potent antitumor agent with significant clinical efficacy against ovarian, breast, and colon carcinomas [113, 114]. The biological activity of Ledakrin is inextricably linked to its metabolic bioactivation. Studies have shown that the presence of the nitro group at position 1 of the acridine ring is critical for its cytotoxicity. Biological reduction of this group yields highly reactive hydroxylamine intermediates [113]. These metabolic products facilitate the formation of covalent interstrand cross-links in DNA, effectively blocking DNA replication and transcription and ultimately leading to cell death [114]. Despite its high efficacy, the clinical application of Ledakrin was severely limited by its substantial toxicity and adverse side effects, including mutagenicity, prompting the search for new derivatives with improved therapeutic indices [113].

Subsequent efforts to mitigate the systemic toxicity of nitroacridines resulted in the synthesis of compounds such as C-1748 (4-methyl-1-nitroacridine). This derivative demonstrated a more favorable toxicity profile in preclinical studies while maintaining high activity against prostate and colon cancers. Additionally, C-1748 exhibited a distinct metabolic profile compared to Ledakrin, particularly in terms of resistance to metabolic degradation in certain cell lines, such as HepG2 liver cancer cells [115, 116]. Parallel to the development of nitroacridines, another class of compounds, the imidazoacridinones, was developed, structurally designed to mimic the chromophore of anthracenediones, such as mitoxantrone, but with a modified mode of action [113]. The most advanced compound from this group, C-1311 (Symadex), has entered phase II clinical trials. Unlike nitroacridine, which forms DNA cross-links, C-1311 primarily acts as a DNA intercalator and topoisomerase II inhibitor, stabilizing the cleavable complex and preventing DNA degradation [117]. A key pharmacological distinction of C-1311 is its metabolic pathway. It is primarily activated by flavin monooxygenases (FMOs) rather than cytochrome P450 isoenzymes (CYP), which contributes to its lower cardiotoxicity compared to anthracyclines and its unique sensitivity profile [118].

The evolution of acridine-based compounds accelerated significantly with the conception and synthesis of bisacridines. The rationale for this design was to create dimeric molecules capable of bis-intercalation, thereby significantly increasing DNA binding affinity and potentially overcoming mechanisms of drug resistance associated with monomeric agents. Initial studies focused on symmetrical bisacridines, but the most promising breakthrough came with the

development of unsymmetrical bisacridines (UAs). These novel compounds are hybrid dimers composed of two distinct monomeric units: an imidazoacridinone ring (analogous to C-1311, Symadex) and a 1-nitroacridine ring (analogous to Ledakrin or C-1748), linked by a flexible polyamine chain [119–122]. The synthesis of these compounds, including the main subjects of this dissertation: C-2028 (9'-{N-[(imidazo[4,5,1-de]-acridin-6-on-5-yl)aminopropyl]-Nmethyl-aminopropylami-no}-1'-nitroacridine×1.5HCl), C-2045 (9'-{N-[(8-hydroxyimidazo[4,5,1-de]-acridin -6-on-5-yl)-aminopro-pyl]-Nmethylaminopropylamino}-4'-methyl-1'-nitroacridine×3HCl), and C-2053 (9'-{N-[(imidazo-[4,5,1-de]-acridin-6-on-5-yl)aminopropyl]-Nmethylaminopropylamino}-4'-methyl-1'-nitroacridine ×3HCl), was achieved in a multi-step process involving the condensation of 9-phenoxy derivatives of acridines with appropriate polyamines [123]. The general chemical scaffold and the specific substituents of the unsymmetrical bisacridines C-2028, C-2045, and C-2053 are presented in **Figure 3.1**. The design strategy aimed to synergize the different mechanisms of action of the parent monomers, intercalation, and topoisomerase inhibition of imidazoacridinones with the bioreductive alkylation potential of nitroacridines, to create agents with high cytotoxicity against solid tumors that are typically refractory to standard chemotherapy, such as pancreatic cancer [123]. The structural diversity among these UAs, such as the presence of a methyl group in the nitroacridine moiety of C-2045 and C-2053, or a hydroxyl group in the imidazoacridinone moiety of C-2045, significantly impacts their physicochemical properties, metabolic stability, and biological activity [123, 124].

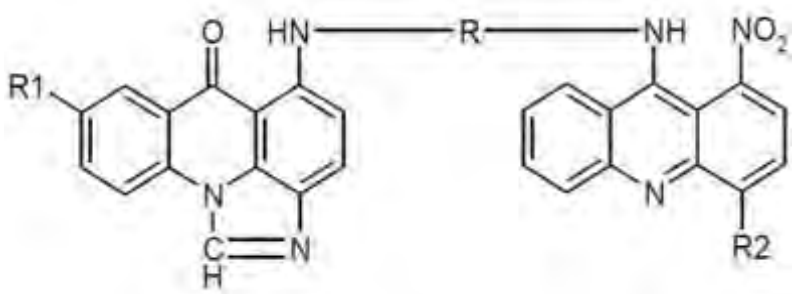

Compound	R	R1	R2
C-2028	-$(CH_2)_3$-N(CH_3)-$(CH_2)_3$-	-H	-H
C-2045	-$(CH_2)_3$-N(CH_3)-$(CH_2)_3$-	-OH	-CH_3
C-2053	-$(CH_2)_3$-N(CH_3)-$(CH_2)_3$-	-H	-CH_3

Figure 3.1. The chemical structures of unsymmetrical bisacridines, based on [123].

3.2. Mechanisms of Action of Unsymmetrical Bisacridines (UAs)

The biological activity of unsymmetrical bisacridines, such as the derivatives C-2028, C-2045, and C-2053, is characterized by a complex mechanism that is fundamentally distinct from that of their monomeric components. While the parent monomers, such as the imidazoacridinone C-1311 and the 1-nitroacridine C-1748, act primarily as potent intercalators of double-stranded DNA (dsDNA), advanced structural investigations using NMR spectroscopy and molecular dynamics (MD) simulations have revealed that UAs do not interact with dsDNA via classical

bis-intercalation [125]. Instead, these dimers exhibit a unique and selective ability to bind to and stabilize G-quadruplex (G4) structures [123, 126].

G-quadruplexes are non-canonical secondary nucleic acid structures formed in guanine-rich regions through the self-association of four guanine residues. Hoogsteen hydrogen bonds hold these residues together to form a planar layer known as a G-tetrad, and the stacking of multiple tetrads creates the G4 core, which is further stabilized by monovalent cations, primarily K^+ and Na^+. G4 structures are strategically located throughout the human genome, particularly in telomeres and the promoter regions of key oncogenes, including *MYC*, *KRAS*, *VEGF*, *BCL-2*, and *c-KIT*. These structures serve as natural regulators of gene expression, often functioning as molecular "switches" for transcription [127]. In the case of the *c-MYC* oncogene, the nuclease hypersensitivity element III1 (NHE III1), also known as Pu27 (or its shorter variant Pu22), controls approximately 80% to 90% of the gene's transcriptional activity, making it an exceptionally attractive target for targeted cancer therapies. The physical stabilization of a G4 structure in such a promoter region can sterically block the transcriptional machinery, including RNA polymerase, or recruit repressor proteins, thereby silencing oncogene expression [126–128].

Unsymmetrical bisacridines demonstrate a high affinity for the G4 structures of the *c-MYC* and *KRAS* promoters, as evidenced by a significant increase in their melting temperatures (ΔT_m values typically ranging from 17.7 to 37.5 °C). Crucially, UAs exhibit only marginal effects on the thermal stability of classical dsDNA, confirming their high selectivity for G4 motifs [123]. Detailed NMR studies have shown that derivatives like C-2045 and C-2053 form well-defined non-covalent adducts with the *c-MYC* G4 (Pu22) with a 1:2 stoichiometry. The binding primarily involves the imidazoacridinone chromophore stacking onto the external G-tetrads, while the aminoalkyl linker and the 1-nitroacridine moiety function as an extended "sidechain" that interacts with the loops and flanking sequences of the quadruplex. Furthermore, UAs possess the ability to induce G4 folding even in the absence of stabilizing potassium ions, underscoring their effectiveness as G4-specific ligands. This selectivity over dsDNA gives UAs a significant therapeutic advantage, potentially minimizing non-specific DNA damage in healthy cells [123, 126].

Metabolic transformation is another pillar of UAs' biological activity. Electrochemical simulations coupled with mass spectrometry (EC-MS) and enzymatic studies have clarified the metabolic pathways of these compounds. A crucial step in the bioactivation of UAs is the reductive metabolism of the nitro group located on the 1-nitroacridine moiety, a pathway shared with the monomeric precursor Ledakrin [124, 129]. This reduction process, mediated by cytochrome P450 enzymes (particularly CYP3A4) and potentially by other reductases, leads to the formation of reactive intermediates, including nitro radical anions, nitroso derivatives, and hydroxylamines. These electrophilic species can covalently bind cellular macromolecules, including DNA and proteins, contributing to the irreversible cytotoxic effects of these compounds. Electrochemical studies have also identified specific oxidation products, including N-oxide derivatives and quinone-imine type structures, particularly for the imidazoacridinone part of the molecule [129]. Importantly, UAs retain their dimeric structure during initial metabolic transformations, preserving their unique DNA-binding capabilities while gaining alkylating potential [124].

Furthermore, phase II metabolism plays a significant role in the disposition of these compounds. Studies proved that C-2045, which has a hydroxyl group, is a substrate for UDP-glucuronosyltransferases (UGTs), specifically UGT1A1, UGT1A9, and UGT1A10. Glucuronidation of C-2045 occurs within tumor cells and may affect the intracellular retention and cytotoxicity [124, 130]. Additionally, it has been shown that C-2028 undergoes conjugation with glutathione (GSH), catalyzed by glutathione S-transferases (GSTs) or occurring non-enzymatically. Although GSH conjugation is typically a detoxification mechanism, the formation of such adducts confirms the generation of reactive electrophilic intermediates during UAs metabolism, which are essential for their biological activity [131].

The cellular response to UAs is multifaceted and context-dependent. In human colon cancer cells (HCT116) and lung cancer cells (H460), treatment with C-2028, C-2045, and C-2053 triggers a sequence of events leading to cell death or growth arrest. A prominent response is the induction of apoptosis, characterized by phosphatidylserine externalization, caspase-3 activation, and chromatin condensation [123, 128]. However, the response profile varies significantly between cell lines. In H460 lung cancer cells, UAs induce substantial accelerated senescence in addition to apoptosis [128, 132]. Interestingly, the induction of senescence in H460 cells was found to be strictly dependent on the complete inhibition of c-Myc protein levels. In cells where c-Myc was only partially inhibited, apoptosis was the dominant pathway. In contrast, HCT116 cells primarily undergo apoptosis upon UAs treatment. This dichotomy suggests that UAs may determine cell fate by modulating specific oncogenic pathways, particularly the c-Myc signaling axis [128].

3.3. Selectivity and Cytotoxicity Toward Cancer vs. Normal Cells

The therapeutic potential of unsymmetrical bisacridines is underscored by their potent cytotoxicity against a broad spectrum of human cancer cell lines and their remarkable selectivity. *In vitro* cytotoxicity assays have demonstrated that C-2028, C-2041, C-2045, and C-2053 exhibit IC_{50} values in the low micromolar range against panels of pancreatic (Panc-1, MIA PaCa-2), colon (HCT116, HT-29), lung (H460, A549), and prostate (DU-145) cancer cell lines [123, 132]. The structural features of UAs, such as linker length and specific substituents, finely tune this activity. Crucially, UA's high potency against cancer cells is accompanied by a significant selectivity window. Comparative studies using normal human lung fibroblasts (MRC-5) and normal colon epithelial cells (CCD 841 CoN) have shown that these nonmalignant cells are far less sensitive to UAs. At concentrations that induce massive apoptosis and complete growth inhibition in cancer cells, normal cells remain viable and exhibit minimal signs of DNA damage or cell cycle dysfunction [128]. This selectivity is a critical attribute for potential clinical candidates, promising a wider therapeutic index and reduced systemic side effects.

The anticancer efficacy of UAs has been further validated in more physiologically relevant models. In multicellular tumor spheroids (MCTS), which mimic the three-dimensional architecture and microenvironment of solid tumors, UAs maintained their potent activity. Studies on HCT116 and A549 spheroids revealed that C-2045 and C-2053 were active within spheroid structure,

inhibited their growth, and reduced cell viability, in contrast to many standard drugs that lose potency in 3D models due to poor penetration or quiescent cell populations [132, 133]. The *in vivo* therapeutic potential of UAs was confirmed using human tumor xenografts in nude mice. Compounds such as C-2028 and C-2045 induced significant tumor growth inhibition (TGI) in models of pancreatic (Panc-1), colorectal (HCT116), and lung (H460) cancers. In some cases, complete tumor regression was observed, highlighting the translational potential of these agents [123].

A main challenge in cancer chemotherapy is the development of multidrug resistance (MDR), often caused by the overexpression of ATP-binding cassette (ABC) transporters that efflux drugs from cells. Studies on the interaction of UAs with these transporters have yielded promising results. Although UAs are substrates for the MDR1 transporter (P-glycoprotein/ ABCB1), they do not induce upregulation of *ABCB1*, *ABCC1*, or *ABCG2* genes, nor do they increase these protein levels in treated cancer cells [130]. This lack of induction suggests that UAs are less likely to promote acquired resistance during treatment. Moreover, the metabolic stability of UAs in the presence of ABC transporters ensures that lethal intracellular concentrations can be maintained [134]. To further enhance the delivery and selectivity of these compounds, recent nanotechnology approaches have been employed. It has been shown that conjugating UAs to quaternary quantum dots (QDs) via non-covalent interactions modulates their cellular uptake and biological responses. These QD-UA nanoconjugates demonstrated improved endocytosis into cancer cells, enhanced cytotoxicity against lung and colon cancer cells, and protection of normal cells [135–137]. The QD-UA also influenced the balance between apoptosis and senescence, further proving that the method of administration can precisely tailor the therapeutic outcome [135]. Collectively, the data position unsymmetrical bisacridines as a potent, selective, and mechanistically distinct class of antitumor agents with significant promise for the treatment of refractory solid tumors.

4. Advanced Cell Culture Models in Cancer Research

The profound complexity of neoplastic diseases continues to challenge the development of effective treatments. Despite decades of substantial investment in pharmaceutical research, the percentage of potential oncology drugs that fail to pass clinical trials remains disproportionately high, with approximately 90% of new antineoplastic agents never receiving regulatory approval [138, 139]. This discrepancy between preclinical success and clinical failure is largely attributed to the inadequacies of conventional experimental models used to predict human responses to treatment. In the specific context of PC, which is characterized by a dense desmoplastic stroma and a hypovascular microenvironment, the inability of traditional models to recapitulate the pathophysiological barriers to drug delivery has been a major obstacle [140]. As a result, a paradigm shift has occurred in cancer biology toward the development of advanced cell culture models that transcend the limitations of existing methodologies. The evolution from monolayer cultures to complex three-dimensional (3D) configurations represents a fundamental stride toward mimicking the *in vivo* tumor microenvironment, thereby enhancing the predictive accuracy of preclinical drug screening [141].

4.1. Limitations of 2D Cell Culture Models

Since the pioneering work of Ross Harrison in the early 20th century, two-dimensional (2D) cell culture has served as the cornerstone of biomedical research, facilitating the fundamental understanding of cellular biology and the initial screening of chemotherapeutic agents [142]. These models, typically involving cells grown as monolayers on a rigid polystyrene or glass surface, offer clear advantages in terms of reproducibility, cost-efficiency, and ease of manipulation. However, it is increasingly recognized that 2D cultures oversimplify biological reality and cannot capture the complex architecture and functioning of solid tumors [142].

The primary limitation of 2D models lies in the artificial geometric constraints imposed on the cells. In a monolayer, cells are forced into a flattened morphology with apical-basal polarity that does not exist in the environment of a tumor mass. This alteration in cell shape leads to significant cytoskeletal rearrangements, which in turn affect intracellular signaling pathways and nuclear mechanics. Additionally, cells in 2D culture are exposed to a uniform, hyper-oxygenated, and nutrient-rich environment that contrasts with the physiological gradients found *in vivo* [141, 143, 144]. In the context of PC, which is notoriously hypoxic and nutrient-deprived, unlimited access to substrates in 2D cultures leads to artificially high proliferation rates, and metabolic profiles reflect neither the Warburg effect nor the metabolic adaptation of cells within a tumor [145].

Moreover, the lack of an extracellular matrix and limited cell-cell interactions in 2D cultures fundamentally alter gene expression and cellular phenotype. Studies have demonstrated that shifting cells from 2D to 3D environments results in profound transcriptional reprogramming [146]. For instance, PC cell lines such as Panc-1 and MIA PaCa-2 exhibit differential expression of epithelial-mesenchymal transition markers when cultured in monolayers compared to 3D

conditions, with 2D cultures often failing to maintain the expression of key structural proteins like E-cadherin or overexpressing mesenchymal markers in a non-physiological manner [147, 148]. Crucially, the 2D environment lacks the physical barriers to drug penetration that characterize solid tumors. In a monolayer, the entire cell surface is accessible to therapeutic agents, leading to an overestimation of compound cytotoxicity and a high rate of false-positive [149]. This lack of predictive accuracy is further exacerbated by the absence of stromal components, such as PSCs, which are integral to the chemoresistance mechanisms observed in patients [150]. Consequently, while 2D models remain useful for basic biochemical assays, they are increasingly viewed as insufficient for translating biological findings into clinical efficacy for complex malignancies like PC. The comparative hierarchy of cancer models, illustrating the trade-off between experimental throughput and physiological relevance, is shown in **Figure 4.1**.

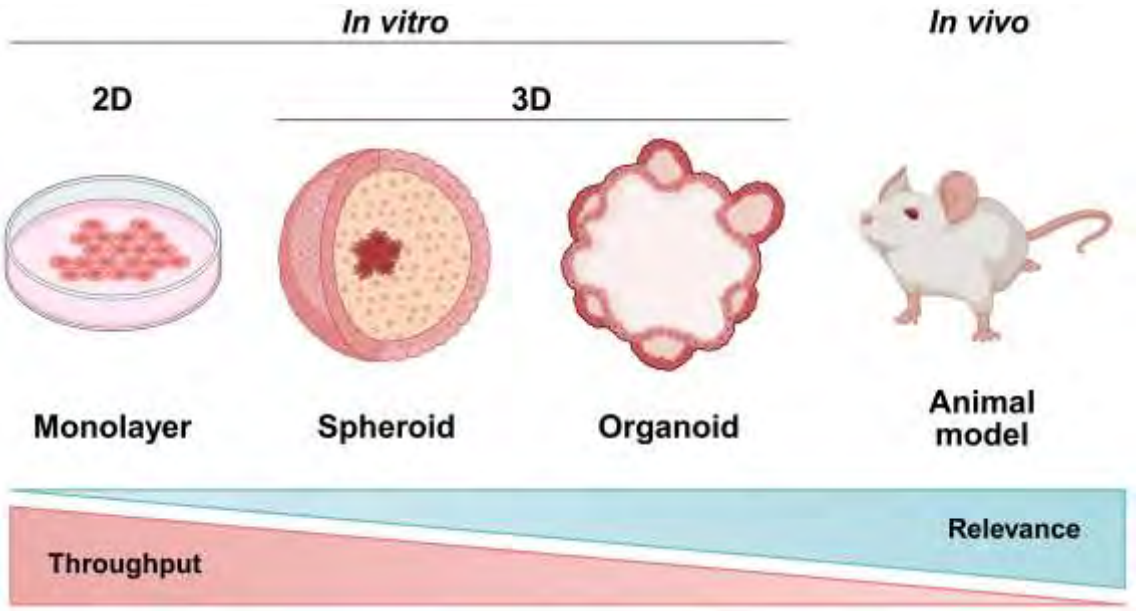

Figure 4.1. Evolution of preclinical cancer models: from 2D to 3D and *in vivo*, based on [151].

4.2. 3D Cell Culture Systems: Spheroids, Organoids, and Scaffold-Based Models

To bridge the gap between *in vitro* simplicity and *in vivo* complexity, three-dimensional cell culture models have been developed to restore the spatial arrangement and microenvironmental cues necessary for authentic tumor biology. These systems can be broadly categorized into scaffold-free models, such as MCTS and organoids, and scaffold-based models that utilize synthetic or natural matrices to support cell growth [139].

4.2.1. Multicellular Tumor Spheroids (MCTS)

Spheroids are among the best-characterized and widely used 3D models in cancer research. Defined as self-assembling cellular aggregates, spheroids form when cell-cell adhesive interactions dominate over cell-surface interactions [149]. This can be achieved through various techniques, including round-bottom wells, the liquid overlay technique (using non-adhesive surfaces such as poly-HEMA or agarose), the hanging drop method, and agitation-based systems

such as spinner flasks [139]. In pancreatic cancer, cell lines such as Panc-1, MIA PaCa-2, AsPC-1, and BxPC-3 have been successfully cultured as spheroids, revealing distinct morphological phenotypes ranging from tight, compact aggregates to loose, irregular clusters, depending on their differentiation status and E-cadherin expression levels [145, 152].

The advantage of spheroid architecture is its ability to recapitulate the physicochemical gradients of avascular tumor nodules or micrometastases [146]. Spheroids with a diameter of about 500 μm typically develop into a layered structure comprising an outer proliferating layer, a middle quiescent zone, and an inner necrotic core [141, 153]. This zonal heterogeneity mimics the pathophysiology of solid tumors, in which oxygen and nutrient diffusion are limited by tissue mass, leading to the formation of hypoxic regions that drive malignant progression and drug resistance [154]. In PC research, modifications to standard spheroid protocols, such as the addition of methylcellulose or the use of concave microwells, have been introduced to improve spheroid homogeneity and compactness, facilitating their use in high-throughput screening applications [155, 156]. The internal architecture of a mature spheroid, characterized by distinct metabolic zones and nutrient gradients, is represented in **Figure 4.2**.

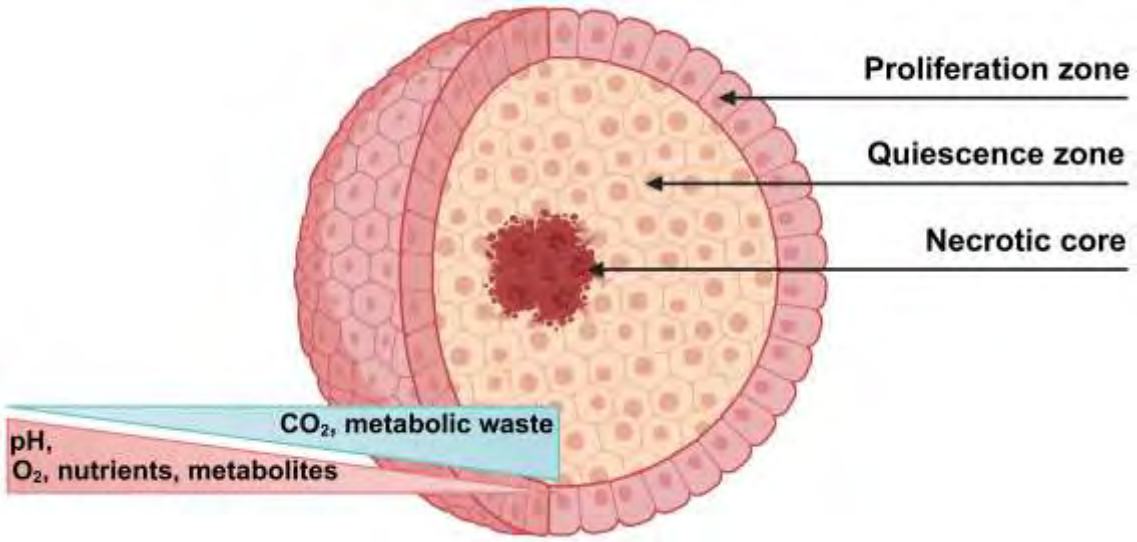

Figure 4.2. Internal architecture and pathophysiological gradients of multicellular tumor spheroids (MCTS), based on [141].

4.2.2. Organoids

Organoids represent a more advanced and biologically complex model system compared to spheroids. Organoids are self-organizing 3D structures derived from stem cells (embryonic, induced pluripotent, or adult tissue stem cells) or primary tumor explants that reproduce the histological architecture and genetic diversity of the original organ [157]. Unlike spheroids, which are typically generated from established immortalized cell lines, organoids are frequently derived directly from patient tissues (patient-derived organoids, PDOs) or patient-derived xenografts (PDX), thus preserving the specific mutation profiles and intratumoral heterogeneity of the donor [157, 158].

The seminal work by the Tuveson and Clevers laboratories has established robust protocols for culturing pancreatic organoids using Matrigel matrices supplemented with specific growth factors (e.g., Wnt, R-spondin, and Noggin) that maintain the stem cell niche. These models have proven superior to cell lines in preserving the differentiation status and molecular signatures of the primary tumor, including the conservation of basal-like or classical transcriptional subtypes [159]. In addition, organoids enable the expansion of both neoplastic and normal ductal epithelial cells, providing a unique platform for comparative studies of carcinogenesis and the identification of patient-specific therapeutic vulnerabilities [157, 159].

4.2.3. Scaffold-Based Models

Scaffold-based 3D cultures utilize exogenous materials to mimic the physical and biochemical properties of the ECM, providing a structural framework for cell attachment, proliferation, and organization [160]. These scaffolds can be engineered from natural polymers (e.g., collagen, gelatin, hyaluronic acid, chitosan) or synthetic polymers (e.g., polycaprolactone, poly(lactic-co-glycolic) acid (PLGA), polyhydroxybutyrate) [160, 161]. In PC research, scaffold-based models are particularly relevant given the intense desmoplastic reaction characterized by excessive deposition of collagen I, fibronectin, and hyaluronic acid [140, 162].

Hydrogels, such as type I collagen or Matrigel, are frequently used to embed PC cells, simulating the stiffness and porosity of fibrotic tumor stroma. These matrices not only provide mechanical support but also engage integrin signaling pathways that regulate cell survival and invasion [154, 163]. Recent advancements include the development of synthetic scaffolds produced via electrospinning or solvent casting with particle leaching techniques, which offer adjustable pore size and topography for controlled study of tumor cell infiltration and migration [164]. Hybrid models incorporating microfluidic devices have also emerged, enabling precise control of nutrient flow and the establishment of vascularized tumor models for the study of dynamic drug transport and immune cell infiltration [140, 165, 166].

4.3. Relevance of 3D Models in Studying Cellular Response

The transition from 2D to 3D culture systems entails fundamental shifts in cellular physiology, underscoring the importance of 3D models for understanding cancer progression mechanisms. The relevance of these models is multifaceted, encompassing changes in gene expression, metabolic adaptation, and the recreation of the TME.

4.3.1. Gene Expression and Phenotypic Plasticity

Cells cultured in 3D environments exhibit gene expression profiles that differ significantly from their 2D counterparts and more closely resemble clinical expression signatures. In PC, it has been shown that the 3D configuration enhances the expression of markers of stem cell properties, such as CD44, CD24, and CD133, as well as transcription factors, including c-Myc, ALDH1, Oct4, Nanog, and Sox2 [167]. This enrichment of cancer stem cell (CSC) populations in spheroids is critical, as CSCs are associated with tumor initiation, metastasis, and recurrence [168]. Research

comparing PC cell lines in 2D and 3D has shown that although cells may appear morphologically similar in monolayers, 3D culture unmasks distinct epithelial or mesenchymal phenotypes. For instance, mesenchymal-type PC cells form loose, invasive aggregates with high vimentin expression in 3D. In contrast, epithelial-type cells form compact spheres with high E-cadherin expression, a distinction often lost in 2D culture [147, 152].

4.3.2. Metabolic Adaptation and Hypoxia

The three-dimensional microenvironment significantly impacts the metabolic reprogramming of cancer cells, a characteristic of malignant tumors. Large spheroids naturally develop gradients of oxygen and nutrients, resulting in a hypoxic core that stabilizes HIF−1α [145]. HIF−1α coordinates the expression of genes involved in anaerobic glycolysis (the Warburg effect), angiogenesis (e.g., VEGF), and drug efflux (e.g., P-glycoprotein), thereby driving a more aggressive and resistant phenotype. Studies on Panc-1 spheroids have confirmed a metabolic shift towards glycolysis, evidenced by increased lactate production and upregulation of glucose transporters (GLUT-1) and lactate dehydrogenase (LDH), mimicking the metabolic state of *in vivo* tumors [145, 159, 169]. This metabolic heterogeneity is absent in 2D cultures, where cells are uniformly exposed to high oxygen levels, making monolayer models unsuitable for studying hypoxia-targeted therapies.

4.3.3. Tumor-Stroma Interactions

A defining feature of PC is the dense, fibrotic stroma, or desmoplasia, which accounts for up to 90% of the tumor volume [140]. The 3D model provides a platform for integrating stromal elements such as PSCs, macrophages, and fibroblasts to study heterotypic cell interactions [140, 160]. Co-cultured spheroids containing PC cells and PSCs have shown that stromal cells secrete ECM proteins (collagen, fibronectin) and cytokines (IL-6, TGF-β), which promote tumor growth and invasiveness. In particular, the interaction between cancer cells and PSCs in 3D matrices triggers PSC activation into a myofibroblast-like phenotype, leading to matrix contraction and increased stiffness, which, in turn, activates signaling pathways involved in tumor progression [162]. These complex interactions, which are critical for maintaining PC's immunosuppressive and chemoresistant properties, cannot be replicated in 2D monocultures.

4.4. Application of 3D Models in Drug Screening and Mechanistic Studies

The ultimate value of advanced cell culture models lies in their application to drug discovery and in elucidating mechanisms of treatment resistance. 3D models have emerged as superior tools for identifying efficacious compounds and filtering out false positives that would otherwise fail in clinical trials.

4.4.1. Mechanisms of Drug Resistance

3D models exhibit multicellular resistance (MCR), a phenomenon in which cells in 3D configurations exhibit significantly reduced sensitivity to chemotherapeutics compared to

monolayer cultures [170]. There are several reasons for this resistance. Firstly, the dense ECM and tight cell-cell junctions in spheroids create a physical barrier that limits the penetration of large molecules and chemotherapeutic agents. Studies have shown that gemcitabine is significantly less effective in 3D spheroids due to limited diffusion and the quiescence of cells in the spheroid interior, as gemcitabine primarily acts on actively dividing cells [150, 154].

Secondly, the hypoxic microenvironment within spheroids upregulates drug efflux pumps and survival signaling pathways (e.g., PI3K/Akt, MAPK), thereby conferring intrinsic resistance [171]. For example, the upregulation of multidrug resistance genes such as *ABCC1* and *ABCG2* has been observed in Panc-1 spheroids, contributing to their refractory nature [152]. Furthermore, cell adhesion-mediated drug resistance (CAM-DR), caused by interactions between integrins and the ECM, is potent in 3D scaffold-based models but negligible in 2D cultures [145]. Recent data also suggest that stromal cells in 3D co-cultures further enhance resistance. For instance, PSCs have been shown to protect PC cells from gemcitabine-induced apoptosis through the secretion of soluble factors and the physical barrier of the collagen matrix [150, 166].

4.4.2. High-Throughput Screening (HTS) and Personalized Medicine

Although historically limited by lower throughput and higher costs, 3D models are increasingly being adapted for high-throughput screening to accelerate drug discovery. Automated platforms utilizing ultra-low attachment microplates, hanging drop arrays, and magnetic levitation have enabled the reproducible generation of uniform spheroids for large-scale library screening [151, 172]. These platforms enable multiplexed analysis of cell viability, invasion, and morphology, providing high-content data that better predict *in vivo* efficacy than simpler 2D assays.

In the era of precision medicine, PDOs serve as "avatars" for predicting individual patient responses to therapy. By establishing organoids from biopsy samples, researchers can screen panels of chemotherapeutics to identify the most effective treatment for a specific patient, correlating *in vitro* sensitivity with clinical outcomes [159]. This approach has shown promise in identifying responders to specific treatments, such as oxaliplatin or targeted therapies, thereby reducing the trial-and-error approach in clinical practice [173]. Moreover, microfluidic "tumor-on-a-chip" systems facilitate the study of complex mechanistic processes, such as immune cell infiltration and metastasis, by perfusing 3D tumor cultures with immune cells and observing their migration and cytotoxic activity in real time [165, 174].

In conclusion, the shift from 2D to 3D cell culture models represents a critical advance in cancer research. By accurately recreating the architectural, metabolic, and microenvironmental features of human tumors, 3D models such as spheroids provide a more rigorous, physiologically relevant platform for investigating pancreatic cancer biology. These models not only elucidate the mechanisms of chemoresistance but also offer transformative potential for developing novel, effective therapeutics, ultimately bridging the gap between preclinical experiments and clinical reality.

RESEARCH OBJECTIVES

The primary aim of this doctoral research was to provide a comprehensive characterization of the biological activity and cellular mechanisms of action of three novel unsymmetrical bisacridine derivatives (C-2028, C-2045, and C-2053) against human pancreatic cancer cells (Panc-1, MIA PaCa-2, AsPC-1, and BxPC-3). The research aimed to elucidate how these compounds modulate key oncogenic drivers and cell death pathways to overcome the inherent resistance and high metastatic potential of pancreatic cancer.

To achieve the central aim of the dissertation, the following specific research objectives were established:

1. **To characterize the fundamental activity and molecular targets of UAs in 2D cell cultures**
    - Determination of the cytotoxic potential of UAs across a panel of pancreatic cancer cell lines with diverse genetic profiles (Panc-1, MIA PaCa-2, AsPC-1, and BxPC-3) compared to normal pancreatic epithelial cells (hTERT-HPNE).
    - Evaluation of the impact of UAs on proliferation, cell cycle distribution, apoptosis induction, and senescence of pancreatic cancer cells.
    - Identification of the molecular targets of UAs involved in the induced cellular response, with particular emphasis on the c-Myc oncoprotein expression and the modulation of regulatory proteins such as p16, p21, p53, and SMAD4.
2. **To validate the therapeutic efficacy of UAs in more physiologically relevant 3D spheroids**
    - Establishment and optimization of three-dimensional multicellular tumor spheroids (MCTS) from PC cell lines to better replicate the tumor microenvironment.
    - Evaluation of the pro-apoptotic efficacy of UA derivatives in 3D tumor spheroids.
    - Comparison of the UA-induced cellular responses between traditional 2D monolayers and 3D MCTS models.
3. **To investigate the role of autophagy and its impact on apoptosis and the migration potential of PC cells exposed to UAs**
    - Assessment of the impact of UAs on autophagic flux by detecting acidic vesicular organelles (AVOs) and examining the levels of autophagy markers such as LC3-I, LC3-II, p62, and Beclin1 proteins.
    - Elucidation of the crosstalk between autophagy and apoptosis, by employment of autophagy inhibitors (wortmannin, chloroquine, and ammonium chloride) and analyzing AVOs level and apoptosis induction.
    - Examination of the anti-migratory properties of UAs and the role of autophagy in mediating these effects, along with the modulation of epithelial-mesenchymal transition markers.

MATERIALS AND METHODS

1. Tested Compounds

The primary research subjects were three novel unsymmetrical bisacridine derivatives: C-2028, C-2045, and C-2053, synthesized as hydrochlorides at the Department of Pharmaceutical Technology and Biochemistry, Gdańsk University of Technology. Stock solutions (10 mM) were prepared in sterile deionized Milli-Q water (Merck/Millipore, Burlington, MA, USA) and stored at –20°C. Clinical reference drugs, gemcitabine (GEM) and irinotecan (IR), were purchased from Merck/Sigma-Aldrich (St. Louis, MO, USA) and dissolved in sterile water or dimethyl sulfoxide (DMSO; POCH S.A., Gliwice, Poland), respectively. Sterile water was used to prepare working solutions (IC_{50} and IC_{80}).

2. Cell Lines and Two-Dimensional (2D) Culture Conditions

The study utilized a panel of human pancreatic cancer cell lines with diverse genetic profiles: Panc-1, MIA PaCa-2, AsPC-1, and BxPC-3 (ATCC, Manassas, VA, USA). The hTERT-HPNE cell line (ATCC, Manassas, VA, USA) served as a normal pancreatic epithelial cell control. PC cells were maintained in either high-glucose Dulbecco's Modified Eagle's Medium (DMEM HG; for Panc-1 and MIA PaCa-2) or RPMI 1640 medium (for AsPC-1 and BxPC-3), supplemented with 10% heat-inactivated fetal bovine serum (FBS) and antibiotics (100 *μ*g/mL streptomycin, 100 units/mL penicillin). hTERT-HPNE cells were maintained in 75% Dulbecco's modified Eagle's medium without glucose (DMEM), 25% Essential 8™ Basal Medium supplemented with heat-inactivated 5% fetal bovine serum, 10ng/mL hEGF, 1 g/L D-glucose, and 1% Penicillin- Streptomycin. Cells were cultured at 37°C in a humidified atmosphere containing 5% CO_2.

3. Three-Dimensional (3D) Spheroid Culture

Multicellular tumor spheroids (MCTS) were generated from Panc-1, MIA PaCa-2, AsPC-1, and BxPC-3 cells using ultra-low attachment (ULA) plates. Following seeding density optimization, spheroids with a diameter of approximately 450 μm on day 3 after seeding were selected using light microscopy (Olympus IX83; Olympus, Tokyo, Japan).

4. Spheroid Size and Morphology Assessment

In generated spheroids after initial imaging (day 0), the culture medium was replaced with either fresh medium (control) or medium containing IC_{80} concentrations of UAs or IC_{50} of the reference compounds. Images (Olympus IX83; Olympus, Tokyo, Japan) of at least 8 spheroids per condition were taken every 2–3 days for up to 14 days, and their diameters were measured using CellSens Dimension software version 1.18 (Olympus, Tokyo, Japan).

5. Cytotoxicity Assays

5.1. 2D MTT Assay

Cytotoxicity was determined by exposing cell monolayers to UAs for 24, 72, or 120 h, followed by quantification of formazan absorbance at 540 nm using an iMark Microplate Absorbance Reader (Bio-Rad, Hercules, CA, USA).

5.2. 3D CellTiter-Glo® Assay

Cell viability in spheroids after compound exposure was evaluated using the CellTiter-Glo® 3D Cell Viability Assay (Promega, Madison, WI, USA), according to the manufacturer's protocol. After spheroids were exposed to UAs and reference compounds for 72 h, the CellTiter-Glo® 3D reagent was added, and after cell lysis and signal stabilization, the luminescence was measured in a Varioskan LUX Multimode Microplate Reader (Thermo Scientific, Waltham, MA, USA).

6. Flow Cytometry Analyses

Quantitative assessment of the cellular response was performed using a FACS Accuri C6 flow cytometer (BD Biosciences, San Jose, CA, USA). At least 10,000 cells per sample were collected, and the results were analyzed using BD Accuri C6 Software (Version 1.0264.21).

6.1. Cell Cycle Distribution

Fixed cells (80% ethanol) were stained with propidium iodide (PI) and RNase A Staining Buffer (BD Biosciences, San Jose, CA, USA) to determine DNA content and identify the sub-G1 (apoptotic/hypodiploid) population.

6.2. Membrane Integrity and Phosphatidylserine Externalization

Apoptotic and necrotic cells were evaluated using Annexin V-FITC/PI dual staining (FITC Annexin V Apoptosis Detection Kit I, BD Biosciences, San Jose, CA, USA). For 3D models, spheroids were first dissociated into single-cell suspensions before staining.

6.3. Cellular Senescence Detection

Senescence-associated β-galactosidase activity was detected at pH 6.0 using a fluorescein-based enzymatic substrate from the CellEvent™ Senescence Green Flow Cytometry Assay Kit (Invitrogen, Thermo Scientific, Waltham, MA, USA). The reaction product remains intracellular and emits a fluorescence (490/514 nm).

6.4. Cell Death Detection

Cell viability was determined by employing 7-aminoactinomycin D (7-AAD; Thermo Scientific, Waltham, MA, USA) staining. While 2D cells were processed directly, MCTS were first

enzymatically dissociated into single-cell suspensions to enable accurate quantification of the non-viable cell population.

6.5. Caspase 3/7 Activity

Activation of caspases 3 and 7 was measured using a fluorogenic caspase substrate by applying the CellEvent™ Caspase-3/7 Green Flow Cytometry Assay Kit (Invitrogen, Thermo Scientific, Waltham, MA, USA).

7. Colony Formation Assay

To evaluate the irreversibility of growth arrest and the long-term proliferative recovery following compound exposure, MIA PaCa-2 cells were treated with UAs at IC_{50} and IC_{80} doses. After treatment, cells were post-incubated in drug-free medium for 14 days, then fixed with ethanol, and stained with Giemsa (Sigma-Aldrich, St Louis, MO, USA) to quantify the colony-forming units.

8. Microscopic Imaging

8.1. Nuclear Morphology

Following incubation with compounds, the cells were stained with Hoechst 33342 (Sigma-Aldrich, St Louis, MO, USA) to detect chromatin condensation and apoptotic bodies, and visualized by fluorescence microscopy using a UV filter (OLYMPUS BX60; Olympus, Tokyo, Japan).

8.2. Cellular Senescence Detection

SA-β-Gal activity was detected at pH 6.0 using X-gal (A&A Biotechnology, Poland) staining. Morphological changes and presence of active SA-β-Gal were observed under light microscopy (OLYMPUS BX60; Olympus, Tokyo, Japan) using Nomarski interference contrast.

8.3. Spheroid Visualization

The LSM 800 inverted laser-scanning confocal microscope (Carl Zeiss, Jena, Germany) was used to capture intact 3D spheroids stained with Calcein AM (live cells), PI (dead cells), and Hoechst 33342 (nuclei) to visualize the spatial distribution of cell death. In turn, apoptotic and necrotic cells were visualized using Annexin V-FITC and PI stains.

8.4. Detection of Autophagic Flux

Acidic vesicular organelles (AVOs) were detected using acridine orange staining and fluorescence microscopy using a blue filter (OLYMPUS BX60; Olympus, Tokyo, Japan). The functional role of autophagy was further investigated using inhibitors, including wortmannin (early-stage), chloroquine, or ammonium chloride (late-stage).

9. Wound Healing Migration Assay

Cell motility was analyzed by generating uniform wounds in cell monolayers using culture inserts (2-well Ibidi culture insert; Ibidi GmbH, Martinsried, Germany). Following pre-treatment with mitomycin C (Merck/Sigma- Aldrich, St. Louis, MO, USA) to inhibit proliferation, migration was monitored by live-cell time-lapse microscopy (Olympus IX83; Olympus, Tokyo, Japan) every 3 h for up to 72 h. Wound closure was quantified using ImageJ software and normalized to the initial wound area.

10. Western Blot Analysis

Protein expression was analyzed in cell lysates prepared in RIPA buffer supplemented with protease and phosphatase inhibitors. Proteins were separated by SDS-PAGE and electrotransferred onto nitrocellulose membranes using a semi-dry blotting system (Bio-Rad, Hercules, CA, USA). Membranes were blocked and incubated with primary antibodies against c-Myc, p53, p21, SMAD4, p16, LC3, p62, Beclin1, Bcl-2, E-cadherin, N-cadherin, and Vimentin. β-actin was used as the loading control. Protein bands were visualized using an enhanced chemiluminescence detection system (Thermo Scientific, Waltham, MA, USA) and quantified by densitometry employing Image Lab software (Bio-Rad, Hercules, CA, USA).

11. Statistical Analysis

Data are presented as means ± SD or medians with interquartile ranges (IQR) from at least three independent experiments. Normality was assessed using the D'Agostino-Pearson test. Statistical significance was determined using Kruskal-Wallis one-way analysis of variance followed by Dunn's post-hoc test for multiple comparisons. Differences were considered statistically significant at $p < 0.05$, with significance levels defined as * $p < 0.05$, ** $p < 0.01$, and *** $p < 0.001$. Analyses were performed using GraphPad Prism software (San Diego, CA, USA).

ARTICLE NO. 1

c-Myc inhibition and p21 modulation contribute to unsymmetrical bisacridines-induced apoptosis and senescence in pancreatic cancer cells

Pharmacological Reports (2025) 77:182–209; doi: 10.1007/s43440-024-00658-6

IF_{2024} = 3.8, Q1, MHES Points: 100

Agnieszka Kurdyn[1], Monika Pawłowska[1], Ewa Paluszkiewicz[1], Mirosława Cichorek[2], Ewa Augustin[1]

[1] Department of Pharmaceutical Technology and Biochemistry, Faculty of Chemistry, Gdańsk University of Technology, Gabriela Narutowicza 11/12, Gdańsk 80-233, Poland

[2] Department of Embryology, Medical University of Gdańsk, Dębinki 1, Gdańsk 80-211, Poland

Pancreatic cancer is one of the most aggressive malignancies, characterized by rapid progression and profound resistance to conventional treatments, which contributes to its status as a leading cause of cancer-related mortality worldwide. The poor prognosis is closely linked to a specific set of genetic alterations, including mutations in *KRAS*, *TP53*, *SMAD4*, and the constitutive overexpression of the c-Myc oncoprotein. As a master regulator of cell proliferation, invasion, metabolic reprogramming, and chemoresistance, c-Myc represents a high-priority therapeutic target in pancreatic cancer.

The primary objective of the first scientific publication presented in this dissertation was to investigate the cellular response induced by unsymmetrical bisacridines (UAs; C-2028, C-2045, and C-2053) in human pancreatic cancer cells. The research specifically focused on characterizing the mechanisms of induced cell death and cellular senescence, thereby identifying the molecular targets of UAs and the regulatory proteins involved in the compound-induced response. To achieve this, a panel of human PC cell lines with distinct genetic profiles (Panc-1, MIA PaCa-2, AsPC-1, and BxPC-3) was employed to evaluate the UAs potential.

The comprehensive biological evaluation was designed to investigate the impact of unsymmetrical bisacridines on cell viability, cell cycle progression, and the activation of specific cell death pathways. The MTT assay was used to assess the cytotoxic potential of the tested derivatives and to determine their IC_{50} and IC_{80} values after a 72 h exposure period. To characterize the drug-induced cellular response over a longitudinal time course (up to 168 h), cell cycle distribution and apoptosis induction were quantified via flow cytometry using propidium iodide DNA staining and Annexin V-FITC/propidium iodide dual staining, respectively. These quantitative analyses were supplemented by fluorescence microscopy observation of nuclear morphology using Hoechst 33342 staining, which enabled the detection of characteristic chromatin condensation and fragmentation. The induction of accelerated cellular senescence was identified by monitoring senescence-associated β-galactosidase activity using two

complementary approaches: light microscopy with Nomarski interference contrast to assess morphological changes (such as cell enlargement and flattening), and flow cytometry for quantitative assessment of enzymatic activity. To elucidate the underlying molecular mechanisms, Western blot analysis was performed to monitor the levels of key regulatory and suppressor proteins, specifically c-Myc, p53, p21, SMAD4, and p16. Furthermore, a colony formation assay was conducted to evaluate the long-term capacity of MIA PaCa-2 cells to recover and resume proliferation after dose-dependent exposure to UAs, thereby determining the reversibility of the drug-induced growth arrest.

Experimental results revealed that all UA derivatives exhibit potent cytotoxicity at sub-micromolar concentrations (**Table 1**), with C-2028 identified as the most active compound (IC_{80} values ranging from 0.042 to 0.102 μM). Significantly, the tested UAs exhibited a favorable selectivity profile, characterized by markedly lower toxicity toward normal hTERT-HPNE pancreatic epithelial cells compared to the malignant lines.

Table 1. Inhibitory concentrations (IC) of unsymmetrical bisacridines (UAs: C-2028, C-2045, and C-2053), and reference compounds gemcitabine (GEM) and irinotecan (IR) against pancreatic cancer cells: Panc-1, MIA PaCa-2, AsPC-1, and BxPC-3, as well as normal hTERT-HPNE pancreatic cells. Doses were determined after 72 h of compound exposure via MTT assay. The results are presented as the means ± SD; N/A – not applicable; (n ≥ 4).

Compound	Dose [μM]	Cell line				
		Panc-1	MIA PaCa-2	AsPC-1	BxPC-3	hTERT-HPNE
C-2028	IC_{50}	0.024 ± 0.005	0.023 ± 0.002	0.027 ± 0.001	0.023 ± 0.003	0.041 ± 0.011
	IC_{80}	**0.043** ± 0.002	**0.042** ± 0,002	**0.102** ± 0.007	**0.043** ± 0.003	**0.366** ± 0.118
C-2045	IC_{50}	0.086 ± 0.007	0.047 ± 0,003	0.096 ± 0.005	0.198 ± 0.005	0.237 ± 0.035
	IC_{80}	**0.323** ± 0,043	**0.086** ± 0.001	**0.463** ± 0.011	**0.393** ± 0.020	**0.830** ± 0.099
C-2053	IC_{50}	0.037 ± 0,007	0.031 ± 0.003	0.097 ± 0.009	0.104 ± 0.009	0.223 ± 0.034
	IC_{80}	**0.080** ± 0,012	**0.072** ± 0.004	**0.486** ± 0.005	**0.303** ± 0.011	**0.853** ± 0.098
GEM	IC_{50}	N/A	0.062 ± 0.010	0.026 ± 0.003	0.025 ± 0.005	N/A
IR	IC_{50}	8.5 ± 0.13	N/A	N/A	N/A	N/A

A central finding of this study was the profound induction of apoptosis across all PC cell lines, as evidenced by time-dependent DNA fragmentation (increased sub-G1 fraction) and significant alterations in cell membrane asymmetry and integrity (annexin V-FITC-positive populations) (**Figure 1A, B**). These quantitative findings were qualitatively confirmed through the microscopic observation of characteristic nuclear changes, including chromatin condensation and the formation of apoptotic bodies (**Figure 1C**). Western blot analysis further revealed that UA exposure led to a significant downregulation of the c-Myc oncoprotein in all tested lines, identifying it as a primary molecular target involved in the apoptotic response (**Figure 1D**). Notably, UA-induced apoptosis was p53-independent, as the compounds remained highly effective in cells harboring either mutant (Panc-1, MIA PaCa-2, and BxPC-3) or null (AsPC-1) *TP53* status. Furthermore, SMAD4 protein induction was shown to facilitate apoptotic cell death in *SMAD4*-positive cell lines.

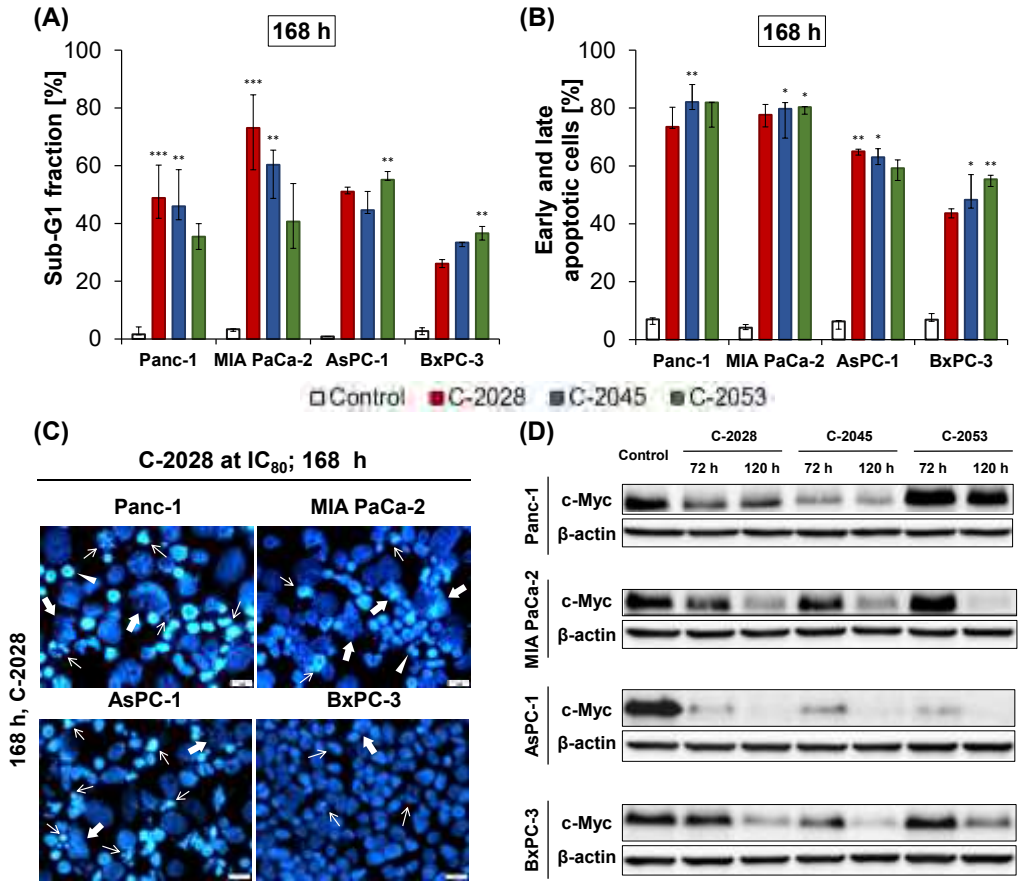

Figure 1. Induction of apoptosis by unsymmetrical bisacridines (UAs: C-2028, C-2045, and C-2053) at IC_{80} doses in pancreatic cancer cells. **(A)** DNA degradation levels are expressed as the percentage of the sub-G1 fraction, based on propidium iodide (PI)/RNase staining and flow cytometry. **(B)** Apoptotic cell population (early and late apoptosis) determined by Annexin V-FITC/PI double staining. **(C)** Nuclear morphology was evaluated by Hoechst 33342 staining and visualized under a fluorescence microscope (400×). **(D)** Western blot analysis showing time-dependent downregulation of c-Myc relative to β-actin. Total protein samples (30 µg/lane) were separated by SDS-PAGE, transferred to membranes using a semi-dry method, and detected with specific antibodies and enhanced chemiluminescence. The results are presented as the median with an interquartile range. Statistical analysis was performed using the Kruskal-Wallis test for non-parametric data and Dunn's post-hoc test. Significantly different from the control at: * $p < 0.05$, ** $p < 0.01$, *** $p < 0.001$; ($n \geq 3$).

In MIA PaCa-2 cells, UAs triggered a dose-dependent induction of accelerated cellular senescence, characterized by enhanced senescence-associated β-galactosidase activity and a significant up to 14-fold increase in p21 protein levels (**Figure 2**). Exposure to IC_{80} doses resulted in irreversible inhibition of cell proliferation, as demonstrated by complete suppression of colony formation, suggesting the potential of UAs to prevent disease recurrence. Remarkably, these senescent cells ultimately transitioned into apoptosis upon prolonged treatment, exhibiting a clear apoptotic phenotype despite their initial senescent state.

Presented findings underscore the multifaceted therapeutic potential of UAs in the treatment of pancreatic cancer. By simultaneously downregulating the c-Myc oncoprotein and upregulating the p21 protein, UAs trigger a unique dual response involving both accelerated cellular senescence and programmed cell death via apoptosis (**Figure 2**). Significantly, these derivatives' ability to exert cytotoxic effects independently of p53 or SMAD4 status suggests a potent capacity to bypass common genetic resistance mechanisms that currently limit the efficacy

of standard clinical regimens. These results, combined with a favorable selectivity profile toward malignant cells, position UA derivatives as promising candidates for future clinical translation in the development of advanced therapeutic strategies for pancreatic cancer.

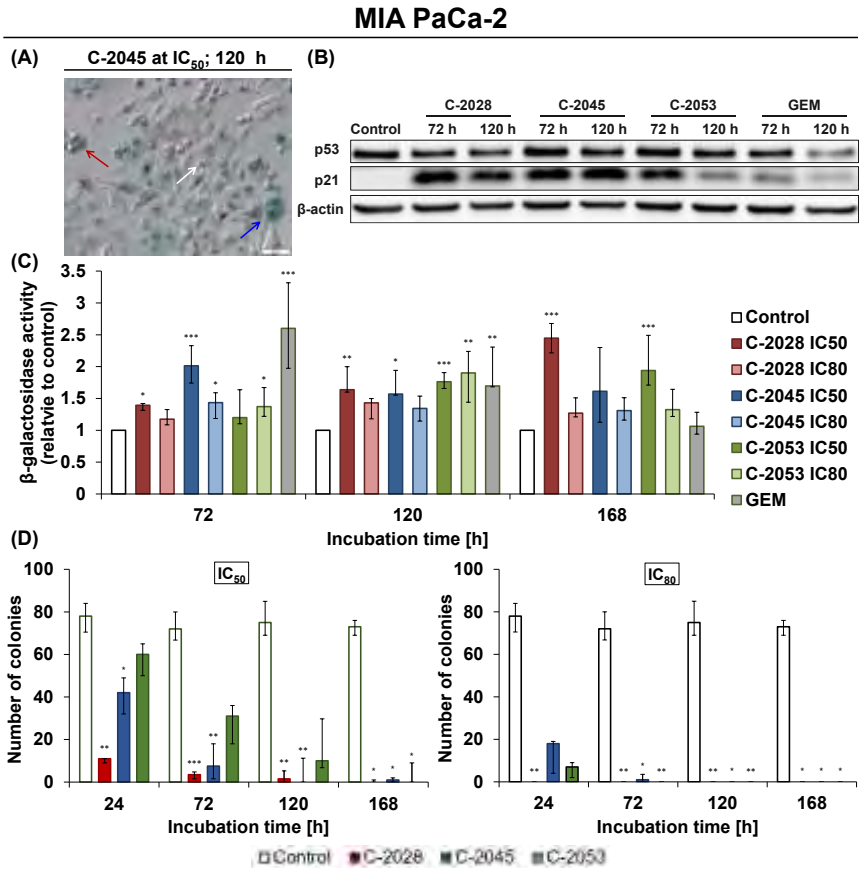

Figure 2. Induction of accelerated cellular senescence and irreversible growth arrest by unsymmetrical bisacridines (UAs; C-2028, C-2045, and C-2053) in MIA PaCa-2 cells in a dose-dependent manner. **(A)** Morphological alterations and activation of senescence-associated β-galactosidase (SA-β-Gal) after treatment with C-2045 at IC_{50} dose (blue arrow: senescent cell; white arrow: apoptotic cell; red arrow: senescent cell transitioning to apoptosis); 200× magnification, scale bar 50 µm. **(B)** Western blot analysis of p21 and p53 protein levels in cells treated with UAs at IC_{80} doses. Total protein samples (30 µg/lane) were separated by SDS-PAGE, transferred to membranes using a semi-dry method, and detected using specific antibodies and enhanced chemiluminescence. **(C)** Changes in SA-β-Gal activity in MIA PaCa-2 cells treated with the compounds, expressed as mean fluorescence intensity (MFI). **(D)** Number of colonies formed after exposure to UAs and followed by 14 days post-incubation in compound-free media. The results are presented as the median with an interquartile range. Statistical analysis was performed using the Kruskal-Wallis test for non-parametric data and Dunn's post-hoc test. Significantly different from the control at: * $p < 0.05$, ** $p < 0.01$, *** $p < 0.001$; ($n \geq 2$).

Pharmacological Reports (2025) 77:182–209
https://doi.org/10.1007/s43440-024-00658-6

RESEARCH

c-Myc inhibition and p21 modulation contribute to unsymmetrical bisacridines-induced apoptosis and senescence in pancreatic cancer cells

Agnieszka Kurdyn[1] · Monika Pawłowska[1] · Ewa Paluszkiewicz[1] · Mirosława Cichorek[2] · Ewa Augustin[1]

Received: 17 July 2024 / Revised: 20 September 2024 / Accepted: 23 September 2024 / Published online: 3 October 2024

Abstract

Background Pancreatic cancer (PC) is one of the most aggressive cancers and is the seventh leading cause of cancer-related death worldwide. PC is characterized by rapid progression and resistance to conventional treatments. Mutations in *KRAS*, *CDKN2A*, *TP53*, *SMAD4/DPC4*, and *MYC* are major genetic alterations associated with poor treatment outcomes in patients with PC. Therefore, optimizing PC therapy is a tremendous challenge. Unsymmetrical bisacridines (UAs), synthesized by our group, are new promising compounds that have exhibited high cytotoxicity and antitumor activity against several solid tumors, including pancreatic cancer.

Methods The cellular efects induced by UAs in PC cells were evaluated by MTT assay (cell growth inhibition), fow cytometry, and fuorescence and light microscopy (cell cycle distribution, apoptosis, and senescence detection). Analysis of the efects of UAs on the levels of proteins (c-Myc, p53, SMAD4, p21, and p16) was performed by Western blotting.

Results Apoptosis was the main triggered mechanism of death after UAs treatment, and induction of the SMAD4 protein can facilitate this process. c-Myc, which is one of the molecular targets of UAs, can participate in the induction of cell death in a p53-independent manner. Moreover, UAs can also induce accelerated senescence through the upregulation of p21. Notably, senescent cells can die via apoptosis after prolonged exposure to UAs.

Conclusions UAs have emerged as potent anticancer agents that induce apoptosis by inhibiting c-Myc protein and triggering cellular senescence in a dose-dependent manner by increasing p21 levels. Thus, UAs exhibit desirable features as promising candidates for future pancreatic anticancer therapies.

Keywords Unsymmetrical bisacridines · Pancreatic cancer · Apoptosis · Senescence · Anticancer activity

Abbreviations

ATCC	American Type Culture Collection
Bcl-2	B-cell lymphoma 2
C-2028	9'-{N-[(imidazo[4,5,1-de]-acridin-6-on-5-yl)aminopropyl]-N-methylaminopropylami-no}-1'-nitroacridine×1.5HCl
C-2045	9'-{N-[(8-hydroxyimidazo[4,5,1-de]-acridin-6-on-5-yl)aminopropyl]-N-methylaminopropylamino}-4'-methyl-1'-nitroacridine×3HCl
C-2053	9'-{N-[(imidazo[4,5,1-de]-acridin-6-on-5-yl)aminopropyl]-N-methylaminopropylamino}-4'-methyl-1'-nitroacridine×3HCl
CDKN2A	Cyclin Dependent Kinase Inhibitor 2 A
c-Myc	Myelocytomatosis Oncogene
DMEM HG	Dulbecco's Modifed Eagle's Medium High-Glucose
DMSO	Dimethyl Sulfoxide
ECL	Enhanced Chemiluminescence
EMT	Epithelial-Mesenchymal Transition
FACS	Fluorescence-Activated Cell Sorting

Ewa Augustin
ewa.augustin@pg.edu.pl

[1] Department of Pharmaceutical Technology and Biochemistry, Faculty of Chemistry, Gdańsk University of Technology, Gabriela Narutowicza 11/12, Gdańsk 80-233, Poland

[2] Department of Embryology, Medical University of Gdańsk, Dębinki 1, Gdańsk 80-211, Poland

FBS	Fetal Bovine Serum
FITC	Fluorescein Isothiocyanate
FOLFIRINOX	Multidrug: fOlinic Acid, Fluorouracil, Irinotecan, and Oxaliplatin
Kit	Tyrosine-Protein Kinase
K-Ras	Kirsten Rat Sarcoma Viral Oncogene Homolog
MTT	3-(4,5-Dimethylthiazol-2-yl)-2,5-diphenyltetrazolium bromide
n	Number of Repetitions
PBS	Phosphate-Bufered Saline
PC	Pancreatic Cancer
PCNA	Proliferating Cell Nuclear Antigen
PDGFRB	Platelet-Derived Growth Factor Receptor Beta
PI	Propidium Iodide
RIPA	Radioimmunoprecipitation Assay Bufer
RPMI 1640	Roswell Park Memorial Institute Medium
SA-β-Gal	Senescence Associated β-Galactosidase
SD	Standard Deviation
SDS-PAGE	Sodium Dodecyl Sulfate-Polyacrylamide Gel Electrophoresis
SMAD4	Mothers Against Decapentaplegic Homolog 4
TBST	Tris-Bufered Saline With Tween ®20
TGF-β	Transforming Growth Factor-β
UAs	Unsymmetrical Bisacridines
X-Gal	5-bromo-4-chloro-3-indolyl-β-D-Galactosidase
VEGF	Vascular Endothelial Growth Factor

Introduction

Pancreatic cancer (PC) is a highly lethal cancer and is the seventh most common cause of cancer-related death worldwide. It is estimated that PC will become the second leading cause of tumor-related mortality in the next 10 years [1]. This negative prognosis results from its late diagnosis, lack of early diagnostic biomarkers [2], and great genetic, intra- and intertumoral heterogeneity compared with other solid tumors [3]. Moreover, the accumulation of genetic alterations in pancreatic cells leads to multistage transformation and, consequently, malignancy, which is often diagnosed at an advanced stage due to the lack of early symptoms [4]. Key mutations detected in PC involve the proto-oncogene *KRAS* and the tumor suppressors *CDKN2A*, *TP53*, and *SMAD4/DPC4*, which are associated with cell cycle deregulation, apoptosis inhibition, invasion, metastasis, and poor treatment outcomes [5]. In addition, the c-Myc protein is commonly overexpressed in pancreatic cancer, enhancing proliferation, invasion, metastasis, angiogenesis, and evasion of the immune response [6, 7].

KRAS mutations are most common in PC, with more than 90% of tumors harboring oncogenic point mutations in this gene. Mutant K-Ras initiates a cascade that provides a strong pro-growth signal, increases cell motility and invasion, and profoundly rearranges cell metabolism to a growth-promoting state. One of the downstream proteins of K-Ras is the transcription factor, c-Myc, which is estimated to regulate 15% of genes in humans [8] and can act as a node in integrating several important pathways that are mutated in pancreatic cancer [9].

Because the inhibition of c-Myc attenuates chemoresistance and enhances immunotherapy, there is a high demand for compounds that directly or indirectly target this protein [6]. c-Myc has been shown to inhibit the transcription of p21, an important regulator of cell cycle control checkpoints, through its interaction and subsequent repression of multiple transcription factors [10]. Furthermore, c-Myc shares a binding domain on p21 with proliferating cell nuclear antigen (PCNA) and thereby can disrupt the interaction of p21 with PCNA, consequently reducing the inhibition of DNA synthesis [11]. Therefore, the protective function of p21 is disabled in tumor cells such as those in pancreatic cancer with high c-Myc levels [12]. In addition to its roles in cell cycle regulation, p21 is involved in diferentiation, cell migration, cytoskeletal dynamics, apoptosis, transcription, DNA repair, reprogramming of induced pluripotent stem cells, autophagy, and the onset of senescence. The p21 protein is transcriptionally controlled by both p53-dependent and p53-independent pathways [10]. Inactivating mutations in the *TP53* gene have been reported in more than 50% of pancreatic cancers and commonly result in apoptosis evasion, loss of cell cycle control, and the disabling of DNA damage repair [13]. *TP53* is typically altered through gain-of-function missense mutations that may further promote cancer beyond the loss of classical functions of this tumor suppressor [14].

Another commonly mutated gene in pancreatic cancer is *CDKN2A* (> 40%), whose alterations are related mainly to cell cycle dysregulation, promoting its progression through the loss of cyclin-dependent kinase CDK4 and CDK6 inhibition [15]. In turn, the gene encoding the tumor suppressor protein SMAD4 is inactivated in 50–55% of pancreatic cancers, and the role of its loss in PC remains controversial but appears to be associated with poorer overall survival and metastasis. SMAD4 is the central signal transducer of the transforming growth factor-β (TGF-β) pathway, which is known to play a role in epithelial–mesenchymal transition (EMT) [16].

According to the latest studies, the standard of care for pancreatic cancer has been gemcitabine, nab-paclitaxel,

and the extremely toxic FOLFIRINOX (folinic acid, fuo - rouracil, irinotecan, and oxaliplatin). However, current chemotherapy approaches for treating PC are still minimally efective in terms of survival rates [17–19]. Considering the poor prognosis of patients with pancreatic cancer and the limited achievements in its treatment, new chemotherapeutic agents are needed to improve its management [6].

Unsymmetrical bisacridines (UAs) (Fig. 1a) are a new group of antitumor compounds among acridine derivatives synthesized at Gdańsk University of Technology. These compounds are patented in Europe [20], the USA [21], Japan [22], and Canada [23] and exhibit high cytotoxicity and antitumor activity toward human tumor xenografts in nude mice, preferentially against human pancreatic cancer and colon, lung, prostate, and breast cancers [24]. We have previously shown that UAs interact with several DNA G-quadruplexes, especially with those present in the promoters of the *KRAS* and *MYC* oncogenes [25]. Additionally, our previous study revealed that UAs afect c-Myc protein levels in a manner dependent on the type of cells treated. A reduction in the c-Myc protein level and the induction of apoptosis after UAs treatment occurred to a greater extent in H460 lung cancer cells than in HCT116 colon cancer cells [26]. Notably, DNA G-quadruplexes are present in the telomeric and promoter regions of oncogenes, which are frequently mutated in various types of cancer and encode the following proteins: c-Myc, Bcl-2, PDFGR-β, VEGR, K-Ras, and Kit [27, 28]. Molecules that can stabilize the DNA G-quadruplex have been shown to exert antiproliferative and chemosensitizing efects in in vitro and in vivo tumor models without appreciably afecting normal cells.

Considering that UAs show diferent activities depend - ing on the type of treated cells [26] and that preliminary in vitro and in vivo studies have shown the high cytotoxic and antitumor activity of UAs against pancreatic cancer cells [24], the present study aimed to investigate the cellular mechanism of action of the selected UA derivatives in pancreatic cancer cells, with a particular focus on the type of induced cell death and the senescence process. To more accurately represent the variety of the patient population, four pancreatic cancer cell lines with diferent genetic pro - fles, namely, Panc-1, MIA PaCa-2, AsPC-1, and BxPC-3, were selected for this study. In addition, to identify the roles of proteins that may be involved in the cellular response induced by UAs, we intend to examine proteins such as c-Myc, p53, p21, and SMAD4, which are frequently mutated in pancreatic cancer or have G-quadruplexes in their promoter regions.

Materials and methods

Materials

2-Mercaptoethanol (Sigma-Aldrich, St Louis, MO, USA, product cat. no. M3148), 5-Fluorouracil (Sigma-Aldrich, St Louis, MO, USA, product cat. no. F6627), Acetic acid 99.5–99.9% (POCH, Gliwice, Poland, product cat. no. 568760114), Acrylamide/Bis-acrylamide, 30% solution (Sigma-Aldrich, St Louis, MO, USA, product cat. no. A3699), Ammonium persulfate (APS, Sigma-Aldrich, St Louis, MO, USA, product cat. no. A3678), Cisplatin (Sigma-Aldrich, St Louis, MO, USA, product cat. no. PHR1624), Citric acid monohydrate pure (POCH, Gliwice, Poland, product cat. no. 538210118), Erlotinib (Cayman Chemical Company, Ann Arbor, MI, USA, product cat. no. 10483) Ethyl alcohol 96% (POCH, Gliwice, Poland, product cat. no. 396420113), Formaldehyde 36–38% (POCH, Gliwice, Poland, product cat. no. 432173111), Gemcitabine hydrochloride (Sigma-Aldrich, St Louis, MO, USA, product cat. no. G6423), Glutaraldehyde solution 25% (POCH, Gliwice, Poland, product cat. no. 461023423), Glycine (Sigma-Aldrich,

(a)

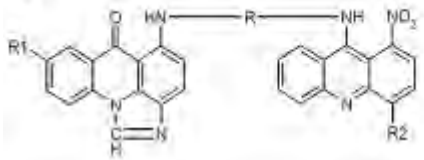

Compound	R	R1	R2
C-2028		-H	-H
C-2045	-(CH$_2$)$_3$-N(CH$_3$)-(CH$_2$)$_2$-	-OH	-CH$_3$
C-2053		-H	-CH$_3$

(b)

Compound	Compound Dose [μM]	Cell line			
		Panc-1	MIA PaCa-2	AsPC-1	BxPC-3
C-2028	IC_{50}	0.024 ± 0.005	0.023 ± 0.002	0.027 ± 0.001	0.023 ± 0.003
	IC_{80}	0.043 ± 0.002	0.042 ± 0.002	0.102 ± 0.007	0.043 ± 0.003
C-2045	IC_{50}	0.086 ± 0.007	0.047 ± 0.003	0.096 ± 0.005	0.198 ± 0.005
	IC_{80}	0.323 ± 0.043	0.086 ± 0.001	0.463 ± 0.011	0.393 ± 0.009
C-2053	IC_{50}	0.037 ± 0.007	0.031 ± 0.003	0.097 ± 0.009	0.104 ± 0.009
	IC_{80}	0.080 ± 0.012	0.072 ± 0.004	0.486 ± 0.005	0.303 ± 0.011
Gemcitabine	IC_{50}	not applicable	0.062 ± 0.010	0.026 ± 0.003	0.025 ± 0.003
Irinotecan	IC_{50}	8.5 ± 0.13	not applicable	not applicable	not applicable

Fig. 1 Chemical structures and IC (inhibitory concentrations) doses of UA compounds. (**a**) The chemical structures of UA derivatives: C-2028, C-2045, and C-2053. (**b**) IC doses of UAs and positive controls (gemcitabine or irinotecan) against Panc-1, MIA PaCa-2, AsPC-1, and BxPC-3 cells after 72 h of treatment. R, R1, R2– substituents. Data are expressed as IC_{50} and IC_{80} (mean ± SD, $n \geq 4$)

St Louis, MO, USA, product cat. no. G8898), Irinotecan hydrochloride (Sigma-Aldrich, St Louis, MO, USA, product cat. no. I1406), L-glutamine solution (Sigma-Aldrich, St Louis, MO, USA, product cat. no. G7513), Magnesium chloride (Sigma-Aldrich, St Louis, MO, USA, product cat. no. M8266), Methanol (POCH, Gliwice, Poland, product cat. no. 621990110), N, N-Dimethyloformamide (POCH, Gliwice, Poland, product cat. no. 355120112), N, N,N′,N′-Tetramethylethylenediamine (TEMED, Sigma-Aldrich, St Louis, MO, USA, product cat. no. T7024), Phosphate bufered saline (PBS, Sigma-Aldrich, St Louis, MO, USA, product cat. no. P4417), Potasium hexacyanoferrate (II) trihydrate (Sigma-Aldrich, St Louis, MO, USA, product cat. no. P9387), Potasium hexacyanoferrate (III) 99% (Sigma-Aldrich, St Louis, MO, USA, product cat. no. P8131), Sodium bicarbonate (Sigma-Aldrich, St Louis, MO, USA, product cat. no. S5761), Sodium chloride 99.9% (POCH, Gliwice, Poland, product cat. no. 363550117), Trizma base (Sigma-Aldrich, St Louis, MO, USA, product cat. no. T1503), Trypsin-EDTA 10× (Biowest, Riverside, MO, USA, product cat. no. X0930), Tween 20 (Sigma-Aldrich, St Louis, MO, USA, product cat. no. P9416).

Methods

Cell lines and culture

In the present study the following cell lines were used: Four human pancreatic cancer cell lines (Panc-1, MIA PaCa-2, AsPC-1, BxPC-3) and one normal pancreatic cell line (hTERT-HPNE). They were purchased from the American Type Culture Collection (Manassas, VA, ATCC). Panc-1 and MIA PaCa-2 cells were maintained in high-glucose Dulbecco's modifed Eagle's medium (DMEM HG, Sigma-Aldrich, St Louis, MO, USA, product cat. no. D5648), whereas AsPC-1 and BxPC-3 cells were maintained in RPMI 1640 medium (Sigma-Aldrich, St Louis, MO, USA, product cat. no. R0883). Both media were supplemented with heat-inactivated 10% fetal bovine serum (FBS; Biowest, Riverside, MO, USA, product cat. no. S1520), 100 µg/mL streptomycin (Sigma-Aldrich, St Louis, MO, USA, product cat. no.S9137), and 100 units/mL penicillin (Sigma-Aldrich, St Louis, MO, USA, product cat. no. P3032). hTERT-HPNE cells were maintained in 75% Dulbecco's modifed Eagle's medium without glucose (DMEM, Sigma-Aldrich, St Louis, MO, USA, product cat. no. D5030), 25% Essential 8™ Basal Medium (Gibco, Thermo Fisher, Waltham, MA, USA, product cat. no. A1517001) supplemented with heat-inactivated 5% fetal bovine serum (FBS; Biowest, Riverside, MO, USA, product cat. no. S1520), 10ng/mL hEGF (Sigma-Aldrich, St Louis, MO, USA, product cat. no. E9644), 1 g/L D-glucose (POCH, Gliwice, Poland, product cat. no. 459560117) and 1% Penicillin-Streptomycin (Sigma-Aldrich, St Louis, MO, USA, product cat. no. P0781). Cells were incubated in a humidifed atmosphere of 5% CO_2 at 37 °C. All experiments were performed on cells in a logarithmic growth phase.

Cell viability assay

To investigate the efect of UAs on cell viability, a colorimetric analysis was performed using MTT (3-(4,5-Dimethyl-2-thiazolyl)-2,5-diphenyl-2 H-tetrazolium bromide, Sigma-Aldrich, St Louis, MO, USA, product cat. no. M2128) based on the reduction of this yellow salt in metabolically active cells to purple formazan crystals. Cells were seeded onto 24-well plates at 2.5×10^4 cells/well for Panc-1 and BxPC-3, 2×10^4 cells/well for MIA PaCa-2 and AsPC-1, and 6.5×10^4 for hTERT-HPNE. After 24 h incubation for cell attachment, cells were treated with concentrations of UAs and gemcitabine up to 5 µM and irinotecan up to 100 µM. Gemcitabine was selected as the reference compound for MIA PaCa-2, AsPC-1, and BxPC-3 cells, while irinotecan for Panc-1 cells. Stock solutions (10 mM) of UAs and gemcitabine were prepared in deionized, sterile water while irinotecan was prepared in DMSO. Dilutions of all compounds were prepared in deionized, sterile water. After 72 h of incubation, 200 µL MTT at a concentration of 4 mg/mL was added to each well for 3–4 h. The culture medium was then aspirated and formazan crystals were dissolved in DMSO. The absorbance of the solutions was measured at 540 nm using an iMark Microplate Absorbance Reader (Bio-Rad, Hercules, CA, USA). The drug concentrations required to inhibit cell growth by 50 (IC_{50}) and 80% (IC_{80}) compared to untreated control cells were determined from curves plotting survival as a function of dose. Results were obtained from at least four independent experiments. The experiment was performed at least four times.

Cell cycle analysis

Cell cycle distribution was assessed by DNA content, which was determined by fow cytometry using propidium iodide (PI), a fuorescent dye that binds stoichiometrically to DNA. Cells were seeded at a density of 1.5×10^6 for Panc-1, 1.2×10^6 for BxPC-3, and 1×10^6 for MIA PaCa-2 and AsPC-1 per 100 mm Petri dish. Cells were then treated with IC_{80} doses of UAs and IC_{50} doses of reference compounds for 24, 72, 120, and 168 h. Following exposure to the test compounds, cells were washed with cold 1X PBS bufer, trypsinized, washed twice with cold 1X PBS, and fxed in 80% (v/v) ethanol at– 20 °C for at least 24 h. Afterward, the fxed cells were washed twice with 1X PBS, stained with PI/RNase Staining Bufer (BD Biosciences, San Jose,

CA, USA, product cat. no. 550,825), and analyzed using a FACS Accuri C6 fow cytometer (BD Biosciences, San Jose, CA, USA). At least 10,000 cells were collected and the results were analyzed using BD Accuri C6 Software (Version 1.0264.21). The experiment was performed at least four times.

Cell death determination by annexin V/propidium iodide (PI) analysis

The type of death induced by the test compounds was assessed using PI/annexin-V-FITC double staining, allowing the identifcation of cells with externalization of phosphatidylserine, a hallmark of apoptotic cells. Panc-1, MIA PaCa-2, AsPC-1, and BxPC-3 cells were seeded and treated with test compounds analogous to cell cycle analysis. After exposure to the compounds, cells were harvested, washed twice with cold 1X PBS, pelleted, and resuspended in 50 µL of binding bufer containing PI and annexin-V-FITC (FITC Annexin V Apoptosis Detection Kit I, BD Biosciences, San Jose, CA, USA, product cat. no. 556,547). The cells were then incubated in the dark for 15 min at room temperature. After incubation, 180 µL of binding bufer was added and samples were analyzed with a FACS Accuri C6 fow cytometer (BD Biosciences, San Jose, CA, USA). At least 10,000 cells were collected and the results were analyzed using BD Accuri C6 Software (Version 1.0264.21). The experiment was performed at least four times.

Assessment of cell nuclei morphology

To determine the morphology of the cell nuclei of cells treated with the test compounds, staining of the fxed cells with Hoechst 33,342 (Sigma-Aldrich, St Louis, MO, USA product cat. no. B2261), the fuorescent dye was used. This allowed analysis of chromatin condensation and fragmentation, as well as the size and multiplicity of cell nuclei. Panc-1, MIA PaCa-2, AsPC-1, and BxPC-3 cells were seeded and treated with test compounds analogous to cell cycle analysis. Successively, cells were washed with 1X PBS, resuspended in 1X PBS, and centrifuged onto slides. The cells were then fxed with methanol: acetic acid (3:1) for 15 min and stained with Hoechst 33,342 (1 mg/mL) for 15 min. The morphology of the nuclei was examined under an OLYMPUS BX60 microscope connected to an U-RFL-T lamp coupled via XC50 CCD camera to a personal computer equipped with cellSens Standard 1.18 software (Olympus, Tokyo, Japan). Images were taken using the UV flter and 400× magnifcation. For each sample slide, 3–4 pictures were taken that showed at least 50 cell nuclei. Cells were identifed as apoptotic based on the presence of condensed, fragmented chromatin. Enlarged cells containing multiple nuclei were considered as mitotic catastrophe. Abnormal distribution of genetic material was considered as abnormal mitosis. The experiment was performed at least three times.

Cellular senescence observation

To determine the morphology characteristic of senescent cells and the expression of senescence-associated β-galactosidase (SA-β-Gal), a marker of this process, microscopic observation was performed. Panc-1, MIA PaCa-2, AsPC-1, and BxPC-3 cells were seeded, in a quantity that prevents the cells from reaching confuence, in 60 mm Petri dishes containing microscope coverslips and treated with UAs (IC_{80} and IC_{50} doses) and reference compounds (IC_{50} dose) for 72, 120, and 168 h. After compound treatment cells were washed twice with 1X PBS and fxed with 2% glutaraldehyde and 0.2% formaldehyde for 5 min. Next cells were washed twice with 1X PBS (pH 6.0) and coverslips were moved to 35 mm Petri dishes and incubated at pH 6.0 with X-gal (5-bromo-4-chloro-3-indolyl-β-D-galactosidase, A&A Biotechnology, Poland, product cat. no. B4252) staining solution (1 mg/mL X-Gal, 40 mmol/L citric acid/sodium phosphate, pH 6.0, 5 mmol/L potassium hexacyanoferrate(II), 5 mmol/L potassium hexacyanoferrate(III), 150 mmol/L NaCl, 2 mmol/L $MgCl_2$). After overnight incubation at 37 °C, cells were washed twice with 1X PBS pH 7.2 and observed under an OLYMPUS BX60 microscope coupled via XC50 CCD camera to a personal computer equipped with a cellSens Standard 1.18 software (Olympus, Tokyo, Japan). Images were taken in light mode using the Nomarski interference contrast at 200× magnifcation. At least 5 images were taken for each slide, a minimum of 400 cells were counted and those stained blue were identifed as senescent cells. The experiment was performed at least two times.

Cytofluorimetric analysis of SA-β-Gal activity

The CellEvent™ Senescence Green Flow Cytometry Assay Kit (Invitrogen, Thermo Fisher, Waltham, MA, USA, product cat. no. C10841) is a fuorescent-based reagent that contains two galactoside moieties (C12FDG; 5-Dodecanoylaminofuorescein di-β-D-Galactopyranoside), making it a specifc substrate for β-galactosidase. The enzyme-cleaved product is retained in the cell due to the covalent binding of intracellular proteins and emits a fuorogenic signal that has an absorption/emission maxima of 490/514 nm. Cells were stained according to the manufacturer's protocol. MIA PaCa-2 cells were seeded in a 100 mm Petri dish and exposed to UAs at IC_{50} and IC_{80} doses and gemcitabine at IC_{50} dose for up to 168 h. After incubation with examined compounds cells were trypsinized, resuspended in 1X PBS, and fxed in 4% paraformaldehyde for 15 min at room temperature,

washed in 1X PBS, and then stained with the CellEvent™ Senescence Green Probe diluted 1/500 in CellEvent™ Senescence Bufer for 3 h in a 37 °C incubator with no CO_2. Cells were washed in 1X PBS and then resuspended in 1X PBS. Data was acquired on the CytoFLEX fow cytometer (Beckman Coulter Life Sciences) and a FACS Accuri C6 fow cytometer (BD Biosciences, San Jose, CA, USA). At least 10,000 cells were collected and the results were analyzed using BD Accuri C6 Software (Version 1.0264.21) and Kaluza C software (Version 1.1. Beckmann Coulter Inc.). Mean fuorescence intensity (MFI) values were calculated as fold change compared with non-treated, stained controls. The experiment was performed at least three times.

Colony formation assay

The ability of MIA PaCa-2 cells to return to proliferation after UAs treatment was examined by performing a colony formation assay. MIA PaCa-2 cells were seeded in 6-well plates and exposed to UAs at IC_{50} and IC_{80} doses and gemcitabine at IC_{50} dose for up to 168 h. After compounds treatment MIA PaCa-2 cells were harvested, and 250 cells per well were seeded in a new 6-well plate with fresh medium. Cells were incubated for 14 days and then fxed with 95% ethanol, stained with Giemsa stain (Sigma-Aldrich, St Louis, MO, USA, product cat. no. GS500), photographed, and counted. The experiment was performed at least three times.

Western blot analysis

Panc-1, MIA PaCa-2, AsPC-1, and BxPC-3 cells were seeded and treated with test compounds analogous to cell cycle analysis. After exposure to the compounds, cells were scraped, harvested together with foating cells, and washed twice with cold 1X PBS. Cells were suspended in RIPA bufer (Abcam, Cambridge, UK, product cat. no. ab156034) with a cocktail of protease (cOmplete Tablets, Roche, Mannheim, Germany, product cat. no. 04693124001), and phosphatase inhibitors (PhosSTOP, Roche, Mannheim, Germany, product cat. no. 049906837001), and 1 mM phenylmethanesulfonyl fuoride (PMSF, Sigma-Aldrich, St Louis, MO, USA, product cat. no. 78830). The cell suspension was maintained on ice for 20 min with brief vortexing every 5 min. The lysates were then centrifuged at 14,000 g for 15 min at 4 °C. Protein concentration was determined using the DC Protein Assay (Bio-Rad, Hercules, CA, USA, product cat. no. 5000113 and no. 5000114). Samples were mixed with Laemmli bufer (Bio-Rad, Hercules, CA, USA, product cat. no. 161–0737) and 2-Mercaptoethanol (Sigma-Aldrich, St. Louis, CA, USA, product cat. no. M3148), then denatured at 100 °C for 5 min. Then 30 µg of total protein was subjected to SDS-PAGE and transfer onto nitrocellulose membranes was performed using a semi-dry blotting apparatus (Bio-Rad, Hercules, CA, USA). The membrane was blocked with every blot-blocking bufer (Bio-Rad, Hercules, CA, USA, product cat. no. 12010020), washed fve times with TBST bufer, and probed with primary antibodies. Rabbit anti-c-Myc (1:2000, product cat. no. 9402), mouse anti-p21 (1:1000, product cat. no. 2946), and rabbit anti-p16 (1:1000, product cat. no. 80772) antibodies were purchased from Cell Signaling Technology (Beverly, MA, USA) and mouse anti-SMAD4 (1:250, product cat. no. sc-7966) was purchased from Santa Cruz Biotechnology (Dallas, TX, USA). Mouse anti-p53 (1:2000, product cat. no. P6874) and anti-β-actin (1:10,000, product cat. no. A5441) antibodies were purchased from Sigma-Aldrich (St. Louis, CA, USA). Secondary anti-mouse (1:2000, product cat. no. 7076) and anti-rabbit (1:2000, product cat. no. 7074) antibodies linked to horseradish peroxidase were purchased from Cell Signaling Technology (Beverly, MA, USA). To reprobe the blot with another antibody, the membrane was washed 5 times with TBST after developing the frst antibody. The membrane was then treated with Restore PLUS Western Blot Stripping Bufer (Thermo Scientifc, Waltham, MA, USA, product cat. no. 46430) for 15 min with gentle shaking. Next, the membrane was washed with TBST, again blocked with blocking bufer, washed, and probed with another primary antibody as described above. For each Western blot, chemiluminescence detection was performed using enhanced chemiluminescence system reagents (Thermo Scientifc, Waltham, MA, USA, product cat. no. 34095). Densitometric analysis was performed using Image Lab software (Bio-Rad, Hercules, CA, USA). The experiment was performed at least three times.

Statistical analysis

All data are presented as median and interquartile ranges (IQR). The normality of data was assessed using the D'Agostino-Pearson test. Statistical analysis was performed using the Kruskal–Wallis one-way analysis of variance for non-parametric data and Dunn's multiple comparison tests due to the non-normal data distribution. Diferences $p < 0.05$ between the group of untreated cells (negative control) and the group of cells treated with the compound were considered statistically signifcant according to the following criteria: * $p < 0.05$, ** $p < 0.01$, and *** $p < 0.001$. Statistical analysis of the data was performed using GraphPad Prism 5 and 8 (GraphPad Software, San Diego, CA, USA).

Results

Cell viability

To examine the efects of unsymmetrical bisacridines and irinotecan or gemcitabine as positive controls on the viability of Panc-1, MIA PaCa-2, AsPC-1, and BxPC-3 cells, the MTT assay was used. Cells were treated with the studied compounds for 72 h in the concentration range 0.00001–5 µM for UAs and 0.0001–100 µM for the positive control. UAs showed a dose-dependent antiproliferative efect, and the determined IC_{50} and IC_{80} values are shown in Fig. 1. The growth inhibition curves are presented in Figs. S1–S4 in the Supplementary Information.

All three UAs strongly inhibited the growth of the four types of pancreatic cancer cells (Fig. 1b). The concentration of UAs that inhibited the growth of pancreatic cancer cells by 50% (IC_{50}) did not exceed 0.198 µM, whereas the concentration that inhibited growth by 80% (IC_{80}) reached a maximum of 0.486 µM. The C-2028 derivative was the most active against all tested cells; for Panc-1, MIA PaCa-2, and BxPC-3 cells, the IC_{50} (0.023–0.024 µM) and IC_{80} (0.042–0.043 µM) values were almost identical, whereas for AsPC-1 cells, the IC_{50} and IC_{80} values reached 0.027 µM and 0.102 µM, respectively. C-2045 was the least active derivative, whereas C-2053 presented IC_{50} and IC_{80} values that were more similar to those of C-2045.

Gemcitabine, a commonly used compound in the treatment of pancreatic cancer, was chosen as the positive control for MIA PaCa-2, AsPC-1, and BxPC-3 cells. Because this compound inhibited the proliferation of the abovementioned cells by a maximum of 60% relative to the control (Figs. S2–S4 in the Supplementary Information), the IC_{50} dose was chosen for further studies (Fig. 1b). For Panc-1 cells, it was not possible to determine the IC_{50} dose of gemcitabine (Fig. S1 in the Supplementary Information), as the compound inhibited cell proliferation by a maximum of 30% relative to the control. Therefore, irinotecan was chosen as the positive control for Panc-1 cells due to its lowest dose (8.5 µM), which inhibited cell growth by 50% (Fig. 1b).

The benefcial properties of UAs were confrmed by their lower toxicity toward hTERT-HPNE normal pancreatic cells (Table S1 in the Supplementary Information). The most active derivative against pancreatic cancer cells, C-2028 was less active against normal cells, and the IC_{80} had a value of 0.366 µM. Moreover, the C-2045 and C-2053 derivatives, which reached greater values than C-2028 in cancer cells, had at least two times higher IC_{80} doses in normal cells, 0.830 and 0.853 µM for C-2045 and C-2053, respectively.

Cell cycle distribution

The promising results of the antiproliferative activity of UAs against the four pancreatic cancer cell lines prompted us to further study the cellular efects induced by these com - pounds. First, cytometric analysis of the cell cycle distribution of pancreatic cancer cells exposed to UAs at IC_{80} doses for 24, 72, 120, and 168 h was performed, and the data are presented in Fig. 2; Table 1, and Tables S2–S5 in the Supplementary Information.

The most important change in the cell cycle of the studied pancreatic cancer cells induced by UAs was a time-dependent increase in the population of hypodiploid cells (DNA content < 2 N, sub-G1 fraction), indicating that the cells were undergoing cell death. Other alternations in cell cycle progression, such as the accumulation of cells in a particular phase of the cycle, were not observed. Only up to 120 h of incubation, a slight increase in the polyploid cell population was observed.

In Panc-1 cells, after 168 h of incubation, the percentages of hypodiploid cells reached 50.7, 51.1, and 35.5% for C-2028, C-2045, and C-2053, respectively. In MIA PaCa-2 cells, the sub-G1 population reached the highest level following 168 h of C-2028 treatment (70.7%). In turn, for C-2045 and C-2053, the percentages of cells with DNA < 2 N reached 58.4 and 49.0%, respectively. In AsPC-1 cells, the percentage of the sub-G1 fraction at 168 h reached maximum levels of 51.3, 46.4, and 56.0% for C-2028, C-2045, and C-2053, respectively. In turn, treatment of BxPC-3 cells with UAs led to an increase in the percentage of cells with fragmented DNA; however, after 168 h, the sub-G1 fraction reached the lowest percentages among all the lines tested, with 26.1, 32.9, and 36.6% for C-2028, C-2045, and C-2053, respectively.

Irinotecan (positive control) caused an increase in the number of Panc-1 cells in the sub-G1 phase, which reached 46.0% after 120 h of incubation. (Fig. 3a–b; Table 2, and Table S2 in the Supplementary Information). Another positive control, gemcitabine, also induced time-dependent increases in the hypodiploid DNA content in pancreatic cells (MIA PaCa-2, AsPC-1, and BxPC-3 cells); however, this increase was less pronounced in AsPC-1 and BxPC-3 cells than following UAs treatment (Fig. 3a–b; Table 2, and Tables S3–S5 in the Supplementary Information).

Induction of apoptosis

To determine the type of cell death caused by the tested compounds, an analysis of cell membrane asymmetry and integrity was performed using annexin V-FITC and PI dual staining. Panc-1, MIA PaCa-2, AsPC-1, and BxPC-3 cells were treated with UAs at IC_{80} doses for 24, 72, 120, and

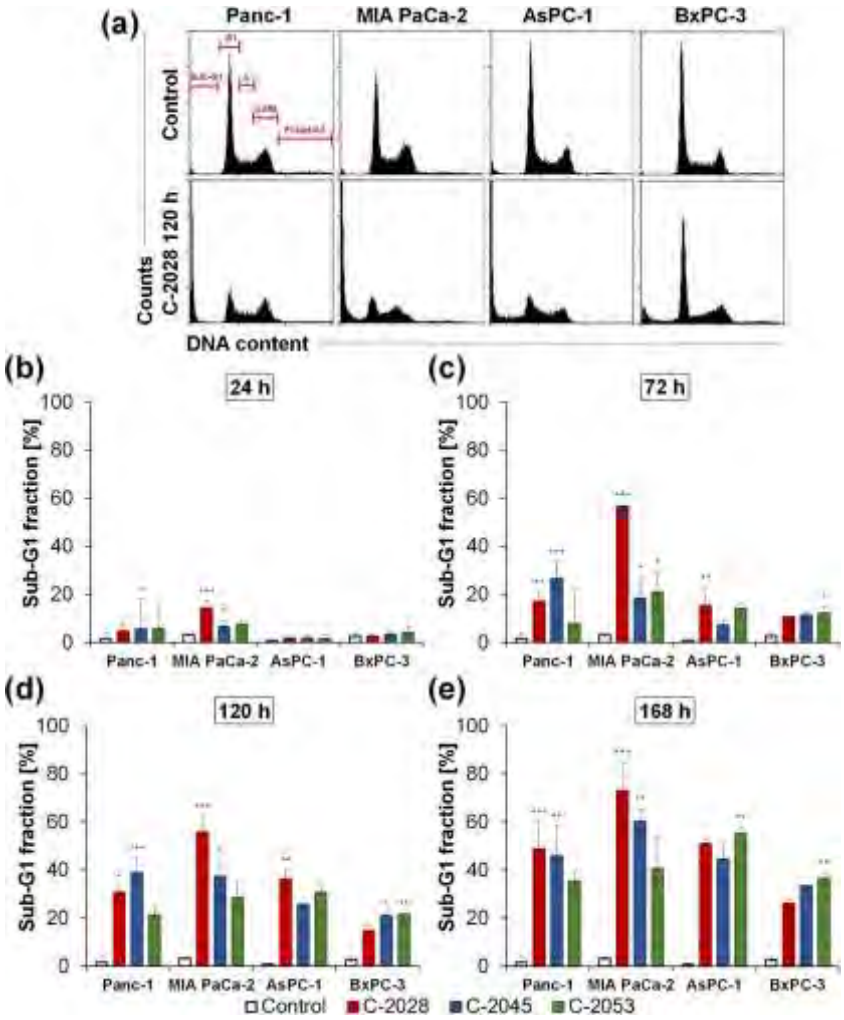

Fig. 2 Cell cycle distribution. Panc-1, MIA PaCa-2, AsPC-1, and BxPC-3 cells were incubated with IC_{80} doses of UAs for 24, 72, 120, and 168 h. After propidium iodide (PI)/ribonuclease (RNase) staining, cells were analyzed by flow cytometry. (**a**) Representative histograms show changes in the PI-signal - DNA content (x-axis) versus cell number (y-axis) in cells after 120 h exposure to the C-2028. (**b-e**) Bar graphs represent data as the median with an interquartile range. Statistical analysis was performed using the Kruskal–Wallis test for non-parametric data and Dunn's post-hoc test. Significantly different from the control at: * $p < 0.05$, ** $p < 0.01$, *** $p < 0.001$; $n \geq 4$

168 h. The cell membrane statuses of pancreatic cancer cells exposed to UAs are presented in Fig. 4; Table 3, and Tables S6–S9 in the Supplementary Information.

In Panc-1 cells, all three UA derivatives caused significant changes (Table 3) in the asymmetry and integrity of the cell membrane, which indicated the induction of cell death. After 168 h of incubation, the number of viable cells (A-/PI-) decreased to less than 22% for all the tested compounds. After 72 h of incubation with the C-2028 and C-2045 derivatives, annexin V-positive cells (i.e., early and late apoptotic cells) accounted for 42.5 and 53.2% of the total cell population, respectively. In contrast, for C-2053, this population reached 31.1%. After the longest incubation time, the percentages of apoptotic cells were similar for all the compounds and ranged from 75.6 to 87.2%. The proportions of necrotic cells for the C-2028 and C-2045 derivatives did not exceed 5.3%, whereas for C-2053, it reached the highest level of 10.2% after 72 h. In MIA PaCa-2 cells, annexin V-positive cells were found at the highest percentage after 72 h of exposure to C-2028 (51%). The apoptotic cell populations reached maximum levels after 168 h: 77.5, 77.7, and 79.4% for C-2028, C-2045, and C-2053, respectively, and greater proportions of these fractions were late-apoptotic cells. Necrotic cells accounted for the highest percentages of the tested cell populations after 72 h, reaching 11.6, 13.6, and 9.4% for C-2028, C-2045, and C-2053, respectively. The fraction of apoptotic AsPC-1 cells gradually increased, reaching 64.9, 63.1, and 58.8% after 168 h of treatment with C-2028, C-2045, and C-2053, respectively. Late apoptotic cells constituted the predominant fraction of annexin-positive cells. The population of necrotic cells did not exceed 5.5% for all the UA derivatives tested. In BxPC-3 cells,

Table 1 The results of statistical analysis for cell cycle analysis (sub-G1 fraction) of pancreatic cancer cells after treatment with UAs at IC_{80} doses (Fig. 2), including a profle of H-values and p-levels of signifcance from Kruskal-Wallis test and Dunn's multiple comparisons test. N– sample size; H– value of Kruskal-Wallis test; n/a– not applicable; *p*– signifcance level; * $p < 0.05$, ** $p < 0.01$, *** $p < 0.001$

			N	Kruskal-Wallis test		Dunn's post hoc test (Control vs. UA)				*N*	Kruskal-Wallis test		Dunn's post hoc test (Control vs. UA)
				H	*p-value*	*p-value*					H	*p-value*	*p-value*
24 h	Panc-1	Control	9	8.8	0.033 *		**72 h**	Panc-1	Control	9	23.5	< 0.001 ***	
		C-2028	6			0.151			C-2028	7			0.007 **
		C-2045	7			0.020 *			C-2045	7			< 0.001 ***
		C-2053	7			0.113			C-2053	7			0.052
	MIA PaCa-2	Control	8	19.1	< 0.001 ***			MIA PaCa-2	Control	8	22.1	< 0.001 ***	
		C-2028	5			< 0.001 ***			C-2028	5			< 0.001 ***
		C-2045	6			0.048 *			C-2045	7			0.021 *
		C-2053	4			0.078			C-2053	8			0.016 *
	AsPC-1	Control	3	4.7	0.209	n/a		AsPC-1	Control	3	10.6	< 0.001 ***	
		C-2028	3			n/a			C-2028	3			0.010 **
		C-2045	3			n/a			C-2045	5			> 0.999
		C-2053	3			n/a			C-2053	3			0.074
	BxPC-3	Control	4	1.9	0.636	n/a		BxPC-3	Control	4	9.6	0.004 **	
		C-2028	4			n/a			C-2028	3			0.391
		C-2045	4			n/a			C-2045	4			0.054
		C-2053	4			n/a			C-2053	3			0.0124 *
120 h	Panc-1	Control	9	21.0	< 0.001 ***		**168 h**	Panc-1	Control	9	19.5	< 0.001 ***	
		C-2028	4			0.012 *			C-2028	6			< 0.001 ***
		C-2045	4			< 0.001 ***			C-2045	5			0.002 **
		C-2053	4			0.244			C-2053	4			0.378
	MIA PaCa-2	Control	8	26.3	< 0.001 ***			MIA PaCa-2	Control	8	21.7	< 0.001 ***	
		C-2028	6			< 0.001 ***			C-2028	7			< 0.001 ***
		C-2045	6			0.015 *			C-2045	6			0.002 **
		C-2053	7			0.068			C-2053	7			0.127
	AsPC-1	Control	3	14.0	0.007 **			AsPC-1	Control	3	9.7	< 0.001 ***	
		C-2028	5			0.006 **			C-2028	3			0.210
		C-2045	3			> 0.999			-2045	3			0.639
		C-2053	3			0.121			C-2053	3			0.007 **
	BxPC-3	Control	4	15.9	0.003 **			BxPC-3	Control	4	13.2	< 0.001 ***	
		C-2028	4			0.618			C-2028	4			0.618
		C-2045	3			0.022 *			C-2045	3			0.084
		C-2053	4			0.006 **			C-2053	4			0.002 **

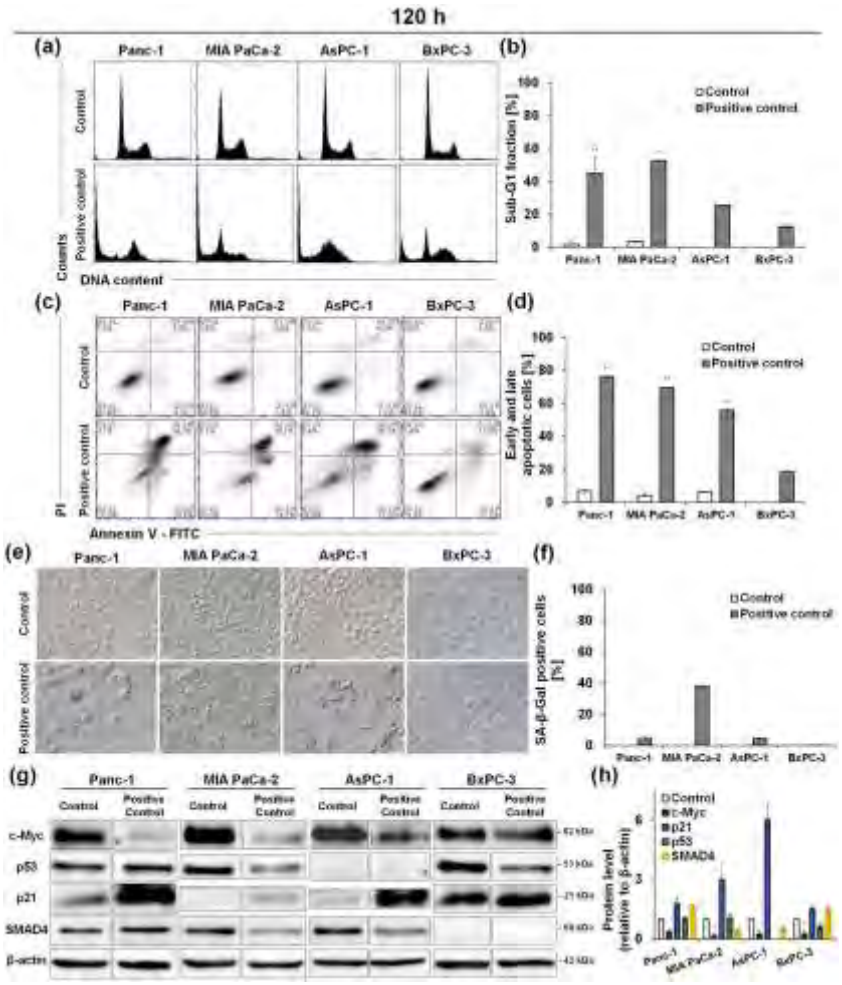

Fig. 3 Effect of the positive control drugs on pancreatic cancer cells. Application of irinotecan (Panc-1 cells) and gemcitabine (MIA PaCa-2, AsPC-1 and BxPC-3 cells) at IC_{50} doses to study the following characteristics: (**a**,**b**) cell cycle distribution, (**c**,**d**) cell membrane integrity, (**e**,**f**) induction of accelerated senescence, and (**g**,**h**) levels of c-Myc, p53, p21 and SMAD4 proteins. (**a**) Representative histograms show changes in the propidium iodide (PI)-signal– DNA content (x-axis) versus cell number (y-axis) analyzed by flow cytometry. (**c**) Representative cytograms show the annexin V- FITC (**a**) signal versus the PI signal analyzed by flow cytometry. Viable cells– A-PI-; early apoptotic cells– A+/PI-; late apoptotic cells– A+/PI+; necrotic cells– A-/PI+. (**e**) Representative images of microscopic observation of accelerated senescence. Cells were fixed, incubated with X-gal (substrate for β-galactosidase) staining solution, and observed under light microscopy using the Nomarski interference contrast at 200× magnification, scale bar 50 μm. Blue stain indicates senescence-associated (SA)-β-galactosidase activity. (**g**) Western blot analysis of c-Myc, p53, p21, and SMAD4 in pancreatic cancer cells. Whole-cell extracts (30 μg of protein/lane) were prepared, separated by polyacrylamide gel electrophoresis, and transferred to the membrane by the semi-dry method. Immunoblotting and enhanced chemiluminescence (ECL) development were performed to determine protein levels by densitometric analysis. (**b**,**d**,**f**,**h**) The bar graphs show the median and interquartile range of indicated parameters. FITC– fluorescein isothiocyanate; SA-β-Gal– senescence-associated-β-galactosidase. Statistical analysis was performed using the Kruskal–Wallis test for non-parametric data and Dunn's post-hoc test. Significantly different from the control at: * $p < 0.05$, ** $p < 0.01$, *** $p < 0.001$; $n \geq 3$

the percentages of the annexin V-positive fraction peaked after 168 h at 43.6, 50.3, and 55.0% for C-2028, C-2045, and C-2053, respectively. The proportions of early and late apoptotic cells were very similar. Conversely, necrotic cells represented very small percentages of the cell population studied, not exceeding 3.8%.

In Panc-1 cells treated with irinotecan, the positive control drug, a time-dependent increase in the number of cells stained with annexin V was observed. After 120 h

Table 2 The results of statistical analysis for cell cycle analysis (sub-G1 fraction) of pancreatic cancer cells after treatment with positive controls (+): irinotecan (IR) or gemcitabine (GEM) (Fig. 3b), including a profle of H-values and p-levels of signifcance from Kruskal-Wallis test and Dunn's multiple comparisons test. N– sample size; H– value of Kruskal-Wallis test; *p*– signifcance level; * $p<0.05$, ** $p<0.01$, *** $p<0.001$

			Kruskal-Wallis test		Dunn's post hoc test (Control vs. (+))
		N	H	*p-value*	*p-value*
Panc-1	Control	9	21.0	< 0.001 ***	
	IR	3			0.001 **
MIA PaCa-2	Control	8	26.3	< 0.001 ***	
	GEM	4			0.001 **
AsPC-1	Control	3	14.0	0.007 **	
	GEM	3			> 0.99
BxPC-3	Control	4	15.9	0.003 **	
	GEM	4			0.840

of incubation, 75.3% of the cells exhibited changes in the asymmetry of the cell membrane (Fig. 3c–d; Table 4, and Table S6 in the Supplementary Information). Necrotic cells accounted for the highest percentage of the tested cell population after 72 h, reaching 13.8%. A strong efect was also triggered by gemcitabine in MIA PaCa-2 and AsPC-1 cells, where after the longest exposure time early and late apoptotic cells were 71.5 and 61.8% for each line, respectively. Compared with UAs, in BxPC-3 cells treated with gemcitabine, apoptosis was induced in the lowest population. Only 31.3% of the cells were annexin V-positive (Fig. 3c–d; Table 4 and Tables S7–S9 in the Supplementary Information). Gemcitabine caused necrosis at levels lower than 8.4% in MIA PaCa-2, AsPC-1, and BxPC-3 cells.

Morphological changes in the cell nuclei

Cell membrane asymmetry and integrity analysis showed a time-dependent induction of apoptosis in cells treated with UAs. To confrm the induction of this type of cell death, an analysis of cell nuclear morphology was performed using Hoechst 33,342 staining. Panc-1, MIA PaCa-2, AsPC-1, and BxPC-3 cells were treated with UAs at IC_{80} doses for 24, 72, 120, and 168 h. Cell nuclear morphology following exposure to UAs is presented in Figs. S5–S8 in the Supplementary Information.

The most profound change in the nuclear morphology of Panc-1 cells was the appearance of condensed chromatin with material collected at the edges of the nuclear envelope, which formed a small pycnotic nucleus, as well as a small group of apoptotic bodies. During incubation, the nuclei became larger, with the exception of the C-2045 derivative, and the proportion of nuclei with altered morphology increased over time. Compared with the other compounds, exposure of Panc-1 cells to the C-2045 derivative resulted in a greater induction of apoptosis. Mitotic catastrophe, which is characterized by the presence of multinucleated cells, was also confrmed, but in a small population of cells. The nuclei of MIA PaCa-2 cells treated with UAs also underwent numerous changes. All the tested compounds induced apoptosis in a large population of cells, as indicated by the multiple cell nuclei that exhibited apoptotic features, the most profoundly after C-2028 exposure. In addition, compared with control cells, exposure of MIA PaCa-2 cells to UAs led to the enlargement of cell nuclei. This efect was mainly observed after 120 h of incubation. Mitotic catastrophe and abnormal mitosis were noted in some of the cell nuclei. In AsPC-1 cells, the strongest induction of apoptosis was observed after exposure to C-2028 and C-2053, with the greatest increase occurring after 120 h of incubation. However, apoptotic bodies were present after 24 h of UA exposure. At 168 h of incubation, some nuclei were signifcantly enlarged, and a few polyploid cells were also observed, as were cells in which mitosis was abnormal. The main change in the morphology of BxPC-3 cell nuclei was the presence of nuclei with condensed chromatin and apoptotic bodies. The cell size did not change signifcantly with incubation time, except in cells exposed to the C-2045 derivative, where the number of nuclei was slightly greater after 72 and 120 h of incubation. Other observed abnormalities included multinucleated cells and abnormal mitosis, but these afected only single cells. The greatest changes indicating apoptosis were triggered in BxPC-3 cells by the C-2053 derivative after 168 h of exposure.

The positive control drugs also triggered many changes in PC cell nuclear morphology (Figs. S5–S8 in the Supplementary Information). After treatment with irinotecan, Panc-1 cells exhibited features characteristic of apoptosis and, to a lesser extent, aberrant mitosis and mitotic catastrophe. Numerous cell nuclei became enlarged. Gemcitabine induced apoptosis in MIA PaCa-2 cells and AsPC-1 cells, and some of the cells underwent aberrations during mitosis. However, cells with normal morphology of nuclei were still observed. Moreover, the nuclei of BxPC-3 cells did not change much after exposure to gemcitabine. Only a few cells exhibited features of abnormal mitosis or mitotic catastrophe.

Detection of accelerated senescence

Previous data have shown that a fraction of pancreatic cancer cells remain viable even after long incubation times with IC_{80} doses of UAs. Therefore, the process of accelerated senescence was investigated following UAs treatment depending on the dose used. In senescent cells, the activity of the SA-β-galactosidase enzyme released into the

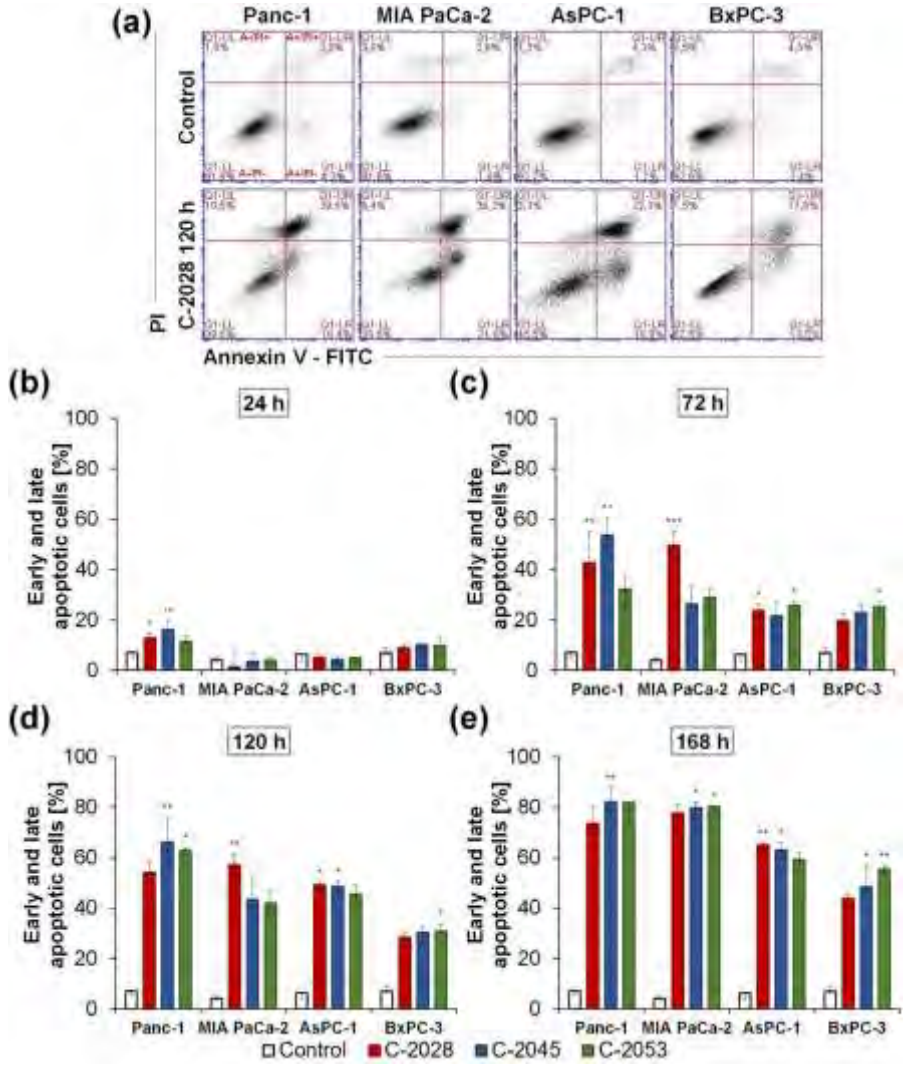

Fig. 4 Phosphatidylserine translocation and membrane integrity. Panc-1, MIA PaCa-2, AsPC-1, and BxPC-3 cells were incubated with IC_{80} doses of UAs for 24, 72, 120, and 168 h. After annexin V-FITC (**a**) and propidium iodide (PI) staining, cells were analyzed by flow cytometry. (**a**) Representative cytograms show the annexin V- FITC signal versus the PI signal in cells after 120 h exposure to the C-2028. Viable cells– A-PI-; early apoptotic cells– A+/PI-; late apoptotic cells– A+/PI+; necrotic cells– A-/PI+. (**b-e**) Bar graphs represent data as the median with an interquartile range. FITC– fluorescein isothiocyanate. Statistical analysis was performed using the Kruskal–Wallis test for non-parametric data and Dunn's post-hoc test. Significantly different from the control at: * $p < 0.05$, ** $p < 0.01$, *** $p < 0.001$; $n \geq 4$

cytoplasm is increased. Its level can be examined by treating cells with an X-gal staining solution, which, at pH 6.0, is metabolized by cytosolic SA-β-galactosidase to a blue insoluble compound, as observed under a light microscope.

Microscopic observation of Panc-1, MIA PaCa-2, AsPC-1, and BxPC-3 cells treated with UAs at IC_{80} and IC_{50} doses for 72, 120, and 168 h revealed that the IC_{50} doses of the compounds triggered accelerated senescence to a greater extent in MIA PaCa-2 cells (Fig. 5a; Table 5). Blue staining was observed after 72, 120, and 168 h of MIA PaCa-2 cell exposure to UAs at the IC_{50} dose (Fig. 5b–e; Table 6). The greatest number of senescent cells was observed after 120 h of incubation with the C-2028 and C-2045 derivatives (Fig. 5e; Table 6). Moreover, these cells were enlarged, flat, and granular. After 168 h of incubation, the cell population was reduced; however, some of the cells exhibited apoptotic

Table 3 The results of statistical analysis for phosphatidylserine translocation and membrane integrity analysis (early- and late apoptotic cells) of pancreatic cancer cells after treatment with UAs at IC_{80} doses (Fig. 4), including a profle of H-values and p-levels of signifcance from Kruskal-Wallis test and Dunn's multiple comparisons test. N– sample size; H– value of Kruskal-Wallis test; n/a– not applicable; *p*– signifcance level; * $p < 0.05$, ** $p < 0.01$, *** $p < 0.001$

			N	Kruskal-Wallis test		Dunn's post hoc test (Control vs. UA)				*N*	Kruskal-Wallis test		Dunn's post hoc test (Control vs. UA)
				H	*p-value*	*p-value*					H	*p-value*	*p-value*
24 h	Panc-1	Control	5	11.6	0.001		**72 h**	Panc-1	Control	5	15.0	0.0018	
		C-2028	4		**	0.036 *			C-2028	6		**	0.007 **
		C-2045	4			0.005 **			C-2045	4			0.002 **
		C-2053	4			0.195			C-2053	4			0.625
	MIA PaCa-2	Control	5	0.8	0.847			MIA PaCa-2	Control	5	14.8	< 0.001	
		C-2028	5			n/a			C-2028	5		***	< 0.001 ***
		C-2045	5			n/a			C-2045	4			0.208
		C-2053	5			n/a			C-2053	4			0.208
	AsPC-1	Control	4	2.1	0.581			AsPC-1	Control	4	9.7	0.0064	
		C-2028	4			n/a			C-2028	4		**	0.043 *
		C-2045	4			n/a			C-2045	4			0.224
		C-2053	4			n/a			C-2053	4			0.011 *
	BxPC-3	Control	3	4.4	0.230			BxPC-3	Control	3	9.3	0.008	
		C-2028	4			n/a			C-2028	4		**	0.459
		C-2045	4			n/a			C-2045	4			0.069
		C-2053	4			n/a			C-2053	4			0.011 *
120 h	Panc-1	Control	5	14.5	0.006 **		**168 h**	Panc-1	Control	5	10.4	0.001	
		C-2028	3			0.571			C-2028	3		**	0.305
		C-2045	3			0.010 **			C-2045	3			0.010 **
		C-2053	3			0.027 *			C-2053	3			0.066
	MIA PaCa-2	Control	5	15.6	0.004 **			MIA PaCa-2	Control	5	10.6	0.004	
		C-2028	4			0.002 **			C-2028	4		**	0.091
		-2045	3			0.157			C-2045	4			0.024 *
		C-2053	3			0.377			C-2053	5			0.013 *
	AsPC-1	Control	4	14.6	0.006			AsPC-1	Control	4	11.4	< 0.001 ***	
		C-2028	4		**	0.02 *			C-2028	4			0.004 **
		C-2045	4			0.025 *			C-2045	4			0.043 *
		C-2053	4			0.2235			C-2053	4			0.413
	BxPC-3	Control	3	14.6	0.006			BxPC-3	Control	4	11.5	< 0.001 ***	
		C-2028	4		**	0.493			-2028	4			0.618
		C-2045	4			0.058			C-2045	3			0.084 *
		C-2053	4			0.013 *			C-2053	4			0.002 **

Table 4 The results of statistical analysis for phosphatidylserine translocation and membrane integrity analysis (early- and late apoptotic cells) of pancreatic cancer cells after treatment with positive controls (+): irinotecan (IR) or gemcitabine (GEM) (Fig. 3d), including a profle of H-values and p-levels of signifcance from Kruskal-Wallis test and Dunn's multiple comparisons test. N– sample size; H– value of Kruskal-Wallis test; *p*– signifcance level; * $p<0.05$, ** $p<0.01$, *** $p<0.001$

			Kruskal-Wallis test		Dunn's post hoc test (Control vs. (+))
		N	H	*p-value*	*p-value*
Panc-1	Control	5	14.5	0.006 **	
	IR	3			0.002 **
MIA PaCa-2	Control	5	15.6	0.004 **	
	GEM	3			0.001 **
AsPC-1	Control	4	14.6	0.006 **	
	GEM	4			< 0.001 ***
BxPC-3	Control	3	14.6	0.006 **	
	GEM	4			> 0.999

cell morphology (shrunken cells with characteristic blebs) and were stained blue (a product of SA-β-galactosidase activity). These fndings suggest that senescent cells may undergo apoptosis, as shown in Fig. 5d, where the red arrow indicates an apoptotic cell with blue staining. Detailed pictures of accelerated senescence observations in all tested pancreatic cancer cells treated with UAs can be found in Figs. S9–S12 in the Supplementary Information. In Panc-1 cells treated only with C-2053 at the IC_{80} dose, single cells with characteristic blue staining were observed after 120 and 168 h of exposure. In AsPC-1 cells, the blue indicator was present only in single cells treated with UAs at the IC_{50} dose and with gemcitabine (Fig. 3e–f; Table 7). Microscopic observation of BxPC-3 cells revealed no induction of accelerated senescence by UAs (Fig. 5a and Fig. S12 in the Supplementary Information). Only single cells with blue staining were observed after exposure to gemcitabine (Fig. 3e–f; Table 7). Despite the presence of single cells with characteristic blue staining in Panc-1, AsPC-1, and BxPC-3 cells, only the MIA PaCa-2 cells underwent accelerated cellular senescence. Moreover, this process occurred in a dose-dependent manner, especially in cells treated with UAs at the IC_{50} dose.

To confrm the increased SA-β-galactosidase activity in MIA PaCa-2 cells, cytometric analysis of SA-β-galactosidase levels after exposure to UAs at the IC_{80} and IC_{50} doses for 72, 120, and 168 h was performed. SA-β-galactosidase activity is shown as a fold change in the mean fuorescence intensity (MFI) after incubation with UAs or the positive control relative to that of untreated cells (Fig. 5f; Table 8, and Table S10 in the Supplementary Information). Exposure of MIA PaCa-2 cells to UAs at the IC_{50} doses resulted in a greater increase in SA-β-galactosidase activity than treatment with the IC_{80} dose. Treatment with the C-2028 and C-2053 derivatives at the IC_{50} dose induced a gradual increase in the population of senescent cells, reaching a maximum after 168 h, with MFIs of 2.5 and 2.0, respectively. In contrast, this parameter value for the C-2045 derivative remained consistently high throughout the analysis (1.7–2.0). When MIA PaCa-2 cells were treated with compounds at the IC_{80} doses, elevated levels of SA-β-galactosidase were observed relative to those in the control, and the MFIs ranged from 1.2 to 1.9, reaching the highest values after 120 h of incubation. These results correlate with the microscopic observations, which indicated that the senescence process was most strongly induced by UAs at IC_{50} concentrations in MIA PaCa-2 cells. Upon exposure to the positive control, gemcitabine caused an increase in SA-β-galactosidase activity to the highest level after 72 h, which was more than 2.6 times greater than that in untreated cells. However, the MFI value gradually decreased with time, reaching the same level as that of the control after 168 h.

Ability of MIA PaCa-2 cells to return to proliferation

Because only MIA PaCa-2 cells underwent accelerated senescence, the reversibility or irreversibility of proliferation arrest was tested. The ability to permanently inhibit cell growth after drug exposure is important from an anticancer therapy perspective due to the possible disease recurrence as well as the induction of the metastatic process. MIA PaCa-2 cells were treated with UAs at the IC_{80} and IC_{50} doses for 24, 72, 120, and 168 h, and after two weeks of post-incubation, their ability to form colonies was investigated.

Exposure of MIA PaCa-2 cells to UAs at the IC_{80} doses resulted in complete inhibition of cell proliferation (Fig. 6a; Table 9, Fig. S13 and Table S11 in the Supplementary Information). Cell division was completely blocked after administration of C-2028 at the IC_{80} dose even after 24 h. The C-2045 and C-2053 derivatives, despite causing signifcant reductions (Table 9) in the number of colonies formed after 24, 72, and 120 h, achieved the same efect as the C-2028 derivative only after 168 h. UAs at the IC_{50} dose caused gradual reductions in the number of colonies formed with the incubation time, and after 168 h, their number did not exceed 5 (Fig. 6a; Table 9). MIA PaCa-2 cells were able to undergo mitosis and divide after exposure to gemcitabine, and the strongest inhibition of proliferation was observed after 72 h of incubation. Interestingly, with longer incubation times (120 and 168 h), an increase in the number of colonies formed was observed (Fig. S13 and Table S11 in the Supplementary Information).

Senescence is classically defned as irreversible arrest of the cell cycle in the G1 phase due to the response to DNA

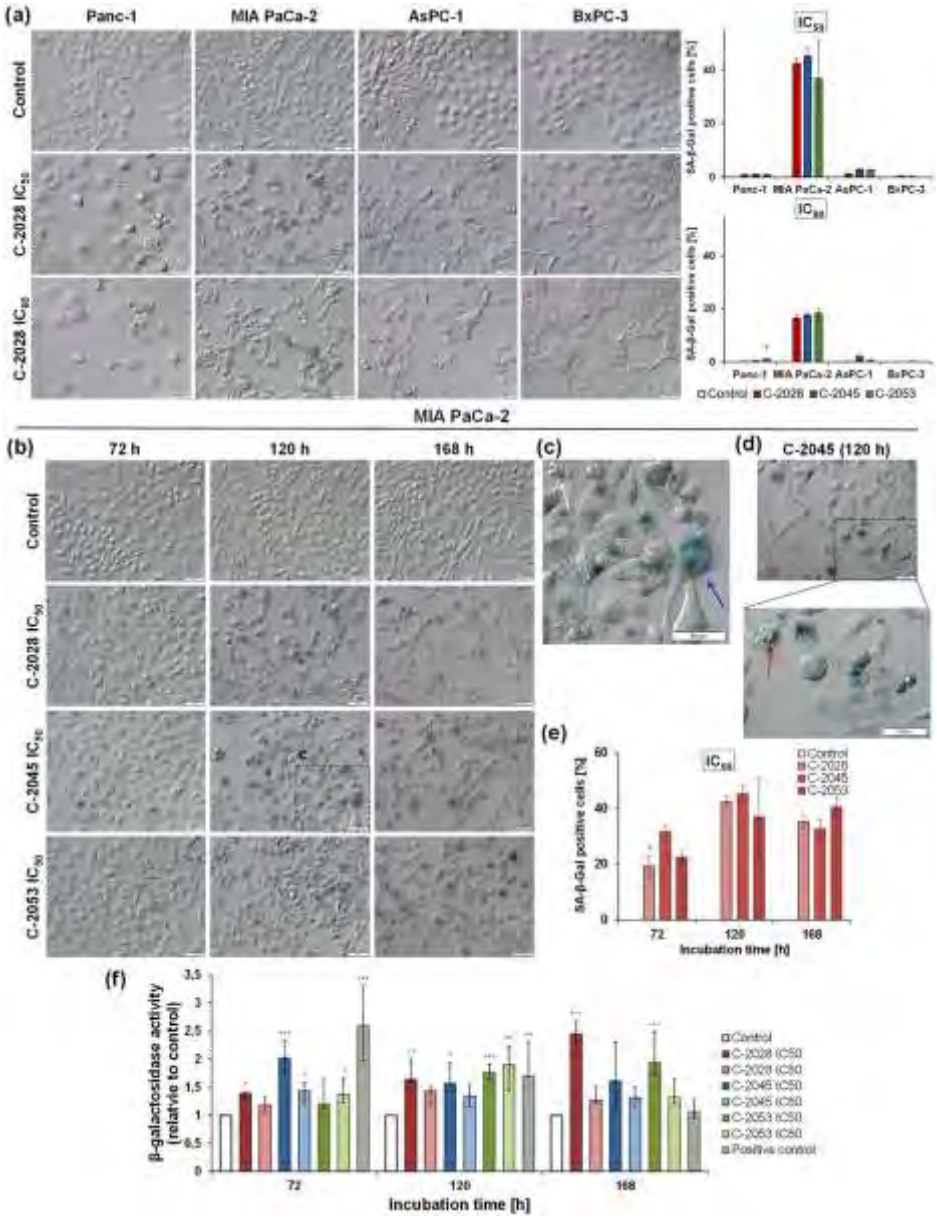

Fig. 5 Accelerated senescence detection. (**a**) Induction of accelerated senescence in Panc-1, MIA PaCa-2, AsPC-1, and BxPC-3 cells by C-2028 at IC50 and IC80 doses after 120 h of incubation. Graphs show the median with an interquartile range of SA-β-Gal (senescence-associated-β-galactosidase) positive cells percentage from the microscopic analysis. (**b-d**) Representative images of MIA PaCa-2 cells after treatment with IC50 doses of UAs for 72, 120, and 168 h. (**c**) Enlarged fragment of the selected image, the blue arrow indicates a senescent cell and the white arrow indicates an apoptotic cell. (**d**) The red arrow indicates an apoptotic cell with a blue stain. (**e**) Graphs represent the median with an interquartile range of SA-β-Gal positive cells percentage from the microscopic analysis. Briefly, cells were fixed, incubated with X-gal (substrate for β-galactosidase) staining solution, and observed under light microscopy using the Nomarski interference contrast at 200× magnification, scale bar 50 µm. (**f**) Changes of the SA-β-Gal activity in MIA PaCa-2 cells after 72, 120, and 168 h of incubation with IC50 and IC80 doses of UAs and positive control (gemcitabine) in comparison to untreated control cells SA-β-Gal activity was estimated by flow cytometry method as mean fluorescence intensity (MFI). Statistical analysis was performed using the Kruskal–Wallis test for non-parametric data and Dunn's post-hoc test. Significantly different from the control at: * $p < 0.05$, ** $p < 0.01$, *** $p < 0.001$; $n \geq 2$

Table 5 The results of statistical analysis for microscopic detection of accelerated senescence (% of SA-β-gal positive cells) in pancreatic cancer cells after treatment with C-2028 at IC_{50} and IC_{80} doses (Fig. 5a), including a profle of H-values and p-levels of signifcance from Kruskal-Wallis test and Dunn's multiple comparisons test. N– sample size; H– value of Kruskal-Wallis test; n/a– not applicable; *p*– signifcance level; * $p < 0.05$, ** $p < 0.01$, *** $p < 0.001$

			N	Kruskal-Wallis test		Dunn's post hoc test (Control vs. UA)				*N*	Kruskal-Wallis test		Dunn's post hoc test (Control vs. UA)
				H	*p-value*	*p-value*					H	*p-value*	*p-value*
IC_{50}	Panc-1	Control	2	7.4	0.052		**IC_{80}**	Panc-1	Control	2	7.5	0.012	
		C-2028	2			n/a			C-2028	2		*	0.658
		C-2045	2			n/a			C-2045	2			0.256
		C-2053	2			n/a			C-2053	2			0.021 *
	MIA PaCa-2	Control	2	5.8	0.216			MIA PaCa-2	Control	2	4.7	0.238	
		C-2028	2			n/a			C-2028	2			n/a
		C-2045	2			n/a			C-2045	2			n/a
		C-2053	2			n/a			C-2053	2			n/a
	AsPC-1	Control	2	7.7	0.048			AsPC-1	Control	2	3.1	0.429	
		C-2028	2		*	> 0.999			C-2028	2			n/a
		C-2045	2			0.072			C-2045	2			n/a
		C-2053	2			0.194			C-2053	2			n/a
	BxPC-3	Control	2	4.9	0.429			BxPC-3	Control	2	3.0	> 0.999	
		C-2028	2			n/a			C-2028	2			n/a
		C-2045	2			n/a			C-2045	2			n/a
		C-2053	2			n/a			C-2053	2			n/a

Table 6 The results of statistical analysis for microscopic detection of accelerated senescence (% of SA-β-gal positive cells) in MIA PaCa-2 cells after treatment with UAs at IC_{50} doses (Fig. 5e), including a profle of H-values and p-levels of signifcance from Kruskal-Wallis test and Dunn's multiple comparisons test. N– sample size; H– value of Kruskal-Wallis test; n/a– not applicable; *p* - signifcance level; * $p < 0.05$, ** $p < 0.01$, *** $p < 0.001$

			N	Kruskal-Wallis test		Dunn's post hoc test (Control vs. UA)
				H	*p-value*	*p-value*
MIA PaCa-2 IC_{50}	72 h	Control	2	6.2	0.029	
		C-2028	2		*	0.914
		C-2045	2			0.041 *
		C-2053	2			0.452
	120 h	Control	2	4.2	0.305	
		C-2028	2			n/a
		C-2045	2			n/a
		C-2053	2			n/a
	168 h	Control	2	5.6	0.0952	
		C-2028	2			n/a
		C-2045	2			n/a
		C-2053	2			n/a

Table 7 The results of statistical analysis for microscopic detection of accelerated senescence (% of SA-β-gal positive cells) in pancreatic cancer cells after treatment with positive controls (+): irinotecan (IR) or gemcitabine (GEM) (Fig. 3f), including a profle of H-values and p-levels of signifcance from Kruskal-Wallis test and Dunn's multiple comparisons test. N– sample size; H– value of Kruskal-Wallis test; n/a– not applicable; *p* - signifcance level; * $p < 0.05$, ** $p < 0.01$, *** $p < 0.001$

			Kruskal-Wallis test		Dunn's post hoc test (Control vs. (+))
		N	H	*p-value*	*p-value*
Panc-1	Control	2	7.4	0.052	
	IR	2			n/a
MIA PaCa-2	Control	2	5.8	0.216	
	GEM	2			n/a
AsPC-1	Control	2	7.7	0.048 *	
	GEM	3			0.071
BxPC-3	Control	2	4.9	0.429	
	GEM	2			n/a

damage. A study of the impact of UAs at IC_{50} doses on MIA PaCa-2 cell cycle progression revealed a gradual increase in the sub-G1 fraction, indicating DNA degradation, but most importantly, the maintenance of the G1 fraction at high levels during the incubation time (Fig. 6b–c; Table 10, and Table S12 in the Supplementary Information). The number of cells with DNA < 2 N peaked at 168 h, with percentages of 39.5, 40.4, and 30.1% for treatments with C-2028, C-2045, and C-2053, respectively. The fraction of cells in the G1 phase prevailed after 72 h of incubation for the C-2028 and C-2045 derivatives (34.5 and 50.2%, respectively) and after 120 h for the C-2053 derivative (49.5%) (Fig. 6c; Table 10). Compared to control cells, the proportions of the cell populations in the S and G2/M phases were slightly higher after 24 h, but the percentages of both fractions decreased during incubation. The distribution of polyploid cells was at a similar level to that in the control.

Western blot analysis

Given that a variety of mutations are observed in pancreatic cancer cells, we determined whether UAs afect the levels of proteins such as c-Myc, p53, p16 (CDKN2A), p21, and SMAD4. Moreover, we compared the levels of selected genes between the studied cell lines, as presented in Fig. 7a; Table 11. c-Myc is an oncogenic protein that plays roles in cell proliferation and the inhibition of apoptosis and, in PC, is often constitutively activated. In all four tested PC cells, signifcant downregulation of c-Myc was observed, espe - cially after prolonged incubation with the three UA derivatives (Fig. 7b; Table 12). The most profound inhibition was observed in AsPC-1 cells, where even after 72 h of exposure, the protein was almost undetectable. The C-2053 compound caused the least reduction in the level of the c-Myc protein. A gene that is mutated in nearly all pancreatic cancer cell lines is *TP53*, which encodes the p53 protein. Panc-1 and MIA PaCa-2 cells expressed the p53 protein (Fig. 7a; Table 11), whose level slightly increased after 72 h of incubation and then, after 120 h, was comparable to the level of the protein in control cells (except following treatment with C-2045 in both cell lines, where the level increased in Panc-1 cells and decreased in MIA PaCa-2 cells) (Fig. 7b; Table 12). In BxPC-3 cells, the p53 protein was also detected (Fig. 7a; Table 11), and its level slightly decreased only after 120 h of incubation with all three UA derivatives (Fig. 7b; Table 12). In AsPC-1 cells, a mutation in the *TP53* gene occurred in such a region that the protein could not be created (Fig. 7a; Table 11) [29]. Western blot analysis confrmed that in these cells, the p53 protein was not detected after UAs treatment (Fig. 7b; Table 12). The level of p21 is strongly connected

Table 8 The results of statistical analysis for cytometric detection of accelerated senescence (SA-β-gal activity) in MIA PaCa-2 cells after treatment with UAs at IC_{50} and IC_{80} doses (Fig. 5f), including a profle of H-values and p-levels of signifcance from Kruskal-Wallis test and Dunn's multiple comparisons test. N– sample size; H– value of Kruskal-Wallis test; *p*– signifcance level; * $p<0.05$, ** $p<0.01$, *** $p<0.001$

			N	Kruskal-Wallis test		Dunn's post hoc test (Control vs. UA)
				H	*p-value*	*p-value*
MIA PaCa-2	72 h	Control	7	31.0	< 0.001 ***	
		C-2028 IC_{50}	6			0.030 *
		C-2028 IC_{80}	5			0.915
		C-2045 IC_{50}	5			< 0.001 ***
		C-2045 IC_{80}	6			0.024 *
		C-2053 IC_{50}	7			0.074
		C-2053 IC_{80}	6			0.024 *
		Positive control	3			< 0.001 ***
	120 h	Control	7	28.7	< 0.001 ***	
		C-2028 IC_{50}	5			0.005 **
		C-2028 IC_{80}	6			> 0.999
		C-2045 IC_{50}	4			0.046 *
		C-2045 IC_{80}	5			> 0.999
		C-2053 IC_{50}	6			< 0.001 ***
		C-2053 IC_{80}	5			0.004 **
		Positive control	4			0.002 **
	168 h	Control	7	32.4	< 0.001 ***	
		C-2028 IC_{50}	6			< 0.001 ***
		C-2028 IC_{80}	5			0.647
		C-2045 IC_{50}	5			0.153
		C-2045 IC_{80}	5			0.614
		C-2053 IC_{50}	7			< 0.001 ***
		C-2053 IC_{80}	5			0.415
		Positive control	6			> 0.999

with p53 and the process of cell proliferation. In cells undergoing mitosis, p21 is inhibited; in turn, its level increases during cell proliferation arrest and the induction of senescence. In Panc-1 and BxPC-3 cells, p21 was observed in control untreated cells, especially in BxPC-3 cells, where the band was very thick, whereas in MIA PaCa-2 and AsPC-1 cells, p21 was not detected (Fig. 7a; Table 11). After UAs treatment in Panc-1 and MIA PaCa-2 cells, the level of p21 strongly increased, especially in MIA PaCa-2 cells, in which accelerated senescence was induced. In AsPC-1 cells, although inhibition of proliferation and apoptosis was observed, p21 was not detected upon UAs treatment (Fig. 7b; Table 12). In BxPC-3 cells, the control level of p21 was very high in comparison with the levels in the other cell lines tested (Fig. 7a; Table 11), and during incubation with UA compounds, its level decreased, especially after C-2045 and C-2053 exposure (Fig. 7b; Table 12). Notably, in these cells, cell division inhibition and apoptosis induction were observed in the smallest population of cells compared with the other cell lines. The next suppressor gene that is mutated in diferent types of cancer is *CDKN2A*, which encodes the p16 protein. In all four studied cell lines, p16 was not detected, indicating the deletion of this gene in pancreatic cells (Fig. 7a; Table 11). Another protein involved in pancreatic cancer initiation and progression is SMAD4, which is a crucial mediator protein in the TGF-β signaling pathway. Three studied cell lines, Panc-1, MIA PaCa-2, and AsPC-1, expressed this protein, whereas the protein was not detected in BxPC-3 cells (Fig. 7a; Table 11). In PC cells exposed to UAs for 72 h, the level of SMAD4 slightly increased, and after 120 h, it returned to the level of that in control untreated cells' (Fig. 7b; Table 12).

In the positive control cells, changes in the levels of the studied proteins were also observed (Fig. 3g–h; Table 13). After 120 h of incubation, the c-Myc levels in Panc-1 and MIA PaCa-2 cells signifcantly decreased (Fig. 3h; Table 13), whereas in AsPC-1 and BxPC-3 cells, only slight downregulation was triggered. Irinotecan did not afect the level of p53 in Panc-1 cells, whereas gemcitabine caused a decrease in its expression in MIA PaCa-2 and BxPC-3 cells. In all four tested cell lines treated with positive control drugs, an increase in p21 was noted, with high levels in Panc-1 and AsPC-1 cells (in UAs-treated cells, p21 was not detected) and lower levels in MIA PaCa-2 and BxPC-3 cells. The level of SMAD4 changed diferently upon positive control drug treatment. Irinotecan increased the level of SMAD4 in Panc-1 cells, whereas gemcitabine decreased it in MIA PaCa-2 and AsPC-3 cells.

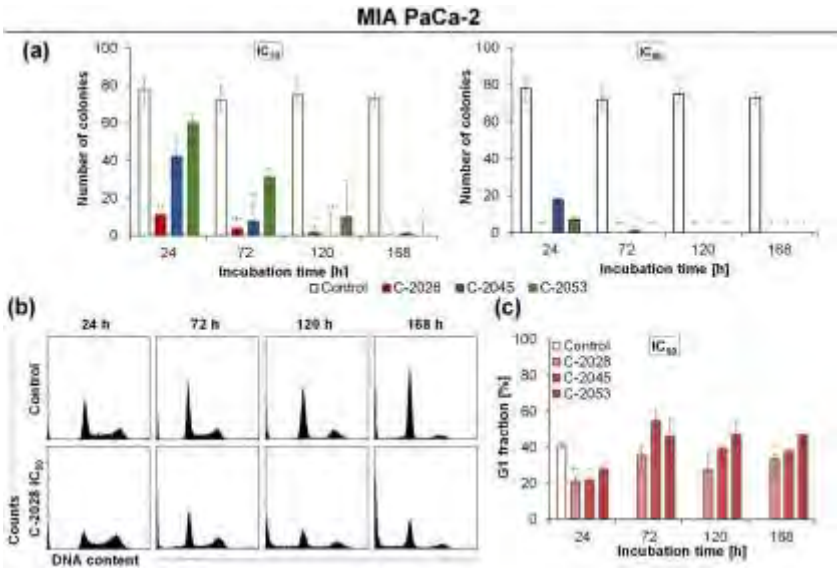

Fig. 6 Ability of MIA PaCa-2 cells to return to proliferation after UAs exposure. (**a**) Bar graphs represent the number of colonies formed as the median with an interquartile range. Cells were exposed to IC_{50} and IC_{80} doses of UAs for 24, 72, 120, and 168 h. Next, 250 cells were seeded onto a fresh plate, post-incubated for 14 days, fixed with ethanol, stained with Giemsa dye, and counted. (**b-c**) Cell cycle distribution of MIA PaCa-2 cells after treatment with C-2028, C-2045, and C-2053. Cells were incubated with IC_{50} doses of UAs for 24, 72, 120, and 168 h. After propidium iodide (PI)/ ribonuclease (RNase) staining, cells were analyzed by flow cytometry. (**b**) Representative histograms show changes in the PI-signal - DNA content (x-axis) versus cell number (y-axis) in cells exposed to the C-2028. (**c**) Bar graphs represent data as the median with an interquartile range. Statistical analysis was performed using the Kruskal–Wallis test for non-parametric data and Dunn's post-hoc test. Significantly different from the control at: * $p < 0.05$, ** $p < 0.01$, *** $p < 0.001$; $n \geq 3$

Discussion

In the present study, we showed that our recently patented compounds, unsymmetrical bisacridines exhibited high antiproliferative activity against the pancreatic cancer cell lines Panc-1, MIA PaCa-2, AsPC-1, and BxPC-3, which display different genetic profiles. UAs inhibited cell proliferation at very low concentrations, leading to induction of cell death via apoptosis in a p53-independent manner. Additionally, in MIA PaCa-2 cells, accelerated senescence was also observed through the upregulation of the p21 protein; however, this process seemed to be transient and ultimately led to cell death. c-Myc inhibition is involved in the induction of apoptosis.

Considering the high cytotoxic and antitumor activity of the UAs against pancreatic cancer cells [24] and the unusual mechanism of interaction of UAs with DNA [25], here we decided to examine the cellular mechanism of action of bisacridine derivatives in different pancreatic cancer cell lines and their impact on proteins that are often mutated in PC or possess G-quadruplexes in the promoter regions of their genes. Our research included the following cell lines: Panc-1, MIA PaCa-2, AsPC-1, and BxPC-3, which were treated with three different derivatives of unsymmetrical bisacridines and an appropriate positive controls. All three tested compounds exhibited very strong antiproliferative effects on the four cell lines. The IC_{50} values ranged from 0.025 μM (average dose against Panc-1) to 0.2 μM (for BxPC-3 cells treated with C-2045). The IC_{80} values were also very low and did not exceed the concentration of 0.5 μM. All the cell lines used in this study were very sensitive to the UA compounds, and C-2028 was the most active compound, whereas C-2045 was the least active. C-2045 possesses a hydroxyl group in its structure, and this group undergoes glucuronidation, which could explain why this derivative has the lowest activity among others [30]. In contrast, the positive control drugs had weaker antiproliferative effects on the tested cell lines. Panc-1 cells are not very sensitive to several widely used clinical medicines, such as gemcitabine, erlotinib, 5-fluorouracil, and cisplatin, for which the IC_{50} values are very high or cannot be established in the concentration range used. Irinotecan administration presented moderate growth inhibition; therefore, this compound was chosen as a positive control in studies triggered on Panc-1 cells. Gemcitabine appeared to be the best and most active clinically used compound against MIA PaCa-2, AsPC-1, and BxPC-3 cells, as the IC_{50} values were very low, comparable to those of the C-2028 derivative (in the

Table 9 The results of statistical analysis for colony formation assay in MIA PaCa-2 cells after treatment with UAs at IC_{50} and IC_{80} doses (Fig. 6a), including a profle of H-values and p-levels of significance from Kruskal-Wallis test and Dunn's multiple comparisons test. N– sample size; H– value of Kruskal-Wallis test; *p*– significance level; * $p<0.05$, ** $p<0.01$, *** $p<0.001$

			N	Kruskal-Wallis test		Dunn's post hoc test (Control vs. UA)			*N*	Kruskal-Wallis test		Dunn's post hoc test (Control vs. UA)
				H	*p-value*	*p-value*				H	*p-value*	*p-value*
MIA PaCa-2 IC_{50}	24 h	Control	4	14.3	< 0.001 ***		**MIA PaCa-2 IC_{80}**	24 h	Control	4	14.5	< 0.001 ***	
		C-2028	3			0.002 **			C-2028	3			0.002 **
		C-2045	3			0.037 *			C-2045	3			0.181
		-2053	3			0.354			C-2053	3			0.057
	72 h	Control	5	19.0	< 0.001 ***			72 h	Control	5	20.3	< 0.001 ***	
		C-2028	4			< 0.001***			C-2028	4			0.003 **
		C-2045	4			0.007 **			C-2045	4			0.027 *
		C-2053	4			0.18			C-2053	4			0.003 **
	120 h	Control	5	18.0	< 0.001 ***			120 h	Control	5	18.0	< 0.001 ***	
		C-2028	4			0.003 **			C-2028	4			0.006 **
		C-2045	4			0.003 **			C-2045	4			0.016 *
		C-2053	4			0.1			C-2053	4			0.006 **
	168 h	Control	4	14.5	< 0.001 ***			168 h	Control	4	15.6	< 0.001 ***	
		C-2028	3			0.014 *			C-2028	3			0.019 *
		C-2045	3			0.049 *			C-2045	3			0.019 *
		C-2053	3			0.027 *			C-2053	3			0.019 *

Table 10 The results of statistical analysis for cell cycle analysis (G1 fraction) of MIA PaCa-2 cells after treatment with UAs at IC_{50} doses (Fig. 6c), including a profle of H-values and p-levels of signifcance from Kruskal-Wallis test and Dunn's multiple comparisons test. N– sample size; H– value of Kruskal-Wallis test; n/a– not applicable; *p*– signifcance level; * $p < 0.05$, ** $p < 0.01$, *** $p < 0.001$

			N	Kruskal-Wallis test		Dunn's post hoc test (Control vs. UA)
				H	*p-value*	*p-value*
MIA PaCa-2 IC_{50}	24 h	Control	4	12.7	< 0.001 ***	
		C-2028	4			0.007 **
		C-2045	4			0.011 *
		C-2053	4			0.704
	72 h	Control	4	3.3	0.368	n/a
		C-2028	4			n/a
		C-2045	3			n/a
		C-2053	4			n/a
	120 h	Control	4	11.2	0.002 **	
		C-2028	5			0.333
		C-2045	4			> 0.999
		C-2053	4			0.371
	168 h	Control	4	10.7	0.002 **	
		C-2028	5			0.0441 *
		C-2045	3			0.633
		C-2053	4			> 0.999

case of AsPC-1 and BxPC-3, not for MIA PaCa-2, for which it was the weakest drug compared with UAs). However, most importantly, the IC_{80} values could not be determined for any of the cell lines. Promisingly, the lower toxicity of UAs against normal pancreatic cells of hTERT-HPNE indicates good selectivity of the tested compounds, which greatly underlines their value as potential agents against pancreatic cancer.

Regarding the cellular mechanism of action, all three unsymmetrical bisacridine derivatives induced time-dependent DNA degradation in the four PC cell lines. This process was the strongest in Panc-1 cells treated with the C-2045 derivative, in MIA PaCa-2 cells treated with C-2028, and in AsPC-1 and BxPC-3 cells treated with the C-2053 derivative. The main type of cell death triggered by UAs in the four human pancreatic cancer cell lines was apoptosis, which was confrmed by annexin V-FITC and PI staining and microscopic observation of the cell nuclei. Necrosis was induced in the PC cells at very low rates under bisacridine treatment. In Panc-1 and MIA PaCa-2 cells, the translocation of phosphatidylserine was triggered in larger populations of cells than in AsPC-1 and BxPC-3 cells. Notably, features of apoptosis in cells treated with C-2028 and C-2045 for Panc-1 cells and C-2028 for MIA PaCa-2 cells were observed much earlier than those in other cell lines and with other derivatives. Microscopic observations also revealed that the most profound induction of apoptosis was observed in Panc-1, MIA PaCa-2, and AsPC-1 cells treated with UAs, whereas this induction was much weaker in BxPC-3 cells. In addition, the exposure of the cells to UAs led to an enlargement of the cell nuclei compared with those of the control cells, except for the BxPC-3 cells.

The strong induction of apoptosis in pancreatic cancer cells by bisacridine derivatives can be explained by the inhibition of the c-Myc protein triggered by these compounds. c-Myc is often overexpressed in pancreatic cancer cells and can promote proliferation, metastasis, chemoresistance, and change metabolism and the immune system response [6]. This is the reason why molecules that can inhibit c-Myc are needed [9]. All UA compounds led to the downregulation of c-Myc in the four tested cell lines. The efect was stronger after prolonged incubation, and after 120 h, c-Myc almost disappeared in some of the UA-treated cells. Our results revealed that one of the molecular targets of UA compounds can be c-Myc, which can contribute to extensive cell death. Interestingly, the apoptosis triggered in PC cells was p53 independent. Three cell lines, Panc-1, MIA PaCa-2, and BxPC-3, express a mutant p53 protein that is unable to bind to target genes, as the DNA-binding domain is disrupted [31, 32]. In AsPC-1 cells, a mutation in the *TP53* gene leads to the complete disappearance of the p53 protein [29]. Moreover, in this cell line, the p21 protein is expressed at a very low level and is not regulated by UAs. The tested compounds in the three p53-expressing PC cell lines caused slight downregulation of this protein after prolonged incubation. The levels of p21 underwent many alternations upon UAs treatment. In Panc-1 and MIA PaCa-2 cells, signif - cant upregulation of p21 was observed, although extensive cell death through apoptosis was observed. p21 is said to be an inhibitor of apoptosis; however, it has been shown that apoptosis can occur in cells where p21 is induced and that these two processes can stimulate each other [33]. In MIA PaCa-2 control cells, the p21 protein was not detected, but its expression increased signifcantly after UAs treatment,

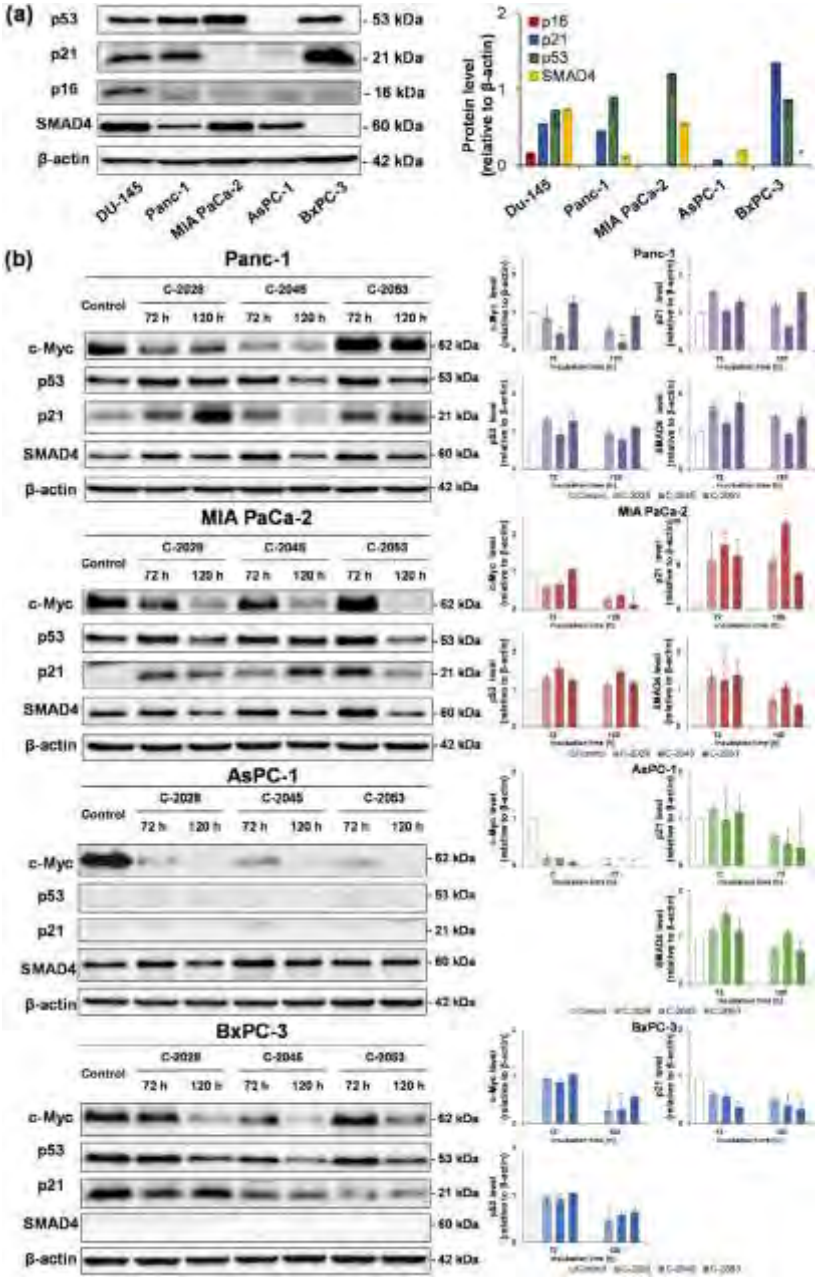

Fig. 7 Western blot analysis of c-Myc, p53, p21, and SMAD4 protein levels. Panc-1, MIA PaCa-2, AsPC-1, and BxPC-3 cells were incubated with IC_{80} doses of C-2028, C-2045, and C-2053 for 72 and 120 h. Whole-cell extracts (30 µg of protein/lane) were prepared, separated by polyacrylamide gel electrophoresis, and transferred to the membrane by a semi-dry method. Immunoblotting and enhanced chemiluminescence (ECL) development were performed to determine protein levels by densitometric analysis. Representative Western blot analysis of (**a**) p53, p21, p16 and SMAD4 protein levels in Panc-1, MIA PaCa-2, AsPC-1 and BxPC-3 cells not treated with compounds compared to Du-145 cells serving as positive control and (**b**) c-Myc, p53, p21, and SMAD4 protein levels in Panc-1, MIA PaCa-2, AsPC-1, and BxPC-3 cells following UAs exposure. Bar graphs represent data as the median with an interquartile range. Statistical analysis was performed using the Kruskal–Wallis test for non-parametric data and Dunn's post-hoc test. Significantly different from the control at: * $p < 0.05$, ** $p < 0.01$, *** $p < 0.001$; $n \geq 3$

Table 11 The results of statistical analysis for Western blot analysis of p16, p21, p53, and SMAD4 protein levels in untreated pancreatic cancer cells (PC) (Fig. 7a), including a profle of H-values and p-levels of signifcance from Kruskal-Wallis test and Dunn's multiple comparisons test. N– sample size; H– value of Kruskal-Wallis test; n/a - not applicable; *p* - signifcance level; * $p<0.05$, ** $p<0.01$, *** $p<0.001$

		N	Kruskal-Wallis test		Dunn's post hoc test (Du-145 vs. PC)			*N*	Kruskal-Wallis test		Dunn's post hoc test (Du-145 vs. PC)
			H	*p-value*	*p-value*				H	*p-value*	*p-value*
p16	Du-145	2	8.9	0.111		**p21**	Du-145	2	8.8	0.001 **	
	Panc-1	2			n/a		Panc-1	2			> 0.999
	MIA PaCa-2	2			n/a		MIA PaCa-2	2			0.187
	AsPC-1	2			n/a		AsPC-1	2			0.74
	BxPC-3	2			n/a		BxPC-3	2			> 0.999
p53	Du-145	2	6.1	0.173		**SMAD4**	Du-145	2	8.8	0.001 **	
	Panc-1	2			n/a		Panc-1	2			0.187
	MIA PaCa-2	2			n/a		MIA PaCa-2	2			> 0.999
	AsPC-1	2			n/a		AsPC-1	2			0.74
	BxPC-3	2			n/a		BxPC-3	2			0.032 *

the most strongly among the cell lines tested. Interestingly, in BxPC-3 cells, the initial level of p21 was very high, and after exposure to UAs, it decreased, especially in C-2053-treated cells, where apoptosis was slightly more induced. The high level of p21 can explain why the BxPC-3 cell line is not prone to undergo apoptosis. Many studies have shown that p21 can act as an oncogenic protein and promotes tumorigenesis and cancer through the inhibition of apoptosis and cell cycle arrest and the induction of the senescence process [34, 35]. The UA compounds and the positive control drug gemcitabine were not able to induce cell death to a similar extent as observed in the other tested cell lines. The slight downregulation of p21 observed in C-2053-treated BxPC-3 cells facilitated the induction of cell death. Another unusual feature of the BxPC-3 cell line is that these cells lack the SMAD4 protein, as our data and reports in the literature have shown [36]. The SMAD4 protein plays a tumor-suppressive role, and cells lacking this protein avoid cell cycle arrest and apoptosis [37]. This fnd - ing may also explain why triggering cell death in BxPC-3 cells with drugs is difcult. In the Panc-1, MIA PaCa-2, and AsPC-1 cell lines, the SMAD4 protein was detected with the wild-type variant (for AsPC-1 cells, the results of the variant are inconsistent, although more studies point to the wild type) [31]. After 72 h of incubation, all the UA compounds upregulated SMAD4 levels in the abovementioned cell lines, which could help in the induction of apoptosis in these cells.

Another studied cellular efect induced by UAs was accelerated senescence, and microscopic observations of X-gal-stained cells revealed that this process was triggered only in MIA PaCa-2 cells, especially after C-2045 treatment. This fnding was confrmed by performing a quantitative cytometric analysis of cells with active SA-β-galactosidase. Interestingly, the cells of the MIA PaCa-2 line, which presented features characteristic of senescence after the frst few days, seemed to die via apoptosis after prolonged incubation. Some of the cells that were stained blue after the metabolic transformation of X-gal shrank, which is typical for apoptotic blebs that form apoptotic bodies. Senescent cells are resistant to apoptosis [38, 39]. However, microscopic observation of MIA PaCa-2 cells treated with UA compounds revealed unusual behavior, in which senescent cells were forced to undergo apoptosis. This unique observation should be investigated more thoroughly, as in the senolytic feld of research, such behavior is in demand [40]. Moreover, MIA PaCa-2 cells underwent irreversible inhibition of proliferation after treatment with the IC_{80} doses of the UAs. In contrast, the IC_{50} doses of the tested bisacridines, which mainly induced accelerated cellular senescence, signifcantly reduced the proliferative capacity of the cells. In addition, cell cycle analysis confrmed that MIA PaCa-2 cells underwent senescence, as indicated by their accumulation in the G1 phase, and the increasing percentage of the sub-G1 cell fraction demonstrated that this dose also induced cell death. The greatest increase in p21 protein levels, up to 14 times greater than that in the controls, was observed in MIA PaCa-2 cells, confrming the induction of cellular senescence through the activation of p21. The p16 protein [41] did not participate in the induction of senescence in MIA PaCa-2 cells because none of the tested PC cell lines expressed this protein, as shown by our results and those in the literature [42, 43].

To summarize, unsymmetrical bisacridine derivatives can be revealed as potent antitumor compounds against pancreatic cancer cells. These compounds exhibit high antiproliferative activity at very low concentrations in PC cells. Although the positive control drugs irinotecan in Panc-1 cells and gemcitabine in MIA PaCa-2, AsPC-1, and BxPC-3 cells triggered efects similar to those of the UA compounds, there are signifcant diferences that demonstrate that UAs are highly potent compounds. The most precise example

Table 12 The results of statistical analysis for Western blot analysis of c-Myc, p53, p21, and SMAD4 protein levels in pancreatic cancer cells after treatment with UAs at IC_{80} doses (Fig. 7b), including a profle of H-values and p-levels of signifcance from Kruskal-Wallis test and Dunn's multiple comparisons test. N– sample size; H– value of Kruskal-Wallis test; n/a - not applicable; *p* - signifcance level; * $p < 0.05$, ** $p < 0.01$, *** $p < 0.001$

				N	Kruskal-Wallis test		Dunn's post hoc test (Control vs. UA)					*N*	Kruskal-Wallis test		Dunn's post hoc test (Control vs. UA)
			[h]		H	*p-value*	*p-value*				[h]		H	*p-value*	*p-value*
Panc-1	c-Myc	Control		4	26.3	< 0.001 ***		**MIA PaCa-2**	c-Myc	Control		4	23.7	0.003 **	
		C-2028	72	3			> 0.999			C-2028	72	3			> 0.999
			120	4			> 0.999				120	4			0.05
		C-2045	72	4			0.496			C-2045	72	3			> 0.999
			120	4			0.007 **				120	4			0.355
		C-2053	72	3			> 0.999			C-2053	72	3			> 0.999
			120	3			> 0.999				120	3			0.018 *
	p53	Control		3	12.6	0.127			p53	Control		3	14.4	0.072	n/a
		C-2028	72	3			n/a			C-2028	72	3			n/a
			120	3			n/a				120	3			n/a
		C-2045	72	3			n/a			C-2045	72	3			n/a
			120	3			n/a				120	3			n/a
		C-2053	72	3			n/a			C-2053	72	3			n/a
			120	3			n/a				120	3			n/a
	p21	Control		4	24.2	0.002 **			p21	Control		4	25.9	0.001 **	
		C-2028	72	3			0.205			C-2028	72	3			0.040 *
			120	3			> 0.999				120	3			0.122
		C-2045	72	3			> 0.999			C-2045	72	4			0.007 **
			120	3			> 0.999				120	3			0.002 **
		C-2053	72	3			> 0.999			C-2053	72	4			0.032 *
			120	3			0.118				120	3			> 0.999
	SMAD4	Control		3	17.9	0.022 *			SMAD4	Control		5	24.7	0.002 **	
		C-2028	72	3			0.511			C-2028	72	4			> 0.999
			120	3			> 0.999				120	5			> 0.999
		C-2045	72	3			> 0.999			C-2045	72	5			> 0.999
			120	3			> 0.999				120	5			> 0.999
		-2053	72	3			0.069			C-2053	72	5			> 0.999
			120	3			> 0.999				120	5			0.568

Table 12 (continued)

				N	Kruskal-Wallis test		Dunn's post hoc test (Control vs. UA)					*N*	Kruskal-Wallis test		Dunn's post hoc test (Control vs. UA)
AsPC-1	c-Myc	Control		4	27.3	< 0.001 ***		**BxPC-3**	c-Myc	Control		4	21.5	0.006 **	
		C-2028	72	4			0.776			C-2028	72	3			> 0.999
			120	4			0.008 **				120	3			0.206
		-2045	72	3			0.382			C-2045	72	3			> 0.999
			120	3			0.001 **				120	4			0.040 *
		C-2053	72	4			0.059			C-2053	72	3			> 0.999
			120	3			0.004 **				120	3			0.46
	p21	Control		4	25.2	0.001 **			p53	Control		4	22.3	0.004 **	
		C-2028	72	3			> 0.999			C-2028	72	3			> 0.999
			120	3			> 0.999				120	4			0.023 *
		C-2045	72	3			> 0.999			C-2045	72	3			> 0.999
			120	4			> 0.999				120	3			0.085
		C-2053	72	3			> 0.999			C-2053	72	3			> 0.999
			120	3			> 0.999				120	4			0.072
	SMAD4	Control		4	28.4	< 0.001 ***			p21	Control		4	23.3	0.003 **	
		C-2028	72	3			> 0.999			C-2028	72	4			> 0.999
			120	3			> 0.999				120	4			0.516
		C-2045	72	4			0.27			C-2045	72	4			> 0.999
			120	3			> 0.999				120	4			0.252
		C-2053	72	4			> 0.999			C-2053	72	4			0.029 *
			120	4			> 0.999				120	4			0.018 *

Table 13 The results of statistical analysis for Western blot analysis of c-Myc, p53, p21, and SMAD4 protein levels in pancreatic cancer cells after treatment with positive controls (+): irinotecan (IR) or gemcitabine (GEM) (Fig. 3h), including a profle of H-values and p-levels of signifcance from Kruskal-Wallis test and Dunn's multiple comparisons test. N– sample size; H– value of Kruskal-Wallis test; n/a - not applicable; *p* - signif - cance level; * $p<0.05$, ** $p<0.01$, *** $p<0.001$

			Kruskal-Wallis test		Dunn's post hoc test (Control vs. (+))				Kruskal-Wallis test		Dunn's post hoc test (Control vs. (+))
		N	H	*p-value*	*p-value*			N	H	*p-value*	*p-value*
Panc-1	Control	4	26.3	< 0.001		**MIA PaCa-2**	Control	4	23.7	0.003	
	c-Myc	4		***	0.07		c-Myc	3		**	0.009 **
	Control	3	12.6	0.127			Control	3	14.4	0.072	
	p53	3			n/a		p53	3			n/a
	Control	4	24.2	0.002			Control	4	25.9	0.001	
	p21	4		**	0.013 *		p21	3		**	> 0.999
	Control	3	17.9	0.022			Control	5	24.7	0.002	
	SMAD4	3		*	0.165		SMAD4	4		**	0.110
AsPC-1	Control	4	27.3	< 0.001		**BxPC-3**	Control	4	21.5	0.006	
	c-Myc	3		***	> 0.999		c-Myc	3		**	0.022 *
	Control	4	25.2	0.001			Control	4	22.3	0.004	
	p21	4		**	0.285		p53	3		**	0.218
	Control	4	28.4	< 0.001			Control	4	23.3	0.003	
	SMAD4	4		***	0.420		p21	3		**	> 0.999

of this is the BxPC-3 cell line, the only one evaluated that lacks SMAD4 expression. Our tests revealed that the most active derivative only against this cell line was C-2053, and more importantly, this compound induced apoptosis in a two-fold greater cell population than the positive control, gemcitabine. Moreover, C-2028 appeared to be very active in MIA PaCa-2 cells at particularly low concentrations. It caused cell death to the greatest extent and completely inhibited cell proliferation at the IC_{80} dose and almost completely at the IC_{50} dose. This study also revealed that one of the molecular targets of UAs might be c-Myc, which can facilitate the induction of cell death in a p53-independent manner. Apoptosis has been identifed as the main mechanism of cell death, and induction of the SMAD4 protein can facilitate this process. The intensity of c-Myc inhibition may contribute to the efcacy of all UA compounds, as may the initial level of p21 protein in control cells. Moreover, UAs can also induce accelerated senescence in a dose-dependent manner through the upregulation of the p21 protein. This phenomenon has been described in several publications, where compounds administered at lower doses or shorter treatment times can induce senescence, whereas higher doses or prolonged incubation times tend to switch the response toward triggering apoptosis [44–46]. We demonstrated such a potential of UAs, as they induced senescence in a dose-dependent manner only in MIA PaCa-2 cells. Importantly, prolonging the incubation time with UAs, even at a lower dose, resulted in the appearance of an apoptotic phenotype in senescent cells. This dose-dependent switch between senescence and apoptosis induction provides an alternative therapeutic approach with reduced toxicity and the potential for synergistic combinations of UAs with immune activators [47] or senolytic agents [45].

The use of cell lines with distinct genetic profles that more accurately represent the diversity in the patient population has revealed that UAs are widely efective, increasing the likelihood of successful translation into clinical practice. Although unsymmetrical bisacridines exhibit unique and desirable features as candidates for anticancer therapy, further research on their molecular targets and interactions with specifc cellular pathways must be undertaken to fully understand the anticancer potential of these compounds.

Supplementary Information The online version contains supplementary material available at https://doi.org/10.1007/s43440-024-00658-6.

Acknowledgements The authors gratefully thank prof. Jan Mazerski from our Department for statistical analysis consultation. This study was funded by a mini-grant from Gdańsk University of Technology no. 036915; part of these experiments were supported by CHDE S.A. Rzeszów, Poland, grant no. 037200.

Author contributions Conceptualization: A.K., M.P., E.A.; methodology: A.K., M.P., M.C., E.A.; validation: A.K., M.P., M.C., E.A.; formal analysis: A.K., M.P., E.A.; investigation: A.K., M.P., M.C.; synthesis of the studied compounds: E.P.; writing - original draft preparation: A.K., M.P., M.C., E.A.; writing– review and editing: A.K., M.P., E.A.; visualization: A.K.; supervision: E.A.; funding acquisition: E.A. All authors have read and agreed to the published version of the manuscript.

Data availability Data obtained during this study are included in this article and Supplementary Information fle. Detailed data are available from the corresponding author upon reasonable request.

Declarations

Conflict of interest The authors declare there is no confict of interest.

References

1. Barcellini A, Peloso A, Pugliese L, Vitolo V, Cobianchi L. Locally advanced pancreatic ductal adenocarcinoma: challenges and progress. Onco Targets Ther. 2020;13:2705–12720. https://doi.org/10.2147/OTT.S220971.
2. Gheorghe G, Bungau S, Ilie M, Behl T, Vesa CM, Brisc C, et al. Early diagnosis of pancreatic Cancer: the Key for Survival. Diagnostics. 2020;10:869. https://doi.org/10.3390/diagnostics10110869.
3. Gutiérrez ML, Muñoz-Bellvís L, Orfao A. Genomic heterogeneity of pancreatic ductal adenocarcinoma and its clinical impact. Cancers. 2021;13:4451. https://doi.org/10.3390/cancers13174451.
4. Singh D, Upadhyay G, Srivastava RK, Shankar S. Recent advances in pancreatic cancer: biology, treatment, and prevention. Biochim Biophys Acta. 2015;1856:13–27. https://doi.org/10.1016/j.bbcan.2015.04.003.
5. Wood LD, Hruban RH. Genomic landscapes of pancreatic neoplasia. J Pathol Transl Med. 2015;49:13–22. https://doi.org/10.4132/jptm.2014.12.26.
6. Ala M. Target c-Myc to treat pancreatic cancer. Cancer Biol Ther. 2022;23:34–50. https://doi.org/10.1080/15384047.2021.2017223.
7. Parasido E, Avetian GS, Naeem A, Graham G, Pishvaian M, Glasgow E, et al. The sustained induction of c-MYC drives nab-Paclitaxel Resistance in primary pancreatic ductal carcinoma cells. Mol Cancer Res. 2019;17:1815–27. https://doi.org/10.1158/1541-7786.MCR-19-0191.
8. Dang CV, O'Donnell KA, Zeller KI, Nguyen T, Osthus RC, Li F. The c-Myc target gene network. Semin Cancer Biol. 2006;16:253–64. https://doi.org/10.1016/j.semcancer.2006.07.014.
9. Wirth M, Mahboobi S, Krämer OH, Schneider G. Concepts to target MYC in pancreatic Cancer. Mol Cancer Ther. 2016;15:1792–8. https://doi.org/10.1158/1535-7163.MCT-16-0050.
10. Kreis NN, Louwen F, Yuan J. The multifaceted p21 (Cip1/Waf1/CDKN1A) in cell diferentiation, Migration and Cancer Therapy. Cancers (Basel). 2019;11:1220. https://doi.org/10.3390/cancers11091220.
11. Kitaura H, Shinshi M, Uchikoshi Y, Ono T, Iguchi-Ariga SM, Ariga H. Reciprocal regulation via protein-protein interaction between c-Myc and p21(cip1/waf1/sdi1) in DNA replication and transcription. J Biol Chem. 2000;275:10477–83. https://doi.org/10.1074/jbc.275.14.10477.
12. Warfel NA, El-Deiry WS. p21WAF1 and tumourigenesis: 20 years after. Curr Opin Oncol. 2013;25:52–8. https://doi.org/10.1097/CCO.0b013e32835b639e.
13. Mizrahi JD, Surana R, Valle JW, Shrof RT. Pancreatic cancer. Lancet. 2020;395:2008–20. https://doi.org/10.1016/S0140-6736(20)30974-0.
14. Morton JP, Timpson P, Karim SA, Ridgway RA, Athineos D, Doyle B, et al. Mutant p53 drives metastasis and overcomes growth arrest/senescence in pancreatic cancer. Proc Natl Acad Sci U S A. 2010;107:246–51. https://doi.org/10.1073/pnas.0908428107.
15. Cortesi M, Zanoni M, Pirini F, Tumedei MM, Ravaioli S, Rapposelli IG, et al. Pancreatic Cancer and Cellular Senescence: Tumor Microenvironment under the spotlight. Int J Mol Sci. 2021;23:254. https://doi.org/10.3390/ijms23010254.
16. Racu ML, Lebrun L, Schiavo AA, Van Campenhout C, De Clercq S, Absil L, et al. The role of SMAD4 inactivation in epithelial-mesenchymal plasticity of pancreatic ductal adenocarcinoma: the missing link? Cancers. 2022;14:973. https://doi.org/10.3390/cancers14040973.
17. Conroy T, Desseigne F, Ychou M, Bouché O, Guimbaud R, Bécouarn Y, et al. FOLFIRINOX versus gemcitabine for metastatic pancreatic cancer. N Engl J Med. 2011;364:1817–25. https://doi.org/10.1056/NEJMoa1011923.
18. Von Hof DD, Ervin T, Arena FP, Chiorean EG, Infante J, Moore M, et al. Increased survival in pancreatic cancer with nab-paclitaxel plus gemcitabine. N Engl J Med. 2013;369:1691–703. https://doi.org/10.1056/NEJMoa1304369.
19. Neoptolemos JP, Kleef J, Michl P, Costello E, Greenhalf W, Palmer DH. Therapeutic developments in pancreatic cancer: current and future perspectives. Nat Rev Gastroenterol Hepatol. 2018;15:333–48. https://doi.org/10.1038/s41575-018-0005-x.
20. Konopa J, Horowska B, Paluszkiewicz EM, Borowa-Mazgaj B, Augustin E, Skwarska A et al. October. Asymmetric bis-acridines with antitumor activity and use thereof. Eur Patent EP 3070078 B1, 4 2017.
21. Konopa J, Horowska B, Paluszkiewicz EM, Borowa-Mazgaj B, Augustin E, Skwarska A et al. Asymmetric bis-acridines with antitumour activity and their uses. U S Patent US10,202,349 B2, 12 February 2019.
22. Konopa J, Horowska B, Paluszkiewicz EM, Borowa-Mazgaj B, Augustin E, Skwarska A, et al. Asymmetric bis-acridines with antitumour activity and their uses. Japanese Patent no. February 2023;7226918:13.
23. Konopa J, Horowska B, Paluszkiewicz EM, Borowa-Mazgaj B, Augustin E, Skwarska A et al. Asymmetric bis-acridines with antitumour activity and their uses. Can Patent No 2 980 084, 07 November 2023.
24. Paluszkiewicz E, Horowska B, Borowa-Mazgaj B, Peszyńska-Sularz G, Paradziej-Łukowicz J, Augustin E, et al. Design, synthesis and high antitumor potential of new unsymmetrical bisacridine derivatives towards human solid tumors, specifically pancreatic cancers and their unique ability to stabilize DNA G-quadruplexes. Eur J Med Chem. 2020;204:112599. https://doi.org/10.1016/j.ejmech.2020.112599.
25. Laskowski T, Kosno M, Andrałojć W, Frackowiak JE, Borzyszkowska-Bukowska J, Szczeblewski P, et al. The interactions of monomeric acridines and unsymmetrical bisacridines (UAs) with DNA duplexes: an insight provided by NMR and MD studies. Sci Rep. 2023;13:3431. https://doi.org/10.1038/s41598-023-30587-y.
26. Pawłowska M, Kulesza J, Augustin E. c-Myc protein level afected by Unsymmetrical Bisacridines Influences Apoptosis and Senescence Induced in HCT116 Colorectal and H460 Lung Cancer cells. Int J Mol Sci. 2022;23:3061. https://doi.org/10.3390/ijms23063061.

27. Bidzinska J, Cimino-Reale G, Zafaroni N, Folini M. G-qua - druplex structures in the human genome as novel therapeutic targets. Molecules. 2013;18:12368–95. https://doi.org/10.3390/molecules181012368.
28. Chen L, Dickerhof J, Sakai S, Yang D. DNA G-Quadruplex in human telomeres and Oncogene promoters: structures, functions, and small molecule targeting. Acc Chem Res. 2022;55:2628–46. https://doi.org/10.1021/acs.accounts.2c00337.
29. Sugimoto H, Nakamura M, Yoda H, Hiraoka K, Shinohara K, Sang M, et al. Silencing of RUNX2 enhances gemcitabine sensitivity of p53-defcient human pancreatic cancer AsPC-1 cells through the stimulation of TAp63-mediated cell death. Cell Death Discov. 2015;1:15010. https://doi.org/10.1038/cddiscovery.2015.10.
30. Mieszkowska A, Nowicka AM, Kowalczyk A, Potęga A, Pawłowska M, Kosno M, et al. Metabolic Profles of New Unsymmetrical Bisacridine Antitumor Agents in Electrochemical and Enzymatic Noncellular systems and in Tumor cells. Pharmaceuticals (Basel). 2021;14:317. https://doi.org/10.3390/ph14040317.
31. Deer EL, González-Hernández J, Coursen JD, Shea JE, Ngatia J, Scaife CL, et al. Phenotype and genotype of pancreatic cancer cell lines. Pancreas. 2010;39:425–35. https://doi.org/10.1097/MPA.0b013e3181c15963.
32. Ozaki T, Nakagawara A. Role of p53 in cell death and human cancers. Cancers (Basel). 2011;3:994–1013. https://doi.org/10.3390/cancers3010994.
33. Abbas T, Dutta A. p21 in cancer: intricate networks and multiple activities. Nat Rev Cancer. 2009;9:400– 14. https://doi.org/10.1038/nrc2657. PMID: 19440234.
34. Karimian A, Ahmadi Y, Yousef B. Multiple functions of p21 in cell cycle, apoptosis and transcriptional regulation after DNA damage. DNA Repair (Amst). 2016;42:63–71. https://doi.org/10.1016/j.dnarep.2016.04.008.
35. Muñoz-Espín D, Serrano M. Cellular senescence: from physiology to pathology. Nat Rev Mol Cell Biol. 2014;15:482–96. https://doi.org/10.1038/nrm3823.
36. Giehl K, Seidel B, Gierschik P, Adler G, Menke A. TGFβ1 represses proliferation of pancreatic carcinoma cells which correlates with Smad4-independent inhibition of ERK activation. Oncogene. 2000;19:4531–41. https://doi.org/10.1038/sj.onc.1203806.
37. Zhao M, Mishra L, Deng CX. The role of TGF-β/SMAD4 signaling in cancer. Int J Biol Sci. 2018;14:111–23. https://doi.org/10.7150/ijbs.23230.
38. Lee S, Lee JS. Cellular senescence: a promising strategy for cancer therapy. BMB Rep. 2019;52:35–41. https://doi.org/10.5483/BMBRep.2019.52.1.294.
39. Salminen A, Ojala J, Kaarniranta K. Apoptosis and aging: increased resistance to apoptosis enhances the aging process. Cell Mol Life Sci. 2011;68:1021–31. https://doi.org/10.1007/s00018-010-0597-y.
40. Hu L, Li H, Zi M, Li W, Liu J, Yang Y, et al. Why senescent cells are resistant to apoptosis: an insight for Senolytic Development. Front Cell Dev Biol. 2022;10:822816. https://doi.org/10.3389/fcell.2022.822816.
41. Rayess H, Wang MB, Srivatsan ES. Cellular senescence and tumor suppressor gene p16. Int J Cancer. 2012;130:1715–25. https://doi.org/10.1002/ijc.27316.
42. Sun C, Yamato T, Furukawa T, Ohnishi Y, Kijima H, Horii A. Characterization of the mutations of the K-ras, p53, p16, and SMAD4 genes in 15 human pancreatic cancer cell lines. Oncol Rep. 2001;8:89–92. https://doi.org/10.3892/or.8.1.89.
43. Ghaneh P, Greenhalf W, Humphreys M, Wilson D, Zumstein L, Lemoine NR, et al. Adenovirus-mediated transfer of p53 and p16(INK4a) results in pancreatic cancer regression in vitro and in vivo. Gene Ther. 2001;8:199–208. https://doi.org/10.1038/sj.gt.3301394.
44. Jo H, Shim K, Jeoung D. The potential of Senescence as a target for developing Anticancer Therapy. Int J Mol Sci. 2023;24:3436. https://doi.org/10.3390/ijms24043436.
45. Wang L, Lankhorst L, Bernards R. Exploiting senescence for the treatment of cancer. Nat Rev Cancer. 2022;22:340–55. https://doi.org/10.1038/s41568-022-00450-9.
46. Petrova NV, Velichko AK, Razin SV, Kantidze OL. Small molecule compounds that induce cellular senescence. Aging Cell. 2016;15:999–1017. https://doi.org/10.1111/acel.12518.
47. Qin S, Schulte BA, Wang GY. Role of senescence induction in cancer treatment. World J Clin Oncol. 2018;9:180–7. https://doi.org/10.5306/wjco.v9.i8.180.
48. Brochure ATCC. *Pancreatic cancer p53 hotspot mutation cell panel*. https://www.atcc.org/-/media/product-assets/documents/panels/cell-biology/pancreatic-p53.pdf?rev=5335112581f94ef6a5441e7cf47e1c97

ARTICLE NO. 2

Pro-Apoptotic Effects of Unsymmetrical Bisacridines in 3D Pancreatic Multicellular Tumor Spheroids

International Journal of Molecular Sciences (2025) 26, 7557; doi: 10.3390/ijms26157557

IF_{2024} = 4.9, Q1, MHES Points: 140

Agnieszka Kurdyn, Ewa Paluszkiewicz, Ewa Augustin

Department of Pharmaceutical Technology and Biochemistry, Faculty of Chemistry, Gdańsk University of Technology, Gabriela Narutowicza 11/12, Gdańsk 80-233, Poland

A primary challenge in oncology is the high failure rate of potential anticancer agents during clinical trials. At the same time, many compounds demonstrate efficacy in traditional two-dimensional monolayer cultures but frequently fail to replicate this performance in patients due to the complex architecture of solid tumors. Multicellular tumor spheroids provide a more physiologically relevant three-dimensional model that successfully recapitulates the nutrient and oxygen gradients, metabolic waste accumulation, and increased chemoresistance characteristic of poorly vascularized tumors *in vivo*.

Given the potent activity of unsymmetrical bisacridine derivatives (C-2028, C-2045, and C-2053) previously observed in 2D pancreatic cultures, the objective of the second scientific article was to validate whether these compounds retain their pro-apoptotic efficacy within a 3D culture model.

The study utilized three human pancreatic cancer cell lines (Panc-1, MIA PaCa-2, and AsPC-1) to generate spheroids using ultra-low attachment (ULA) plates. Following the optimization of cell densities and growth conditions, MCTS were treated with IC_{80} doses of UAs (determined from previous 2D studies). Spheroid growth kinetics and morphological alterations were monitored over 14 days through light microscopy and automated diameter measurements. To quantify the cellular response within the 3D architecture, spheroids were dissociated into single-cell suspensions and subjected to flow cytometry using 7-AAD for viability and Annexin V-FITC/propidium iodide for apoptosis detection. Furthermore, confocal laser scanning microscopy with multiple fluorescent stains (Calcein AM, propidium iodide, Annexin V-FITC, and Hoechst 33342) was used to visualize the spatial distribution of viable, apoptotic, and necrotic cells within the intact 3D structure.

UAs significantly inhibited growth and fundamentally altered the morphology of PC spheroids across all tested lines, leading to growth inhibition and a visible loss of compactness. Panc-1 spheroids were identified as the most sensitive model, exhibiting a total loss of integrity that likely facilitated drug diffusion. Flow cytometric analysis confirmed a substantial increase in the non-viable ($7\text{-}AAD^+$) cell population in both culture models (**Figure 3A**), with specific derivatives showing peak activity against certain lines: C-2045 for Panc-1, C-2028 for

MIA PaCa-2, and C-2053 for AsPC-1. Confocal imaging provided direct evidence of the compounds' efficacy. A marked increase in propidium iodide fluorescence and a corresponding decrease in Calcein AM-positive cells were observed throughout the entire 3D structure, indicating biological activity of UAs within deeper spheroid layers, associated with compromised viability and membrane integrity (**Figure 3B**).

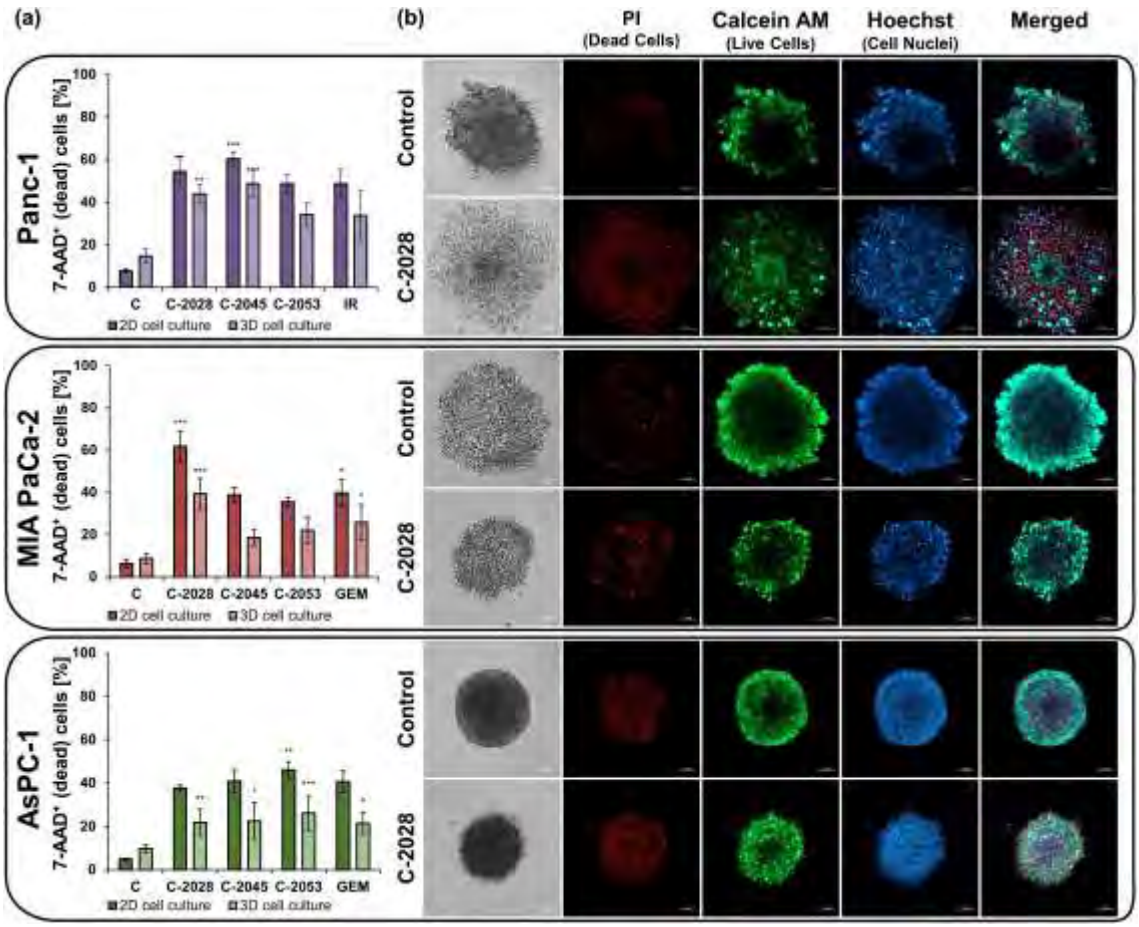

Figure 3. Viability of pancreatic cancer cells cultured in 2D and 3D conditions. Cells were treated with unsymmetrical bisacridine derivatives (UAs; C-2028, C-2045, and C-2053) at IC_{80} doses and positive control compounds (gemcitabine–GEM or irinotecan–IR) at IC_{50} doses for 72 h. **(A)** Bar graphs show the flow cytometry-quantified percentage of dead (7-AAD^+) cells in 2D and 3D cultures after exposure to the tested compounds. **(B)** Representative images of spheroids treated with C-2028 derivative and stained with propidium iodide (PI), calcein AM, and Hoechst 33342. Scale bar 100 µm. The results are presented as the means ± SD. Statistical analysis was performed using the Kruskal–Wallis test for non-parametric data and Dunn's post-hoc test. Significantly different from the control at: * $p < 0.05$, ** $p < 0.01$, *** $p < 0.001$; ($n \geq 2$).

Flow cytometric analysis using Annexin V-FITC/propidium iodide double staining confirmed that apoptosis was the dominant cell death pathway in the 3D model (**Figure 4**). Notably, a specific distribution pattern emerged. In contrast to 2D monolayers, where late-apoptotic cells typically prevailed after 72 h, 3D spheroids showed a predominance of early-apoptotic cells. This disproportion was most statistically significant in Panc-1 spheroids treated with the C-2045 derivative (34.6% early vs. 20.1% late apoptosis). These findings suggest delayed kinetics of cell death in 3D environments, likely due to the gradual penetration of UAs through the compact spheroid structure. Nevertheless, the relative potency of the derivatives

remained consistent across models, as UAs maintained high activity against their respective sensitive cell lines despite the challenges posed by the 3D microenvironment.

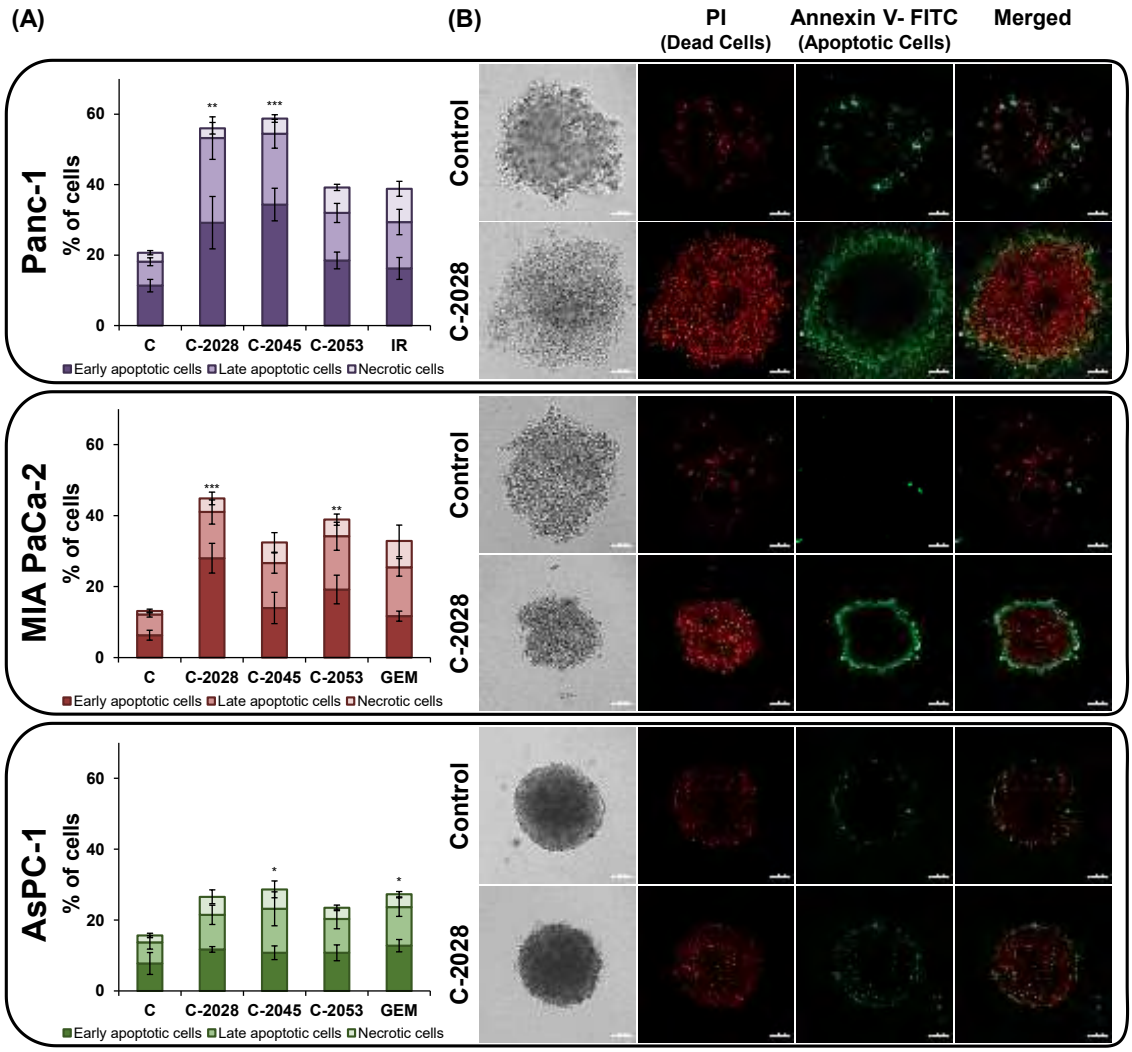

Figure 4. Phosphatidylserine externalization and membrane disruption of pancreatic cancer cells cultured in 3D conditions after treatment with unsymmetrical bisacridine derivatives (UAs; C- 2028, C-2045, and C-2053) at IC_{80} doses and positive control compounds (gemcitabine–GEM or irinotecan–IR) at IC_{50} doses for 72 h. Following compound incubation, propidium iodide (PI)/annexin V–fluorescein isothiocyanate (FITC) dual staining was performed. Early apoptotic cells - annexin V–FITC positive, PI negative; late apoptotic cells - annexin V–FITC positive, PI positive; necrotic cells - annexin V–FITC negative, PI positive. **(A)** Bar graphs show the percentage of early apoptotic, late apoptotic, and necrotic cells in 3D culture after exposure to the tested compounds. **(B)** Representative images of spheroids treated with C-2028 derivative and stained with PI and annexin V–FITC. Scale bar 100 µm. The results are presented as the means ± SD. Statistical analysis was performed using the Kruskal–Wallis test for non-parametric data and Dunn's post-hoc test. Significantly different from the control at: * $p < 0.05$, ** $p < 0.01$, *** $p < 0.001$; ($n \geq 2$).

The research demonstrates that unsymmetrical bisacridines retain robust pro-apoptotic activity, overcoming the inherent resistance associated with the MCTS environment. These findings confirm that the therapeutic potential of UAs is not significantly limited by the physical barriers observed in solid tumors. By sustaining efficacy in a more physiologically relevant model characterized by hypoxia and nutrient gradients, this study provides a vital scientific bridge between initial *in vitro* screening and future *in vivo* validation.

International Journal of Molecular Sciences

MDPI

Article

Pro-Apoptotic Effects of Unsymmetrical Bisacridines in 3D Pancreatic Multicellular Tumor Spheroids

Agnieszka Kurdyn, Ewa Paluszkiewicz and Ewa Augustin*

Department of Pharmaceutical Technology and Biochemistry, Faculty of Chemistry, Gdansk University of Technology, Gabriela Narutowicza Str. 11/12, 80-233 Gdansk, Poland; agnieszka.kurdyn@pg.edu.pl (A.K.); ewa.paluszkiewicz@pg.edu.pl (E.P.)

* Correspondence: ewa.augustin@pg.edu.pl; Tel.: +48-58-347-14-68

Abstract

Pancreatic cancer (PC) is an aggressive malignancy with a poor prognosis, requiring innovative approaches to evaluate new therapies. Considering the high activity of unsymmetrical bisacridines (UAs) in PC monolayer cultures, we employed multicellular tumor spheroids (MCTS) to assess whether UAs retain pro-apoptotic activity under more physiologically relevant conditions. Ultra-low attachment plates were used to form spheroids from three PC cell lines (Panc-1, MIA PaCa-2, and AsPC-1) with different genotypes and phenotypes. The effects of UA derivatives (C-2028, C-2045, and C-2053) were evaluated using microscopy and flow cytometry (7-AAD for viability and annexin V-FITC/PI for membrane integrity). UAs altered the morphology of the spheroids and reduced their growth. Notably, Panc-1 spheroids exhibited compromised integrity. The increase in 7-AAD$^+$ cells confirmed diminished cell viability, and annexin V-FITC assays showed apoptosis as the dominant death pathway. Interestingly, the exact derivative was most active against a given cell line regardless of culture conditions. These results confirm that UAs maintain anticancer activity in 3D cultures and induce apoptosis, with varying efficacy across different cell lines. This underscores the value of diverse cellular models in compound evaluation and supports UAs as promising candidates for pancreatic cancer therapy.

Keywords: unsymmetrical bisacridines; pancreatic cancer; multicellular tumor spheroids; apoptosis; anticancer activity

Academic Editor: Emily Capone

Received: 14 July 2025
Revised: 31 July 2025
Accepted: 1 August 2025
Published: 5 August 2025

Citation: Kurdyn, A.; Paluszkiewicz, E.; Augustin, E. Pro-Apoptotic Effects of Unsymmetrical Bisacridines in 3D Pancreatic Multicellular Tumor Spheroids. *Int. J. Mol. Sci.* **2025**, *26*, 7557. https://doi.org/10.3390/ijms26157557

1. Introduction

Despite modern methods of cancer treatment and diagnosis, there is still a high demand for anticancer drugs with the highest possible efficacy and the lowest toxicity. Pancreatic cancer (PC) is notorious for its poor prognosis and high treatment resistance [1,2]. The overall five-year survival rate of less than 13% [3] reflects the aggressive nature of this cancer. Current treatment options, including surgery, chemotherapy, and radiation therapy, can extend survival time, but rarely provide a cure. The multidrug FOLFIRINOX (irinotecan, 5-fluorouracil, leucovorin, and oxaliplatin), which improves the median survival to 11.7 months, compared to 6.8 months with previous standard treatment with gemcitabine [4]. Recently, the FDA approved NALIRIFOX, which substitutes irinotecan with liposomal irinotecan, offering a new first-line therapy for metastatic PC [5]. However, pancreatic cancer exhibits pronounced resistance to standard therapies through several mechanisms. Its tumor microenvironment is marked by extensive desmoplastic stroma and poor vascularization, both of which hinder the delivery of drugs to cancer cells [6].

Additionally, pancreatic cancer cells often display intrinsic resistance via the overexpression of drug efflux pumps, such as multidrug resistance protein 1 (MDR1), also known as P-glycoprotein [7]. They also possess enhanced DNA damage repair mechanisms, altered apoptotic pathways, and activated pro-survival signaling pathways, including the PI3K/Akt and NF-κB pathways [8]. These factors collectively reduce the effectiveness of standard chemotherapy, contributing to rapid disease progression and recurrence. Consequently, overcoming chemoresistance remains a key goal in the development of new treatment strategies for pancreatic cancer.

Unsymmetrical bisacridine derivatives (UAs), as presented in Figure 1, are patented compounds with high anticancer properties that have been developed and widely studied by researchers from the Gdańsk University of Technology [9]. The chemical structure of UAs consists of an imidazoacridone and 1-nitroacridine moieties linked with an aminoalkyl chain (Figure 1). Extensive preliminary studies enabled the selection of three UA derivatives, C-2028, C-2045, and C-2053, which showed high activity against pancreatic cancer cells in particular [9]. Notably, UAs preferentially bind with G-quadruplex structures in oncogene promoters such as *KRAS* and *MYC* [9,10], rather than double-stranded DNA [11]. Modulation of c-Myc protein level by UAs resulted in apoptosis induction in colorectal (HCT116) and lung (H460) cancer cells [12]. Most importantly, this selective binding in pancreatic cancer monolayer (2D) cultures leads to the downregulation of the c-Myc protein level, inducing apoptosis, a process also facilitated by SMAD4 upregulation. In addition, UAs promote accelerated cellular senescence in MIA PaCa-2 cells by upregulating p21, with senescent cells eventually undergoing apoptosis following prolonged exposure [13]. Previous studies have also demonstrated the effectiveness of these compounds in three-dimensional (3D) culture models [14]. In colorectal (HCT116) and lung (A549) cancer cell-derived spheroids, UAs significantly inhibited spheroid growth and viability, confirming their ability to penetrate and act within the compact spheres. Further studies confirmed that UAs induce apoptosis in this culture model, consistent with their mechanism in monolayer cultures [14].

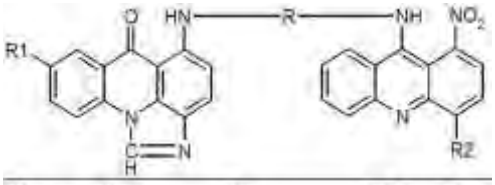

Compound	R	R1	R2
C-2028		-H	-H
C-2045	$-(CH_2)_3-N(CH_3)-(CH_2)_3-$	-OH	$-CH_3$
C-2053		-H	$-CH_3$

Figure 1. Chemical structures of tested unsymmetrical bisacridine derivatives: C-2028, C-2045, and C-2053.

Considering the 2D culture results, this study aimed to test whether three UA derivatives—C-2028, C-2045, and C-2053—would exhibit similarly effective pro-apoptotic activity in PC cells cultured under 3D conditions. The application of multicellular tumor spheroids (MCTS) provides a robust and widely used platform for cancer research due to the diversity of methods used to generate them [15] and, most importantly, by more accurately representing the tumor microenvironment compared to traditional 2D cultures [16]. Spheroids consist of diverse zones defined by gradients of nutrients, oxygen, metabolites, waste, and pH, also present in poorly vascularized tumors [17]. MCTS are increasingly used

for screening of new compounds, especially in PC cells that exhibit distinct morphological and functional characteristics in 3D cultures [18], which better reflect the complexity of this tumor biology [19].

The cell lines used in the current study, Panc-1, MIA PaCa-2, and AsPC-1, differ in their genetic profile [20] as well as the phenotype and expression of molecules responsible for cell–cell contacts [21]. Panc-1 and MIA PaCa-2 cells exhibit quasi-mesenchymal (epithelial and mesenchymal) features [22]. However, the Panc-1 cells express E-cadherin, reflecting a more epithelial-like phenotype, in contrast to MIA PaCa-2, which completely lacks this protein [23,24]. AsPC-1 cells are characterized by high levels of E-cadherin expression [23] and exhibit features of an intermediate phenotype between epithelial and mesenchymal states [25]. This morphological distinction within applied cell lines influences nutrient and oxygen gradients, affecting drug penetration and efficacy.

Since MCTS are more resistant to chemo- and radiotherapy compared to cells cultured in monolayers [26,27], this study examined whether UAs retain high anticancer activity against Panc-1, MIA PaCa-2, and AsPC-1 cells cultured under 3D conditions. To address this, we determined changes in the morphology, size, and viability of pancreatic cancer spheroids treated with UAs, as well as identified the main type of cellular response induced by these compounds.

2. Results

1. Optimization of 3D Culture Conditions

The first necessary step when starting research on a 3D cell culture model is to verify the ability of the tested cells to form multicellular tumor spheroids (MCTS), and if so, to determine the culture conditions. Generation of spheroids from cells at different densities using the ULA (ultra-low attachment) plates proved that the studied Panc-1, MIA PaCa-2, and AsPC-1 cells can form spheres (Figures S1–S3 in Supplementary Materials). Both Panc-1 and MIA PaCa-2 spheres exhibit similar morphometric features, such as a nearly spherical shape with jagged edges. In turn, AsPC-1 cell-derived spheroids were more condensed compared to the spheroids of the other tested lines, with an almost perfectly spherical shape and even edges. Moreover, the obtained spheroids exhibited a constant increase in size during incubation time and a high content of viable cells, which did not differ between spheroids, despite the varying numbers of cells from which they were generated. Cell viability on day 3 was assessed by flow cytometry using 7–AAD dye, and in Panc-1 cells, the content of 7–AAD$^-$ (viable) cells ranged from 79.8% to 85.8%. In MIA PaCa-2 and AsPC-1 cell-derived spheroids, the percentage of viable cells was approximately 90%. Due to these observations, the spheroids of the studied cell lines are a promising culture model, and their steady growth and high viability of the cells that form MCTS allow further research on this model. Considering that the required spheroids diameter on day 0 (72 h after seeding) should be in the range of 300–500 µm [28], spheroids that were about 450 µm were used for further experiments, i.e., those generated from 1200 cells/well for Panc-1 cells, 500 cells/well for MIA PaCa-2 cells, and 4500 cells/well for AsPC-1 cells were used for further experiments.

2. Spheroid Size and Morphology Assessment After UAs Treatment

The study of the effect that UAs induce in spheroids began with microscopic observation. Spheroids generated under the conditions determined in the previous paragraph, *Optimization of 3D culture conditions*, were exposed to UAs at a dose of IC_{80} and positive control compounds at a dose of IC_{50} (Table 1), and then subjected to 14 days of observation by taking photographs and diameter measurements every 2–3 days (Figure 2 and Figures S4–S6 in the Supplementary Materials). The selection of reference compounds and

the doses of all compounds were based on previously conducted studies using pancreatic cancer cells cultured in 2D [13].

Table 1. Cytotoxicity of unsymmetrical bisacridine derivatives (C-2028, C-2045, and C-2053) and positive control (gemcitabine—GEM or irinotecan—IR) against Panc-1, MIA PaCa-2, and AsPC-1 cells after 72 h of treatment. Data are expressed as IC_{50} and IC_{80} values, based on previously conducted studies on pancreatic cancer cells cultured in 2D [13].

Compound	Compound Dose [μM]	Cell Line		
		Panc-1	MIA PaCa-2	AsPC-1
C-2028	IC_{80}	0.043 ± 0.002	0.042 ± 0.002	0.102 ± 0.007
C-2045	IC_{80}	0.323 ± 0.043	0.086 ± 0.001	0.463 ± 0.011
C-2053	IC_{80}	0.080 ± 0.012	0.072 ± 0.004	0.486 ± 0.005
GEM	IC_{50}	not applicable	0.062 ± 0.010	0.026 ± 0.003
IR	IC_{50}	8.5 ± 0.13	not applicable	not applicable

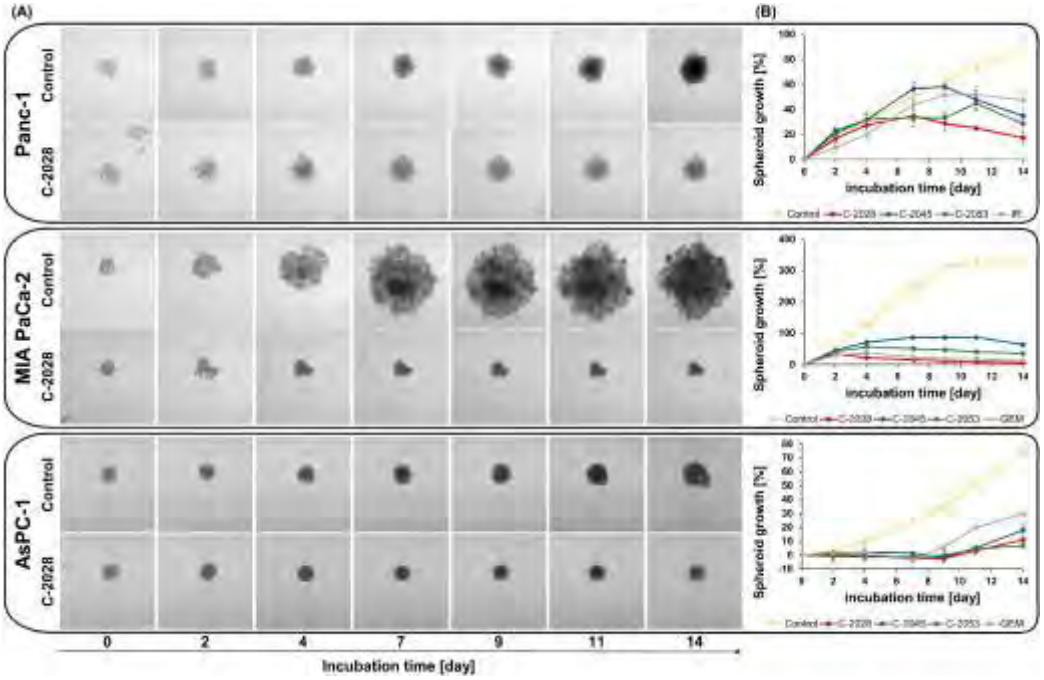

Figure 2. Morphology and kinetics of spheroids derived from pancreatic cancer cells after treatment with unsymmetrical bisacridine derivatives (UAs): C-2028, C-2045, and C-2053. Panc-1, MIA PaCa-2, and AsPC-1 spheroids were incubated with UAs at IC_{80} doses and positive control compounds (gemcitabine–GEM or irinotecan–IR) at IC_{50} doses for 14 days, and spheroid images were taken and their diameters were measured every 2–3 days. (**A**) Representative images of spheroids obtained from Panc-1, MIA PaCa-2, and AsPC-1 cells treated with C-2028 derivative. (**B**) Spheroid growth kinetics after exposure to UAs and positive control compounds are shown as spheroid growth compared to day 0 over time. Scale bar 200 μm. (n = 4).

Control Panc-1 cell spheroids showed a steady increase in growth over time and became more compact and spherical. Treatment with the tested unsymmetrical bisacridines and irinotecan (IR) resulted in the morphology changes in the obtained spheroids

(Figure 2 and Figure S4 in the Supplementary Materials). After only 4 days of incubation, compound-treated spheroids became loose with irregular edges, and the cells forming the spheroids shrank. Spheroids treated with the C-2028 derivative showed the strongest growth inhibition, only a 17% increase, while C-2045 and irinotecan led to more diffuse spheroids with 35% and 47% increases, respectively, after 14 days of incubation.

Control spheroids generated from MIA PaCa-2 cells (Figure 2) exhibited rapid growth, with a growth rate of 338% after 14 days (Figure S5 in the Supplementary Materials). Their structure was heterogeneous, characterized by areas of higher cell density and jagged, uneven edges. Treatment of the spheroids with the compounds significantly reduced their proliferative capacity, resulting in them being much smaller than the control spheroids. The spheroids exposed to the C-2028 derivative were the most compact. They were characterized by the smallest diameter already on the fourth day of incubation—a 21% increase in size compared to day 0 (Figure S5 in the Supplementary Materials). Treatment with C-2045 and C-2053 resulted in reduced proliferation and the formation of loose, irregular spheroids. After 14 days, their diameters increased by 63% and 35%, respectively, whereas C-2028 showed the most effective growth inhibition, with only a 5% increase in diameter. Treatment with gemcitabine (GEM), as with the C-2028 derivative, caused shrinkage of the spheroids, except that this occurred after the seventh day of incubation, and their structure was less compact.

The morphology of the spheroids generated from AsPC-1 cells (Figure 2 and Figure S6 in the Supplementary Materials), not treated with the compounds, was homogeneous, and they maintained their spherical shape even up to the 11th day of incubation. Compared to MIA PaCa-2 spheroids, those obtained from AsPC-1 cells showed slower and more restricted growth. Treatment of AsPC-1 spheroids with UAs and GEM resulted in morphology changes after the seventh day of exposure (Figure S6 in the Supplementary Materials). The spheroids had a smooth periphery up to day 4 of incubation, while a diffuse outer layer of cells was observed from day 7 onward. All UAs similarly reduced the spheroid growth after 14 days (7–18%) (Figure S6 in the Supplementary Materials). In contrast, gemcitabine caused loss of spheroid integrity with the largest diameter increase among the tested compounds (30%) (Figure S6 in the Supplementary Materials). In general, C-2028 showed the most substantial growth inhibitory effect in all cell lines.

2.3. The Impact of UAs on Cell Viability in 2D and 3D

Exposure to UAs altered MCTS morphology, indicating reduced cell proliferation and induction of cell death. To determine viability, cells were cultured under 2D and 3D conditions and then treated for 72 h with UAs at IC_{80} and positive control compounds at IC_{50}. The cells were then stained with 7–AAD, which binds to the DNA of damaged cells, and subjected to flow cytometry analysis (Figure 3A and Tables S1 and S2 in Supplementary Materials).

In monolayer culture, Panc-1 cells treated with UAs for 3 days exhibited a higher percentage of dead cells compared to the untreated control (Figure 3A and Table S1 in the Supplementary Materials). Among the compounds tested, C-2045 induced cell death to the greatest extent (60.4%, $p < 0.001$, Figure 3A), while C-2028 and C-2053 caused a moderate effect (48.6–54.5% of 7-AAD$^+$ cells, Table S1 in the Supplementary Materials). In contrast, the spherical culture initially had a lower content of viable cells compared to the 2D culture, and the viable cell content in the control spheroids reached 85.3% after 72 h of incubation (Figure 3A and Table S2 in the Supplementary Materials). The Panc-1 cells cultured in 3D conditions were also the most sensitive to the C-2045 derivative, inducing death in 48.7% ($p < 0.001$, Figure 3A) of the cells. The percentage of 7-AAD$^+$ cells after exposure to the

C-2028 derivative was 43.8% ($p < 0.01$, Figure 3A), while C-2053 and IR had a very similar effect of 34.3–33.7% non-viable cells (Table S2 in the Supplementary Materials).

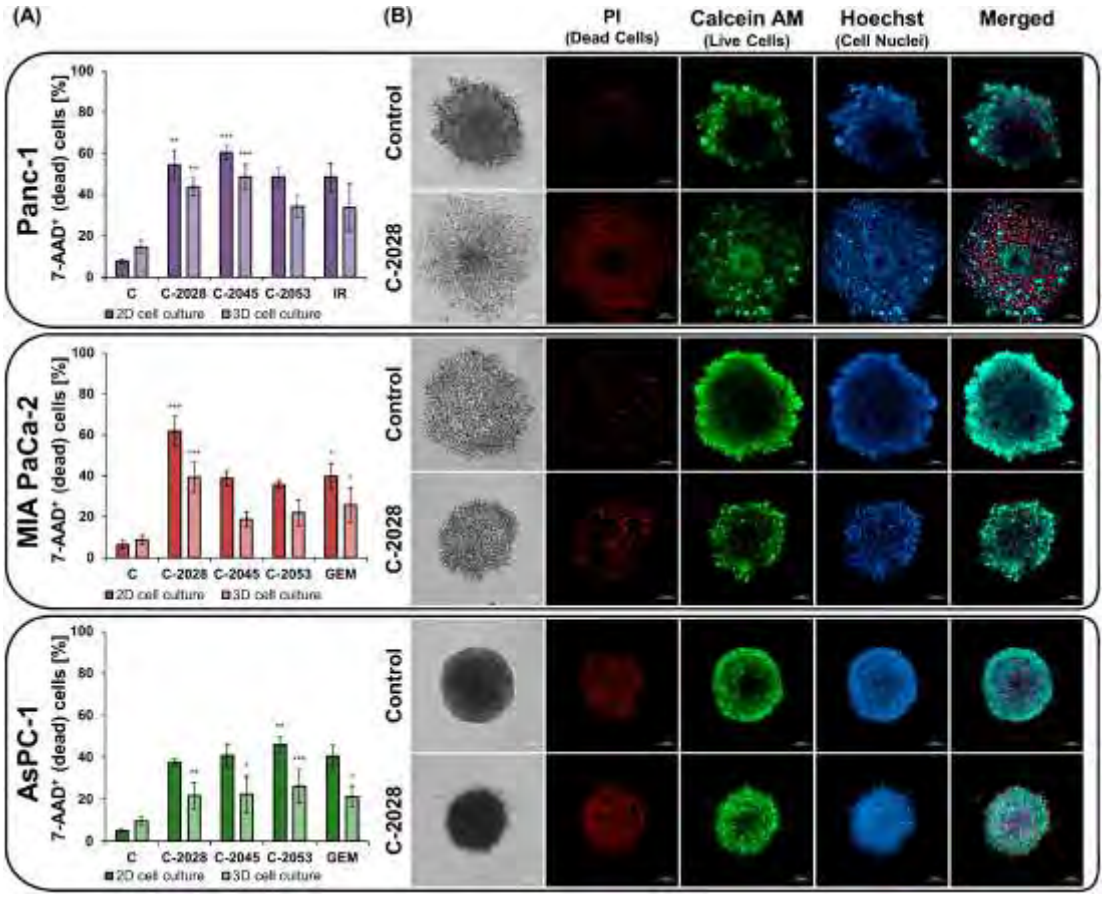

Figure 3. Viability of pancreatic cancer cells cultured in 2D and 3D conditions after treatment with unsymmetrical bisacridine derivatives (UAs): C-2028, C-2045, and C-2053. Panc-1, MIA PaCa-2, and AsPC-1 cells were incubated with UAs at IC_{80} doses and positive control compounds (gemcitabine–GEM or irinotecan–IR) at IC_{50} doses for 72 h, followed by viability analysis using flow cytometry (2D and 3D) and imaging using confocal microscopy (3D). (**A**) Bar graphs show the flow cytometry-quantified percentage of dead (7-AAD$^+$) cells in 2D and 3D cultures after exposure to the tested compounds. (**B**) Representative images of spheroids treated with C-2028 derivative and stained with propidium iodide (PI), calcein AM, and Hoechst 33342. Scale bar 100 µm. Statistical analysis was performed using the Kruskal–Wallis test followed by Dunn's post hoc test. Differences versus control: * $p < 0.05$, ** $p < 0.01$, *** $p < 0.001$. ($n \geq 2$).

MIA PaCa-2 cells cultured in 2D conditions were characterized by a high content of alive cells—93.6% (Figure 3A and Table S1 in the Supplementary Materials). Exposure to UAs significantly increased the 7-AAD$^+$ dead cell population to the greatest extent for the C-2028 derivative—61.8% ($p < 0.001$, Figure 3A). The percentage of dead cells after treatment with C-2045, C-2053, and GEM was similar, reaching 38.8%, 35.6%, and 39.8%, respectively ($p < 0.05$, Figure 3A). Untreated cells cultured in both 3D and 2D conditions also showed a high content of viable cells—90.4% (Figure 3A and Table S2 in the Supplementary Materials). Similarly to the 2D culture, C-2028 was the most potent in spheroid culture,

inducing cell death in 39.4% of cells ($p < 0.001$, Figure 3A), followed by C-2045, C-2053, and GEM with a non-viable cell population in the range of 18.7–25.8% (Table S2 in the Supplementary Materials).

AsPC-1 cells cultured as monolayers also demonstrated high viability, reaching 95% of the cell population (Figure 3A and Table S1 in the Supplementary Materials). Exposure of the cells to UAs and GEM increased the dead cell population to a range of 37.7–46.1% (Table S1 in the Supplementary Materials), and the best effect was produced by the C-2053 derivative—46.1% ($p < 0.01$, Figure 3A). Control spheroids were characterized by a high level of viable cells, 90.3%, and exposure to the test compounds, as in 2D cultures, caused an effect at a similar level (Figure 3A and Table S2 in the Supplementary Materials). The C-2028 derivative induced death in 21.7% ($p < 0.01$, Figure 3A) of cells, C-2045—22.5% ($p < 0.05$, Figure 3A), and GEM—21.4% ($p < 0.05$, Figure 3A). As in 2D culture, C-2053 proved to be the most active against AsPC-1 spheroids, resulting in the death of 26.1% of the cell population ($p < 0.001$, Figure 3A).

To visualize and confirm the results of cytometric analysis for 3D cultures, spheroid imaging was performed after 72 h of compound treatment (Figure 3B and Figures S7–S9 in the Supplementary Materials). Hoechst 33342 was used to determine the total cell count, while calcein AM marked only metabolically active cells. Propidium iodide (PI) was used to distinguish between dead cells with compromised membranes and live cells.

As shown in Figure 3B, control spheroids Panc-1, MIA PaCa-2, and AsPC-1 showed mainly calcein AM-positive cells. Green staining was predominantly localized in the outer layers of the 3D structure, where cells have easier access to nutrients and oxygen. Weak PI positivity was observed, indicating that only a small percentage of cancer cells forming spheroids underwent cell death. In contrast, spheroids treated with UAs and positive control compounds (Figure 3B and Figures S7–S9 in the Supplementary Materials) exhibited an increase in PI fluorescence accompanied by a decrease in the number of calcein-positive cells. As in the control, in compound-treated spheroids, calcein AM-positive cells were present mainly at the periphery of their structure. In contrast, cells labeled with propidium iodide were observed throughout the spheroid structure. These observations demonstrate the induction of cell death in the spheroids exposed to UAs and confirm the results of cytometric analysis.

2.4. AnnexinV–FITC/PI Double Staining

Considering that UAs cause cell death in spheroids and that the main type of death induced under 2D conditions was apoptosis [13], the next step was to test whether the same kind of cell death would occur in spheroids. Accordingly, spheroids were incubated for 72 h with UAs at IC_{80} doses and reference compounds at IC_{50} doses. Then, the cells were stained with annexin V–FITC/PI and subjected to flow cytometry analysis (Figure 4A and Table S3 in the Supplementary Materials).

Cytometric analysis showed an increase in the population of dead cells, mainly apoptotic cells, in UA-treated spheroids compared to controls (Figure 4A and Table S3 in the Supplementary Materials). A slight predominance of early-apoptotic cells over late-apoptotic cells was observed for most compounds studied; however, this difference reached statistical significance only in Panc-1 spheroids treated with C-2045 ($p < 0.05$). Necrosis was induced in a small percentage of all cells tested in 3D culture. For UAs, the population of PI-positive cells did not exceed 7.2%, whereas for reference compounds, it reached a maximum of 9.5%.

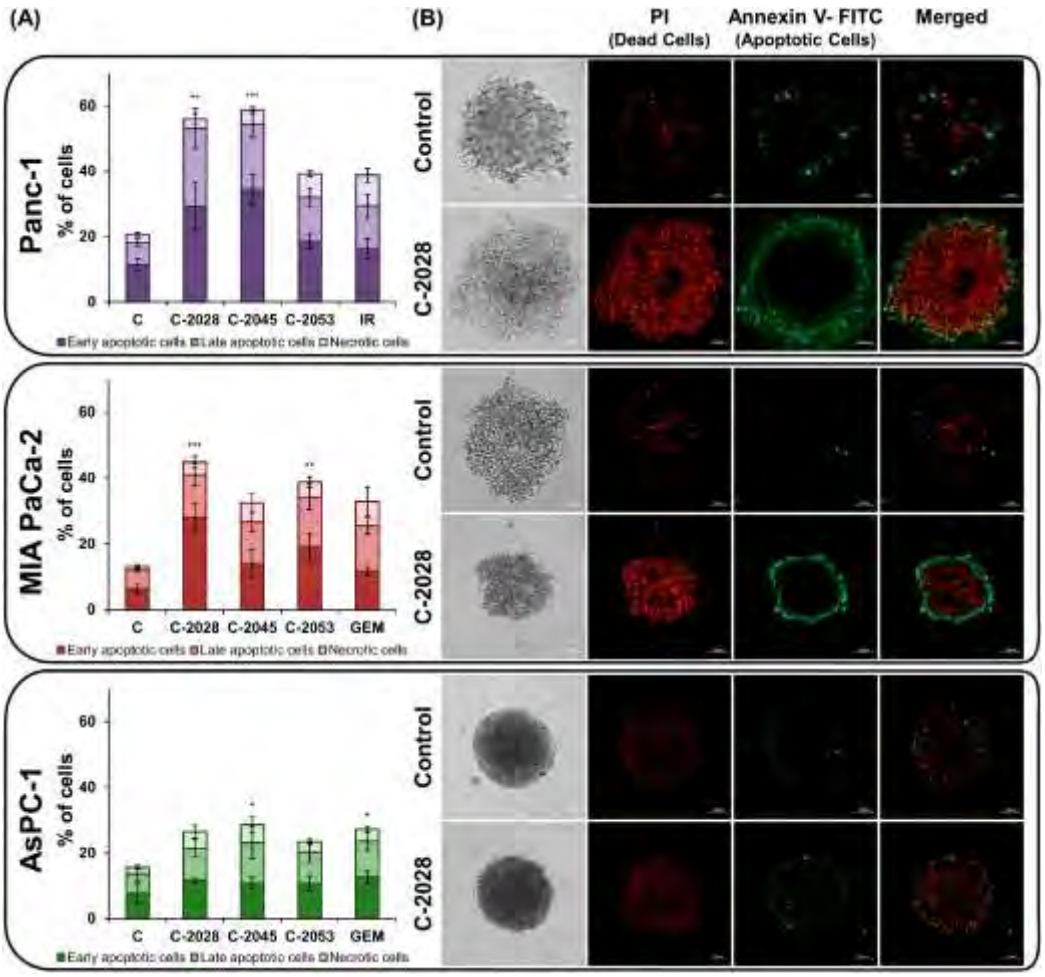

Figure 4. Phosphatidylserine externalization and membrane disruption of pancreatic cancer cells cultured in 3D conditions after treatment with unsymmetrical bisacridine derivatives (UAs): C-2028, C-2045, and C-2053. Panc-1, MIA PaCa-2, and AsPC-1 spheroids were incubated with UAs at IC_{80} doses, and positive control compounds (gemcitabine–GEM or irinotecan–IR) at IC_{50} doses for 72 h, followed by propidium iodide (PI)/annexin V–fluorescein isothiocyanate (FITC) dual staining. Early apoptotic cells—annexin V–FITC positive, PI negative; late apoptotic cells—annexin V–FITC positive, PI positive; necrotic cells—annexin V–FITC negative, PI positive. (**A**) Bar graphs show the percentage of early apoptotic, late apoptotic, and necrotic cells in 3D culture after exposure to the tested compounds. (**B**) Representative images of spheroids treated with C-2028 derivative and stained with PI and annexin V–FITC. Scale bar 100 µm. Statistical analysis was performed using the Kruskal–Wallis test followed by Dunn's post hoc test. Differences versus control: * $p < 0.05$, ** $p < 0.01$, *** $p < 0.001$. ($n \geq 2$).

Spheroids generated from Panc-1 and MIA PaCa-2 cells, which were characterized by a less compact structure, appeared to be more sensitive to UA derivatives compared to AsPC-1 spheroids. Panc-1 spheroids were similarly susceptible to C-2028 and C-2045; apoptosis was induced in 53.2 and 54.0% of the cell population, respectively (Table S3 in the Supplementary Materials). Total number of dead cells, including necrosis, was 56.0% ($p < 0.01$, Figure 4A) for C-2028 and 58.4% ($p < 0.001$, Figure 4A) for C-2045. The

C-2045 induced the greatest disproportion between early (34.6%) and late (20.1%) apoptosis. C-2053 was less effective (32.0% apoptotic cells), while irinotecan induced apoptosis in only 29.4% of cells (Table S3 in the Supplementary Materials). In MIA PaCa-2 cells, exposure to the C-2028 derivative resulted in phosphatidylserine translocation in the highest percentage of cells—41.0%, of which 28.0% were early apoptotic cells, and the total number of dead cells was 44.8% ($p < 0.001$, Figure 4A). C-2053 caused a weaker effect, resulting in 34.2% apoptotic cells, and when including necrotic cells, a total of 38.9% ($p < 0.01$, Figure 4A), whereas C-2045 and GEM induced cell death by apoptosis at similar levels, 26.6 and 25.4% (Table S3 in the Supplementary Materials). AsPC-1 spheroids were more resistant, with a comparable degree of apoptosis induction across all compounds, ranging from 20.3% to 23.7% (Table S3 in the Supplementary Materials). C-2045 led to 23.2% of apoptotic cells, and including necrosis, a total of 28.7% ($p < 0.05$, Figure 4A) dead cells. In comparison, GEM had an equivalent effect, inducing 23.7% (Table S3 in the Supplementary Materials) apoptotic cells and a total of 27.3% ($p < 0.05$, Figure 4A) dead cells. In turn, C-2028 and C-2053 triggered early and late apoptosis in 21.5% and 20.3% of cells, respectively (Table S3 in the Supplementary Materials).

Spheroid imaging was used to detect early- and late-apoptotic cells, as well as necrotic cells, after 72 h of compound treatment. As in the cytometric analysis, annexin V–FITC stained apoptotic cells, while PI stained necrotic and late apoptotic cells (Figure 4B).

As shown in Figure 4B and Figures S10–S12 in the Supplementary Materials, the fraction of apoptotic and necrotic cells was significantly lower in untreated spheroids of all tested cell lines, compared to spheroids exposed to UA compounds. In the merged images, especially of compound-treated spheroids, it is possible to distinguish between early-apoptotic cells, whose cell membranes were stained green with annexin V–FITC, and late-apoptotic cells, which were stained with both annexin V–FITC and propidium iodide. Accordingly, late-apoptotic cells are observed as red-stained interiors where PI has bound to DNA, surrounded by a green envelope, containing red-stained DNA inside. These observations qualitatively confirm the results of the cytometric analysis—the induction of apoptosis in spheroids formed from pancreatic cancer cells.

3. Discussion

The results presented in the current study on multicellular tumor spheroids derived from Panc-1, MIA PaCa-2, and AsPC-1 cells provide critical insights into the efficacy of three highly active unsymmetrical bisacridine derivatives. UAs significantly altered the morphology of treated spheroids and reduced their growth. These changes were caused by the induction of cell death, particularly apoptosis, demonstrating the anticancer nature of the tested compounds against pancreatic cancer cells cultured under 3D conditions.

Our recently published work proved that UAs exhibit high anticancer potential against pancreatic cancer cells cultured as monolayers [13]. Given the increasing popularity of the three-dimensional culture model, studies were conducted to evaluate the effect of UAs on cells with different phenotypes, specifically Panc-1, MIA PaCa-2, and AsPC-1, cultured under 3D conditions. The use of a 3D culture model has many advantages, including a closer representation of in vivo conditions; however, anticancer compounds may appear effective in 2D but lose potency in a more biologically relevant 3D environment [29]. Therefore, the present study aimed to determine whether UA derivatives retain potent pro-apoptotic efficacy under more physiologically relevant conditions.

Morphological distinction within applied cell lines can affect drug penetration and efficacy. As a result, loose spheroids may allow for better diffusion of therapeutic agents compared to compact spheroids, potentially leading to varied responses to treatment across different cell lines [16]. Such phenomena were observed in our study. Tested UAs inhibited

spheroid growth to the greatest extent in highly proliferative MIA PaCa-2 cells, with C-2028 being the most active derivative. The less dense structure of these spheres with jagged edges allowed for reaching the interior of the spheroid, thus facilitating the compound action. In most dense AsPC-1 cell-derived spheroids, all UAs inhibited growth more than GEM, with C-2053 showing the most substantial effect. A different impact from that observed in MIA PaCa-2 and AsPC-1 occurred in Panc-1 spheres treated with the compounds. In addition to a reduction in the size of spheroids exposed to compounds, a significant dispersion of their structure was observed, mainly after C-2028 treatment. Inhibition of the growth of the spheroid as well as loss of its integrity under the influence of the anticancer compound are the most frequently observed changes, which strictly depend on the mechanism of action of the compounds [30], but also on the cell lines applied. In our previous studies, after using the same UA derivatives, a reduction in the size of A549 spheroids, along with an incoherent layer of peripheral cells, was observed in HCT116 spheroids [14]. Notably, the spheroids of lung and colon cancers had a distinct morphology from the spheroids presented in this study, most closely resembling those observed for AsPC-1 cells.

Alternations of spheroids' morphology after treatment with UAs indicated a reduction in cell viability and proliferation; therefore, cytometric 7–AAD viability analysis was conducted. Since cells in 3D cultures can exhibit drug resistance and different survival characteristics, making them less susceptible to cytotoxic compounds compared to those grown in 2D [31,32], here we assessed the distribution of pancreatic cancer cell viability cultured under 2D and 3D conditions. Firstly, untreated cells cultured as a monolayer exhibited a lower population of dead cells compared to 3D conditions. This distinction can be explained by the gradients of oxygen and nutrients that can lead to a necrotic core in the three-dimensional structure of spheroids. At the same time, monolayer cultures do not experience such gradients [33]. Most importantly, the results proved that UAs reduced the population of viable cells in 3D compared to the control. In addition, cells cultured under both conditions and exposed to UA were most sensitive to the exact derivative: C-2045 for Panc-1, C-2028 for MIA PaCa-2, and C-2053 for AsPC-1. Positive control drugs caused less cell death than at least one UA derivative in all cells. Moreover, Panc-1 cell-derived spheroids were the most sensitive to UAs, likely due to the UA-induced loss of spheroid integrity, which facilitates the diffusion of drugs. Fluorescence staining confirmed decreased viability and membrane integrity after UA exposure, as evidenced by the increase in PI-positive cells along with the decrease in calcein AM-positive cells [34,35]. Calcein also indicated uptake, efflux, and inward diffusion within spheroids, revealing the dynamics of the drug in a 3D environment [36]. The peripheral fluorescence suggested active efflux transporter activity, such as MDR1 [37,38]. Although UAs are MDR1 substrates, they do not affect the expression of ABCB1, ABCC1, and ABCC2 genes in certain cancer cells, suggesting a lower risk of developing resistance and highlighting their strong anticancer potential [39].

Identification of the type of cell death induced by UAs using annexin V-FITC and propidium iodide staining indicated apoptosis, with a low level of necrosis observed. Moreover, the early-apoptotic cell fraction was slightly higher in spheroids exposed to compounds, although statistical significance was achieved only in Panc-1 spheroids treated with C-20245. In contrast, as reported in our previous work [13], after 72 h of compound treatment, the late-apoptotic cell fraction prevailed in 2D. This shift suggests delayed compound action by limited penetration through the spheroid structure [40]. Nevertheless, all the UA derivatives studied had high activity in 3D, sometimes slightly better than in 2D [13]. For instance, C-2028 caused more cell death in Panc-1 spheroids (56%) than in 2D (42.5%). Similarly, C-2045 was about 5% more active in 3D across all cell lines, and C-2028

caused nearly 14% more death in MIA PaCa-2 spheroids than in 2D [13]. However, it is worth noting that baseline cell death was higher in untreated spheroids than in monolayers.

The high potential of UAs in pancreatic MCTS may be related to the acidic spheroid microenvironment [41], which enhances UAs' solubility, uptake, and stability. Our previous studies indicate that UAs exhibit enhanced anticancer activity under acidic conditions due to the protonation of functional groups at lower pH, which increases their solubility and promotes interactions with cancer cell membranes, thereby improving cellular uptake [42]. Conversely, positive controls (IR or GEM) performed worse in 3D, aligning with other studies reporting diminished GEM efficacy in MIA PaCa-2 spheroids [27], whereas a common approach in the literature to overcome the resistance of MIA PaCa-2 and AsPC-1 spheroids to GEM is its administration in combination with other anticancer compounds [40,43]. Although the search for new combination therapies with gemcitabine is still ongoing to potentially increase efficacy against pancreatic cancer, it is essential to note that its use may carry risks related to toxicity and the development of resistance, leading to only marginal survival benefits [44].

Summing up, this study highlights the pro-apoptotic potential of UAs against PC cells, a notoriously drug-resistant malignancy. The morphological differences among spheroids of Panc-1, MIA PaCa-2, and AsPC-1 cells, along with their varied responses to UA treatment, underscore the importance of three-dimensional models in evaluating anticancer compounds. Based on our previous studies using a 2D pancreatic cancer culture model, UAs were found to induce apoptosis by downregulating the c-Myc protein, the primary molecular target of these compounds [13]. Although the molecular profile in 3D cultures may differ from that observed in 2D, it is promising that UAs triggered a similar final cellular response while sustaining robust anticancer activity, even in the more challenging 3D spheroids. These findings lay the groundwork for future research on unsymmetrical bisacridines in more advanced 3D models and, subsequently, in animal models, supporting their continued evaluation as candidates for pancreatic cancer therapy.

4. Materials and Methods

1. Tested Compounds

Three unsymmetrical bisacridine derivatives (UAs), C-2028, C-2045, and C-2053, were synthesized as hydrochlorides at the Department of Pharmaceutical Technology and Biochemistry, Gdańsk University of Technology, according to the procedure previously published [9]. Stock solutions of the UAs were prepared in sterile, deionized Milli-Q water (Merck/Millipore, Burlington, MA, USA). The positive control drugs, gemcitabine and irinotecan (Merck/Sigma-Aldrich, St. Louis, MO, USA), were prepared as stock solutions in sterile, deionized Milli-Q water and dimethyl sulfoxide (DMSO; POCH S.A., Gliwice, Poland), respectively. Working solutions of all compounds were prepared in sterile, deionized Mili-Q water. The selection of reference compounds and the doses of all compounds were based on previously conducted studies using pancreatic cancer cells cultured in 2D [13].

2. Cell Lines and Culture Conditions

Three human pancreatic cancer cell lines, Panc-1 (CRL-1469), MIA PaCa-2 (CRL-1420), and AsPC-1 (CRL-1682), were purchased from the American Type Culture Collection (ATCC, Manassas, VA, USA). Panc-1 and MIA PaCa-2 cells were maintained in high-glucose Dulbecco's modified Eagle's medium (DMEM HG, Merck/Sigma-Aldrich, St. Louis, MO, USA). In contrast, AsPC-1 cells were maintained in RPMI 1640 medium (Merck/Sigma-Aldrich, St. Louis, MO, USA). Both media were supplemented with heat-inactivated 10% fetal bovine serum (FBS), 100 µg/mL streptomycin, and 100 units/mL penicillin. Cells were

maintained in a Falcon 75 cm^2 rectangular, canted-neck cell culture flask with a vented cap (Corning Incorporated, Kennebunk, ME, USA) and incubated in a humidified atmosphere containing 5% CO_2 at 37 °C. All experiments were performed on cells in a logarithmic growth phase.

3. Generation of Multicellular Tumor Spheroids

Multicellular tumor spheroids (MCTS) were generated using Corning® Costar® Ultra-Low Attachment (ULA) 96-well round-bottom plates (Corning Incorporated, Kennebunk, ME, USA). A cell density gradient was used to determine the number of cells used to generate spheroids, selecting those that formed spheroids with a diameter of about 450 µm on day 3 after seeding. During optimization, the following spheroid generation conditions were selected: Panc-1-1200 (cells/well), MIA PaCa-2-500 (cells/well), and AsPC-1-4500 (cells/well). Briefly, to generate MCTS from monolayer cultures, cells were trypsinized, counted, and centrifuged to remove trypsin. Then, cells were resuspended in fresh medium at a density suitable for spheroid formation. Next, 200 µL/well of cell suspension was added to each well of a ULA plate, which was centrifuged for 15 min at 1200 rpm (A-4-62 rotor) at room temperature to initiate aggregation. Plates were incubated at 37 °C in a humidified atmosphere with 5% CO_2 for 3 days. On day 3 (designated as day 0), 100 µL of the medium was replaced with fresh medium. Spheroids were imaged using a ×4 objective on an Olympus IX83 inverted microscope (Olympus, Tokyo, Japan) with an XC50 camera (Olympus, Tokyo, Japan) and CellSens Dimension software version 1.18 (Olympus, Tokyo, Japan).

4. Spheroid Size and Morphology Assessment

The pancreatic cancer MCTS were generated as described in the previous paragraph *Generation of Multicellular Tumor Spheroids* and photographed at day 0; next, 100 µL of culture medium was replaced with a fresh medium in the control spheroids or a fresh medium with IC_{80} concentrations of UAs and IC_{50} concentrations of positive control in the treated spheroids. Images of at least 8 spheroids grown under given conditions were taken every 2–3 days (up to 14 days). Along with the photos taken, the diameters of the spheroids were measured using the cellSens Dimension software version 1.18. The kinetics of spheroid size change were expressed as the ratio of the mean spheroid diameter value on the day of measurement (d_x) minus the mean spheroid diameter value on day 0 (d_0) to the d_0 value, according to the formula below. Results were obtained from four independent experiments (n = 4).

$$pheroid\ growth\ [\%] = \frac{d_x - d_0}{d_0} \cdot 100\%$$

4.5. Cell Death Assay

The cell death assay was performed using 7-aminoactinomycin D (7–AAD) dye (Thermo Scientific, Waltham, MA, USA). Briefly, pancreatic cancer cells cultured as monolayers were seeded at a density of 1.5 × 10^6 for Panc-1 and 1 × 10^6 for MIA PaCa-2 and AsPC-1 per Falcon 100 mm cell culture dish (Corning Incorporated, Kennebunk, ME, USA). Cells were then treated with IC_{80} doses of UAs and IC_{50} doses of positive controls for 72 h. Following exposure to the test compounds, 0.5 × 10^6 cells were collected from the plates, centrifuged at 1000 rpm (A–4–62 rotor) for 5 min at RT, and washed twice with cold PBS. Next, cells were resuspended in 150 µL of PBS and stained with 7–AAD dye (1 µg/mL) for 15 min in the dark at RT. In turn, the pancreatic cancer MCTS were generated as described in the paragraph *Generation of Multicellular Tumor Spheroids*, and on day 0, 100 µL of culture medium was replaced with a fresh medium in the control spheroids or a fresh medium with IC_{80} concentrations of UAs and IC_{50} concentrations of positive

control in the treated spheroids. After compound exposure, the spheroids (16–48 spheroids, dependent on cell line) were collected and trypsinized to obtain a single-cell suspension. Next, a fresh medium was added to neutralize the trypsin, and cells were centrifuged, washed twice with PBS, resuspended in 150 µL of PBS, and stained with 1 µg/mL 7–AAD for 15 min in the dark at RT. After staining, samples were analyzed using a FACS AccuriTM C6 (BD, San Jose, CA, USA) flow cytometer. At least 10,000 cells were collected, and the results were analyzed using BD AccuriTM C6 Software Version 1.0.264.21. Results were obtained from four independent experiments (n = 4).

6. Annexin V/PI Dual Staining

Apoptosis detection was performed by analyzing changes in the cytoplasmic membrane using flow cytometry with the FITC Annexin V Apoptosis Detection Kit (BD Biosciences, San Jose, CA, USA) according to the manufacturer's instructions. Briefly, spherical cultures of Panc-1, MIA PaCa-1, and AsPC-1 cells were exposed to UAs and a positive control for 72 h and harvested as described in the previous paragraph *Cell Death Assay*. Cell pellets were resuspended in 50 µL of a binding buffer containing Annexin V–FITC and PI and incubated for 15 min in the dark at RT. Next, the samples were diluted with 180 µL of binding buffer and analyzed using an FACS Accuri C6 flow cytometer (BD, San Jose, CA, USA). At least 10,000 cells were collected, and the results were analyzed using BD AccuriTM C6 Software Version 1.0.264.21. Results were obtained from four independent experiments (n = 4).

7. Spheroid Staining

Panc-1, MIA PaCa-2, and AsPC-1 spheroids were exposed for 72 h to UAs and positive controls as described in the paragraph *Cell Death Assay*. Following incubation, spheroids were stained using either (1) Hoechst 33342, calcein AM, and propidium iodide (PI), or (2) Annexin V-FITC and PI dye mixtures. Calcein AM (Invitrogen, Thermo Scientific, Waltham, MA, USA) and Hoechst 33342 (Sigma-Aldrich, St. Louis, MO, USA) were obtained in lyophilized form and reconstituted according to the manufacturers' instructions to yield 1 mg/mL stock solutions in DMSO and ultrapure water, respectively. For each spheroid suspended in 200 µL of culture medium, 0.3 µL of calcein AM and 0.5 µL of Hoechst 33342 stock solution were added, resulting in final concentrations of 1.5 µg/mL and 2.5 µg/mL, respectively. PI and Annexin V-FITC (BD Biosciences, San Jose, CA, USA) were purchased as ready-to-use liquid formulations. For each well, 0.8 µL of PI and 0.8 µL of Annexin V-FITC were added. Dye mixtures were prepared immediately before use in bulk for the total number of samples. Then, 1.6 µL of the mixed dye solution was added to each well containing a spheroid, and the samples were incubated for 2–3 h at 37 °C in a humidified atmosphere with 5% CO_2 before imaging. To avoid spheroid disintegration, staining was performed in complete culture medium without washing steps. Image sections were acquired at 15 µm intervals using an LSM 800 inverted laser scanning confocal microscope (Carl Zeiss, Jena, Germany), equipped with an Airyscan detector for high-resolution confocal scanning, and a ×10 objective (Carl Zeiss, Jena, Germany). Images were processed with ZEN 2.6 software (Carl Zeiss, Jena, Germany). Results were obtained from two independent experiments (n = 2).

8. Statistical Analysis

The results are presented as the means ± SDs from at least three independent experiments. The normality of data was assessed using the D'Agostino–Pearson test. Statistical analysis was performed using the Kruskal–Wallis one-way analysis of variance for non-parametric data and Dunn's multiple comparison tests due to the non-normal distribution of the data. Differences $p < 0.05$ between the group of untreated cells (negative control)

and the group of cells treated with the compound were considered statistically significant according to the following criteria: * $p < 0.05$, ** $p < 0.01$, and *** $p < 0.001$. Statistical analysis of the data was performed using GraphPad Prism, version 5.00 (GraphPad Software, San Diego, CA, USA).

Supplementary Materials: The following supporting information can be downloaded at https://www.mdpi.com/article/10.3390/ijms26157557/s1.

Author Contributions: Conceptualization, A.K. and E.A.; methodology, A.K., E.P. and E.A.; validation, A.K.; formal analysis, A.K. and E.A.; investigation, A.K.; resources, E.A.; data curation, A.K. and E.A.; writing—original draft preparation, A.K.; writing—review and editing, A.K. and E.A.; visualization, A.K.; supervision, E.A.; project administration, E.A.; funding acquisition, E.A. All authors have read and agreed to the published version of the manuscript.

Funding: This research was partially funded by CHDE S.A., Rzeszów, Poland, grant no. 037200.

Institutional Review Board Statement: Not applicable.

Informed Consent Statement: Not applicable.

Data Availability Statement: Data obtained during this study are included in this article and the Supplementary Materials file. Detailed data are available from the corresponding author upon reasonable request.

Acknowledgments: We acknowledge the financial support of the Gdańsk University of Technology in maintaining the research facilities used in this study under grant DEC-2/2021/IDUB/V0.6/Si under the SILICIUM SUPPORTING CORE R&D FACILITIES—"Excellence Initiative—Research University" program.

Conflicts of Interest: The authors declare no conflicts of interest.

Abbreviations

The following abbreviations are used in this manuscript:

2D	Two-dimensional
3D	Three-dimensional
7-AAD	7-aminoactionomycin D
ABC	ATP-binding cassette
DMEM HG	High-glucose Dulbecco's modified Eagle's medium
DMSO	Dimethylsulfoxide
FACS	Fluorescence-Activated Cell Sorting
FOLFIRINOX	Multidrug: 5-fluorouracil, leucovorin, irinotecan and oxaliplatin
GEM	Gemcitabine
IR	Irinotecan
KRAS	Kirsten rat sarcoma virus gene
MCTS	Multicellular tumor spheroids
MDR	Multidrug resistance
NALIROX	Multidrug: 5-fluorouracil, leucovorin, liposomal irinotecan, and oxaliplatin
PBS	Phosphate-buffer saline
PC	Pancreatic cancer
PI	Propidium iodide
RPMI	Roswell Park Memorial Institute
RT	Room temperature
SMAD4	Mothers against decapentaplegic homolog 4
UAs	Unsymmetrical bisacridines
ULA	Ultra-low attachment

References

1. Quiñonero, F.; Mesas, C.; Doello, K.; Cabeza, L.; Perazzoli, G.; Jimenez-Luna, C.; Rosa Rama, A.; Melguizo, C.; Prados, J. The Challenge of Drug Resistance in Pancreatic Ductal Adenocarcinoma: A Current Overview. *Cancer Biol. Med.* **2019**, *16*, 688–699. [CrossRef]
2. Jain, A.; Bhardwaj, V. Therapeutic Resistance in Pancreatic Ductal Adenocarcinoma: Current Challenges and Future Opportunities. *World J. Gastroenterol.* **2021**, *27*, 6527–6550. [CrossRef]
3. National Cancer Institute Cancer Stat Facts: Pancreatic Cancer. Available online: https://seer.cancer.gov/statfacts/html/pancreas.html (accessed on 1 March 2025).
4. Conroy, T.; Desseigne, F.; Ychou, M.; Bouché, O.; Guimbaud, R.; Bécouarn, Y.; Adenis, A.; Raoul, J.-L.; Gourgou-Bourgade, S.; de la Fouchardière, C.; et al. FOLFIRINOX versus Gemcitabine for Metastatic Pancreatic Cancer. *N. Engl. J. Med.* **2011**, *364*, 1817–1825. [CrossRef] [PubMed]
5. Nichetti, F.; Rota, S.; Ambrosini, P.; Pircher, C.; Gusmaroli, E.; Droz Dit Busset, M.; Pusceddu, S.; Sposito, C.; Coppa, J.; Morano, F.; et al. NALIRIFOX, FOLFIRINOX, and Gemcitabine With Nab-Paclitaxel as First-Line Chemotherapy for Metastatic Pancreatic Cancer. *JAMA Netw. Open* **2024**, *7*, e2350756. [CrossRef] [PubMed]
6. Wang, S.; Li, Y.; Xing, C.; Ding, C.; Zhang, H.; Chen, L.; You, L.; Dai, M.; Zhao, Y. Tumor Microenvironment in Chemoresistance, Metastasis and Immunotherapy of Pancreatic Cancer. *Am. J. Cancer Res.* **2020**, *10*, 1937–1953.
7. Marin, J.; Monte, M.; Macias, R.; Romero, M.; Herraez, E.; Asensio, M.; Ortiz-Rivero, S.; Cives-Losada, C.; Di Giacomo, S.; Gonzalez-Gallego, J.; et al. Expression of Chemoresistance-Associated ABC Proteins in Hepatobiliary, Pancreatic and Gastrointestinal Cancers. *Cancers* **2022**, *14*, 3524. [CrossRef] [PubMed]
8. Rajabpour, A.; Rajaei, F.; Teimoori-Toolabi, L. Molecular Alterations Contributing to Pancreatic Cancer Chemoresistance. *Pancreatology* **2017**, *17*, 310–320. [CrossRef]
9. Paluszkiewicz, E.; Horowska, B.; Borowa-Mazgaj, B.; Peszyńska-Sularz, G.; Paradziej-Łukowicz, J.; Augustin, E.; Konopa, J.; Mazerska, Z. Design, Synthesis and High Antitumor Potential of New Unsymmetrical Bisacridine Derivatives towards Human Solid Tumors, Specifically Pancreatic Cancers and Their Unique Ability to Stabilize DNA G-Quadruplexes. *Eur. J. Med. Chem.* **2020**, *204*, 112599. [CrossRef] [PubMed]
10. Laskowski, T.; Kosno, M.; Andrałojc´, W.; Pakuła, J.; Stojałowski, R.; Borzyszkowska-Bukowska, J.; Paluszkiewicz, E.; Mazerska, Z. The Interactions of Pu22 G-Quadruplex, Derived from c-MYC Promoter Sequence, with Antitumor Acridine Derivatives—An NMR/MD Combined Study. *Mol. Ther. Nucleic Acids* **2025**, *36*, 102513. [CrossRef]
11. Laskowski, T.; Kosno, M.; Andrałojc´, W.; Frackowiak, J.E.; Borzyszkowska-Bukowska, J.; Szczeblewski, P.; Radoń, N.; Świerżewska, M.; Woz´ny, A.; Paluszkiewicz, E.; et al. The Interactions of Monomeric Acridines and Unsymmetrical Bisacridines (UAs) with DNA Duplexes: An Insight Provided by NMR and MD Studies. *Sci. Rep.* **2023**, *13*, 3431. [CrossRef]
12. Pawłowska, M.; Kulesza, J.; Augustin, E. C-Myc Protein Level Affected by Unsymmetrical Bisacridines Influences Apoptosis and Senescence Induced in HCT116 Colorectal and H460 Lung Cancer Cells. *Int. J. Mol. Sci.* **2022**, *23*, 3061. [CrossRef]
13. Kurdyn, A.; Pawłowska, M.; Paluszkiewicz, E.; Cichorek, M.; Augustin, E. C-Myc Inhibition and P21 Modulation Contribute to Unsymmetrical Bisacridines-Induced Apoptosis and Senescence in Pancreatic Cancer Cells. *Pharmacol. Rep.* **2025**, *77*, 182–209. [CrossRef]
14. Kulesza, J.; Paluszkiewicz, E.; Augustin, E. Cellular Effects of Selected Unsymmetrical Bisacridines on the Multicellular Tumor Spheroids of HCT116 Colon and A549 Lung Cancer Cells in Comparison to Monolayer Cultures. *Int. J. Mol. Sci.* **2023**, *24*, 15780. [CrossRef]
15. Delle Cave, D.; Rizzo, R.; Sainz, B.; Gigli, G.; del Mercato, L.L.; Lonardo, E. The Revolutionary Roads to Study Cell–Cell Interactions in 3D In Vitro Pancreatic Cancer Models. *Cancers* **2021**, *13*, 930. [CrossRef] [PubMed]
16. Han, S.J.; Kwon, S.; Kim, K.S. Challenges of Applying Multicellular Tumor Spheroids in Preclinical Phase. *Cancer Cell Int.* **2021**, *21*, 152. [CrossRef] [PubMed]
17. Mitrakas, A.G.; Tsolou, A.; Didaskalou, S.; Karkaletsou, L.; Efstathiou, C.; Eftalitsidis, E.; Marmanis, K.; Koffa, M. Applications and Advances of Multicellular Tumor Spheroids: Challenges in Their Development and Analysis. *Int. J. Mol. Sci.* **2023**, *24*, 6949. [CrossRef] [PubMed]
18. Minami, F.; Sasaki, N.; Shichi, Y.; Gomi, F.; Michishita, M.; Ohkusu-Tsukada, K.; Toyoda, M.; Takahashi, K.; Ishiwata, T. Morphofunctional Analysis of Human Pancreatic Cancer Cell Lines in 2- and 3-Dimensional Cultures. *Sci. Rep.* **2021**, *11*, 6775. [CrossRef]
19. Truong, L.-H.; Pauklin, S. Pancreatic Cancer Microenvironment and Cellular Composition: Current Understandings and Therapeutic Approaches. *Cancers* **2021**, *13*, 5028. [CrossRef]
20. Deer, E.L.; González-Hernández, J.; Coursen, J.D.; Shea, J.E.; Ngatia, J.; Scaife, C.L.; Firpo, M.A.; Mulvihill, S.J. Phenotype and Genotype of Pancreatic Cancer Cell Lines. *Pancreas* **2010**, *39*, 425–435. [CrossRef]

21. Svirshchevskaya, E.; Doronina, E.; Grechikhina, M.; Matushevskaya, E.; Kotsareva, O.; Fattakhova, G.; Sapozhnikov, A.; Felix, K. Characteristics of Multicellular Tumor Spheroids Formed by Pancreatic Cells Expressing Different Adhesion Molecules. *Life Sci.* **2019**, *219*, 343–352. [CrossRef]
22. Shichi, Y.; Gomi, F.; Sasaki, N.; Nonaka, K.; Arai, T.; Ishiwata, T. Epithelial and Mesenchymal Features of Pancreatic Ductal Adenocarcinoma Cell Lines in Two- and Three-Dimensional Cultures. *J. Pers. Med.* **2022**, *12*, 746. [CrossRef] [PubMed]
23. Kopantzev, E.P.; Kopantseva, M.R.; Grankina, E.V.; Mikaelyan, A.; Egorov, V.I.; Sverdlov, E.D. Activation of IGF/IGF-IR Signaling Pathway Fails to Induce Epithelial-Mesenchymal Transition in Pancreatic Cancer Cells. *Pancreatology* **2019**, *19*, 390–396. [CrossRef]
24. Ungefroren, H.; Thürling, I.; Färber, B.; Kowalke, T.; Fischer, T.; De Assis, L.V.M.; Braun, R.; Castven, D.; Oster, H.; Konukiewitz, B.; et al. The Quasimesenchymal Pancreatic Ductal Epithelial Cell Line PANC-1—A Useful Model to Study Clonal Heterogeneity and EMT Subtype Shifting. *Cancers* **2022**, *14*, 2057. [CrossRef] [PubMed]
25. Rice, A.J.; Cortes, E.; Lachowski, D.; Cheung, B.C.H.; Karim, S.A.; Morton, J.P.; del Río Hernández, A. Matrix Stiffness Induces Epithelial–Mesenchymal Transition and Promotes Chemoresistance in Pancreatic Cancer Cells. *Oncogenesis* **2017**, *6*, e352. [CrossRef]
26. Liao, Q.; Hu, Y.; Zhao, Y.-P.; Zhou, T.; Zhang, Q. Assessment of Pancreatic Carcinoma Cell Chemosensitivity Using a Three-Dimensional Culture System. *Chin. Med. J. (Engl.)* **2010**, *123*, 1871–1877. [CrossRef]
27. Wen, Z.; Liao, Q.; Hu, Y.; You, L.; Zhou, L.; Zhao, Y. A Spheroid-Based 3-D Culture Model for Pancreatic Cancer Drug Testing, Using the Acid Phosphatase Assay. *Braz. J. Med. Biol. Res.* **2013**, *46*, 634–642. [CrossRef] [PubMed]
28. Singh, S.K.; Abbas, S.; Saxena, A.K.; Tiwari, S.; Sharma, L.K.; Tiwari, M. Critical Role of Three-Dimensional Tumorsphere Size on Experimental Outcome. *Biotechniques* **2020**, *69*, 333–338. [CrossRef]
29. Alwahsh, M.; Al-Doridee, A.; Jasim, S.; Awwad, O.; Hergenröder, R.; Hamadneh, L. Cytotoxic and Molecular Differences of Anticancer Agents on 2D and 3D Cell Culture. *Mol. Biol. Rep.* **2024**, *51*, 721. [CrossRef]
30. Paškevic̆iu ̄te˙, M.; Petrikaite˙, V. Differences of Statin Activity in 2D and 3D Pancreatic Cancer Cell Cultures. *Drug Des. Devel. Ther.* **2017**, *11*, 3273–3280. [CrossRef]
31. Tidwell, T.R.; Røsland, G.; Tronstad, K.J.; Søreide, K.; Hagland, H.R. Comparing in Vitro Cytotoxic Drug Sensitivity in Colon Andpancreatic Cancer Using 2D and 3D Cell Models: Contrastingviability and Growth Inhibition in Clinically Relevant Doseand Repeated Drug Cycles. *Cancer Med.* **2024**, *13*, e7318. [CrossRef] [PubMed]
32. Breslin, S.; O'Driscoll, L. The Relevance of Using 3D Cell Cultures, in Addition to 2D Monolayer Cultures, When Evaluating Breast Cancer Drug Sensitivity and Resistance. *Oncotarget* **2016**, *7*, 45745–45756. [CrossRef]
33. Ascione, F.; Ferraro, R.; Dogra, P.; Cristini, V.; Guido, S.; Caserta, S. Gradient-Induced Instability in Tumour Spheroids Unveils the Impact of Microenvironmental Nutrient Changes. *Sci. Rep.* **2024**, *14*, 20837. [CrossRef]
34. Lee, J.-H.; Kim, S.-K.; Khawar, I.A.; Jeong, S.-Y.; Chung, S.; Kuh, H.-J. Microfluidic Co-Culture of Pancreatic Tumor Spheroids with Stellate Cells as a Novel 3D Model for Investigation of Stroma-Mediated Cell Motility and Drug Resistance. *J. Exp. Clin. Cancer Res.* **2018**, *37*, 4. [CrossRef]
35. Jaros, S.W.; Komarnicka, U.K.; Kyzioł, A.; Pucelik, B.; Nesterov, D.S.; Kirillov, A.M.; Smoleński, P. Therapeutic Potential of a Water-Soluble Silver-Diclofenac Coordination Polymer on 3D Pancreatic Cancer Spheroids. *J. Med. Chem.* **2022**, *65*, 11100–11110. [CrossRef] [PubMed]
36. Achilli, T.-M.; McCalla, S.; Meyer, J.; Tripathi, A.; Morgan, J.R. Multilayer Spheroids To Quantify Drug Uptake and Diffusion in 3D. *Mol. Pharm.* **2014**, *11*, 2071–2081. [CrossRef]
37. Hagmann, W.; Faissner, R.; Schnölzer, M.; Löhr, M.; Jesnowski, R. Membrane Drug Transporters and Chemoresistance in Human Pancreatic Carcinoma. *Cancers* **2010**, *3*, 106–125. [CrossRef]
38. Harpstrite, S.E.; Gu, H.; Natarajan, R.; Sharma, V. Interrogation of Multidrug Resistance (MDR1) P-Glycoprotein (ABCB1) Expression in Human Pancreatic Carcinoma Cells. *Nucl. Med. Commun.* **2014**, *35*, 1067–1070. [CrossRef]
39. Pawłowska, M.; Kulesza, J.; Paluszkiewicz, E.; Augustin, E.; Mazerska, Z. Unsymmetrical Bisacridines' Interactions with ABC Transporters and Their Cellular Impact on Colon LS 174T and Prostate DU 145 Cancer Cells. *Molecules* **2024**, *29*, 5582. [CrossRef] [PubMed]
40. Hassan, S.; Peluso, J.; Chalhoub, S.; Idoux Gillet, Y.; Benkirane-Jessel, N.; Rochel, N.; Fuhrmann, G.; Ubeaud-Sequier, G. Quercetin Potentializes the Respective Cytotoxic Activity of Gemcitabine or Doxorubicin on 3D Culture of AsPC-1 or HepG2 cells, through the inhibition of HIF-1α and MDR1. *PLoS ONE* **2020**, *15*, e0240676. [CrossRef]
41. Tidwell, T.R.; Røsland, G.V.; Tronstad, K.J.; Søreide, K.; Hagland, H.R. Metabolic Flux Analysis of 3D Spheroids Reveals Significant Differences in Glucose Metabolism from Matched 2D Cultures of Colorectal Cancer and Pancreatic Ductal Adenocarcinoma Cell Lines. *Cancer Metab.* **2022**, *10*, 9. [CrossRef]
42. Pilch, J.; Pote¸ga, A.; Kowalczyk, A.; Kasprzak, A.; Kowalik, P.; Bujak, P.; Paluszkiewicz, E.; Augustin, E.; Nowicka, A.M. PH-Responsive Drug Delivery Nanoplatforms as Smart Carriers of Unsymmetrical Bisacridines for Targeted Cancer Therapy. *Pharmaceutics* **2023**, *15*, 201. [CrossRef] [PubMed]

43. Patki, M.; Saraswat, A.; Bhutkar, S.; Dukhande, V.; Patel, K. In Vitro Assessment of a Synergistic Combination of Gemcitabine and Zebularine in Pancreatic Cancer Cells. *Exp. Cell Res.* **2021**, *405*, 112660. [CrossRef] [PubMed]
44. Samanta, K.; Setua, S.; Kumari, S.; Jaggi, M.; Yallapu, M.M.; Chauhan, S.C. Gemcitabine Combination Nano Therapies for Pancreatic Cancer. *Pharmaceutics* **2019**, *11*, 574. [CrossRef] [PubMed]

Unpublished results as a supplement to Article No. 2

Results published in article no. 2, *Pro-Apoptotic Effects of Unsymmetrical Bisacridines in 3D Pancreatic Multicellular Tumor Spheroids,* focused on the spheroids obtained from Panc-1, MIA PaCa-2, and AsPC-1 cells. Since this doctoral dissertation also discusses BxPC-3 cells, this chapter aims to clarify why spheroids obtained from cells of this cell line weren't included in the mentioned article.

Preliminary screening was conducted to assess the BxPC-3 cells' ability to form MCTS suitable for further analysis. However, the results indicated that BxPC-3-derived spheres remained relatively small, with diameters of approximately 346–376 µm (Figure 5). Notably, the spheroid size barely differed despite increasing the initial seeding density from 4500 to 7000 cells/well. Furthermore, during incubation, even untreated control spheroids tend to lose their integrity spontaneously. Since the primary cellular responses expected after treatment with UAs, specifically growth inhibition and structural dispersion, were already occurring in the untreated BxPC-3 models, it was decided to exclude this cell line from the study part regarding spheroids. Including BxPC-3 spheroids would have precluded a reliable interpretation of the UAs' effects and could have led to false conclusions about the compounds' actual anticancer activity.

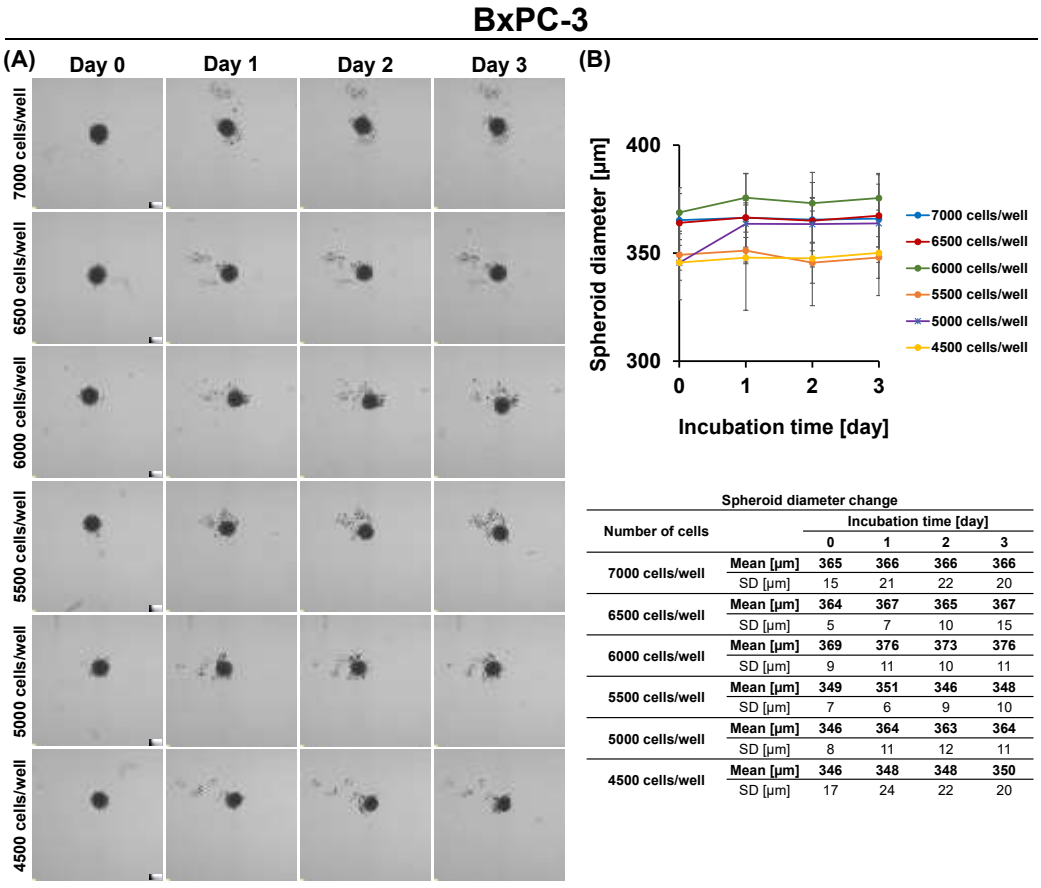

Spheroid diameter change

Number of cells		Incubation time [day]			
		0	1	2	3
7000 cells/well	Mean [µm]	365	366	366	366
	SD [µm]	15	21	22	20
6500 cells/well	Mean [µm]	364	367	365	367
	SD [µm]	5	7	10	15
6000 cells/well	Mean [µm]	369	376	373	376
	SD [µm]	9	11	10	11
5500 cells/well	Mean [µm]	349	351	346	348
	SD [µm]	7	6	9	10
5000 cells/well	Mean [µm]	346	364	363	364
	SD [µm]	8	11	12	11
4500 cells/well	Mean [µm]	346	348	348	350
	SD [µm]	17	24	22	20

Figure 5. Establishment of seeding conditions for BxPC-3 spheroids. **(A)** Representative light microscopy images of spheroids generated from varying cell densities. **(B)** The spheroid's growth curves. Scale bar 200 µm.

Another test performed regarding spheroids was the determination of UAs cytotoxicity in pancreatic cancer spheroids (**Table 2**). The test was conducted according to the methodology described in the *MATERIALS AND METHODS* section.

The cytotoxicity of the studied UAs was further evaluated by comparing IC_{50} and IC_{80} values across 2D and 3D culture models for three pancreatic cancer cell lines (Panc-1, MIA PaCa-2, and AsPC-1), as presented in **Table 2**. In the case of Panc-1 and MIA PaCa-2 cells, the IC_{50} values for the C-2028 derivative remained highly consistent between both models, maintaining levels around 0.020–0.025 μM. However, for C-2045 and C-2053, a noticeable increase in inhibitory concentrations was observed in spheroids compared to monolayers. For instance, the IC_{50} for C-2045 in MIA PaCa-2 cells rose nearly fourfold, from 0.047 μM in 2D to 0.186 μM in 3D. The most significant disparities were observed in the AsPC-1 cell line, where the 3D environment resulted in a substantial decrease in sensitivity to all UAs. Specifically, the IC_{50} dose of C-2053 in AsPC-1 was ten times higher in the spheroid model (0.968 μM) than in the monolayer (0.097 μM). These results suggest that the more compact structure of AsPC-1 spheroids may impede compound penetration more effectively than in other cell lines. Despite these differences, the potency of all tested UAs remained significantly higher than that of the reference drug irinotecan, which required micromolar concentrations (ranging from approximately 13 to 80 μM) to achieve comparable effects in 3D models.

Table 2. Comparison of IC_{50} and IC_{80} doses of UAs (C-2028, C-2045, and C-2053) and positive controls (gemcitabine - GEM or irinotecan - IR) against Panc-1, MIA PaCa-2, AsPC-1, and BxPC-3 cells cultured in 2D (MTT assay) and 3D (CellTiter-Glo®) conditions after 72 h of treatment.

Panc-1				
	IC_{50} [μM]		**IC_{80} [μM]**	
Compound	2D	**3D**	2D	**3D**
C-2028	0.024 ± 0.005	**0.020 ± 0.003**	0.043 ± 0.002	**0.038 ± 0.004**
C-2045	0.086 ± 0.007	**0.209 ± 0.009**	0.323 ± 0.043	**0.373 ± 0.015**
C-2053	0.037 ± 0.007	**0.067 ± 0.007**	0.080 ± 0.012	**0.105 ± 0.022**
IR	8.5 ± 0.13	**44.307 ± 2.353**	-	**80.124 ± 6.059**
MIA PaCa-2				
	IC_{50} [μM]		**IC_{80} [μM]**	
Compound	2D	**3D**	2D	**3D**
C-2028	0.023 ± 0.002	**0.025 ± 0.005**	0.042 ± 0.002	**0.043 ± 0.012**
C-2045	0.047 ± 0.003	**0.186 ± 0.014**	0.086 ± 0.001	**0.338 ± 0.009**
C-2053	0.031 ± 0.003	**0.074 ± 0.002**	0.072 ± 0.004	**0.142 ± 0.008**
GEM	0.062 ± 0.010	**-**	-	**-**
IR	-	**13.004 ± 0.904**	-	**44.900 ± 0.292**
AsPC-1				
	IC_{50} [μM]		**IC_{80} [μM]**	
Compound	2D	**3D**	2D	**3D**
C-2028	0.027 ± 0.001	**0.184 ± 0.008**	0.102 ± 0.007	**0.427 ± 0.034**
C-2045	0.096 ± 0.005	**0.858 ± 0.057**	0.463 ± 0.011	**2.237 ± 0.217**
C-2053	0.097 ± 0.009	**0.968 ± 0.065**	0.486 ± 0.005	**2.537 ± 0.147**
GEM	0.026 ± 0.003	**-**	-	**-**
IR	-	**54.534 ± 3.877**	-	**83.733 ± 2.876**

To ensure a more uniform and comparable evaluation of the cellular response in 3D, it was decided to apply the IC_{80} doses determined in 2D models for all subsequent experiments involving spheroids. This approach allowed for a direct comparison of the compounds' efficacy across different culture models. This choice was further justified by the observation that, even in the more resistant AsPC-1 cell line, where the 3D IC_{80} values were significantly higher (up to 6-fold) than in 2D, the differences in cell death induction were not as pronounced as the concentration disparity might suggest. Furthermore, the decision to rely on 2D-derived doses was influenced by the inability to determine IC_{50} and IC_{80} values for gemcitabine in the 3D spheroid models. Consequently, using the 2D-established doses provided a consistent framework to assess morphological alterations and apoptosis induction across all cell lines, confirming that UAs maintain potent activity even when applied at lower concentrations in a more challenging 3D environment.

ARTICLE NO. 3

Apoptosis-promoting autophagy mediates anti-migratory effects of unsymmetrical bisacridines in pancreatic cancer cells

Biomedicine & Pharmacotherapy (2025) 193, 118786; doi: 10.1016/j.biopha.2025.118786

IF_{2024} = 7.5, Q1, MHES Points: 100

Agnieszka Kurdyn, Bożena Pezała, Ewa Paluszkiewicz, Ewa Augustin

Department of Pharmaceutical Technology and Biochemistry, Faculty of Chemistry, Gdańsk University of Technology, Gabriela Narutowicza 11/12, Gdańsk 80-233, Poland

Pancreatic cancer is distinguished by its extreme aggressiveness, early metastatic dissemination, and profound resistance to standard chemotherapeutic regimens. A critical and complex factor in PC progression and therapy resistance is autophagy, a lysosomal degradation process that frequently serves as a cytoprotective survival mechanism, allowing tumor cells to adapt to metabolic stress, hypoxia, and nutrient deprivation. In the context of established tumors like PC, autophagy typically supports malignancy. However, its role is highly context-dependent and can be reprogrammed to act in a pro-death capacity.

The third scientific article in this doctoral dissertation investigates the biological effects of three unsymmetrical bisacridine derivatives (C-2028, C-2045, and C-2053) on autophagic flux in pancreatic cancer cells. The primary research objective was to elucidate the intricate crosstalk between autophagy, apoptosis, and the modulation of the migratory potential of PC cells.

The biological activity of UAs was evaluated across four human PC cell lines (Panc-1, MIA PaCa-2, AsPC-1, and BxPC-3) and a normal human pancreatic epithelial line (hTERT-HPNE) as a control. To assess the selectivity of UAs, the cellular response in normal hTERT-HPNE cells was characterized using flow cytometry to determine cell cycle distribution (propidium iodide staining), membrane integrity (Annexin V-FITC/propidium iodide), and caspase 3/7 activity, supplemented by nuclear morphology analysis via Hoechst 33342 staining. Autophagic flux in PC cells was assessed by microscopic detection of acidic vesicular organelles (AVOs) via acridine orange staining and by quantitative Western blot analysis of key molecular markers (LC3-I/II, p62, Beclin1, and Bcl-2). The functional role of autophagy was further dissected using autophagy inhibitors: wortmannin (an early-stage inhibitor) and chloroquine or ammonium chloride (late-stage inhibitors). These were used alone or in combination with selected UA derivatives to analyze their combined impact on AVO levels, cell viability (MTT assay), and apoptosis induction. Finally, the anti-migratory effects of UAs and the specific role of autophagy in mediating this process were assessed using a wound healing migration assay monitored by live-cell time-lapse microscopy over 72 h. This was accompanied by a Western blot analysis of EMT markers, including E-cadherin, N-cadherin, and vimentin.

UAs exhibited high selectivity, inducing significant apoptosis in PC cancer cells while sparing the normal hTERT-HPNE cells, which showed only moderate sensitivity at higher concentrations (**Figure 6**).

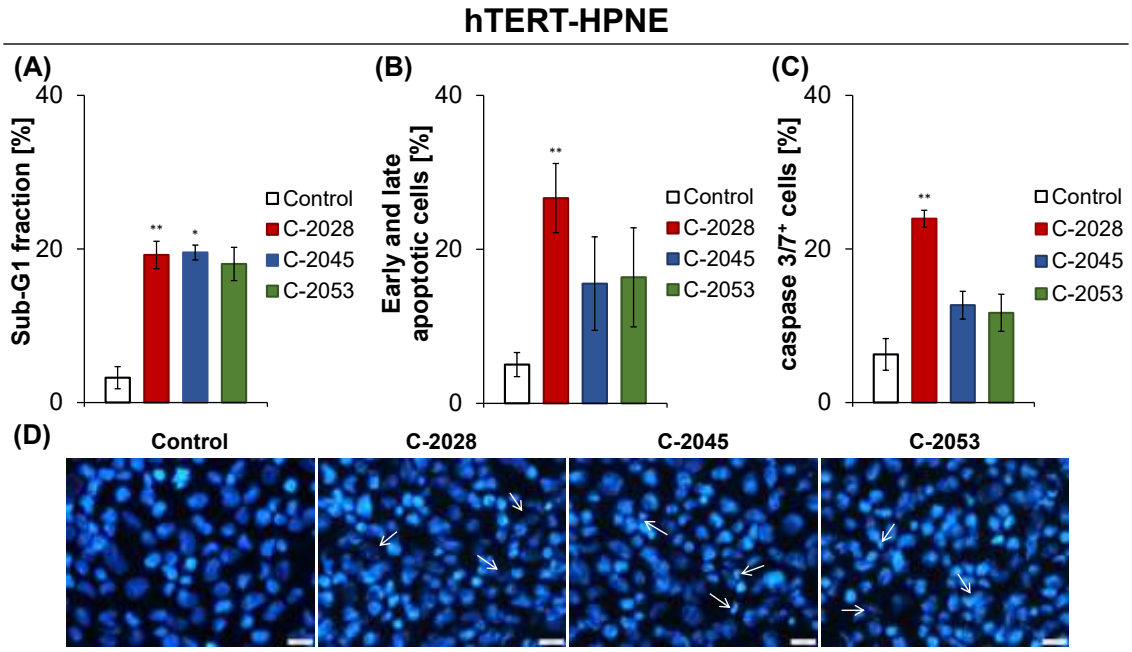

Figure 6. Cellular response induced by unsymmetrical bisacridines (UAs; C-2028, C-2045, and C-2053) at IC_{80} doses in normal pancreatic hTERT-HPNE cells treated for 120 h. **(A)** DNA degradation level expressed as the percentage of sub-G1 fraction, based on PI/RNase staining and flow cytometry. **(B)** Apoptotic cell population (early and late apoptosis) determined by Annexin V-FITC/PI double staining. **(C)** Caspase 3/7 activation was measured by flow cytometry using a fluorogenic caspase substrate. **(D)** Nuclear morphology was evaluated by Hoechst 33342 staining and visualized under a fluorescence microscope (400×); white arrows indicate apoptotic bodies. The results are presented as the means ± SD. Statistical analysis was performed using the Kruskal–Wallis test for non-parametric data and Dunn's post-hoc test. Significantly different from the control at: * $p < 0.05$, ** $p < 0.01$, *** $p < 0.001$; ($n \geq 4$).

Treatment with UAs triggered a substantial, time-dependent increase in autophagic flux, evidenced by the conversion of LC3-I to LC3-II and the significant degradation of the p62 protein (**Figure 7A**), particularly in Panc-1 and AsPC-1 cells. Notably, this autophagic induction was found to be Beclin1-independent, suggesting that UAs activate a non-canonical pathway that bypasses the traditional autophagy initiation complex. The functional interplay between autophagy and cell death was found to be cell-line specific (**Figure 7B**). In Panc-1 and AsPC-1 cells, inhibition of autophagy significantly reduced UA-induced apoptosis and increased cell viability, indicating that autophagy is pro-death. MIA PaCa-2 cells also demonstrated sensitivity; however, while the C-2028 derivative successfully induced pro-death autophagy, the C-2045 and C-2053 derivatives appeared to disrupt autophagic flux, leading to the accumulation of p62. Conversely, in BxPC-3 cells, autophagy inhibition enhanced UA-induced cytotoxicity, suggesting that in this specific molecular subtype, autophagy retains a cytoprotective role.

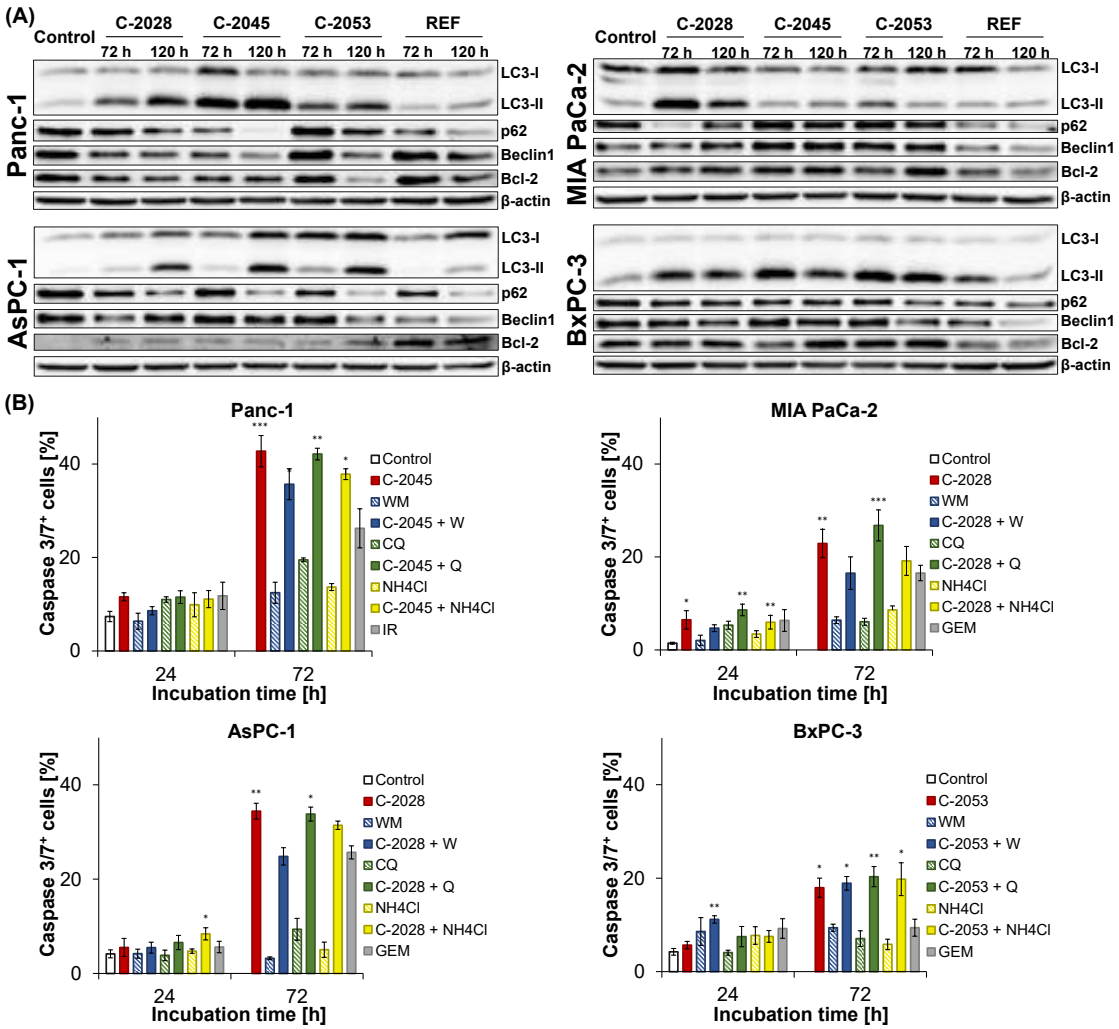

Figure 7. Autophagy induction by unsymmetrical bisacridines. Cells were treated with unsymmetrical bisacridine derivatives (UAs; C-2028, C-2045, and C-2053) at IC_{80} doses and positive control compounds (gemcitabine–GEM or irinotecan–IR) at IC_{50} doses. **(A)** Western blot analysis of LC3-I/II, p62, Beclin1, and Bcl-2 protein levels. Total protein samples (30 µg/lane) were separated by SDS-PAGE, transferred to membranes using a semi-dry method, and detected with specific antibodies and enhanced chemiluminescence. **(B)** Apoptosis detection by flow cytometry based on the percentage of caspase3/7-positive cells. Pancreatic cancer cells were preincubated for 1 h with autophagy inhibitors: wortmannin (WM), chloroquine (CQ), or ammonium chloride (NH_4Cl), and subsequently treated with IC_{80} doses of selected UA. The results are presented as the means ± SD. Statistical analysis was performed using the Kruskal–Wallis test for non-parametric data and Dunn's post-hoc test. Significantly different from the control at: * $p < 0.05$, ** $p < 0.01$, *** $p < 0.001$; ($n \geq 4$).

Furthermore, all UA derivatives significantly inhibited PC cell migration, outperforming reference compounds such as gemcitabine. Crucially, in Panc-1 cells, blocking autophagy partially restored migratory capacity and accelerated wound closure (**Figure 8A**). This demonstrates that the anti-migratory effect of UAs is directly mediated by the induction of autophagy and the subsequent modulation of EMT-related markers via a non-canonical mechanism characterized by decreased N-cadherin and E-cadherin levels and a paradoxical increase in vimentin, suggesting a disrupted EMT signaling response rather than a classical mesenchymal shift (**Figure 8B**).

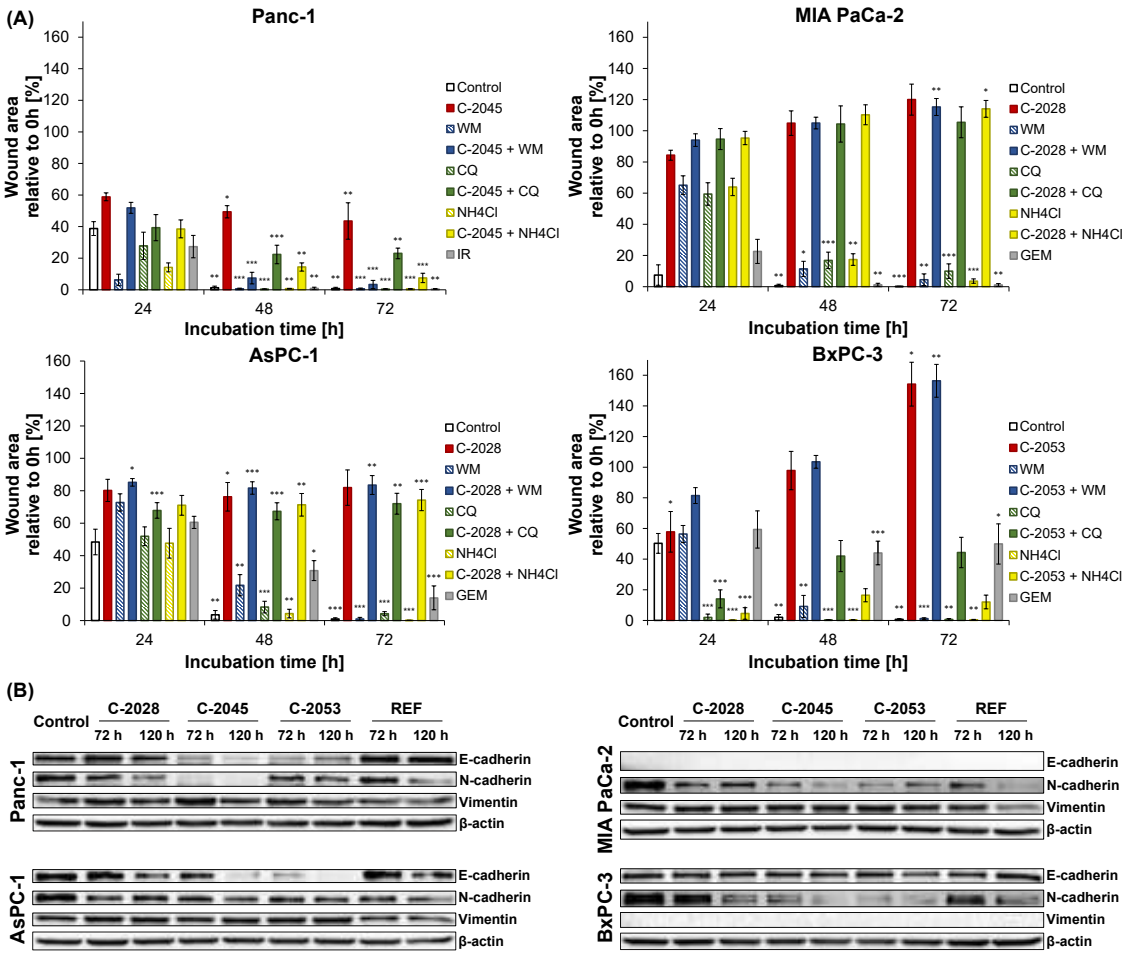

Figure 8. Suppression of pancreatic cancer cell migration and non-canonical epithelial-mesenchymal transition modulation. **(A)** Cells were preincubated for 1 h with autophagy inhibitors (wortmannin (WM), chloroquine (CQ), or ammonium chloride (NH_4Cl)) and subsequently treated with IC_{80} doses of selected unsymmetrical bisacridines (UAs; C-2028, C-2045, and C-2053). Positive control compounds (gemcitabine–GEM or irinotecan–IR) at IC_{50} doses were applied. Bar graphs showing the wound area after treatment with individual UA compounds or in combination with an autophagy inhibitor, expressed as a percentage relative to the wound area at the beginning of the experiment. **(B)** Western blot analysis of epithelial (E-cadherin) and mesenchymal (N-cadherin and vimentin) markers expression. Total protein samples (30 µg/lane) were separated by SDS-PAGE, transferred to membranes using a semi-dry method, and detected with specific antibodies and enhanced chemiluminescence. The results are presented as the means ± SD. Statistical analysis was performed using the Kruskal–Wallis test for non-parametric data and Dunn's post-hoc test. Significantly different from the control at: * $p < 0.05$, ** $p < 0.01$, *** $p < 0.001$; ($n \geq 4$).

This study establishes that unsymmetrical bisacridines exert a potent dual therapeutic effect by simultaneously promoting cell death and inhibiting migration. By inducing autophagic flux, UAs effectively reprogram autophagy from a cytoprotective survival mechanism into a cytotoxic process that facilitates apoptosis. Furthermore, the discovery that UA-induced autophagy suppresses the migratory potential of pancreatic cancer cells through a non-canonical mechanism provides a strong scientific rationale for developing UAs as multifunctional compounds. These findings underscore the potential of UA derivatives to overcome pancreatic cancer's inherent resistance by exploiting autophagic vulnerabilities, supporting their continued translational development toward clinical application.

Biomedicine & Pharmacotherapy 193 (2025) 118786

Contents lists available at ScienceDirect

Biomedicine & Pharmacotherapy

journal homepage: www.elsevier.com/locate/biopha

Apoptosis-promoting autophagy mediates anti-migratory effects of unsymmetrical bisacridines in pancreatic cancer cells

Agnieszka Kurdyn [1], Boz˙ena Pezala [2], Ewa Paluszkiewicz, Ewa Augustin [*,3]

Department of Pharmaceutical Technology and Biochemistry, Faculty of Chemistry, Gdan´sk University of Technology, Gabriela Narutowicza Str. 11/12, Gdan´sk 80-233, Poland

ARTICLE INFO

Keywords:
Unsymmetrical bisacridines
Pancreatic cancer
Autophagy
Apoptosis
Migration
Anticancer activity

ABSTRACT

Pancreatic cancer (PC) remains one of the most lethal malignancies, underscoring the urgent need for new therapeutic strategies. Our previous studies demonstrated that unsymmetrical bisacridines (UAs) exhibit strong anticancer activity against PC cells by inducing apoptosis. Given the complex role of autophagy in tumor progression, particularly its association with poor prognosis in PC, this study aimed to evaluate the effects of UAs on autophagy and its crosstalk with apoptosis and migration in PC cells. Three UA derivatives (C-2028, C-2045, and C-2053) were tested on pancreatic cancer (Panc-1, MIA PaCa-2, AsPC-1, BxPC-3), and normal (hTERT-HPNE) cell lines. The biological evaluation included assessment of cell viability (MTT), apoptosis (Annexin V-FITC, caspase 3/7, and nuclear staining), and autophagy (acidic vesicular organelles staining and molecular markers). Cell migration and related molecular markers were also analyzed. UAs exhibited markedly greater cytotoxicity and induced substantially higher levels of apoptosis in pancreatic cancer cells compared to normal cells. UAs triggered increased autophagic flux in a cell line-dependent and Beclin1-independent manner. The interplay between autophagy and apoptosis was complex but predominantly pro-death. All UAs significantly inhibited PC cell migration, with antimigratory effects linked to autophagic activity. These findings demonstrate that UAs exert a dual pro-apoptotic and anti-migratory effect on PC cells through autophagy. Their selective activity and limited toxicity toward normal pancreatic cells support further development of UA derivatives as promising therapeutic candidates for pancreatic cancer.

1. Introduction

Pancreatic cancer (PC) is an aggressive malignancy, that ranks as the 11th most common cancer worldwide and is characterized by early metastasis and high resistance to standard chemotherapy [1,2]. These factors contribute to the limited effectiveness of current treatment regimens, including multidrug combinations such as FOLFIRINOX (fluorouracil, leucovorin, irinotecan, and oxaliplatin), NALIRIFOX (fluorouracil, leucovorin, liposomal irinotecan, and oxaliplatin), and GEM-NABP (gemcitabine with nab-paclitaxel). Although combination therapies have modestly improved patient survival compared with gemcitabine monotherapy, the efficacy of treatment protocols may still be limited due to high toxicity and adverse events [3]. Therefore, there is an urgent need to identify new compounds that have greater selectivity for cancer cells and possess the ability to surmount resistance mechanisms.

One promising research direction involves the development of unsymmetrical bisacridines (UAs; Fig. 1) which are acridine based compounds synthesized and characterized at the Gdan´sk University of Technology [4–8]. Acridines and their derivatives are well-known DNA-intercalating agents with broad antitumor potential [9]. Researchers from our University developed the first Polish anticancer drug Ledakrin (Nitracrine^{R}, C-283) [10], a 1-nitro-9-aminoacridine derivative. However, despite its promising therapeutic potential, Ledakrin was withdrawn because of mutagenic properties and induction of adverse events [11]. Another acridine analog synthesized by our research team, Symadex (C-1311) - imidazoacrodinone derivative, exhibited strong cytotoxic activity combined with markedly lower mutagenic potential

* Corresponding author.
E-mail address: ewa.augustin@pg.edu.pl (E. Augustin).
[1] 0000–0002-6650–2738
[2] 0009–0008-1589–9350
[3] 0000–0002-0807–021X

https://doi.org/10.1016/j.biopha.2025.118786
Received 30 September 2025; Received in revised form 13 November 2025; Accepted 17 November 2025
Available online 21 November 2025

[12]. Nevertheless, it reached only II phase of clinical trials, and clinical application has been limited by systemic toxicity and insufficient selectivity toward cancer cells.

The design of UAs aimed to overcome these limitations by combining two different heterocyclic acridine rings through an aminoalkyl chain, which allows modulation of DNA-binding affinity, cellular uptake, and target selectivity [4]. In contrast to classic acridines that intercalate into double-stranded DNA, UAs have the unique ability to stabilize G-quadruplex DNA structures. These DNA configurations are presentin key regulatory regions of oncogenes such as *MYC* and *KRAS*. Stabilization of G-quadruplexes is associated with the downregulation of oncogene expression, contributing to the anticancer properties of UAs [13].

Previous studies from our group have demonstrated that UAs display strong cytotoxic activity against a broad spectrum of human tumor cell lines, including pancreatic, lung, and colon cancers, while exhibiting significantly lower toxicity toward normal cells [4,14]. Based on screening studies on PC cells, three derivatives, C-2028, C-2045, and C-2053, were selected for the present study. These compounds showed high cytotoxicity and potent antitumor activity against human tumor xenografts in nude mice [4]. The structural differences among derivatives include the presence or absence of methyl and hydroxyl substituents, which influence their physicochemical and metabolic properties. It has been shown that these substituents distinctly modulate enzymatic activity: only C-2045 derivative undergoes glucuronidation, whereas both C-2045 and C-2053 inhibit CYP3A4, the major P450 isoform responsible for xenobiotic metabolism. In contrast, C-2028 derivative inhibits UGT1A1 and 2B7 [15].

Studies performed so far in PC models have revealed that C-2028, C-2045, and C-2053 induce apoptosis through c-Myc protein downregulation, which is further enhanced by SMAD4 activation [16]. Notably, UAs maintain their pro-apoptotic activity in three-dimensional (3D) cell culture models that more accurately reflect the tumor microenvironment [17]. Interestingly, the tested PC cell lines displayed diverse sensitivity to these compounds. The differences may result from the distinct substituents present in the UAs structures, which could influence cellular uptake, metabolic stability, or the efficiency of G-quadruplex stabilization.

Apoptosis and autophagy are interconnected processes that play central roles in cancer cell responses to chemotherapy. While apoptosis is a well-established target in cancer therapy, autophagy can act as a double-edged sword, either supporting cancer cell survival under stress or promoting cell death [18]. Recent work by El Mahi has shown that Rhus coriaria extract induces autophagy that precedes and supports apoptosis via survivin downregulation [13]. In contrast, autophagy inhibition paradoxically accelerates apoptotic death in sonodynamic therapy settings studied by Du et al. [14], underscoring the context-dependent roles of autophagy in the response of PC cells. A key marker of autophagy is the LC3 protein, which is involved in the formation of autophagosomes. Initially cleaved at the carboxyl terminus to form LC3-I, it is subsequently conjugated with phosphoethanolamine to produce LC3-II, which integrates into autophagosome membranes. Another critical protein, p62, binds ubiquitinated cargo and directs it to autophagosomes for degradation. Hence, the accumulation or clearance of p62 assesses autophagic flux [19,20]. Beclin1 plays a crucial role in the initiation of autophagy, as well as in the regulation of autophagy, and represents a key link between apoptosis and the initiation of autophagy. Functionally, its BH3 (Bcl-2 homology) domain interacts with anti-apoptotic proteins, Bcl-2 and Bcl-xL, making Beclin1 an important molecule for linking autophagy regulation to apoptosis control [21].

In PC, autophagy is frequently upregulated and associated with enhanced cancer cell survival, metastasis, and resistance to therapy. Although it may act as a tumor suppressor mechanism in early tumorigenesis, in established tumors such as PC, autophagy often supports adaptation to metabolic stress and hypoxia. Therefore, the role of autophagy in its interaction with chemotherapeutic agents remains unresolved and highly context dependent [22,23].

Autophagy also has a multifaced influence on cell motility, showing both pro- and anti-migratory effects [24,25]. Considering that cell migration is an early and essential step in the metastatic cascade of pancreatic cancer, understanding how autophagy modulates this process is crucial for identifying new therapeutic strategies that aim to limit tumor spread [26]. Apart from pro-apoptotic action, the anti-migratory effect is equally valuable in designing effective PC therapies, as this tumor type is very aggressive with a high metastatic capacity. Epithelial-mesenchymal transition (EMT), a significant factor in metastasis, primarily contributes to the rapid invasion, motility, and drug resistance of cancer cells [27]. In essence, EMT reduces the expression of epithelial markers (E-cadherin) and increases the expression of mesenchymal markers (N-cadherin and vimentin), which promote migration and invasion [28].

Given the critical role of autophagy in regulating apoptosis and migration in cancer cells, this study aimed to investigate the effects of three UA derivatives, C-2028, C-2045, and C-2053, on pancreatic cancer cells. In addition, the apoptosis-inducing properties of these compounds were examined in normal pancreatic cells. UAs' impact on cancer cell viability, apoptosis, autophagy, and migration, as well as the associated molecular markers, was evaluated. Furthermore, the functional role of autophagy was analyzed using autophagy inhibitors to better understand its contribution to the UA-induced response. By comparing the cellular effects triggered by UAs in normal and cancer cells and integrating these findings with the existing literature, this study provides a comprehensive characterization of the cellular and molecular mechanisms of action of UAs in pancreatic cancer cells, supporting further translational research on these promising compounds.

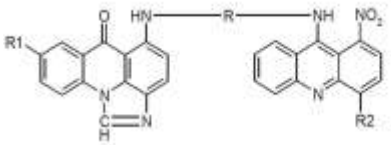

Compound	R	R1	R2
C-2028	$-(CH_2)_3-N(CH_3)-(CH_2)_3-$	-H	-H
C-2045		-OH	$-CH_3$
C-2053		-H	$-CH_3$

Compound	Compound Dose [μM]	Cell line				
		Panc-1	MIA PaCa-2	AsPC-1	BxPC-3	hTERT-HPNE
C-2028	IC_{50}	0.024 ± 0.005	0.023 ± 0.002	0.027 ± 0.001	0.023 ± 0.003	0.041 ± 0.011
	IC_{90}	**0.043** ± 0.002	**0.042** ± 0.002	**0.102** ± 0.007	**0.043** ± 0.003	**0.366** ± 0.118
C-2045	IC_{50}	0.086 ± 0.007	0.047 ± 0.003	0.096 ± 0.005	0.196 ± 0.005	0.237 ± 0.035
	IC_{90}	**0.323** ± 0.043	**0.086** ± 0.001	**0.463** ± 0.011	**0.393** ± 0.020	**0.830** ± 0.099
C-2053	IC_{50}	0.037 ± 0.007	0.031 ± 0.003	0.097 ± 0.009	0.104 ± 0.009	0.223 ± 0.034
	IC_{90}	**0.080** ± 0.012	**0.072** ± 0.004	**0.486** ± 0.005	**0.303** ± 0.011	**0.853** ± 0.098
GEM	IC_{50}	n/a	0.062 ± 0.010	0.026 ± 0.003	0.025 ± 0.005	n/a
IR	IC_{50}	8.5 ± 0.13	n/a	n/a	n/a	n/a

Fig. 1. Structures and doses of tested compounds**.** Chemical structure of tested unsymmetrical bisacridines (UAs: C-2028, C-2045, and C-2053) and their inhibitory concentrations (IC), along with those of the reference compounds gemcitabine (GEM) and irinotecan (IR) against pancreatic cancer cells: Panc-1, MIA PaCa-2, AsPC-1, and BxPC-3, as well as normal hTERT-HPNE pancreatic cells. Doses were determined after 72 h of compound exposure by MTT assay [9], ($n \geq 4$).

2. Materials and methods

2.1. Tested compounds

Unsymmetrical bisacridine derivatives (C-2028, C-2045, and C-2053) were synthesized as hydrochlorides in the Department of Pharmaceutical Technology and Biochemistry, Gdan´sk University of Technology, following a previously published procedure [4]. Stock solutions of the UAs were prepared in sterile, deionized Milli-Q water (Merck/-Millipore, Burlington, MA, USA). Stock solutions of the positive control drugs, gemcitabine and irinotecan (Merck/Sigma-Aldrich, St. Louis, MO, USA), selected based to our previous work [16], were prepared in sterile deionized Mili-Q water and dimethylsulfoxide (DMSO; POCH S.A., Gliwice, Poland), respectively. Working solutions of all compounds, corresponding to the IC_{50} and IC_{80} doses determined previously [16], were prepared in sterile, deionized Mili-Q water.

2.2. Cell lines and culture conditions

Four human pancreatic cancer cell lines, Panc-1 (CRL-1469), MIA PaCa-2 (CRL-1420), AsPC-1 (CRL-1682), and BxPC-3 (CRL-1687), were purchased from the American Type Culture Collection (ATCC, Manassas, VA, USA). Panc-1 and MIA PaCa-2 cells were maintained in high-glucose Dulbecco's modified Eagle's medium (DMEM HG, Merck/Sigma-Aldrich, St. Louis, MO, USA), while AsPC-1 and BxPC-3 cells were maintained in Roswell Park Memorial Institute 1640 medium (RPMI 1640, Merck/Sigma-Aldrich, St. Louis, MO, USA). Both media were supplemented with heat-inactivated 10 % fetal bovine serum (FBS; Biowest, Riverside, MO, USA), 100 μg/mL streptomycin, and 100 units/mL penicillin. Normal pancreatic cells, hTERT-HPNE (ATCC, Manassas, VA, USA), were maintained in 75 % Dulbecco's modified Eagle's medium without glucose (Merck/Sigma-Aldrich, St. Louis, MO, USA), 25 % Essential 8™ Basal Medium (Gibco, Thermo Fisher, Waltham, MA, USA) supplemented with heat-inactivated 5 % FBS, 10 ng/mL human Epidermal Growth Factor (hEGF, Merck/Sigma-Aldrich, St. Louis, MO, USA), 1 g/L D-glucose (POCH, Gliwice, Poland), and 1 % Penicillin-Streptomycin. Cells were maintained at 37 °C in a humidified atmosphere with 5 % CO_2. All experiments were performed on cells in a logarithmic growth phase.

2.3. Cell viability assay

Cell viability was investigated using a colorimetric, MTT (3-(4,5-dimethyl-2-thiazolyl)-2,5-diphenyl-2H-tetrazolium bromide, Merck/Sigma-Aldrich, St. Louis, MO, USA) analysis based on the reduction of this yellow salt in metabolically active cells to purple formazan crystals. Cells were seeded onto 24-well plates at 2.5×10^4 cells/well for Panc-1 and BxPC-3, 2×10^4 cells/well for MIA PaCa-2 and AsPC-1. After 24 h incubation, necessary for cell attachment, cells were treated with the reference compound at $IC_{50,}$ or autophagy inhibitors for 1 h, followed by UAs at IC_{80}. The concentrations of autophagy inhibitors used were: wortmannin (WM) at 2 μM [29], chloroquine (CQ) at 20 μM [29,30], and ammonium chloride (NH_4Cl) at 5 mM, only in Panc-1 cells at 15 mM [31,32]. After 24 and 72 h of incubation, 200 μL MTT at a concentration of 4 mg/mL was added to each well for 3–4 h. The culture medium was then aspirated, and formazan crystals were dissolved in DMSO. The absorbance of the solutions was measured at 540 nm using an iMark Microplate Absorbance Reader (Bio-Rad, Hercules, CA, USA). The cell viability was assessed relative to untreated control cells. The experiment was independently repeated at least four times.

2.4. Cell cycle analysis

Cell cycle distribution of hTERT-HPNE cells was assessed by DNA content, which was determined by flow cytometry using propidium iodide (PI), a fluorescent dye that binds stoichiometrically to DNA. Cells were seeded at a density of 1.5×10^6 per 100 mm Petri dish. Cells were then treated with IC_{80} doses of UAs for 120 h. Next, the cells were washed with cold 1X PBS buffer, trypsinized, and then washed twice with cold 1X PBS. They were subsequently fixed in 80 % (v/v) ethanol at –20 °C for at least 24 h. Afterward, samples were washed twice with 1X PBS, stained with PI/RNase Staining Buffer (BD Biosciences, San Jose, CA, USA), and analyzed using a FACS Accuri C6 flow cytometer (BD Biosciences, San Jose, CA, USA). At least 10,000 cells were collected, and the results were analyzed using BD Accuri C6 Software (Version 1.0264.21). The experiment was independently repeated at least four times.

2.5. Cell death determination by annexin V/propidium iodide (PI) analysis

The type of cell death induced by the UAs in hTERT-HPNE cells was assessed using PI/annexin V-FITC double staining. Cells were seeded and treated with test compounds as in the cell cycle analysis. After UAs' exposure, cells were harvested, washed twice with cold 1X PBS, pelleted, and resuspended in 50 μL of binding buffer containing PI and annexin V-FITC (FITC Annexin V Apoptosis Detection Kit I, BD Biosciences, San Jose, CA, USA). Samples were then incubated in the dark for 15 min at room temperature. Afterward, 180 μL of binding buffer was added, and samples were analyzed with a FACS Accuri C6 flow cytometer (BD Biosciences, San Jose, CA, USA). At least 10,000 cells were collected, and the results were analyzed using BD Accuri C6 Software (Version 1.0264.21). The experiment was independently repeated at least four times.

2.6. Assessment of cell nuclei morphology

Cell nucleus morphology was determined by staining cells with the fluorescent dye Hoechst 33342 (Merck/Sigma-Aldrich, St. Louis, MO, USA), which specifically binds to DNA. hTERT-HPNE cells were seeded and treated with test compounds, analogous to cell cycle analysis. Successively, cells were washed with 1X PBS, resuspended in 1X PBS, and centrifuged onto slides. After 15 min fixing with methanol: acetic acid (3:1), samples were stained with Hoechst 33342 (1 mg/mL) for 15 min. The morphology of the nuclei was examined under an OLYMPUS BX60 microscope connected to a U-RFL-T lamp coupled via XC50 CCD camera to a computer equipped with cellSens Standard 1.18 software (Olympus, Tokyo, Japan). Images were taken using the UV filter and 400 × magnification. The experiment was independently repeated at least three times.

2.7. Acidic vesicular organelles (AVOs) detection

The amount of acidic vesicular organelles (AVOs) was assessed by staining cells with acridine orange (AO), a cell-permeable green fluorescent dye that can be protonated and trapped in acidic vesicular organelles, where it shifts to red fluorescence. Cells were seeded at a density of 0.55×10^6 for Panc-1, 0.44×10^6 for BxPC-3, and 0.37×10^6 for MIA PaCa-2 and AsPC-1 per 60 mm Petri dish. Cells were treated with the reference compound at $IC_{50,}$ or autophagy inhibitors (at the doses given in the *Cell Viability Assay*) for 1 h, followed by UAs at IC_{80} for 24, 72, and 120 h. Next, cells were stained with 1 μg/mL acridine orange for 15 min. After incubation, cells were washed with cold 1X PBS, trypsinized, and then washed twice with cold 1X PBS. They were subsequently suspended in 200 μL of 1X PBS and centrifuged onto slides. The presence of AVOs was examined under an Olympus BX60 microscope, connected to a U-RFL-T lamp and coupled via an XC50 CCD camera to a computer equipped with CellSens Standard 1.18 software (Olympus, Tokyo, Japan). Images were taken using the blue filter and 200 × magnification. For each experimental replicate, 3–4 non-overlapping microscopic fields were imaged that showed at least 50 cells. These images were used for quantitative analysis, and

representative images are presented in the manuscript. The amount of AVOs was defined as the ratio of AVOs fluorescence intensity to the total fluorescence intensity of living cells. Cells were identified as apoptotic based on the presence of intensely bright green apoptotic bodies and were excluded from the fluorescence intensity analysis. Fluorescence intensity was measured in CellProfiler 4.2.8 [33]. The experiment was independently repeated at least three times.

2.8. Western blot analysis

To assess the selected protein levels, cells were seeded at densities of 1.5×10^6 for Panc-1, 1.2×10^6 for BxPC-3, and 1×10^6 for MIA PaCa-2 and AsPC-1 per 100 mm Petri dish. After treatment with IC_{80} doses of UAs and IC_{50} doses of reference compounds, cells were scraped, harvested, and washed twice with cold 1X PBS. Cells suspension in RIPA buffer (Abcam, Cambridge, UK), cocktail of proteases (cOmplete Tablets, Roche, Mannheim, Germany), phosphatase inhibitors (PhosSTOP, Roche, Mannheim, Germany), and 1 mM phenylmethanesulfonyl fluoride (PMSF, Merck/Sigma-Aldrich, St Louis, MO, USA) was maintained on ice for 20 min with brief vortexing every 5 min. Following the lysis, the samples were centrifuged at 14,000 g for 15 min at 4 °C. The protein concentration was determined using the DC Protein Assay (Bio-Rad, Hercules, CA, USA). Equal amounts of cell lysates (30 μg) were denatured at 100°C for 5 min in a buffer consisting of Laemmli buffer (Bio-Rad, Hercules, CA, USA) and 2-Mercaptoethanol (Merck/Sigma-Aldrich, St. Louis, CA, USA). Then, samples were subjected to SDS-PAGE and electrotransferred onto nitrocellulose membranes using a semi-dry blotting apparatus (Bio-Rad, Hercules, CA, USA). Next, the membrane was blocked with every blot-blocking buffer (Bio-Rad, Hercules, CA, USA), washed five times with TBST buffer, and probed with relevant primary antibodies. Rabbit anti-Beclin1 (1:1000), rabbit anti-Bcl-2 (1:1000), and rabbit anti-p62 (1:1000) antibodies were purchased from Cell Signaling Technology (Beverly, MA, USA). Rabbit anti-LC3B (1:500) and mouse anti-β-actin (1:10,000) antibodies were purchased from Merck/Sigma-Aldrich (St. Louis, MO, USA). Rabbit anti-E-Cadherin (1:1000), rabbit anti-N-Cadherin/CDH2 (1:1000), and rabbit anti-Vimentin (1:1000) antibodies were purchased from Boster Biological Technology (Pleasanton, CA, USA). Secondary anti-mouse (1:2000) and anti-rabbit (1:2000) antibodies linked to horseradish peroxidase were purchased from Cell Signaling Technology (Beverly, MA, USA). Membranes were reprobed with another antibody after stripping with Restore PLUS Western Blot Stripping Buffer (Thermo Scientific, Waltham, MA, USA) for 15 min with gentle shaking. Finally, membrane development was performed via chemiluminescence detection using enhanced chemiluminescence system reagents (Thermo Scientific, Waltham, MA, USA). Bands were quantified by densitometric analysis using Image Lab software (Bio-Rad, Hercules, CA, USA), and the expression levels were normalized to β-actin. The experiment was independently repeated at least two times.

2.9. Apoptosis detection – caspase 3/7

Detection of activated caspases 3 and 7 in apoptotic cells was performed using the CellEvent™ Caspase-3/7 Green Flow Cytometry Assay Kit (Invitrogen, Thermo Fisher, Waltham, MA, USA). Cells were seeded onto a 60 mm Petri dish at a density of 0.55×10^6 for Panc-1, 0.44×10^6 for BxPC-3, and 0.37×10^6 for MIA PaCa-2 and AsPC-1. Cells were then treated with the reference compound at the IC_{50} and autophagy inhibitors at the doses specified in the *Cell Viability Assay* for 1 h, followed by UAs at the IC_{80} for 24 and 72 h. Next, the cells were washed with cold 1X PBS buffer, trypsinized, and then washed twice with cold 1X PBS before being resuspended in culture medium containing a caspase 3/7 probe. Cells were then incubated for 20 min in a humidified atmosphere of 5 % CO_2 at 37°C and analyzed with a FACS Accuri C6 flow cytometer (BD Biosciences, San Jose, CA, USA). At least 10,000 cells were collected, and the results were analyzed using BD Accuri C6 Software (Version 1.0264.21). The experiment was independently repeated at least four times.

2.10. Wound healing migration assay

Mobility of cells was analyzed by seeding in a culture-insert (Ibidi culture-insert 2 well; Ibidi GmbH, Martinsried, Germany) at a density of 3×10^4 for Panc-1 and BxPC-3, 2.3×10^4 for MIA PaCa-2, and 2.5×10^4 for AsPC-1 per well. After 24 h the culture insert was removed, and the attached cells were washed with the appropriate medium. Following 1 h preincubation with mitomycin C (Merck/Sigma-Aldrich, St. Louis, MO, USA) to prevent cell proliferation, cells were washed twice with fresh medium and exposed to the reference compound at $IC_{50,}$ and autophagy inhibitors for 1 h, at doses given in the *Cell Viability Assay,* followed by UAs at IC_{80}. The plate was placed in an imaging chamber (CellVivo incubation system; Olympus, Tokyo, Japan) at 37 °C with 5 % CO_2. Cell migration was monitored using live-cell microscopy with time-lapse photography every 3 h for 72 h under 10 × magnification. Images were acquired using a phase-contrast fluorescence microscope (IX83 Inverted Microscope; Olympus, Tokyo, Japan) connected to an XC50 digital color camera (Olympus, Tokyo, Japan). Images were combined using CellSens Dimension software version 1.18, and the wound closure percentage was quantified with ImageJ software. The experiment was independently repeated at least four times.

2.11. Statistical analysis

The results are presented as the means ± SD from at least three independent experiments. The normality of data was assessed using the D'Agostino-Pearson test. Statistical analysis was performed using the Kruskal-Wallis one-way analysis of variance for non-parametric data and Dunn's multiple comparison tests due to the non-normal data distribution. Differences $p < 0.05$ between the group of untreated cells (negative control) or the initial wound area and the group of cells treated with the compound were considered statistically significant according to the following criteria: * $p < 0.05$, ** $p < 0.01$, and *** $p < 0.001$. Statistical analysis of the data was performed using GraphPad Prism Version 5.00 (GraphPad Software, San Diego, CA, USA).

3. Results

3.1. Impact of UAs on normal pancreatic cells – hTERT-HPNE

Our previous studies confirmed the favorable properties of UA derivatives, showing lower cytotoxicity toward normal hTERT-HPNE pancreatic cells compared with cancer cells [16]. The detailed results of cytotoxicity of UAs in cancer and normal cells are presented in Fig. 1. The most active derivative against pancreatic cancer cells, C-2028, exhibited reduced activity in normal cells, with an IC_{80} value of 0.366 μM. In contrast, the less active derivatives C-2045 and C-2053 showed at least twice the IC_{80} in normal cells, at 0.830 and 0.853 μM, respectively.

The present study began with an assessment of the cellular response induced by UAs in normal cells after 120 h of incubation. The flow cytometric analysis was performed to determine the cell cycle distribution, the membrane asymmetry, and integrity using Annexin V-FITC/PI double staining, and to measure the levels of caspases 3 and 7. Additionally, nuclear morphology was examined (Fig. 2 and Fig. S1 in the SI).

The main change in cell cycle distribution was an increase in the sub-G1 fraction, which indicated DNA fragmentation (Fig. 2a**)**. Kruskal–Wallis analysis confirmed a significant overall treatment effect ($H(3) = 12.0$, $p = 0.001$, $N = 19$). Post-hoc Dunn's test revealed that both C-2028 (19.2 %; $p = 0.006$) and C-2045 (19.5 %; $p = 0.03$) significantly increased the hypodiploid cell population compared with the control.

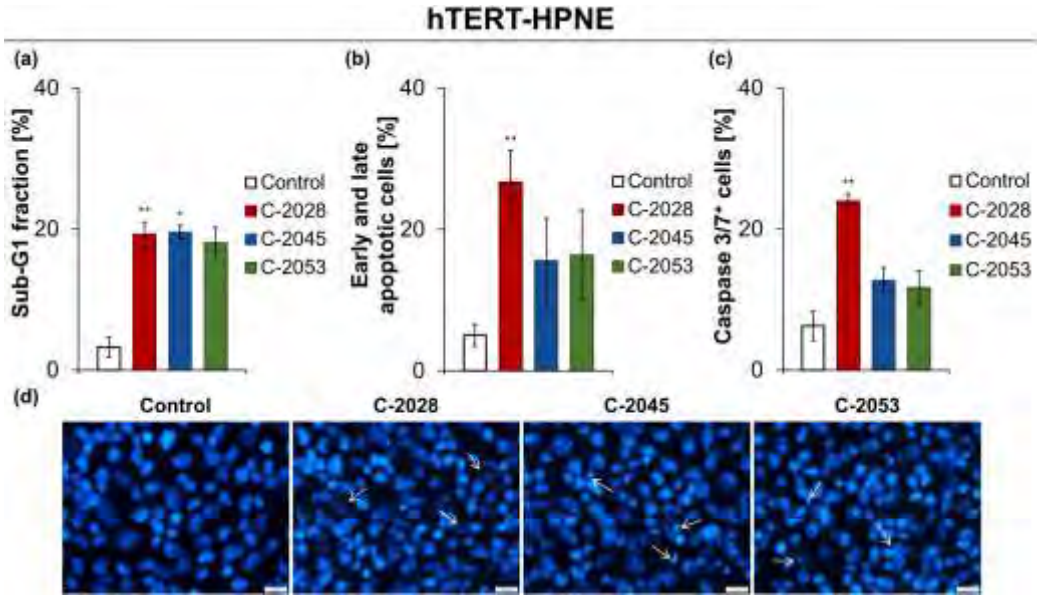

Fig. 2. Cellular response induced by UA derivatives in normal pancreatic hTERT-HPNE cells. Cells were treated for 120 h with IC_{80} doses of C-2028, C-2045, and C-2053. **(a)** DNA degradation level expressed as the percentage of sub-G1 cells, based on PI/RNase staining and flow cytometry. **(b)** Apoptotic cell population (early and late apoptosis) determined by Annexin V-FITC/PI double staining. **(c)** Caspase 3/7 activation was measured by flow cytometry using a fluorogenic caspase substrate. **(d)** Nuclear morphology was evaluated by Hoechst 33342 staining and visualized under a fluorescence microscope (400 ×); white arrows indicate apoptotic bodies. The results are presented as the means ± SD. Statistical analysis was performed using the Kruskal-Wallis test followed by Dunn's post hoc test; **(a)**: $H(3) = 12.0$, $p = 0.001$, $N = 19$; **(b)**: $H(3) = 12.8$, $p < 0.001$, $N = 17$; **(c)**: $H(3) = 10.6$, $p < 0.001$, $N = 14$. Differences versus control: $^{*}p < 0.05$, $^{**}p < 0.01$, $^{***}p < 0.001$; $n \geq 4$.

Interestingly, after 120 h of incubation, C-2028 induced DNA fragmentation in 57.2 % of the MIA PaCa-2 cancer cell population [16]. Annexin V-FITC/PI staining confirmed that DNA fragmentation resulted from apoptosis (Fig. 2b). Again, treatment effects were significant ($H(3) = 12.8$, $p < 0.001$, $N = 17$). The percentage of annexin V-positive cells ranged from 15.6 % to 26.7 %, with C-2028 (26.7 %; $p = 0.001$) triggering the strongest apoptotic response. In contrast, among PC cells, the highest proportion of apoptotic cells was observed in Panc-1 cells treated with C-2045 for 120 h, 67.2 % [16]. Moreover, caspase 3/7 activity was significantly elevated in normal cells following UAs treatment ($H(3) = 10.6$, $p < 0.001$, $N = 14$), ranging from 11.7 % to 23.9 %, with the highest activation again observed for C-2028 (23.9 %; $p = 0.004$) (Fig. 2c). Apoptosis induction was further supported by nuclear morphology analysis, where the formation of apoptotic bodies was the predominant alteration caused by UA treatment (Fig. 2d).

UA derivatives demonstrated selective cytotoxicity, being less toxic to normal pancreatic cells than cancer cells. After 120 h of treatment, UA exposure resulted in moderate apoptosis in normal cells, with the most substantial pro-apoptotic effect consistently observed for C-2028. These findings confirm that UAs induce apoptosis in normal cells to a lesser extent than in cancer cells [16], supporting their therapeutic potential with limited off-target effects.

3.2. Autophagy detection

Analysis was first assessed by microscopic evaluation of acidic cell organelles (AVOs), including autophagosomes, autolysosomes, lysosomes, and other acidic vesicles. These structures, after fusion with autophagosomes, play the executive role of degrading the absorbed cargo by lysosomal enzymes, and their increased presence can serve as an indicator of this process (Fig. 3 and Figs. S2-S5 in the SI) [34].

In Panc-1 cells treated with UAs, an increase in AVOs level was noted, particularly after 72 h of C-2028 treatment and 120 h of C-2045, both of which reached a mean fluorescence intensity (MFI) ratio of 2.0 (Fig. S2 in the SI). Kruskal–Wallis tests indicated no significant differ-ences at 24 h ($H(4) = 8.14$, $p = 0.06$, $N = 16$), but treatment effects became significant at later time points (72 h: $H(4) = 11.1$, $p = 0.003$, $N = 15$; 120 h: $H(4) = 11.1$, $p = 0.003$, $N = 15$). Post-hoc analysis, however, did not reveal statistically significant pairwise differences versus control (all $p > 0.07$). In parallel, IR induced progressive AVOs accumulation, maintaining a 2.0 MFI ratio at the longest time point. In MIA PaCa-2 cells, the highest red fluorescence signal was observed after 24 h of C-2028 treatment (MFI 2.1), followed by a marked decline (Fig. S3 in the SI). Statistically, Kruskal–Wallis tests showed significant treatment effects across all time points (24 h: $H(4) = 9.02$, $p = 0.03$, $N = 16$; 72 h: $H(4) = 8.70$, $p = 0.04$, $N = 15$; 120 h: $H(4) = 10.1$, $p = 0.01$, $N = 15$). Post-hoc Dunn's test identified a significant increase only after 120 h for C-2053 ($p = 0.02$ vs control), while other comparisons remained nonsignificant ($p > 0.1$). GEM and other UAs gradually reduced the AVOs level, reaching as low as 0.1 MFI ratio after 120 h. The most pronounced accumulation of AVOs occurred in AsPC-1 cells (Fig. S4 in the SI). Kruskal–Wallis analyses showed highly significant effects (24 h: $H(4) = 13.1$, $p < 0.001$, $N = 15$; 72 h: $H(4) = 13.0$, $p < 0.001$, $N = 15$; 120 h: $H(4) = 11.4$, $p = 0.002$, $N = 15$). Dunn's test confirmed significant increases in red fluorescence at 72 h for C-2028 (MFI 10.0; $p = 0.01$) and GEM (MFI 8.6; $p = 0.02$), as well as at 120 h for C-2028 (MFI 5.8; $p = 0.01$). Although the AVO levels decreased by 120 h, they remained elevated compared to the control. This pattern of increased and subsequently reduced red fluorescence may indicate the induction of autophagy followed by effective autophagic flux. An opposite trend was observed in BxPC-3 cells, which have the highest levels of AVOs at baseline, where exposure to all tested compounds led

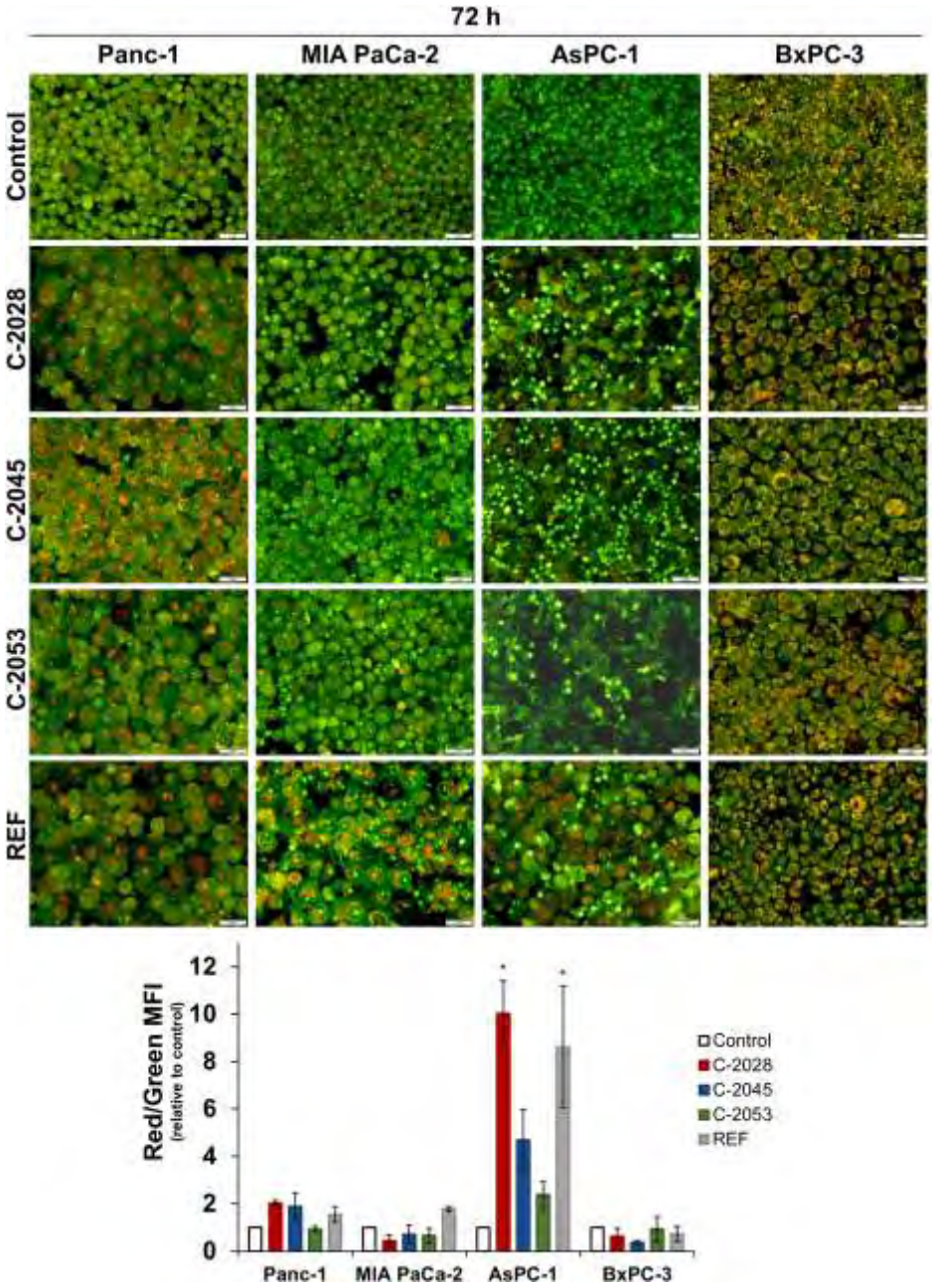

Fig. 3. Acidic vesicular organelles (AVOs) detection in pancreatic cancer (PC) cells treated with UAs. Cells were exposed to IC_{80} doses of unsymmetrical bisacridines (UAs): C-2028, C-2045, and C-2053, and IC_{50} doses of reference compounds (REF; irinotecan for Panc-1 and gemcitabine for MIA PaCa-2, AsPC-1, and BxPC-3). Representative images showing AVOs (red fluorescence) as well as the cytoplasm and nucleus (green fluorescence) in PC cells after 72 h of treatment. Cells were stained with acridine orange (1 μg/mL) and analyzed by fluorescence microscopy (200 ×). Red/Green mean fluorescence intensity (MFI) was measured in CellProfiler and related to the control. The results are presented as the means ± SD. Statistical analysis was performed using the Kruskal–Wallis test followed by Dunn's post hoc test; H(8) = 8.7–13.3, $p < 0.04$, N = 15–16. Differences versus control: $^{*}p < 0.05$, $^{**}p < 0.01$, $^{***}p < 0.001$; $n \geq 3$.

to a decrease in acidic organelle levels below that of the untreated control. Statistical analyses did not confirm significant differences at any time point (24 h: H(4) = 8.26, $p = 0.05$, N = 15; 72 h: H(4) = 5.54, $p = 0.25$, N = 15; 120 h: H(4) = 5.24, $p = 0.28$, N = 15).

Because changes in AVO accumulation suggested autophagy induction, the key protein indicators of autophagic activity were evaluated. Among these are the conversion of the LC3 from LC3-I to LC3-IIand p62 proteins [19,20]. Pancreatic cancer cells, particularly Panc-1 and BxPC-3, exhibit high baseline levels of autophagy, as evidenced by the predominance of the LC3-II form over LC3-I (Fig. 4, Fig. S6 in the SI, and Fig. S2.1 in the Western Blot). In all UA-treated cell lines, LC3-II protein levels increased relative to LC3-I (Fig. 4, Figs. S7–S11, Table 1 in the SI, and Figs. S2.2-S2.5 in the Western Blot). In Panc-1 cells, UAs treatment significantly enhanced the lipidation of LC3 protein. Kruskal–Wallis analysis confirmed a robust effect for LC3-II (72 h: H(4) = 17.7, $p = 0.001$, N = 15; 120 h: H(4) = 20.4, $p < 0.001$, N = 18) with Dunn's post hoc analysis showing highly signisicant increases after treatment with C-2028 for 120 h (5.5-fold; $p = 0.007$), C-2045 for 72 h (5.4-fold; $p < 0.001$), and especially C-2045 for 120 h (11.4-fold; $p < 0.001$). p62 levels also decreased significantly (H(4) = 11.3, $p = 0.002$, N = 15), particularly after C-2045 at 120 h ($p = 0.01$), indicating efficient autophagic flux. In AsPC-1 cells, autophagy activation was even stronger. LC3-II levels showed a highly significant increase after 120 h of treatment (H(4) = 16.1, $p = 0.003$, N = 18). Post hoc analysis revealed that compounds C-2053 and C-2045 induced substantial effects, resulting in 31.7-fold ($p = 0.008$) and 33.5-fold ($p = 0.003$) increases in LC3-II protein levels, respectively. Simultaneously, a significant reduction in p62 levels was observed at 120 h (H(4) = 11.2, $p = 0.003$, N = 15), particularly after extended exposure to C-2053, which resulted in a decrease to 0.1 ($p = 0.02$). BxPC-3 cells also responded strongly to UA treatment. LC3-II levels increased significantly, particularly after 120 h (H(4) = 12.3, $p < 0.001$, N = 15), with marked effects observed for C-2045 (3.5-fold increase) and C-2053 (3.6-fold increase). A parallel reduction in p62 was detected (120 h: H = 11.9, $p = 0.02$, N = 18), though less pronounced than in AsPC-1. In MIA PaCa-2 cells, LC3-II induction was weaker and more variable. Although overall effects were significant (72 h: H(4) = 14.8, $p = 0.005$, N = 17; 120 h: H(4) = 12.6, $p = 0.01$, N = 17), the increases were mainly attributable to C-2028, which induced a 6.0- fold (p = 0.002) and a 3.3-fold ($p = 0.004$) increase in LC3-II levels after 72 and 120 h, respectively. Notably, p62 levels increased up to 1.8-fold relative to control following treatment with C-2045 and C-2053 (120 h: H = 12.3, $p < 0.001$, N = 15), indicating a disruption of autophagic flux. In contrast, only C-2028 led to a reduction in p62 levels (to 0.6-fold of control after 72 h), suggesting that effective autophagy was restored only by this compound. Reference compounds in all cell lines caused only a slight increase in LC3-II and a decrease in p62.

To determine whether UA-induced autophagy in PC cells is Beclin1-dependent and related to apoptosis, cell death strongly induced by UAs [16], Beclin1 and Bcl-2 protein levels were analyzed (Fig. 4, Figs. S7–S11, Table 1 in the SI, and Figs. S2.2-S2.5 in the Western Blot). The Beclin1-dependent complex can initiate autophagy. In contrast, the anti-apoptotic protein Bcl-2 negatively regulates this process by interacting with the BH3 domain of Beclin1 [21].

In Panc-1 cells, both Beclin1 and Bcl-2 levels decreased significantly after 120 h (H(4) = 12.7, $p = 0.01$, N = 18 for Beclin1; H = 11.2, $p = 0.02$, N = 17 for Bcl-2), consistent with a shift in the autophagy-–apoptosis balance toward apoptosis and Beclin1-independent autophagy. In contrast, AsPC-1 and BxPC-3 cells exhibited reduced Beclin1 levels and increased Bcl-2 expression following compound exposure, indicating inhibition of autophagy and further supporting a Beclin1-independent induction mechanism. A significant increase in both Beclin1 and Bcl-2 levels was observed exclusively in MIA PaCa-2 cells treated with UAs (120 h: H(4) = 13.8, $p = 0.008$, N = 17 for Beclin1; H = 14.6, $p < 0.001$, N = 16 for Bcl-2), with Beclin1 levels elevated by 1.5–2.0-fold and Bcl-2 by 1.1–2.6-fold. The concurrent rise in Bcl-2, particularly under C-2053 after 120 h (2.6-fold increase; $p = 0.03$), may represent a feedback mechanism to limit excessive autophagy activation. Notably, the weakest Bcl-2 induction was observed in C-2028-treated cells, which also exhibited LC3-II upregulation and a reduction in p62.

To conclude, the results indicated that UA treatment triggered autophagy in all four PC cell lines, although the extent and role of this process varied. Specifically, autophagy appeared to be primarily pro-death for both Panc-1 and AsPC-1 cells, partially protective for BxPC-3 cells, and had an intermediate effect on MIA PaCa-2 cells which are indicative of the cell line's combined responses to both apoptosis and autophagy induction. Overall, despite differences in Beclin1 and Bcl-2 modulation across cell lines, these results show that UAs induce autophagy in PC cells through a Beclin1-independent mechanism.

3.3. The UAs-induced cellular response following autophagy inhibition

To investigate whether UAs induce pro-survival or pro-death autophagy, their effect on AVOs level, cell viability, and apoptosis was evaluated following treatment with selected UA derivatives in combination with autophagy inhibitors: wortmannin (WM) [29], chloroquine (CQ) [29,30], and ammonium chloride (NH_4Cl) [31,32]. For each PC cell line, one UA derivative was selected: C-2028 for MIA PaCa-2 and AsPC-1, C-2045 for Panc-1, and C-2053 for BxPC3 cells, based on its high pro-apoptotic potential [16] and strong autophagy-inducing capacity.

First, changes in the AVOs level were evaluated (Fig. 5a and Figs. S12–S15 in the SI). In Panc-1 cells, Kruskal–Wallis analysis indicated significant treatment effects after 24 h (H(8) = 16.7, $p = 0.03$, N = 28) and 72 h (H(8) = 22.7, $p = 0.004$, N = 27). However, Dunn's post-hoc test did not identify significant pairwise differences versus control ($p > 0.5$ for all). Treatment with C-2045 combined with CQ or NH_4Cl resulted in reduced AVOs accumulation, while co-treatment with WM produced a similar AVOs level to that observed with C-2045 alone. In MIA PaCa-2 cells, co-treatment with either CQ or NH_4Cl led to a marked increase in AVOs accumulation, reaching a maximum of 5.1 and 2.8 MFI ratios after 72 h, respectively. Statistically, significant effects were observed both at 24 h (H(8) = 16.0, $p = 0.04$, N = 28) and 72 h (H(8) = 23.7, $p = 0.003$, N = 27), but post-hoc tests showed no significant pairwise differences ($p > 0.09$). Similar to Panc-1 cells, the addition of WM to the UA derivative did not significantly alter the effect of the UA alone. In AsPC-1 cells, strong accumulation of AVOs was observed after 24 h and 72 h of C-2028 treatment. Kruskal–Wallis confirmed significant treatment effects (24 h: H(8) = 21.0, $p = 0.007$, N = 27; 72 h: H(8) = 23.7, $p = 0.003$, N = 28). Dunn's tests revealed significant increases at 24 h for CQ ($p = 0.03$), C-2028 +CQ ($p = 0.003$), and C-2028 +NH_4Cl ($p = 0.04$), as well as at 72 h for C-2028 +CQ ($p = 0.008$). Consistent with these data, co-treatment with CQ or NH_4Cl for 72 h further increased AVO formation beyond the levels induced by C-2028 alone (MFI 10.0), reaching 16.7 and 11.8, respectively. In contrast, co-treatment with WM reduced AVO generation to an MFI of 2.4. In BxPC-3 cells, which had the highest basal AVO levels, Kruskal–Wallis tests showed significant effects at 24 h (H(8) = 21.9, $p = 0.005$, N = 27) and 72 h (H(8) = 21.2, $p = 0.007$, N = 27). Dunn's analysis demonstrated that CQ ($p = 0.009$) and C-2053 +CQ ($p = 0.002$) significantly suppressed AVO formation after 24 h, while after 72 h, only C-2053 +CQ remained significant ($p = 0.02$). Overall, all autophagy inhibitors tended to suppress AVO accumulation when combined with C-2053.

Subsequently, cell viability was assessed to determine whether autophagy inhibition enhances the cytotoxic effect of selected UAs (Fig. 5b and Fig. S16 in the SI). In Panc-1 cells, Kruskal–Wallis analysis revealed significant treatment effects after both 24 h (H(8) = 19.7, $p = 0.01$, N = 28) and 72 h (H(8) = 23.7, $p = 0.003$, N = 27). Dunn's post-hoc test confirmed that C-2045 ($p = 0.03$) alone and in combination with NH_4Cl ($p = 0.01$) significantly reduced viability compared with control after 24 h, resulting in 68.7 % viability. After 72 h, several

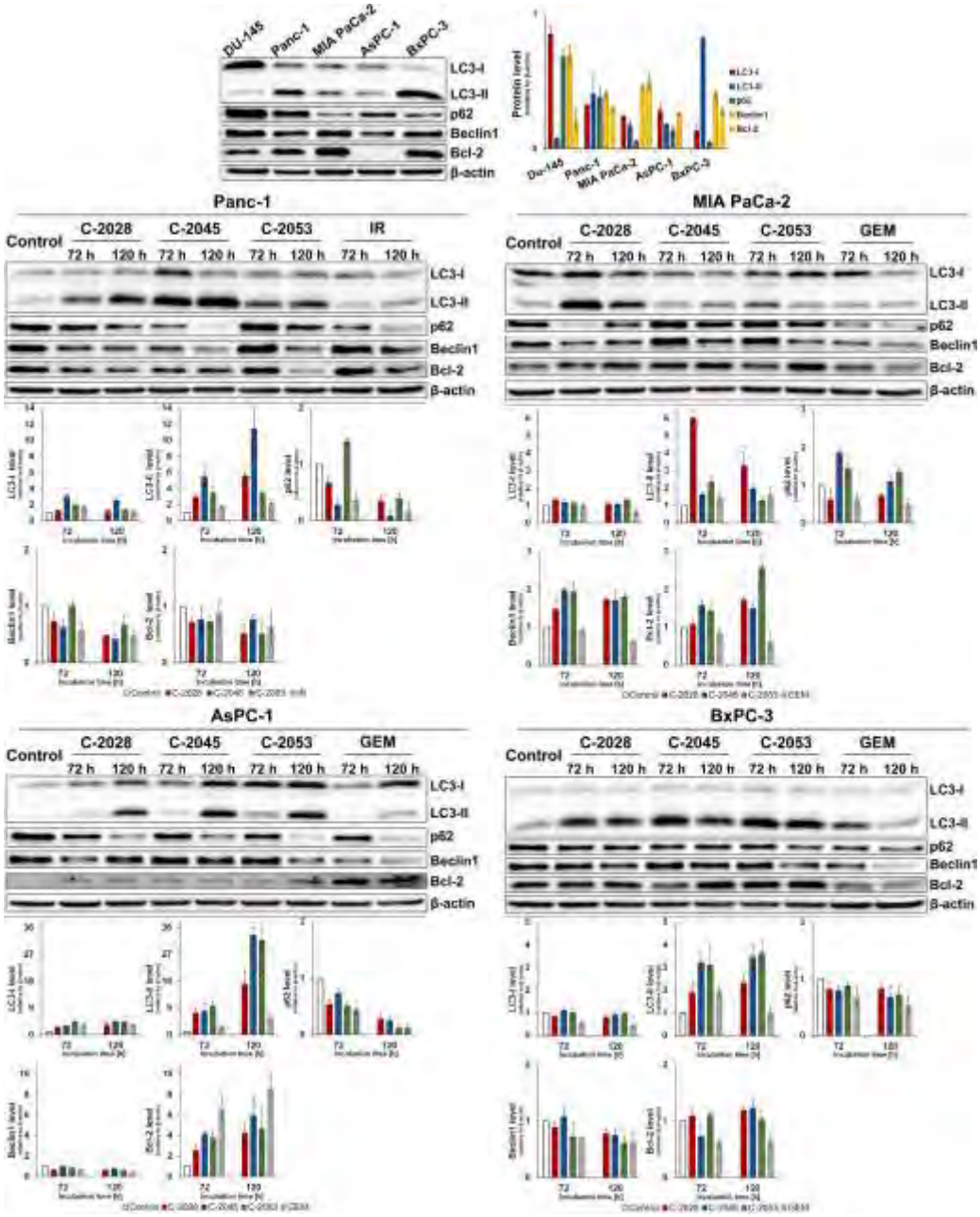

Fig. 4. Western blot analysis of LC3-I/II, p62, Beclin1, and Bcl-2 protein levels in PC cells. DU-145 cells were used as a positive control. Cells were exposed to IC_{80} doses of unsymmetrical bisacridines (UAs): C-2028, C-2045, and C-2053, and IC_{50} doses of reference compounds (IR -irinotecan for Panc-1 and GEM - gemcitabine for MIA PaCa-2, AsPC-1, and BxPC-3) for 72 and 120 h. Total protein samples (30 μg/lane) were separated by SDS-PAGE, transferred to membranes using a semi-dry method, and detected using specific antibodies and enhanced chemiluminescence. The results are presented as the means ± SD. Statistical analysis was performed using the Kruskal–Wallis test followed by Dunn's post hoc test; H(4) = 9.3–20.4, $p < 0.09$, N = 15–20. Differences versus control: $^{*}p < 0.05$, $^{**}p < 0.01$, $^{***}p < 0.001$; $n \geq 2$.

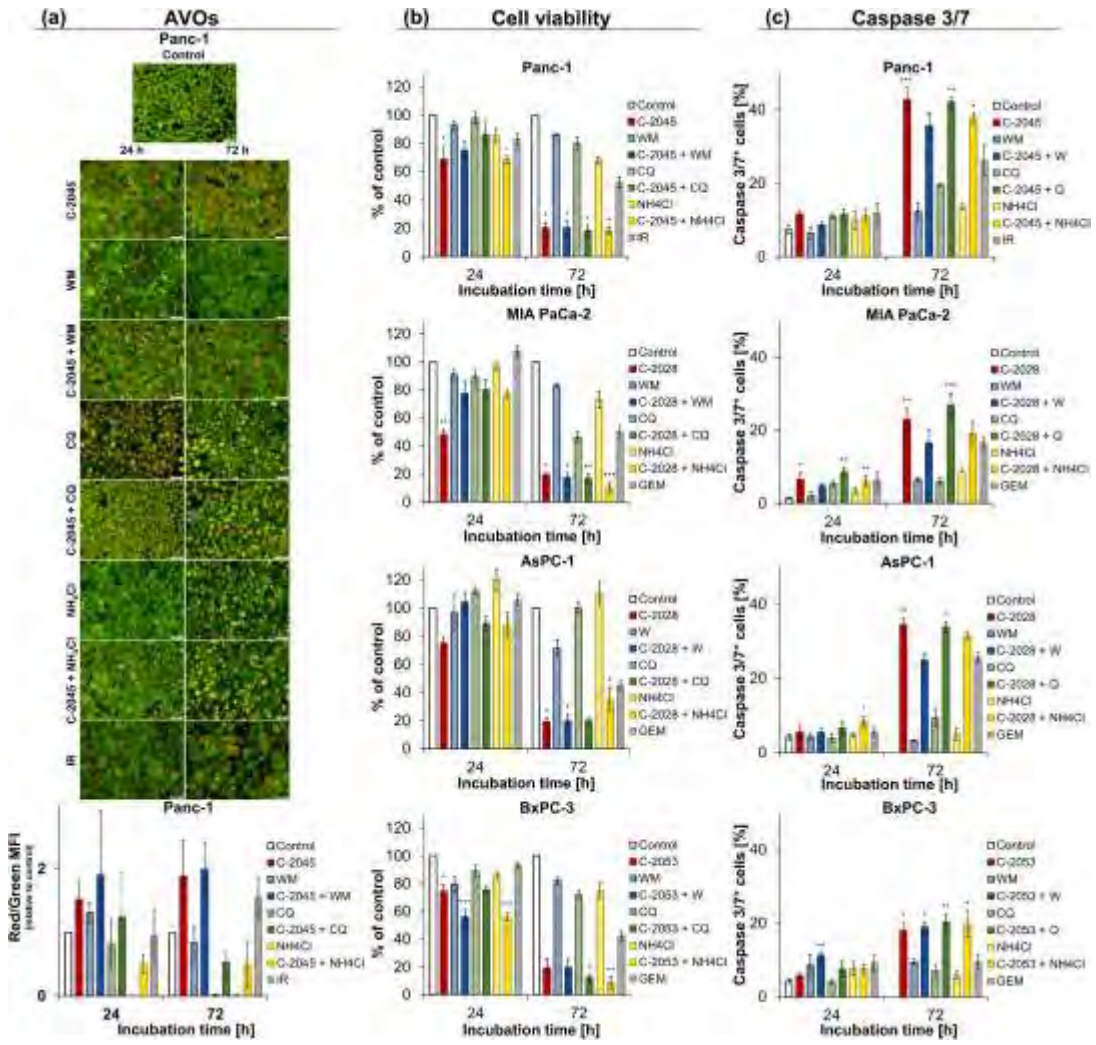

Fig. 5. Cellular response following autophagy inhibition. Pancreatic cancer (PC) cells were preincubated for 1 h with autophagy inhibitors: wortmannin (WM), chloroquine (CQ), or ammonium chloride (NH_4Cl), and subsequently treated with IC_{80} doses of selected unsymmetrical bisacridines (UAs): C-2028, C-2045, or C-2053. As a positive control, IC_{50} doses of reference compounds gemcitabine (GEM) and irinotecan (IR) were used. **(a)** Representative images of Panc-1 cells after 72 h of treatment, showing acidic vesicular organelles (AVOs; red fluorescence), cytoplasm, and nuclei (green fluorescence). Cells were stained with acridine orange (1 μg/mL) and analyzed by fluorescence microscopy (200 ×). Red/Green mean fluorescence intensity (MFI) was measured in CellProfiler and related to the control. (b) Cell viability of PC cells was assessed using the colorimetric MTT (4 mg/mL) assay. The percentage of viable cells was normalized to the untreated control. **(c)** Apoptosis detection by flow cytometry based on the percentage of caspase3/7-positive cells. The results are presented as the means ± SD. Statistical analysis was performed using the Kruskal–Wallis test followed by Dunn's post hoc test; **(a):** H(8) = 16.0–23.7, $p < 0.04$, N = 27–28; **(b)**: H(8) = 19.7–30.1, $p < 0.01$, N = 27–33; (c): H(8) = 16.3–30.5, $p < 0.04$, N = 31–36. Differences versus control: $*p < 0.05$, $**p < 0.01$, $***p < 0.001$; $n \geq 3$.

treatments, including C-2045 alone ($p = 0.03$), C-2045 +WM ($p = 0.03$), C-2045 +CQ ($p = 0.02$), and C-2045 +NH_4Cl ($p = 0.01$), markedly decreased viability to 18.3–20.5 %, with no substantial differences between UA alone and its combinations with inhibitors. In MIA PaCa-2 (H(8) = 27.5, $p < 0.001$, N = 31) and AsPC-1 (H(8) = 22.0, $p = 0.005$, N = 29) cells, the strongest reduction in viability was observed after 24 h of treatment with C-2028 alone, reaching up to 48.2 % ($p = 0.009$) in MIA PaCa-2 cells. However, after 72 h, C-2028 co-treatment with NH_4Cl significantly enhanced cytotoxicity in MIA PaCa-2 cells (10.7 %, $p < 0.001$). Whereas, in AsPC-1 cells, this combination was less effective (35.0 %) compared to other combinations and C-2028 alone (19.2–19.8 %). In BxPC-3 cells, treatment effects were again significant at both 24 h (H(8) = 29.4, $p < 0.001$, N = 33) and 72 h (H(8) = 26.2, $p < 0.001$, N = 29). Autophagy inhibition enhanced cytotoxicity of C-2053, particularly in the C-2053 +NH_4Cl combination after 72 h (8.6 %, $p = 0.001$), compared to 19.2 % for UA alone. This effect enhancement was most evident in BxPC-3 cells, while in other tested cells, the cytotoxicity was either comparable to or lower than that of the

UA alone (after 24 h). Notably, autophagy inhibitors alone exhibited some cytotoxicity, especially after 72 h, highlighting their independent contribution to reduced cell viability.

Given that apoptosis is the primary mechanism of UA-induced cytotoxicity [16], caspase-3/7 activation was evaluated following treatment with UA and autophagy inhibitors (Fig. 5c and Figs. S17–S20 in the SI). In Panc-1 cells, Kruskal–Wallis analysis revealed significant overall treatment effects both at 24 h ($H(8) = 19.2$, $p = 0.01$, $N = 35$) and 72 h ($H(8) = 30.5$, $p < 0.001$, $N = 33$). At 24 h, Dunn's post-hoc test did not detect significant pairwise differences compared with control (all $p > 0.09$). However, after 72 h, C-2045 induced the highest level of apoptosis (42.8 %), with a significant increase versus control ($p < 0.001$). In MIA PaCa-2 cells treated for 72 h ($H(8) = 29.7$, $p < 0.001$, $N = 34$), combining C-2028 with CQ modestly increased caspase-3/7 activity from 22.9 % (C-2028, $p = 0.002$) to 26.0 % (C-2028 +CQ, $p < 0.001$), while co-treatment with WM or NH_4Cl yielded lower levels (16.5 % and 19.2 %, respectively). In AsPC-1 cells, apoptosis induction was modest at 24 h but reached clear significance after 72 h. Kruskal–Wallis analysis confirmed treatment effects at both 24 h ($H(8) = 16.3$, $p = 0.04$, $N = 36$) and 72 h ($H(8) = 28.2$, $p < 0.001$, $N = 31$). After 72 h, C-2028 alone induced apoptosis in 34.4 % of cells ($p = 0.004$), and the CQ combination slightly reduced this effect to 33.8 % ($p = 0.02$), while the weakest response was observed with C-2028 +WM (24.8 %). Interestingly, in BxPC-3 cells, all combinations modestly enhanced C-2053-induced apoptosis after 72 h ($H(8) = 25.9$, $p = 0.001$, $N = 31$). The caspase-3/7-positive cell population increased from 18.0 % ($p = 0.02$) for C-2053 alone to 20.3 % ($p = 0.004$) for C-2053 +CQ.

The relationship between autophagy and apoptosis differed across the examined cell lines. In Panc-1, MIA PaCa-2, and AsPC-1 cells, autophagy blockade generally resulted in reduced UA-induced apoptosis, implying that UAs predominantly trigger pro-death autophagy. Conversely, in BxPC-3 cells, autophagy inhibition enhanced UA-induced apoptosis, suggesting a cytoprotective role of autophagy. These findings demonstrate that the efficacy of UA treatment in PC cells may depend on the autophagic status of each cell line.

3.4. Impact of UAs on cell migration

To clarify whether autophagy promotes or suppresses cell migration, a wound healing migration assay was performed, and EMT-related proteins were analyzed in the next step.

All tested UA derivatives inhibited migration in PC cells (Fig. 6a, and Figs. S21–S24 in the SI). MIA PaCa-2 cells showed high motility, as the wound area of untreated cells was fully closed after 24 h of incubation. UAs significantly reduced cell migration already after 24 h, most profoundly the C-2028 in MIA PaCa-2 cells ($H(3) = 11.8$, $p < 0.001$, $N = 16$), where the wound area reached 84 % of the initial state compared to 7.4 % for the control. The wound area gradually increased after UAs exposure up to 72 h, reaching its largest size in BxPC-3 cells treated with C-2053 ($H(3) = 23.6$, $p < 0.001$, $N = 28$), 154.3 % ($p = 0.04$). The reference compounds reduced cell migration to a lesser extent compared to UAs. The anti-migratory properties were observed after treatment with all UAs, particularly derivatives with the greatest pro-apoptotic and pro-autophagic potential.

Considering the reduced migration potential observed in the wound healing assay, a comprehensive investigation was undertaken to determine whether this phenotype correlates with modulation of EMT-related proteins. Although the wound healing assay lasted up to 72 h, EMT markers can also exhibit changes with prolonged compound treatment. To determine whether the observed reduction in cell migration correlates with changes in EMT-related protein expression, western blot analysis was performed at 72 and 120 h following UAs treatment (Fig. 6b, Figs. S25–S29, Table 2 in the SI, and Figs. S2.6-S2.10 in the Western Blot). During EMT, a process that promotes cell migration, E-cadherin decreases, while N-cadherin and vimentin increase [28]. Moreover, as shown in Fig. 6b, E-cadherin protein was undetectable in MIA PaCa-2 [35] as well as vimentin in BxPC-3 cells [36]. In BxPC-3 cells, which were the most susceptible to migration inhibition by UAs, E-cadherin levels dropped the weakest, reaching a minimum value of 0.9 after 72 h treatment with C-2045 and C-2053. N-cadherin was almost undetectable in BxPC-3 cells treated with UAs ($H = 11.4$, $p = 0.002$, $N = 15$), which correlates with the anti-migratory effect observed in the wound healing assay. Interestingly, despite the anti-migratory potential of UAs in Panc-1, MIA PaCa-2, and AsPC-1, the decrease in both E-cadherin and N-cadherin levels, along with an increase in vimentin levels, was observed after compound treatment. The reduction in E-cadherin after 72 h, up to 0.3 ($p < 0.05$) for Panc-1 ($H = 14.6$, $p = 0.006$, $N = 18$) as well as for AsPC-1 ($H = 14.8$, $p = 0.005$, $N = 20$) cells treated with C-2045 and C-2053, respectively, may indicate impaired intercellular interactions. Meanwhile, the unusual increase in vimentin levels after 72 h to 1.4–3.3 in Panc-1 ($H = 10.0$, $p = 0.004$, $N = 18$), MIA PaCa-2 ($H = 8.83$, $p = 0.03$, $N = 15$), and AsPC-1 cells suggests a shift toward a mesenchymal phenotype; however, the inhibition of migration may be indicative of activation mechanisms independent of vimentin. In turn, the decrease in N-cadherin in these cell lines ($H = 11.2–12.2$, $p < 0.02$, $N = 15–18$), even to a level of 0.1 after 72 h, correlates with the results of the wound healing assay, confirming the reduction in cell migration.

Comparatively, when evaluating the effect of UA on cell migration, all tested PC cell lines exhibited high responsiveness, showing a marked reduction in wound closure. In particular, MIA PaCa-2 and BxPC-3 cells displayed the strongest inhibition of migration. The modulation of EMT-related proteins was generally consistent across PC cells, resulting in decreased levels of E-cadherin and N-cadherin, accompanied by an increase in vimentin expression.

3.5. Impact of autophagy inhibition on cell migration

To further explore whether the observed anti-migratory effect of UAs was dependent on autophagic activity, the wound healing migration assay was performed in the presence of autophagy inhibitors (Fig. 7 and Figs. S30–S33 in the SI).

In Panc-1, the combination of C-2045 with all autophagy inhibitors resulted in elevated cell migration compared to the UA compound alone. The wound area after 72 h of C-2045 ($H(3) = 13.0$, $p < 0.001$, $N = 16$) exposure reached 43.5 % ($p = 0.005$) of the beginning value, while the addition of wortmannin stimulated cell migration, as evidenced by a reduced wound area to 3.4 % ($p < 0.001$). In MIA PaCa-2 cells, both inhibitors alone and in combination with C-2028 significantly reduced cell migration ($H(3) = 17.8–24.9$, $p < 0.001$, $N = 16–28$), as observed by an increase in wound area compared to untreated control cells. After 24 h of incubation, the addition of inhibitors slightly improved the antimigratory effect of C-2028. However, after 72 h, this UA derivative (120 % of wound area) caused greater reduction in cell motility than in combination with inhibitors (105.4–115.3 % of wound area). In AsPC-1 and BxPC-3 cells, the combination of UA derivative with the early autophagy phase inhibitor – WM showed a similar effect to the individual compound. After 72 h, the wound area in AsPC-1 cells ($H(3) = 9.43–31.5$, $p < 0.009$, $N = 16–32$) treated with UA reached 82.0 % and UA+WM 83.5 % ($p = 0.01$), while in BxPC-3 cells ($H(3) = 12.9–30.0$, $p < 0.003$, $N = 18–35$), 154.3 % ($p = 0.04$) and 156.4 % ($p = 0.005$), respectively. In turn, late autophagy inhibitors – CQ and NH_4Cl combined with UA were weaker in limiting cell migration, mainly in BxPC-3 cells, reaching a wound area of 12.0 % for C-2053 +NH_4Cl.

Inhibition of autophagy differentially affected the antimigratory activity of UAs across PC cell lines. In Panc-1 cells, blocking autophagy weakened the antimigratory effect of UA, while in MIA PaCa-2, AsPC-1, and BxPC-3 cells, the impact depended on the inhibitor type and treatment duration. The faster wound closure observed after autophagy inhibition, particularly at the late stage, suggests that autophagy is necessary for the anti-migratory activity of UAs in PC cells.

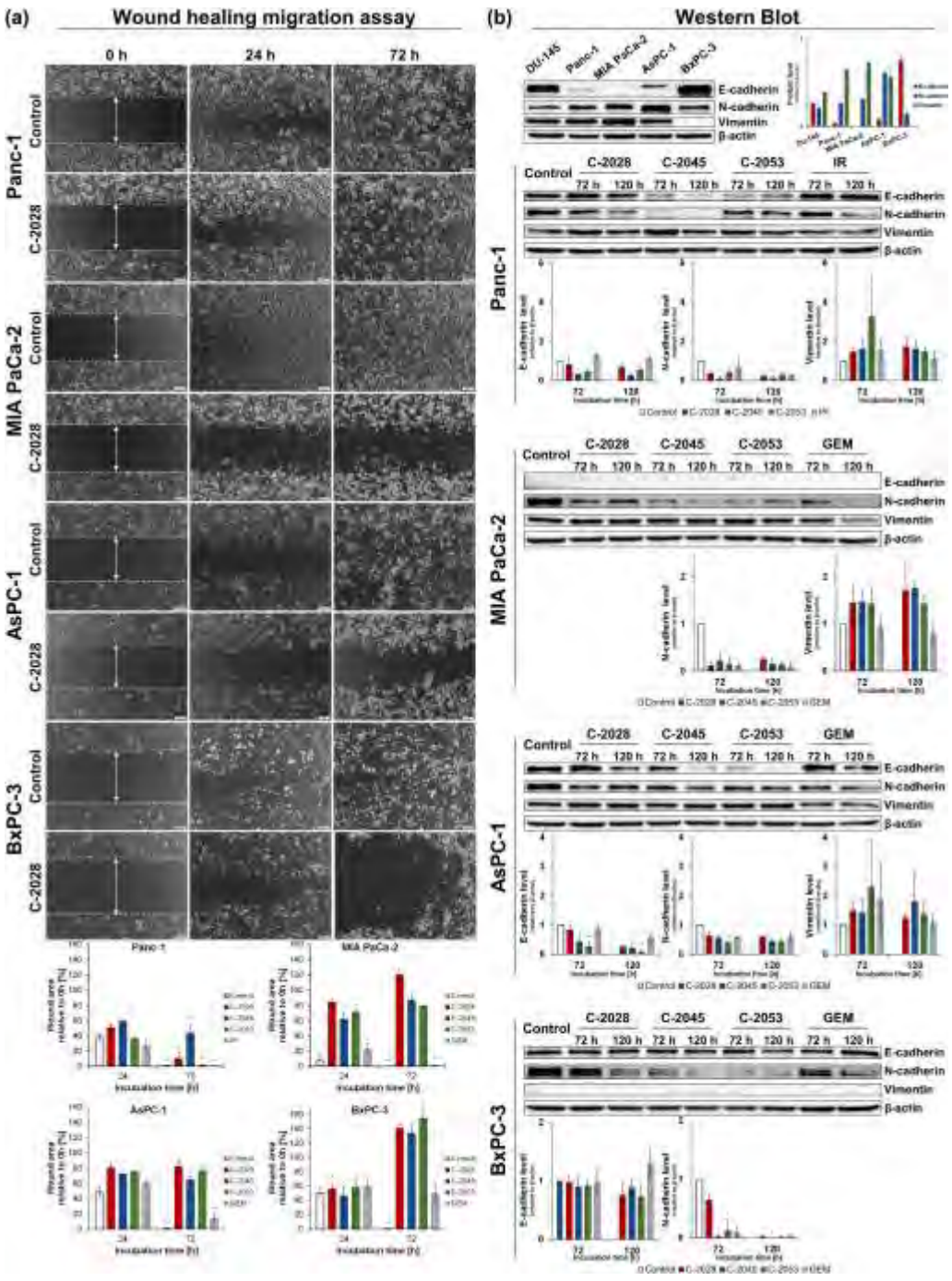

(caption on next page)

Fig. 6. Cell migration following treatment with unsymmetrical bisacridines (UAs). Pancreatic cancer (PC) cells were incubated for 72 and 120 h with IC_{80} doses of unsymmetrical bisacridines (UAs): C-2028, C-2045, and C-2053. As a positive control, IC_{50} doses of reference compounds were used: IR - irinotecan for Panc-1 and GEM - gemcitabine for MIA PaCa-2, AsPC-1, and BxPC-3. **(a)** Representative images from the wound healing migration assay of PC cells after 24 and 72 h of treatment with C-2028 derivative. Cell migration was monitored using live-cell microscopy with time-lapse imaging at 3 h intervals (10 ×; scale bar: 100 μm). Bar graphs showing the wound area after compound exposure, expressed as a percentage relative to the wound area at the beginning of the experiment. **(b)** Western blot analysis of epithelial (E-cadherin) and mesenchymal (N-cadherin and vimentin) markers expression. DU-145 cells were used as a positive control. Total protein samples (30 μg/lane) were separated by SDS-PAGE, transferred to membranes using a semi-dry method, and detected using specific antibodies and enhanced chemiluminescence. The results are presented as the means ± SD. Statistical analysis was performed using the Kruskal–Wallis test followed by Dunn's post hoc test; **(a)**: H (3) = 9.43–23.6, $p < 0.01$, N = 15–28; **(b)**: H(4) = 8.8-15.6, $p < 0.04$, N = 15–20. Differences versus initial wound area: $*p < 0.05$, $**p < 0.01$, $***p < 0.001$; $n \geq 3$.

4. Discussion

The obtained findings confirm that UAs selectively target PC cells while sparing normal hTERT-HPNE pancreatic epithelial cells. This selectivity is crucial for potential clinical safety, as it minimizes off-target effects and supports the therapeutic potential of UAs. Among the tested cell lines, Panc-1 and AsPC-1 cells were the most susceptible to UAs treatment, exhibiting strong apoptotic and pro-death autophagic responses. MIA PaCa-2 cells also showed sensitivity, with C-2028 derivative inducing pro-death autophagy, whereas treatment with C-2045 and C-2053 disrupted autophagic flux. BxPC-3 cells were the least responsive and displayed a cytoprotective form of autophagy, which may reflect their distinct molecular subtype and lower dependence on c-Myc signaling [16]. Despite these variations, all tested PC cell lines demonstrated that UAs induce autophagy through a Beclin1-independent mechanism. Furthermore, UAs inhibited cell migration of all PC cells via autophagy induction, accompanied by the modulation of EMT-related proteins through a non-canonical mechanism.

The preferential induction of apoptosis in PC cells [16] compared to normal hTERT-HPNE cells mirrors the previous findings of our research team [14], which showed selective cytotoxicity and apoptosis triggered by UAs in colon and lung cancer cells, as opposed to normal cells from these tissues.

This study aimed to determine whether UAs modulate autophagy, a complex and context-dependent process that plays a significant role in cancer therapy. The results showed that UAs induced autophagy in PC cells, as indicated by increased AVOs formation, elevated LC3-II levels, and reduced p62 expression, which are markers of active autophagic flux. In contrast, impaired flux in MIA PaCa-2 cells treated with C-2045 and C-2053 (increased p62 despite LC3-II accumulation) points toward autophagy dysfunction, phenomenon also observed in response to the SHP2 allosteric inhibitor – IACS-13909 [37]. Since Beclin1 is a central autophagy initiator in PC and its upregulation is associated with pancreatic neoplasm progression and aggressiveness, this protein is a promising molecular target [38]. A recent study reported that the Beclin1 targeting stapled peptide Tat-SP4 enhances autophagy in several pancreatic cancer cell lines, including Panc-1, MIA PaCa-2, and BxPC-3, thereby increasing autophagic flux and leading to anti-proliferative effects and non-apoptotic cell death [39]. Interestingly, the observed induction of autophagy by UAs was independent of Beclin1. This suggests alternative pathways of autophagy activation, a phenomenon increasingly recognized in cancer biology that may offer advantages in tumors with defective canonical autophagy pathways. The correlation between non-canonical, Beclin1-independent autophagy induction and subsequent apoptosis has been described by other researchers in pancreatic cancer cells [40] and breast cancer cells [41].

In PC, autophagy plays a dual role, varying by cell line, and our research supports that. In BxPC-3 cells, co-treatment with autophagy inhibitors, especially chloroquine, enhanced the cytotoxic and pro-apoptotic effects of C-2053. This suggests a protective role for autophagy, reinforcing findings by Chen et al. and Fu et al., who showed that autophagy inhibition with chloroquine sensitized BxPC-3 cells to pterostilbene and gemcitabine, respectively [42,43]. Conversely, in Panc-1 and AsPC-1 cells, autophagy inhibition reduced UA-induced apoptosis, indicating that UAs trigger pro-death autophagy, which represents a desirable therapeutic mechanism [44,45]. Interestingly, in MIA PaCa-2 cells, only co-treatment with CQ enhanced the apoptotic effect of UA, while the addition of WM and NH_4Cl significantly reduced the potency of C-2028. Studies performed by other researchers [46] proved that CQ combinations potentiate apoptosis in MIA PaCa-2 cells. The observed antagonistic effect in the current study, where co-treatment with WM and NH_4Cl was employed, demonstrates that C-2028 requires a specific blockade of the autophagic pathway to exert its full activity. It is also noteworthy that UA-induced dysfunctional autophagy mechanism, observed only in MIA PaCa-2 cells, may contribute to the development of accelerated cellular senescence. Our previous studies showed that only these cells underwent senescence after UA exposure through upregulation of p21, and interestingly, the senescent cells transitioned into apoptosis after prolonged treatment with the compounds [16]. This correlation between impaired autophagy and senescence may be due to the accumulation of damaged cellular components that interfere with cellular metabolism [47]. Although further mechanistic studies are needed to elucidate this phenomenon, the relevant observation is that C-2028 alone, without autophagy inhibition, triggers apoptosis at a similar level as when combined with CQ.

The wound healing migration assay showed that UAs alone inhibited cell migration more effectively than the reference compound, and the highest anti-migratory potential was observed in a derivative that induced the strongest autophagy and apoptosis [16]. The molecular pattern obtained in this study suggests a non-classical EMT signaling response, possibly reflecting a disrupted or partial activation of the EMT signaling pathway. Importantly, the molecular profile of EMT did not translate into reduced migratory capacity observed in the wound healing assay of PC cells following UAs treatment. Decreased E- and N-cadherin levels may reflect impaired cell-cell interactions in general, and inhibition of E-cadherin alone is not sufficient to induce EMT [48]. In contrast, the elevation of vimentin may be a response to UAs-induced stress, rather than a shift toward a mesenchymal phenotype, as evidenced by reduced migration capacity after UAs exposure. The study of Ostrowska-Podhorodecka et al. presents that vimentin's role extends beyond EMT and migration, and it can be upregulated by cellular stress, differentiation cues, or drug treatments, independent of the acquisition of mesenchymal traits or motility [49]. Moreover, unusual changes in molecular marker levels can result from activation of non-canonical pathways, which inhibit cell migration independently of E-cadherin, vimentin, or EMT in general, but by disrupting cytoskeletal dynamics, interfering with integrin or focal adhesion signaling, or altering secretion of migration-promoting factors, while paradoxically inducing a stress response that upregulates vimentin [50]. Although further studies are required to determine the molecular mechanism by which UAs inhibit the migration of PC cells, the obtained results clearly demonstrate that these compounds exhibit the desired anti-migratory effects. Notably, inhibition of autophagy was found to stimulate cell migration, suggesting that autophagy has a suppressive impact on this process in PC cells. Treatment with UAs showed that these compounds may impair cell motility through autophagy induction, highlighting the complex role of autophagy in the cellular response induced by bisacridine derivatives. This confirms previous findings that autophagy inhibition promotes EMT and invasion, particularly in *RAS*-mutated cancer cells, by disrupting epithelial integrity and enhancing mesenchymal features [51]. Similarly, studies in gastric cancer models show that blocking autophagy

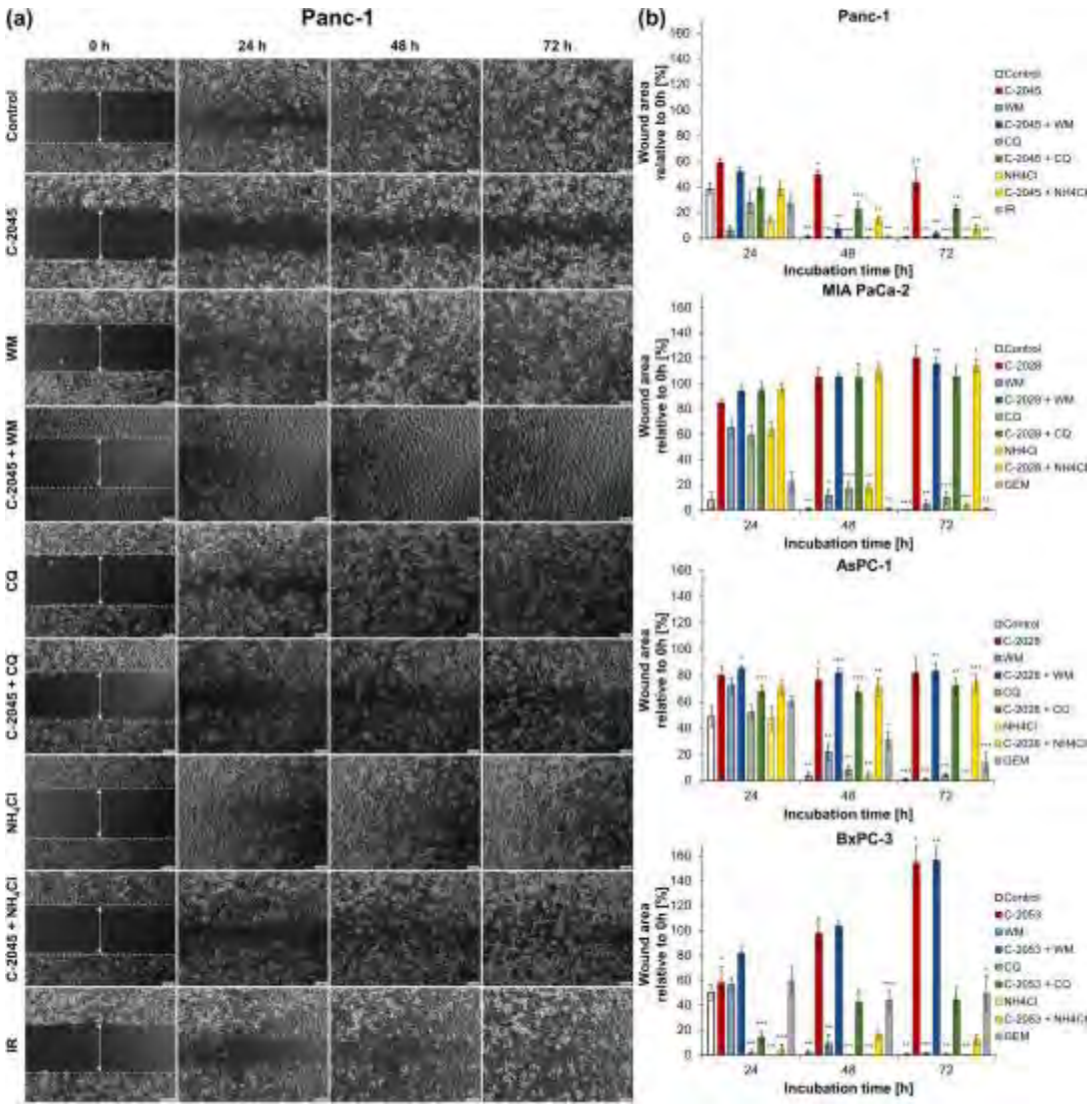

Fig. 7. Cell migration following autophagy inhibition. Pancreatic cancer (PC) cells were preincubated for 1 h with autophagy inhibitors: wortmannin (WM), chloroquine (CQ), or ammonium chloride (NH_4Cl), and subsequently treated with IC_{80} doses of selected unsymmetrical bisacridines (UAs): C-2028, C-2045, or C-2053. As positive controls, IC_{50} doses of gemcitabine (GEM) and irinotecan (IR) were used. **(a)** Representative images from the wound healing migration assay of Panc-1 cells after 24, 48, and 72 h of treatment. Cell migration was monitored using live-cell microscopy with time-lapse imaging every 3 h (10 ×; scale bar: 100 μm). **(b)** Bar graphs showing the wound area after treatment with individual UA compounds or in combination with an autophagy inhibitor, expressed as a percentage relative to the wound area at the beginning of the experiment. The results are presented as the means ± SD. Statistical analysis was performed using the Kruskal–Wallis test followed by Dunn's post hoc test; **(b)**: H(3) = 9.43–31.5, $p < 0.009$, N = 16–35. Differences versus initial wound area: $^{*}p < 0.05$, $^{**}p < 0.01$, $^{***}p < 0.001$; $n \geq 3$.

increases migration and metastasis through ROS accumulation and metabolic reprogramming, further highlighting the suppressive role of autophagy in cell motility [52].

In our previous study, UAs induced apoptosis in PC cells through c-Myc protein downregulation [16]. C-Myc is an oncogenic transcription factor that is significantly overexpressed in pancreatic cancer, regulating various tumor-promoting processes, including proliferation, differentiation, apoptosis, angiogenesis, metastasis, chemoresistance, and metabolic reprogramming [53]. The UAs reduce c-Myc levels by stabilizing G-quadruplexes, and, as suggested by the work of Zang et al., also by promoting its selective autophagic degradation, a mechanism mediated by the ubiquitination of c-Myc via the E3 ligase TRIM21, which is bound to K63, directing it to autophagic removal [54]. This autophagy-dependent degradation reduces c-Myc protein levels, which

in turn triggers apoptosis and enhances autophagy flux, as reflected by LC3-II accumulation and reduced p62. Thus, our findings are consistent with these mechanistic insights and show that c-Myc downregulation and autophagy induction are interrelated processes that mediate the anticancer activity of UA compounds in PC cells [54]. Moreover, a study by Liu et al. showed that c-Myc knockout inhibits PC cell invasion and migration, suggesting that the observed anti-migratory properties of UAs may also be due to the downregulation of this protein [55].

The mechanism of action of unsymmetrical bisacridines differs considerably from that of chemotherapeutic agents currently used in PC treatment, including those administered as part of multidrug regimens such as FOLFIRINOX, NALIRIFOX, and GEM-NABP. The FOLFIRINOX and NALIRIFOX protocols, which combine fluorouracil, leucovorin, irinotecan, and oxaliplatin, primarily act by interfering with DNA replication and repair, thereby inducing apoptosis through genotoxic stress [56]. Similarly, gemcitabine, a nucleoside analog used in GEM-NABP therapy, inhibits DNA synthesis and promotes cell death by disrupting the S phase of the cell cycle [57], while nab-paclitaxel interferes with microtubule dynamics and mitotic progression [58]. Although these regimens have improved survival outcomes compared with gemcitabine monotherapy, their clinical use is frequently limited by severe systemic toxicity and development of drug resistance.

In contrast, UAs target multiple molecular pathways that are essential for pancreatic cancer cell survival. They stabilize G-quadruplex DNA structures in promoter regions of oncogenes such as *MYC*, leading to the downregulation of this key driver of tumor proliferation. Moreover, UAs induce apoptosis and a Beclin1-independent form of pro-death autophagy, which together contribute to a potent cytotoxic response. This mechanism is fundamentally different from that of the cytotoxic agents used in standard chemotherapy, as UAs do not rely solely on DNA damage to trigger cell death. Instead, they convert autophagy from a cytoprotective to a cytotoxic process, thereby overcoming one of the major resistance mechanisms that are characteristic of pancreatic cancer cells.

Furthermore, compared with combination regimens that often cause high levels of hematological and gastrointestinal toxicity [3], UAs exhibit pronounced selectivity toward malignant cells and limited toxicity in normal pancreatic epithelial cells [16]. Their multitargeted mode of action, which includes G-quadruplex stabilization [4,13], c-Myc downregulation [16], and modulation of autophagy, positions them as promising candidates for future therapeutic strategies. Such properties suggest that UAs could potentially complement or enhance the efficacy of existing chemotherapy protocols while reducing adverse effects and the likelihood of resistance development.

The present study provides mechanistic insight into the complex activity of UAs in PC cells, but several limitations should be acknowledged. The data were obtained exclusively from *in vitro* cellular models and therefore require validation *in vivo* to confirm the therapeutic relevance and safety profile of UAs. Although the current results clearly indicate that c-Myc downregulation and the interaction between autophagy and apoptosis are central to the observed effects, additional pathway analyses such as phosphoproteomic profiling or bioinformatic mapping of AKT/mTOR and MAPK signaling are necessary to define the upstream regulators involved. Future research will focus on verifying the proposed molecular mechanism of UAs in more advanced 3D and animal models of PC, and on exploring potential synergistic effects of UAs with standard agents such as gemcitabine. These studies will help to establish the translational potential of unsymmetrical bisacridines as multifunctional anticancer compounds that exploit specific vulnerabilities of pancreatic cancer cells.

In conclusion, our study demonstrates that UAs selectively target PC cells by inducing pro-apoptotic Beclin1 independent autophagy, while sparing normal pancreatic cells, supporting their high therapeutic potential and favorable safety profile. UAs also inhibit PC cell migration, likely through complex non-canonical mechanisms involving autophagy induction and c-Myc downregulation. These findings underscore that UAs are promising agents for pancreatic cancer therapy, combining selective cytotoxicity, autophagy-mediated apoptosis, and anti-migratory activity.

Abbreviations

AO	Acridine orange
AVOs	Acidic vesicular organelles
BH3	Bcl-2 homology 3 domain
CQ	Chloroquine
DMSO	Dimethylsulfoxide
DMEM HG	High-glucose Dulbecco's modified Eagle's medium
EMT	Epithelial-mesenchymal transition
FACS	Fluorescence-Activated Cell Sorting
FBS	Fetal bovine serum
FITC	Fluorescein Isothiocyanate
FOLFIRINOX	Multidrug: fluorouracil, leucovorin, irinotecan, and oxaliplatin
GEM	Gemcitabine
IC	Inhibitory Concentration
IR	Irinotecan
MTT	3-(4,5-dimethyl-2-thiazolyl)-2,5-diphenyl-2H-tetrazolium bromide
NABP	Nab-paclitaxel
NALIRIFOX	Multidrug: fluorouracil, leucovorin, liposomal irinotecan, and oxaliplatin
PBS	Phosphate buffer saline
PC	Pancreatic cancer
PI	Propidium Iodide
RPMI 1640	Roswell Park Memorial Institute 1640 medium
UAs	Unsymmetrical bisacridines
WM	Wortmannin

Funding

This study was partially funded by CHDE S.A., Rzeszo´w, Poland, grant no. 037200, and was additionally supported through co-financing of publication costs by the BioTechMed Center, Gdan´sk University of Technology.

CRediT authorship contribution statement

Ewa Augustin: Writing – review & editing, Supervision, Resources, Project administration, Funding acquisition, Formal analysis, Conceptualization. **Ewa Paluszkiewicz:** Methodology. **Boz˙ena Pezała:** Methodology, Investigation. **Agnieszka Kurdyn:** Writing – review & editing, Writing – original draft, Visualization, Validation, Software, Methodology, Investigation, Formal analysis, Data curation, Conceptualization.

Declaration of Competing Interest

The authors declare the following financial interests/personal relationships which may be considered as potential competing interests: Ewa Augustin reports financial support was provided by CHDE S.A., Rzeszo´w, Poland. If there are other authors, they declare that they have no known competing financial interests or personal relationships that could have appeared to influence the work reported in this paper.

Appendix A. Supporting information

Supplementary data associated with this article can be found in the online version at doi:10.1016/j.biopha.2025.118786.

Data availability

Data obtained during this study are included in this article and its

Supplementary Information file. Additional detailed data are available from the corresponding author upon reasonable request.

References

1 J. Ushio, A. Kanno, E. Ikeda, K. Ando, H. Nagai, T. Miwata, et al., Pancreatic ductal adenocarcinoma: epidemiology and risk factors, Diagnostics 11 (2021) 562, https://doi.org/10.3390/diagnostics11030562.

2 C. Kan, N. Liu, K. Zhang, D. Wu, Y. Liang, W. Cai, et al., Global, regional, and national burden of pancreatic cancer, 1990-2019: results from the global burden of disease study 2019, Ann. Glob. Heal 89 (2023) 33, https://doi.org/10.5334/aogh.4019.

3 F. Nichetti, S. Rota, P. Ambrosini, C. Pircher, E. Gusmaroli, M. Droz Dit Busset, et al., NALIRIFOX, FOLFIRINOX, and gemcitabine with nab-paclitaxel as first-line chemotherapy for metastatic pancreatic cancer, JAMA Netw. Open 7 (2024) e2350756, https://doi.org/10.1001/jamanetworkopen.2023.50756.

4 E. Paluszkiewicz, B. Horowska, B. Borowa-Mazgaj, G. Peszyn´ska-Sularz, J. Paradziej-Łukowicz, E. Augustin, et al., Design, synthesis and high antitumor potential of new unsymmetrical bisacridine derivatives towards human solid tumors, specifically pancreatic cancers and their unique ability to stabilize DNA G-quadruplexes, Eur. J. Med. Chem. 204 (2020) 112599, https://doi.org/10.1016/j.ejmech.2020.112599.

[5] J. Konopa, B. Horowska, E.M. Paluszkiewicz, B. Borowa-Mazgaj, E.A. Augustin, A. Skwarska, et al., Asymmetric Bis-acridines with Antitumour Activity and Their Uses, University of Technology, 2023 (Cancadian Patent CA 2980084).

6 J. Konopa, B. Horowska, E.M. Paluszkiewicz, B. Borowa-Mazgaj, E.A. Augustin, A. Skwarska, et al., Asymmetric Bis-Acridines with Antitumor Activity and Use Thereof, Gdansk University of Technology, 2019 (U.S. Patent US 10202349 B2).

[7] J. Konopa, B. Horowska, E.M. Paluszkiewicz, B. Borowa-Mazgaj, E.A. Augustin, A. Skwarska, et al., Asymmetric Bis-Acridines with Antitumor Activity and Use Thereof, Gdansk University of Technology, 2017 (European Patent EP 3070078).

[8] J. Konopa, B. Horowska, E.M. Paluszkiewicz, B. Borowa-Mazgaj, E.A. Augustin, A. Skwarska, et al., Asymmetric Bis-Acridines with Antitumour Activity and Their Uses, Gdansk University of Technology, 2023 (Japanese Patent 7226918).

9 G. Cholewin´ski, K. Dzierzbicka, A.M. Kołodziejczyk, Natural and synthetic acridines/acridones as antitumor agents: their biological activities and methods of synthesis, Pharmacol. Rep. 63 (2011) 305–336, https://doi.org/10.1016/S1734-1140(11)70499-6.

10 WHO Chronicle. Geneva: World Health Organization 1976;30 (3):11.

11 J. Piotrowska-Sowin´ska, Clinical observations of the Ledakrin effects in treatment of patients with malignant neoplasms, Mater. Med. Pol. 8 (1976) 266–272.

12 N. Isambert, M. Campone, E. Bourbouloux, M. Drouin, A. Major, W. Yin, et al., Evaluation of the safety of C-I311 (SYMADEX) administered in a phase 1 dose escalation trial as a weekly infusion for 3 consecutive weeks in patients with advanced solid tumours, Eur. J. Cancer 46 (2010) 729–734, https://doi.org/10.1016/j.ejca.2009.12.005.

13 T. Laskowski, M. Kosno, W. Andraloj´c, J. Pakula, R. Stojalowski, J. Borzyszkowska-Bukowska, et al., The interactions of Pu22 G-quadruplex, derived from c-MYC promoter sequence, with antitumor acridine derivatives—an NMR/MD combined study, Mol. Ther. Nucleic Acids 36 (2025) 102513, https://doi.org/10.1016/j.omtn.2025.102513.

14 M. Pawlowska, J. Kulesza, E. Augustin, c-Myc protein level affected by unsymmetrical bisacridines influences apoptosis and senescence induced in HCT116 colorectal and H460 lung cancer cells, Int. J. Mol. Sci. 23 (2022) 3061, https://doi.org/10.3390/ijms23063061.

15 A. Mieszkowska, A.M. Nowicka, A. Kowalczyk, A. Potęga, M. Pawlowska, M. Kosno, et al., Metabolic profiles of new unsymmetrical bisacridine antitumor agents in electrochemical and enzymatic noncellular systems and in tumor cells, Pharmaceuticals 14 (2021) 317, https://doi.org/10.3390/ph14040317.

16 A. Kurdyn, M. Pawlowska, E. Paluszkiewicz, M. Cichorek, E. Augustin, c-Myc inhibition and p21 modulation contribute to unsymmetrical bisacridines-induced apoptosis and senescence in pancreatic cancer cells, Pharmacol. Rep. 77 (2025) 182–209, https://doi.org/10.1007/s43440-024-00658-6.

17 A. Kurdyn, E. Paluszkiewicz, E. Augustin, Pro-apoptotic effects of unsymmetrical bisacridines in 3D pancreatic multicellular tumor spheroids, Int. J. Mol. Sci. 26 (2025) 7557, https://doi.org/10.3390/ijms26157557.

18 M. Su, Y. Mei, S. Sinha, Role of the crosstalk between autophagy and apoptosis in cancer, J. Oncol. 2013 (2013) 1–14, https://doi.org/10.1155/2013/102735.

19 X. Zhang, S. Chen, K. Huang, W. Le, Why should autophagic flux be assessed? Acta Pharmacol. Sin. 34 (2013) 595–599, https://doi.org/10.1038/aps.2012.184.

20 N. Mizushima, T. Yoshimori, How to interpret LC3 immunoblotting, Autophagy 3 (2007) 542–545, https://doi.org/10.4161/auto.4600.

21 R. Kang, H.J. Zeh, M.T. Lotze, D. Tang, The Beclin 1 network regulates autophagy and apoptosis, Cell Death Differ. 18 (2011) 571–580, https://doi.org/10.1038/cdd.2010.191.

22 M. Piffoux, E. Eriau, P.A. Cassier, Autophagy as a therapeutic target in pancreatic cancer, Br. J. Cancer 124 (2021) 333–344, https://doi.org/10.1038/s41416-020-01039-5.

23 D. Troumpoukis, A. Papadimitropoulou, C. Charalampous, P. Kogionou, K. Palamaris, P. Sarantis, et al., Targeting autophagy in pancreatic cancer: the cancer stem cell perspective, Front. Oncol. 12 (2022) 1049436.

[24] J. Gillson, Y.S. Abd El-Aziz, L.Y.W. Leck, P.J. Jansson, N. Pavlakis, J.S. Samra, et al., Autophagy: a key player in pancreatic cancer progression and a potential drug target, Cancers 14 (2022) 3528, https://doi.org/10.3390/cancers14143528.

25 J. Yang, Y. Liu, S. Liu, The role of epithelial-mesenchymal transition and autophagy in pancreatic ductal adenocarcinoma invasion, Cell Death Dis. 14 (2023) 506, https://doi.org/10.1038/s41419-023-06032-3.

26 V.B. Joshi, O.L. Gutierrez Ruiz, G.L. Razidlo, The cell biology of metastatic invasion in pancreatic cancer: updates and mechanistic insights, Cancers 15 (2023) 2169, https://doi.org/10.3390/cancers15072169.

27 M. Beuran, I. Negoi, S. Paun, A.D. Ion, C. Bleotu, R.I. Negoi, et al., The epithelial to mesenchymal transition in pancreatic cancer: a systematic review, Pancreatology 15 (2015) 217–225, https://doi.org/10.1016/j.pan.2015.02.011.

28 A.R. Safa, Epithelial-mesenchymal transition: a hallmark in pancreatic cancer stem cell migration, metastasis formation, and drug resistance, J. Cancer Metastas. Treat. 6 (2020) 36, https://doi.org/10.20517/2394-4722.2020.55.

29 D. Hashimoto, M. Bl˝auer, M. Hirota, N.H. Ikonen, J. Sand, J. Laukkarinen, Autophagy is needed for the growth of pancreatic adenocarcinoma and has a cytoprotective effect against anticancer drugs, Eur. J. Cancer 50 (2014) 1382–1390, https://doi.org/10.1016/j.ejca.2014.01.011.

30 C.G. Kinsey, S.A. Camolotto, A.M. Boespflug, K.P. Guillen, M. Foth, A. Truong, et al., Protective autophagy elicited by RAF→MEK→ERK inhibition suggests a treatment strategy for RAS-driven cancers, Nat. Med. (2019) 620–627, https://doi.org/10.1038/s41591-019-0367-9.

31 I.A. Elliott, A.M. Dann, S. Xu, S.S. Kim, E.R. Abt, W. Kim, et al., Lysosome inhibition sensitizes pancreatic cancer to replication stress by aspartate depletion, Proc. Natl. Acad. Sci. USA 116 (2019) 6842–6847, https://doi.org/10.1073/pnas.1812410116.

32 D. Kumar, V.K. Kommalapati, M.K. Jerald, A.D. Tangutur, Fluorinated thiazolidinol drives autophagic cell death in pancreatic cancer cells via AMPK activation and perturbation of critical sentinels of oncogenic signaling, Chem. Biol. Interact. 343 (2021) 109433, https://doi.org/10.1016/j.cbi.2021.109433.

33 D.R. Stirling, M.J. Swain-Bowden, A.M. Lucas, A.E. Carpenter, B.A. Cimini, A. Goodman, CellProfiler 4: improvements in speed, utility and usability, BMC Bioinforma. 22 (2021) 433, https://doi.org/10.1186/s12859-021-04344-9.

34 K.R. Parzych, D.J. Klionsky, An overview of autophagy: morphology, mechanism, and regulation, Antioxid. Redox Signal. 20 (2014) 460–473, https://doi.org/10.1089/ars.2013.5371.

35 W. Wang, L. Dong, B. Zhao, J. Lu, Y. Zhao, E-cadherin is downregulated by microenvironmental changes in pancreatic cancer and induces EMT, Oncol. Rep. 40 (2018) 1641–1649, https://doi.org/10.3892/or.2018.6528.

36 C. Rosty, M. GogginsIdentification of differentially expressed proteins in pancreatic cancer using a global proteomic approach. Pancreat. Cancer, vol. 9, New Jersey: Humana Press; 2012, pp. 189–198. https://doi.org/10.1385/1-59259-780-7:189.

37 Y. Miao, Y. Bai, J. Miao, A.A. Murray, J. Lin, J. Dong, et al., Off-target autophagy inhibition by SHP2 allosteric inhibitors contributes to their antitumor activity in RAS-driven cancers, J. Clin. Investig. 134 (2024) e177142, https://doi.org/10.1172/JCI177142.

38 S. Song, B. Wang, S. Gu, X. Li, S. Sun, Expression of Beclin 1 and Bcl-2 in pancreatic neoplasms and its effect on pancreatic ductal adenocarcinoma prognosis, Oncol. Lett. 14 (2017) 7849–7861, https://doi.org/10.3892/ol.2017.7218.

39 N. Li, X. Zhang, J. Chen, S. Gao, L. Wang, Y. Zhao, Perturbation of autophagy by a beclin 1-targeting stapled peptide induces mitochondria stress and inhibits proliferation of pancreatic cancer cells, Cancers 15 (2023) 953, https://doi.org/10.3390/cancers15030953.

40 Y. El Mahi, Z.N. Nizami, A.F. Wali, A. Al Neyadi, M. Magramane, M. Al Azzani, et al., Rhus coriaria induces autophagic and apoptotic cell death in pancreatic cancer cells, Front. Pharmacol. 15 (2024) 1412565.

41 L. Sun, N. Liu, S.-S. Liu, W.-Y. Xia, M.-Y. Liu, L.-F. Li, et al., Beclin-1-independent autophagy mediates programmed cancer cell death through interplays with endoplasmic reticulum and/or mitochondria in colbat chloride-induced hypoxia, Am. J. Cancer Res. 5 (2015) 2626–2642.

42 R.-J. Chen, Y.-J. Lyu, Y.-Y. Chen, Y.-C. Lee, M.-H. Pan, Y.-S. Ho, et al., Chloroquine potentiates the anticancer effect of pterostilbene on pancreatic cancer by inhibiting autophagy and downregulating the RAGE/STAT3 Pathway, Molecules 26 (2021) 6741, https://doi.org/10.3390/molecules26216741.

43 Z. Fu, X. Cheng, J. Kuang, H. Feng, L. Chen, J. Liang, et al., CQ sensitizes human pancreatic cancer cells to gemcitabine through the lysosomal apoptotic pathway via reactive oxygen species, Mol. Oncol. 12 (2018) 529–544, https://doi.org/10.1002/1878-0261.12179.

44 A. Ranjan, S.K. Srivastava, Penfluridol suppresses pancreatic tumor growth by autophagy-mediated apoptosis, Sci. Rep. 6 (2016) 26165, https://doi.org/10.1038/srep26165.

45 D. Muilenburg, C. Parsons, J. Coates, S. Virudachalam, R.J. Bold, Role of autophagy in apoptotic regulation by Akt in pancreatic cancer, Anticancer Res. 34 (2014) 631–637.

46 H. Monma, Y. Iida, T. Moritani, T. Okimoto, R. Tanino, Y. Tajima, et al., Chloroquine augments TRAIL-induced apoptosis and induces G2/M phase arrest in human pancreatic cancer cells, PLOS One 13 (2018) e0193990, https://doi.org/10.1371/journal.pone.0193990.

47 L.D. Cassidy, M. Narita, Autophagy at the intersection of aging, senescence, and cancer, Mol. Oncol. 16 (2022) 3259–3275, https://doi.org/10.1002/1878-0261.13269.

48 Y. Song, M. Ye, J. Zhou, Z. Wang, X. Zhu, Restoring E-cadherin expression by natural compounds for anticancer therapies in genital and urinary cancers, Mol. Ther. Oncol. 14 (2019) 130–138, https://doi.org/10.1016/j.omto.2019.04.005.

49 Z. Ostrowska-Podhorodecka, I. Ding, M. Norouzi, C.A. McCulloch, Impact of vimentin on regulation of cell signaling and matrix remodeling, Front. Cell Dev. Biol. 10 (2022) 869069, https://doi.org/10.3389/fcell.2022.869069.

50 X. Deng, Y.V. Yu, Y.N. Jin, Non-canonical translation in cancer: significance and therapeutic potential of non-canonical ORFs, m6A-modification, and circular RNAs, Cell Death Discov. 10 (2024) 412, https://doi.org/10.1038/s41420-024-02185-y.
51 Y. Wang, H. Xiong, D. Liu, C. Hill, A. Ertay, J. Li, et al., Autophagy inhibition specifically promotes epithelial-mesenchymal transition and invasion in RAS-mutated cancer cells, Autophagy 15 (2019) 886–899, https://doi.org/10.1080/15548627.2019.1569912.
52 W. Qin, C. Li, W. Zheng, Q. Guo, Y. Zhang, M. Kang, et al., Inhibition of autophagy promotes metastasis and glycolysis by inducing ROS in gastric cancer cells, Oncotarget 6 (2015) 39839–39854, https://doi.org/10.18632/oncotarget.5674.
53 M. Ala, Target c-Myc to treat pancreatic cancer, Cancer Biol. Ther. 23 (2022) 34–50, https://doi.org/10.1080/15384047.2021.2017223.
54 Y. Zang, L. Zhu, T. Li, Q. Wang, J. Li, Y. Qian, et al., EI24 Suppresses tumorigenesis in pancreatic cancer via regulating c-Myc, Gastroenterol. Res. Pract. 2018 (2018) 1–12, https://doi.org/10.1155/2018/2626545.
55 X. Liu, Y. Zhou, J. Peng, B. Xie, Q. Shou, J. Wang, Silencing c-Myc enhances the antitumor activity of bufalin by suppressing the HIF-1α/SDF-1/CXCR4 Pathway in Pancreatic Cancer Cells, Front. Pharmacol. 11 (2020) 495, https://doi.org/10.3389/fphar.2020.00495.
56 S. J Paul, A.N. Lalaji, S. Shubra Saha, V. Patel, C. Sneha Arvind, T. Bairagi, et al., Nalirifox in the treatment of metastatic pancreatic ductal adenocarcinoma (mPDAC): a comprehensive review, J. Neonatal Surg. 14 (2025) 175–182, https://doi.org/10.52783/jns.v14.2383.
57 W. Plunkett, P. Huang, Y.Z. Xu, V. Heinemann, R. Grunewald, V. Gandhi, Gemcitabine: metabolism, mechanisms of action, and self-potentiation, Semin. Oncol. 22 (1995) 3–10.
58 C. Zhang, N. Awasthi, M.A. Schwarz, S. Hinz, R.E. Schwarz, Superior antitumor activity of nanoparticle albumin-bound paclitaxel in experimental gastric cancer, PLOS One 8 (2013) e58037, https://doi.org/10.1371/journal.pone.0058037.

CONCLUSIONS

The research presented in this doctoral dissertation provides a comprehensive characterization of the biological activity and cellular mechanisms of action of three novel unsymmetrical bisacridine derivatives, C-2028, C-2045, and C-2053, against human pancreatic cancer cells (**Figure 9)**. By integrating protein expression analysis using western blotting, kinetic studies in traditional 2D cultures, and 3D multicellular tumor spheroid models, this work identifies UAs as a highly active and multifaceted class of potential therapeutics for the treatment of PC.

The integrated mechanism of action and the diverse cellular responses triggered by unsymmetrical bisacridines in both traditional 2D cultures and more physiologically relevant 3D pancreatic cancer spheroids are schematically presented in **Figure 9**.

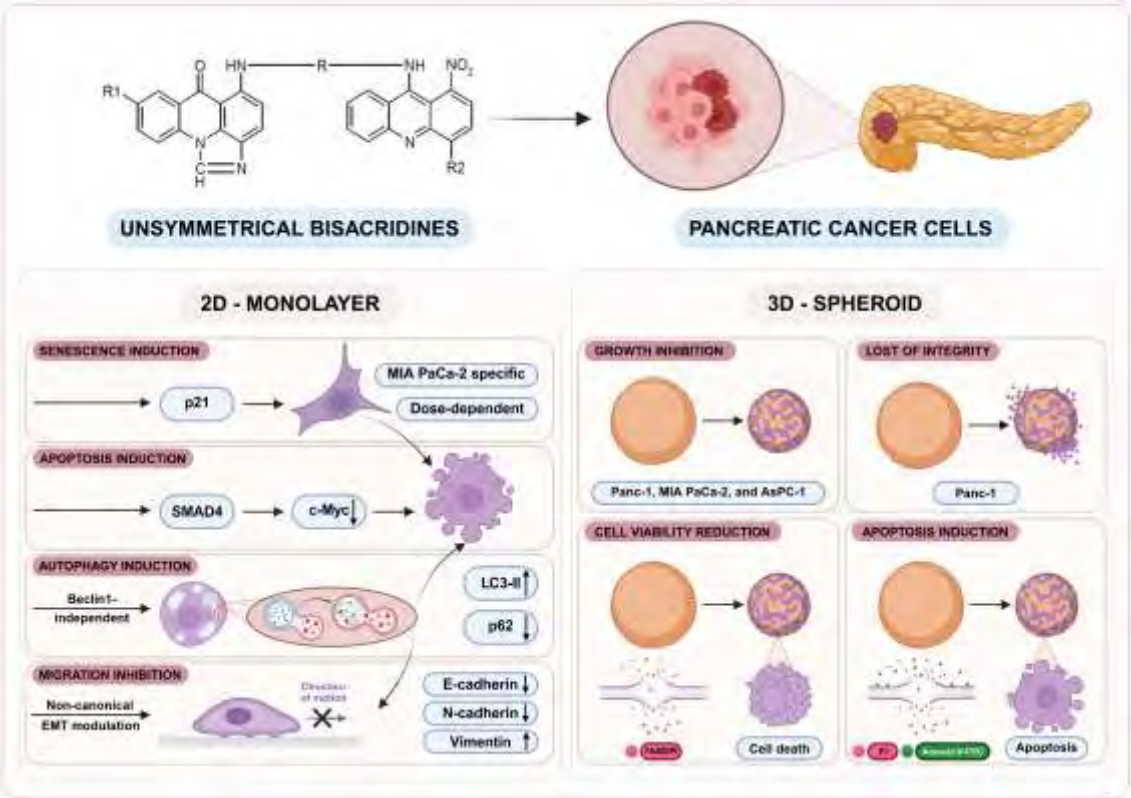

Figure 9. Schematic representation of the multifaceted biological activity and mechanism of action of unsymmetrical bisacridines (UAs) in pancreatic cancer models. The diagram summarizes the cellular responses induced in 2D monolayers (senescence via p21 upregulation, apoptosis involving c-Myc downregulation and SMAD4 induction, Beclin1-independent cytotoxic autophagy, and migration inhibition through non-canonical EMT modulation) and 3D multicellular tumor spheroids (growth inhibition, loss of structural integrity, and induction of apoptosis).

The collective findings of the three scientific publications lead to the following conclusions:

1. Selective cytotoxicity and favorable safety profile

A significant finding of this doctoral research is the high selectivity of unsymmetrical bisacridines toward cancer cells, which is a crucial requirement for potential clinical applications. UA derivatives exhibit markedly greater cytotoxicity and induce substantially higher levels of apoptosis in pancreatic cancer cells compared to normal human pancreatic epithelial cells (hTERT-HPNE). Quantitative evaluation demonstrated that the IC_{80} values for derivatives C-2045 and C-2053 in normal cells were at least twice as high as those observed in cancer cells. Furthermore, while UAs trigger profound programmed cell death in PC models, they induce only moderate apoptosis in normal cells, thereby minimizing potential off-target effects and providing a significant therapeutic window.

2. Targeted downregulation of the c-Myc and p21 modulation

A fundamental discovery is that UAs exert their potent anticancer effects by targeting the c-Myc oncoprotein, a master regulator overexpressed in the majority of PC cases. The UAs, which stabilize G-quadruplex DNA structures in oncogene promoters, induce a profound, time-dependent downregulation of c-Myc protein levels across all tested PC cell lines (Panc-1, MIA PaCa-2, AsPC-1, and BxPC-3).

- p53-independent activity: Crucially, UA-induced cytotoxicity and apoptosis occur independently of the p53 tumor suppressor status. UAs remain highly effective in cells harboring mutant *TP53* (Panc-1, MIA PaCa-2, BxPC-3) or in those with a *TP53*-null cells (AsPC-1), a critical clinical advantage given that *TP53* mutations are a primary cause of resistance to standard DNA-damaging agents.
- SMAD4 and p21 modulation: In *SMAD4*-positive lines, the induction of the SMAD4 protein further facilitates the apoptotic response. Simultaneously, UAs trigger a significant upregulation of the cyclin-dependent kinase inhibitor p21, particularly in MIA PaCa-2 cells, where a 14-fold increase in protein levels was observed, signaling a shift toward cell cycle arrest and senescence.

2. Induction of a dual therapeutic response: apoptosis and senescence

UAs do not merely inhibit growth but actively eliminate PC cells through diverse pathways, depending on the dose and duration of exposure.

- Programmed cell death: Apoptosis was identified as the predominant mechanism of cell death, characterized by time-dependent DNA fragmentation, phosphatidylserine externalization, and the formation of apoptotic bodies.
- Accelerated cellular senescence: In MIA PaCa-2 cells, UAs uniquely induce accelerated cellular senescence, characterized by increased SA-β-galactosidase activity and morphological changes (enlargement and flattening).
- The senescence-to-apoptosis switch: A notable and clinically desirable finding is that senescent cells ultimately transition into apoptosis upon prolonged treatment. This

ensures that the compound-induced growth arrest is irreversible, as further confirmed by the complete inhibition of colony-forming capacity in MIA PaCa-2 cells following UA exposure, thereby minimizing the risk of tumor recurrence.

3. Resiliency and efficacy in 3D tumor MTCS

The successful translation of UAs' activity from 2D monolayers to 3D multicellular tumor spheroids represents a significant validation of their therapeutic potential in more complex, physiologically relevant environments.

- Sustained activity and cytotoxicity: UAs remained biologically active within 3D spheroids, overcoming the physical barriers and nutrient gradients that typically limit drug efficacy in solid tumors. This resulted in significant growth inhibition and loss of spheroid integrity.
- Delayed kinetics in 3D: While apoptosis remains the dominant death pathway in 3D, its kinetics are delayed compared to 2D cultures, with early-apoptotic cells predominating at 72 h. This delay likely reflects the gradual diffusion of the compounds through the compact 3D architecture.
- Consistent potency: Importantly, the relative potency of the derivatives remained consistent between 2D and 3D models, confirming that UAs retain their high efficacy even under conditions of increased resistance and metabolic stress characteristic of the tumor microenvironment.

4. Reprogramming of autophagy from a survival to a pro-death process

The presented research provides critical insights into the role of autophagy, which often acts as a cytoprotective mechanism in PC to survive metabolic stress.

- Beclin1-independent induction: UAs triggered a robust increase in autophagic flux across all PC lines. Remarkably, this induction is Beclin1-independent, suggesting that UAs activate non-canonical pathways that bypass traditional autophagy initiation complexes.
- Pro-apoptotic autophagy: In the majority of tested cell lines (Panc-1, AsPC-1, and MIA PaCa-2) treated with the tested compounds, the UA-induced autophagy acts as a pro-death process. Inhibition of autophagy in these cells reduced UA-induced apoptosis, confirming that UAs effectively convert a potential survival mechanism into a death-promoting pathway.

5. Suppression of the migration and EMT proteins modulation

Beyond primary cytotoxicity, this dissertation establishes the anti-migratory potential of UAs, which is essential for limiting the early systemic spread characteristic of PC.

- Effective inhibition of migration: All tested UA derivatives significantly inhibited PC cell migration, outperforming clinical reference compounds such as gemcitabine.
- Autophagy-mediated anti-migratory effect: Using the wound healing migration assay, it was demonstrated that autophagy is necessary for the anti-migratory activity of UAs. In Panc-1 cells, blocking autophagy partially restored migratory capabilities.

- Non-canonical EMT modulation: UAs modulate markers of the epithelial-mesenchymal transition, notably decreasing N-cadherin and E-cadherin levels. While vimentin levels paradoxically increased, likely as a stress response, the overall phenotype remained non-migratory, indicating a disrupted EMT signaling response rather than a classical mesenchymal shift.

The findings of this dissertation identify unsymmetrical bisacridines as highly promising candidates for further research regarding the treatment of pancreatic cancer. By simultaneously downregulating c-Myc, bypassing p53 mutations, reprogramming autophagy toward cell death, and inhibiting the metastatic phenotype, UAs address the fundamental biological drivers of PC. Their ability to maintain activity within complex 3D structures provides a robust scientific foundation for advancing these compounds to *in vivo* animal studies and subsequent clinical evaluation if favorable preclinical outcomes are achieved. This research underscores the potential of UA derivatives to shift the current treatment paradigm for pancreatic cancer from non-specific genotoxicity toward targeted, multi-pathway tumor elimination.

FUTURE PERSPECTIVES

The findings presented in this dissertation provide a robust scientific foundation for the further development of unsymmetrical bisacridines as potential therapeutics for pancreatic cancer, while simultaneously opening several promising avenues for future research.

A primary area for investigation is the "vimentin paradox" observed in the migration studies. Although UAs effectively inhibited cell motility, they induced a non-canonical modulation of EMT markers characterized by an unexpected increase in vimentin levels. Future studies should focus on determining whether this response is a general cellular stress mechanism or if UAs directly interfere with cytoskeletal dynamics and focal adhesion signaling independently of the classical mesenchymal phenotype.

Furthermore, although multicellular tumor spheroid models successfully validated UA efficacy in 3D, the exclusion of the BxPC-3 cell line due to its structural instability underscores the limitations of scaffold-free models for certain phenotypes. To bridge this gap, subsequent research should utilize more advanced 3D platforms, such as patient-derived organoids or hybrid scaffold-based co-cultures incorporating pancreatic stellate cells, to better replicate the dense desmoplastic niche and its impact on drug resistance.

The significant disparities in inhibitory concentrations (IC_{50} and IC_{80}) observed between 2D and compact 3D models, particularly in the AsPC-1 line, also emphasize the need for detailed pharmacokinetic profiling. Investigating how the physical barriers of the extracellular matrix and the hypoxic core of solid tumors affect the diffusion and intracellular accumulation of UAs will be critical for successful translation to *in vivo* animal models.

Finally, fully elucidating the non-canonical pathways triggered by UAs, including Beclin1-independent autophagy and its specific link to G-quadruplex stabilization in oncogene promoters, remains a priority.

Connecting these molecular insights with the multifaceted cellular response of apoptosis and senescence will be essential for establishing UAs as a new class of targeted, multi-pathway anticancer agents.

AUTHORS CONTRIBUTION

Article No. 1

Agnieszka Kurdyn, MSc Eng.
Gdańsk University of Technology
Faculty of Chemistry
Department of Pharmaceutical Technology and Biochemistry
Narutowicza Str. 11/12, Gdańsk 80-233, Poland
e-mail: agnieszka.kurdyn@pg.edu.pl
phone: +48 58 347 12 97

GDAŃSK UNIVERSITY OF TECHNOLOGY

May 15, 2026

Author Contribution

I hereby declare that my contribution to the publication entitled *"c-Myc inhibition and p21 modulation contribute to unsymmetrical bisacridines-induced apoptosis and senescence in pancreatic cancer cells"* included the following:

- Planning and performing laboratory experiments.
- Analysis and interpreting the experimental data.
- Preparing figures and tables.
- Drafting the original manuscript, as well as reviewing and editing the final version.

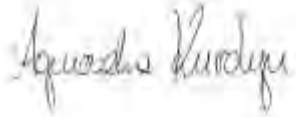

Monika Pawlowska, PhD, Eng.
Gdańsk University of Technology
Faculty of Chemistry
Department of Pharmaceutical Technology and Biochemistry
Narutowicza Str. 11/12, Gdańsk 80-233, Poland
e-mail: monpawlo@pg.edu.pl
phone: +48 58 347 12 97

GDAŃSK UNIVERSITY OF TECHNOLOGY

May 15, 2026

Author Contribution

I hereby declare that my contribution to the publication entitled *"c-Myc inhibition and p21 modulation contribute to unsymmetrical bisacridines-induced apoptosis and senescence in pancreatic cancer cells"* included the following:

- Performing selected Western blot experiments and participating in the subsequent data analysis.
- Conducting part of the microscopic imaging and visualization for the SA-β-galactosidase activity assessment.
- Substantive participation in the interpretation of research findings.
- Drafting the original manuscript, as well as reviewing and editing the final version.

Monika Pawłowska

Ewa Paluszkiewicz, PhD, Eng.
Gdańsk University of Technology
Faculty of Chemistry
Department of Pharmaceutical Technology and Biochemistry
Narutowicza Str. 11/12, Gdańsk 80-233, Poland
e-mail: ewapalus@pg.edu.pl
phone: +48 58 347 13 93

GDAŃSK UNIVERSITY OF TECHNOLOGY

May 15, 2026

Author Contribution

I hereby declare that my contribution to the publication entitled *"c-Myc inhibition and p21 modulation contribute to unsymmetrical bisacridines-induced apoptosis and senescence in pancreatic cancer cells"* included the following:

- Performing the chemical synthesis of the unsymmetrical bisacridine derivatives (C-2028, C-2045, and C-2053) used in the study.

Ewa Paluszkiewicz

Prof. Mirosława Anna Cichorek, PhD, DSc
Medical University of Gdańsk
Faculty of Medicine
Division of Embryology
Skłodowskiej-Curie Str. 3a, 80-210 Gdańsk
e-mail: miroslawa.cichorek@gumed.edu.pl
phone: + 48 58 349 14 95

May 15, 2026

Author Contribution

I hereby declare that my contribution to the publication entitled *"c-Myc inhibition and p21 modulation contribute to unsymmetrical bisacridines-induced apoptosis and senescence in pancreatic cancer cells"* included the following:

- Performing the flow cytometric analysis of cellular senescence induced by the C-2045 derivative and gemcitabine in MIA PaCa-2 cells.
- Data analysis and interpretation of the experimental results regarding the quantification of senescence markers.
- Providing methodological consultations.
- Drafting of the original manuscript.

M Cichorek

Ewa Augustin, PhD, DSc
Gdańsk University of Technology
Faculty of Chemistry
Department of Pharmaceutical Technology and Biochemistry
Narutowicza Str. 11/12, Gdańsk 80-233, Poland
e-mail: ewa.augustin@pg.edu.pl
phone: +48 58 347 14 68

GDAŃSK UNIVERSITY OF TECHNOLOGY

May 15, 2026

Author Contribution

I hereby declare that my contribution to the publication entitled *"c-Myc inhibition and p21 modulation contribute to unsymmetrical bisacridines-induced apoptosis and senescence in pancreatic cancer cells"* included the following:

- Conceptualization and design of the study.
- Data interpretation and evaluation.
- Provision of research resources and funding.
- Supervision and coordination of the project.
- Scientific guidance throughout the study.
- Drafting the original manuscript, as well as reviewing and editing the final version.

Ewa Augustin

Article No. 2

Agnieszka Kurdyn, MSc Eng.
Gdańsk University of Technology
Faculty of Chemistry
Department of Pharmaceutical Technology and Biochemistry
Narutowicza Str. 11/12, Gdańsk 80-233, Poland
e-mail: agnieszka.kurdyn@pg.edu.pl
phone: +48 58 347 12 97

GDAŃSK UNIVERSITY OF TECHNOLOGY

May 15, 2026

Author Contribution

I hereby declare that my contribution to the publication entitled *"Pro-Apoptotic Effects of Unsymmetrical Bisacridines in 3D Pancreatic Multicellular Tumor Spheroids"* included the following:

- Planning and performing laboratory experiments.
- Analysis and interpreting the experimental data.
- Preparing figures and tables.
- Drafting the original manuscript, as well as reviewing and editing the final version.

Agnieszka Kurdyn

Ewa Paluszkiewicz, PhD, Eng.
Gdańsk University of Technology
Faculty of Chemistry
Department of Pharmaceutical Technology and Biochemistry
Narutowicza Str. 11/12, Gdańsk 80-233, Poland
e-mail: ewapalus@pg.edu.pl
phone: +48 58 347 13 93

GDAŃSK UNIVERSITY OF TECHNOLOGY

May 15, 2026

Author Contribution

I hereby declare that my contribution to the publication entitled *"Pro-Apoptotic Effects of Unsymmetrical Bisacridines in 3D Pancreatic Multicellular Tumor Spheroids"* included the following:

- Performing the chemical synthesis of the unsymmetrical bisacridine derivatives (C-2028, C-2045, and C-2053) used in the study.

Ewa Paluszkiewicz

Ewa Augustin, PhD, DSc
Gdańsk University of Technology
Faculty of Chemistry
Department of Pharmaceutical Technology and Biochemistry
Narutowicza Str. 11/12, Gdańsk 80-233, Poland
e-mail: ewa.augustin@pg.edu.pl
phone: +48 58 347 14 68

GDAŃSK UNIVERSITY OF TECHNOLOGY

May 15, 2026

Author Contribution

I hereby declare that my contribution to the publication entitled *"Pro-Apoptotic Effects of Unsymmetrical Bisacridines in 3D Pancreatic Multicellular Tumor Spheroids"* included the following:

- Conceptualization and design of the study.
- Data interpretation and evaluation.
- Provision of research resources and funding.
- Supervision and coordination of the project.
- Scientific guidance throughout the study.
- Reviewing the final version of the manuscript.

Ewa Augustin

Article No. 3

Agnieszka Kurdyn, MSc Eng.
Gdańsk University of Technology
Faculty of Chemistry
Department of Pharmaceutical Technology and Biochemistry
Narutowicza Str. 11/12, Gdańsk 80-233, Poland
e-mail: agnieszka.kurdyn@pg.edu.pl
phone: +48 58 347 12 97

GDAŃSK UNIVERSITY OF TECHNOLOGY

May 15, 2026

Author Contribution

I hereby declare that my contribution to the publication entitled *"Apoptosis-promoting autophagy mediates anti-migratory effects of unsymmetrical bisacridines in pancreatic cancer cells"* included the following:

- Planning and performing laboratory experiments.
- Analysis and interpreting the experimental data.
- Preparing figures and tables.
- Drafting the original manuscript, as well as reviewing and editing the final version.

Bożena Pezala, MSc Eng.
Gdańsk University of Technology
Faculty of Chemistry
Department of Pharmaceutical Technology and Biochemistry
Narutowicza Str. 11/12, Gdańsk 80-233, Poland
e-mail: bozena.pezala@pg.edu.pl
phone: +48 58 347 12 97

GDAŃSK UNIVERSITY OF TECHNOLOGY

May 15, 2026

Author Contribution

I hereby declare that my contribution to the publication entitled *"Apoptosis-promoting autophagy mediates anti-migratory effects of unsymmetrical bisacridines in pancreatic cancer cells"* included the following:

- Performing part of the microscopic observations of acidic vesicular organelles in pancreatic cancer cells using acridine orange staining and fluorescence microscopy.
- Conducting the quantitative analysis and quantification of fluorescence intensity of the captured images.

Bożena Pezala

Ewa Paluszkiewicz, PhD, Eng.
Gdańsk University of Technology
Faculty of Chemistry
Department of Pharmaceutical Technology and Biochemistry
Narutowicza Str. 11/12, Gdańsk 80-233, Poland
e-mail: ewapalus@pg.edu.pl
phone: +48 58 347 13 93

GDAŃSK UNIVERSITY OF TECHNOLOGY

May 15, 2026

Author Contribution

I hereby declare that my contribution to the publication entitled *"Apoptosis-promoting autophagy mediates anti-migratory effects of unsymmetrical bisacridines in pancreatic cancer cells"* included the following:

- Performing the chemical synthesis of the unsymmetrical bisacridine derivatives (C-2028, C-2045, and C-2053) used in the study.

Ewa Paluszkiewicz

Ewa Augustin, PhD, DSc
Gdańsk University of Technology
Faculty of Chemistry
Department of Pharmaceutical Technology and Biochemistry
Narutowicza Str. 11/12, Gdańsk 80-233, Poland
e-mail: ewa.augustin@pg.edu.pl
phone: +48 58 347 14 68

GDAŃSK UNIVERSITY OF TECHNOLOGY

May 15, 2026

Author Contribution

I hereby declare that my contribution to the publication entitled *"Apoptosis-promoting autophagy mediates anti-migratory effects of unsymmetrical bisacridines in pancreatic cancer cells"* included the following:

- Conceptualization and design of the study.
- Data interpretation and evaluation.
- Provision of research resources and funding.
- Supervision and coordination of the project.
- Scientific guidance throughout the study.
- Reviewing the final version of the manuscript.

Ewa Augustin

SCIENTIFIC ACHIEVEMENTS

Publications

1. **Kurdyn A.**, Pezała B., Paluszkiewicz E., Augustin E. Apoptosis-promoting autophagy mediates anti-migratory effects of unsymmetrical bisacridines in pancreatic cancer cells. *Biomedicine & Pharmacotherapy;* 2025; 193:118786; doi:10.1016/j.biopha.2025.118786; MHES Points 100; Q1; IF: 7.5
2. **Kurdyn A.**, Paluszkiewicz E., Augustin E. Anticancer activity of unsymmetrical bisacridines in 3D pancreatic multicellular tumor spheroids. *International Journal of Molecular Sciences*; 2025; 26:7557; doi:10.3390/ijms26157557; MHES Points 140; Q1; IF: 4.9
3. Walczak, J.; Iwaszkiewicz-Grześ, D.; Śliwka-Kaszyńska, M.; **Kurdyn, A.**; Augustin, E.; Viapiana, A.; Plenis, A.; Cholewiński, G. Direct synthesis of mycophenolic acid aryl esters with antioxidant and antiproliferative properties. *Scientific Reports*; 2025, 15, 26006; doi:10.1038/s41598-025-11871-5; MHES Points 140; Q1; IF: 3.9
4. **Kurdyn, A.**; Pawłowska, M.; Paluszkiewicz, E; Cichorek, M.; Augustin, E. c-Myc inhibition and p21 modulation contribute to unsymmetrical bisacridines-induced apoptosis and senescence in pancreatic cancer cells. *Pharmacological Reports*; 2025; 77:182–209; doi: 10.1007/s43440-024-00658-6; MHES Points 100; Q1; IF: 3.8
5. Piłat, E.; Gnatowski, P.; **Kurdyn, A.**; Cieśliński, H.; Augustin, E.; Kucińska-Lipka, J. Investigation of bioprintable modified agar-based hydrogels with antimicrobial properties. *International Journal of Biological Macromolecules*; 2025; 289:138707; doi: 10.1016/j.ijbiomac.2024.138707; MHES Points 100; Q1; IF: 8.5
6. Piłat, E.; **Kurdyn, A.**; Kucińska-Lipka, J. Naturally-derived Hydrogels for 3D Pancreatic Tumor Models: A short review. *Polymers from Renewable Resources*; 2023;14(4):279-288; doi: 10.1177/20412479231200321; MHES Points 20; Q2; IF-
7. Gnatowski, P.; Gwizdała, K.; **Kurdyn, A.**; Skorek, A.; Augustin, E.; Kucińska-Lipka, J. Investigation on Filaments for 3D Printing of Nasal Septum Cartilage Implant. *Materials*; 2023; 16, 3534; doi: 10.3390/ma16093534; MHES Points 140; Q2; IF: 3.1
8. Kosno, M.; Laskowski, T.; Frąckowiak, J.E.; Potęga, A.; **Kurdyn, A.**; Andrałojć, W.; Borzyszkowska-Bukowska, J.; Szwarc-Karabyka, K.; Mazerska, Z. Acid–Base Equilibrium and Self-Association in Relation to High Antitumor Activity of Selected Unsymmetrical Bisacridines Established by Extensive Chemometric Analysis. *Molecules*; 2022; 27, 3995; doi: 10.3390/molecules27133995; MHES Points 140; Q2; IF: 4.6

Submitted publication

1. Dagdelen, S.; Mestizo, P. D.; Mackiewicz, M.; **Kurdyn, A.**; Augustin, E.; Karbarz, M.; Zelder, F. H.; Vitamin B12-functionalized nanogels for doxorubicin delivery. *ChemBioChem*

Poster communications

1. **Kurdyn A.**, Pezała B., Augustin E.: Crosstalk between autophagy and apoptosis induced by unsymmetrical bisacridines in pancreatic cancer cells. The EACR 2025 Congress, Lisbon, Portugal, 16 – 19 June 2025
2. Piłat, E.; Gnatowski, P.; **Kurdyn, A.**; Cieśliński, H.; Augustin, E.; Kucińska-Lipka, J. Agar-based hydrogels with antimicrobial properties. 30th International Student Scientific Conference, Gdańsk, Poland, 10 – 12 April 2025
3. **Kurdyn A.**, Augustin E.: Studies of the cellular response induced by highly active unsymmetrical bisacridines in pancreatic cancer cells cultured in 2D and 3D. *The 48th FEBS Congress,* Milano, Italy, 29 June – 03 July 2024, and *the 23rd FEBS Young Scientists' Forum 2024,* Pavia, Italy, 26 – 29 June 2024
4. **Kurdyn, A.**; Pawłowska, M.; Augustin, E. Biological effects induced by new anticancer unsymmetrical bisacridines in human chemoresistant pancreatic cancer cells. *The 47th FEBS Congress*, Tours, France, 8 – 12 July 2023.
5. **Kurdyn, A.**; Kulesza, J.; Pawłowska, M.; Paluszkiewicz, E.; Augustin, E. Unsymmetrical bisacridine derivatives show anticancer potential by inducing apoptosis in human prostate, colon, and pancreatic cancer cells. *The 28th Conference of ECDO*, Bonn, Germany, 26 – 29 September 2022.

Awards and scholarships

1. PROM Program – short-term mobility – Grant funding participation in the EACR 2025 Congress, Lisbon, Portugal, 16–19 June 2025
2. Mini-grant of the Faculty of Chemistry, Gdańsk University of Technology, 2025
3. Francium Supporting Outstanding Doctoral Candidates – scholarship from the IDUB program, October 2024 – September 2025.
4. Grant from the Federation of European Biochemical Societies (FEBS) funding conference participation, accommodation, and 80% of travel costs: The 48th FEBS Congress, Milan, Italy, 29 June – 3 July 2024, and The 23rd FEBS Young Scientists' Forum 2024, Pavia, Italy, 26 – 29 June 2024.
5. Francium Supporting Outstanding Doctoral Candidates – scholarship from the IDUB program, October 2023 – September 2024
6. Scholarship from the Federation of European Biochemical Societies (FEBS) supporting participation in The 47th FEBS Congress, Tours, France, 8 – 12 July 2023
7. Mini-grant of the Faculty of Chemistry, Gdańsk University of Technology, 2023
8. Francium Supporting Outstanding Doctoral Candidates – scholarship from the IDUB program, October 2022 – September 2023
9. Gold Graduate Badge of Gdańsk University of Technology for obtaining a Master's degree with distinction, 2021
10. „Najlepsi z najlepszych! 4.0." – Grant of PLN 225,000 for the implementation of the student project Stardust, carried out by the Biotechnology Students' Association (KSB; Koło Studentów Biotechnologii) and Simply Learn Experience (SimLE), August 2019 – October 2020

Professional experience

1. Researcher on a project conducted at Gdańsk University of Technology, in the Department of Pharmaceutical Technology and Biochemistry, in collaboration with CHDE Polska S.A., Rzeszów, January 2024 – February 2025

   Project: “Preclinical *in vitro* studies of unsymmetrical bisacridines with high anticancer activity – a 3D culture model of human pancreatic cancer cells as an introduction to *in vivo* toxicology studies.”

REFERENCES

[1] World Health Organization, International Agency for Research on Cancer, CANCER TODAY. *Globocan 2022 (version 1.1) - 08.02.2024; date of access: 01.10.2025*.

[2] World Health Organization, International Agency for Research on Cancer, CANCER TOMORROW. *Globocan 2022 (version 1.1) - 08.02.2024; date of access: 01.10.2025*.

[3] Capasso M, Franceschi M, Rodriguez-Castro KI, et al. Epidemiology and risk factors of pancreatic cancer. *Acta Biomed* 2018; 89: 141–146.

[4] Xu F, Huang M, Bai Y, et al. Landmarks in pancreatic cancer studies. *Cancer Cell Int* 2022; 22: 383.

[5] Halbrook CJ, Lyssiotis CA, Pasca di Magliano M, Maitra A. Pancreatic cancer: Advances and challenges. *Cell* 2023; 186: 1729–1754.

[6] Hu J, Zhao C, Chen W, et al. Pancreatic cancer: A review of epidemiology, trend, and risk factors. *World J Gastroenterol* 2021; 27: 4298–4321.

[7] Rahib L, Smith BD, Aizenberg R, Rosenzweig AB, Fleshman JM, Matrisian LM. Projecting Cancer Incidence and Deaths to 2030: The Unexpected Burden of Thyroid, Liver, and Pancreas Cancers in the United States. *Cancer Res* 2014; 74: 2913–2921.

[8] Seyhan AA. Circulating microRNAs as Potential Biomarkers in Pancreatic Cancer-Advances and Challenges. *Int J Mol Sci* 2023; 24: 13340.

[9] Rawla P, Sunkara T, Gaduputi V. Epidemiology of Pancreatic Cancer: Global Trends, Etiology and Risk Factors. *World J Oncol* 2019; 10: 10–27.

[10] Bazeed AY, Day CM, Garg S. Pancreatic Cancer: Challenges and Opportunities in Locoregional Therapies. *Cancers (Basel)* 2022; 14: 4257.

[11] Moletta L, Serafini S, Valmasoni M, Pierobon ES, Ponzoni A, Sperti C. Surgery for Recurrent Pancreatic Cancer: Is It Effective? *Cancers (Basel)* 2019; 11: 991.

[12] Hu C, Chen Y, Yin X, et al. Pancreatic endocrine and exocrine signaling and crosstalk in physiological and pathological status. *Signal Transduct Target Ther* 2025; 10: 39.

[13] Khalaf N, El-Serag HB, Abrams HR, Thrift AP. Burden of Pancreatic Cancer: From Epidemiology to Practice. *Clin Gastroenterol Hepatol* 2021; 19: 876–884.

[14] Partyka O, Pajewska M, Kwaśniewska D, et al. Overview of Pancreatic Cancer Epidemiology in Europe and Recommendations for Screening in High-Risk Populations. *Cancers (Basel)* 2023; 15: 3634.

[15] Wood LD, Canto MI, Jaffee EM, Simeone DM. Pancreatic Cancer: Pathogenesis, Screening, Diagnosis, and Treatment. *Gastroenterology* 2022; 163: 386-402.e1.

[16] Graham S, Dmitrieva M, Vendramini-Costa DB, et al. From precursor to cancer: decoding the intrinsic and extrinsic pathways of pancreatic intraepithelial neoplasia progression. *Carcinogenesis* 2024; 45: 801–816.

[17] Wang S, Zheng Y, Yang F, et al. The molecular biology of pancreatic adenocarcinoma: translational challenges and clinical perspectives. *Signal Transduct Target Ther* 2021; 6: 249.

[18] Fan Z, Fan K, Yan C, et al. Critical role of KRAS mutation in pancreatic ductal adenocarcinoma. *Transl Cancer Res* 2018; 7: 1728–1736.

[19] Lin J, Liu T, Yang P. CDKN2A-Inactivated Pancreatic Ductal Adenocarcinoma Exhibits Therapeutic Sensitivity to Paclitaxel: A Bioinformatics Study. *J Clin Med* 2020; 9: 4019.

[20] Han G, Yang G, Hao D, et al. 9p21 loss confers a cold tumor immune microenvironment and primary resistance to immune checkpoint therapy. *Nat Commun* 2021; 12: 5606.

[21] Wang Z, Li Y, Zhan S, et al. SMAD4 Y353C promotes the progression of PDAC. *BMC Cancer* 2019; 19: 1037.

[22] Morton JP, Timpson P, Karim SA, et al. Mutant p53 drives metastasis and overcomes growth arrest/senescence in pancreatic cancer. *Proc Natl Acad Sci* 2010; 107: 246–251.

[23] Maddalena M, Mallel G, Nataraj NB, et al. TP53 missense mutations in PDAC are associated with enhanced fibrosis and an immunosuppressive microenvironment. *Proc Natl Acad Sci*; 118. Epub ahead of print 8 June 2021. DOI: 10.1073/pnas.2025631118.

[24] Racu M, Lebrun L, Schiavo AA, et al. The Role of SMAD4 Inactivation in Epithelial-Mesenchymal Plasticity of Pancreatic Ductal Adenocarcinoma: The Missing Link? *Cancers (Basel)* 2022; 14: 973.

[25] Tie Y, Tang F, Peng D, Zhang Y, Shi H. TGF-beta signal transduction: biology, function and therapy for diseases. *Mol Biomed* 2022; 3: 45.

[26] O'Sullivan EA, Wallis R, Mossa F, Bishop CL. The paradox of senescent-marker positive cancer cells: challenges and opportunities. *npj Aging* 2024; 10: 41.

[27] Vaskovich-Koubi D, Green Buzhor M, Krinsky A, et al. Patient-Derived 3D-Bioprinted Models of Pancreatic Cancer: Toward Personalized Therapy and Overcoming Tumor Microenvironment Challenges. *Adv Drug Deliv Rev* 2025; 225: 115670.

[28] Deng D, Patel R, Chiang C-Y, Hou P. Role of the Tumor Microenvironment in Regulating Pancreatic Cancer Therapy Resistance. *Cells* 2022; 11: 2952.

[29] Polani F, Grierson PM, Lim K. Stroma-targeting strategies in pancreatic cancer: Past lessons, challenges and prospects. *World J Gastroenterol* 2021; 27: 2105–2121.

[30] Sherman MH, Beatty GL. Tumor Microenvironment in Pancreatic Cancer Pathogenesis and Therapeutic Resistance. *Annu Rev Pathol Mech Dis* 2023; 18: 123–148.

[31] Wang H, Lin Y, Hsu C, et al. Pancreatic stellate cells activated by mutant KRAS-mediated PAI-1 upregulation foster pancreatic cancer progression via IL-8. *Theranostics* 2019; 9: 7168–7183.

[32] Louault K, Li R-R, DeClerck YA. Cancer-Associated Fibroblasts: Understanding Their Heterogeneity. *Cancers (Basel)* 2020; 12: 3108.

[33] Özdemir BC, Pentcheva-Hoang T, Carstens JL, et al. Depletion of Carcinoma-Associated Fibroblasts and Fibrosis Induces Immunosuppression and Accelerates Pancreas Cancer with Reduced Survival. *Cancer Cell* 2014; 25: 719–734.

[34] Rhim AD, Oberstein PE, Thomas DH, et al. Stromal Elements Act to Restrain, Rather Than Support, Pancreatic Ductal Adenocarcinoma. *Cancer Cell* 2014; 25: 735–747.

[35] Tarannum M, Vivero-Escoto JL. Nanoparticle-based therapeutic strategies targeting major clinical challenges in pancreatic cancer treatment. *Adv Drug Deliv Rev* 2022; 187: 114357.

[36] Ahmad RS, Eubank TD, Lukomski S, Boone BA. Immune Cell Modulation of the Extracellular Matrix Contributes to the Pathogenesis of Pancreatic Cancer. *Biomolecules* 2021; 11: 901.

[37] Burris HA, Moore MJ, Andersen J, et al. Improvements in survival and clinical benefit with gemcitabine as first-line therapy for patients with advanced pancreas cancer: a randomized trial. *J Clin Oncol* 1997; 15: 2403–2413.

[38] de Sousa Cavalcante L, Monteiro G. Gemcitabine: Metabolism and molecular mechanisms of action, sensitivity and chemoresistance in pancreatic cancer. *Eur J Pharmacol* 2014; 741: 8–16.

[39] Conroy T, Castan F, Lopez A, et al. Five-Year Outcomes of FOLFIRINOX vs Gemcitabine as Adjuvant Therapy for Pancreatic Cancer. *JAMA Oncol* 2022; 8: 1571.

[40] Zhou K, Liu Y, Tang C, Zhu H. Pancreatic Cancer: Pathogenesis and Clinical Studies.

MedComm; 6. Epub ahead of print 2 April 2025. DOI: 10.1002/mco2.70162.

[41] Kindler HL. A New Direction for Pancreatic Cancer Treatment: FOLFIRINOX in Context. *Am Soc Clin Oncol Educ B* 2012; 232–237.

[42] Okada K, Kimura K, Yamashita Y, et al. Efficacy and safety of neoadjuvant nab-paclitaxel plus gemcitabine therapy in patients with borderline resectable pancreatic cancer: A multicenter single-arm phase <scp>II</scp> study (<scp>NAC-GA</scp> trial). *Ann Gastroenterol Surg* 2023; 7: 997–1008.

[43] Von Hoff DD, Ervin T, Arena FP, et al. Increased Survival in Pancreatic Cancer with nab-Paclitaxel plus Gemcitabine. *N Engl J Med* 2013; 369: 1691–1703.

[44] Buckley CW, O'Reilly EM. Next-generation therapies for pancreatic cancer. *Expert Rev Gastroenterol Hepatol* 2024; 18: 55–72.

[45] Wainberg ZA, Melisi D, Macarulla T, et al. NALIRIFOX versus nab-paclitaxel and gemcitabine in treatment-naive patients with metastatic pancreatic ductal adenocarcinoma (NAPOLI 3): a randomised, open-label, phase 3 trial. *Lancet* 2023; 402: 1272–1281.

[46] Dilly J, Hoffman MT, Abbassi L, et al. Mechanisms of Resistance to Oncogenic KRAS Inhibition in Pancreatic Cancer. DOI: 10.1158/2159-8290.CD-24-0177.

[47] Hall MJ, Park JO, Ph D, et al. Maintenance Olaparib for Germline. 2019; 317–327.

[48] Melisi D, Garcia-Carbonero R, Macarulla T, et al. Galunisertib plus gemcitabine vs. gemcitabine for first-line treatment of patients with unresectable pancreatic cancer. *Br J Cancer* 2018; 119: 1208–1214.

[49] Arnold SA, Rivera LB, Carbon JG, et al. Losartan Slows Pancreatic Tumor Progression and Extends Survival of SPARC-Null Mice by Abrogating Aberrant TGFβ Activation. *PLoS One* 2012; 7: e31384.

[50] O'Hara MH, O'Reilly EM, Varadhachary G, et al. CD40 agonistic monoclonal antibody APX005M (sotigalimab) and chemotherapy, with or without nivolumab, for the treatment of metastatic pancreatic adenocarcinoma: an open-label, multicentre, phase 1b study. *Lancet Oncol* 2021; 22: 118–131.

[51] Morrison AH, Diamond MS, Hay CA, Byrne KT, Vonderheide RH. Sufficiency of CD40 activation and immune checkpoint blockade for T cell priming and tumor immunity. *Proc Natl Acad Sci* 2020; 117: 8022–8031.

[52] Balachandran VP, Beatty GL, Dougan SK. Broadening the Impact of Immunotherapy to Pancreatic Cancer: Challenges and Opportunities. *Gastroenterology* 2019; 156: 2056-2072.

[53] Babiker HM, Picozzi V, Chandana SR, et al. Tumor Treating Fields With Gemcitabine and Nab-Paclitaxel for Locally Advanced Pancreatic Adenocarcinoma: Randomized, Open-Label, Pivotal Phase III PANOVA-3 Study. *J Clin Oncol* 2025; 43: 2350–2360.

[54] Liaki V, Barrambana S, Kostopoulou M, et al. A targeted combination therapy achieves effective pancreatic cancer regression and prevents tumor resistance. *Proc Natl Acad Sci*; 122. Epub ahead of print 9 December 2025. DOI: 10.1073/pnas.2523039122.

[55] Shen MJ, Jamali A, Katona BW. Challenges of early detection of pancreatic cancer. *J Clin Invest*; 135. Epub ahead of print 15 October 2025. DOI: 10.1172/JCI191942.

[56] Zheng Z, Lu Z, Yan F, Song Y. The role of novel biomarkers in the early diagnosis of pancreatic cancer: A systematic review and meta-analysis. *PLoS One* 2025; 20: e0322720.

[57] Hu H, Ye Z, Qin Y, et al. Mutations in key driver genes of pancreatic cancer: molecularly targeted therapies and other clinical implications. *Acta Pharmacol Sin* 2021; 42: 1725-1741.

[58] Deer EL, González-Hernández J, Coursen JD, et al. Phenotype and Genotype of

Pancreatic Cancer Cell Lines. *Pancreas* 2010; 39: 425–435.

[59] Watanabe M. Metabolic Profiling Comparison of Human Pancreatic Ductal Epithelial Cells and Three Pancreatic Cancer Cell Lines using NMR Based Metabonomics. *J Mol Biomark Diagn* 2012; 03: 139–148.

[60] Gradiz R, Silva HC, Carvalho L, Botelho MF, Mota-Pinto A. MIA PaCa-2 and PANC-1 – pancreas ductal adenocarcinoma cell lines with neuroendocrine differentiation and somatostatin receptors. *Sci Rep* 2016; 6: 21648.

[61] Sun C, Yamato T, Furukawa T, Ohnishi Y, Kijima H, Horii A. Characterization of the mutations of the K-ras, p53, p16, and SMAD4 genes in 15 human pancreatic cancer cell lines. *Oncol Rep* 2001; 8: 89–92.

[62] Waters AM, Der CJ. KRAS: The Critical Driver and Therapeutic Target for Pancreatic Cancer. *Cold Spring Harb Perspect Med* 2018; 8: a031435.

[63] LEGENDRE O, SOOKDEO A, FOSTER DA. BxPC3 pancreatic cancer cells express a truncated Smad4 protein upon PI3K and mTOR inhibition. *Oncol Lett* 2014; 7: 1165–1168.

[64] Arlt A, Müerköster SS, Schäfer H. Targeting apoptosis pathways in pancreatic cancer. *Cancer Lett* 2013; 332: 346–358.

[65] Modi S, Kir D, Banerjee S, Saluja A. Control of Apoptosis in Treatment and Biology of Pancreatic Cancer. *J Cell Biochem* 2016; 117: 279–288.

[66] Pfeffer C, Singh A. Apoptosis: A Target for Anticancer Therapy. *Int J Mol Sci* 2018; 19: 448.

[67] Eser S, Schnieke A, Schneider G, Saur D. Oncogenic KRAS signalling in pancreatic cancer. *Br J Cancer* 2014; 111: 817–822.

[68] Mehra S, Deshpande N, Nagathihalli N. Targeting pi3k pathway in pancreatic ductal adenocarcinoma: Rationale and progress. *Cancers (Basel)* 2021; 13: 1–10.

[69] Shen X, Niu N, Xue J. Oncogenic KRAS triggers metabolic reprogramming in pancreatic ductal adenocarcinoma. *J Transl Intern Med* 2023; 11: 322–329.

[70] Dorji JP, Chen Q, Perera SG, et al. c-MYC mRNA destabilization inhibited lethal pancreatic cancer in vivo with significant survival outcomes. *Front Pharmacol* 2025; 16: 1–12.

[71] Liu Y, Gan Y, Chen J, Jiang Y, Huang F, Tang D. Targeting MYC to Combat Pancreatic Cancer. *J Explor Res Pharmacol* 2022; 000: 000–000.

[72] Ji S, Qin Y, Liang C, et al. FBW7 (F-box and WD Repeat Domain-Containing 7) Negatively Regulates Glucose Metabolism by Targeting the c-Myc/TXNIP (Thioredoxin-Binding Protein) Axis in Pancreatic Cancer. *Clin Cancer Res* 2016; 22: 3950–3960.

[73] Ala M. Target c-Myc to treat pancreatic cancer. *Cancer Biol Ther* 2022; 23: 34–50.

[74] Chen H, Liu H, Qing G. Targeting oncogenic Myc as a strategy for cancer treatment. *Signal Transduct Target Ther* 2018; 3: 5.

[75] Mori T, Doi R, Kida A, et al. Effect of the XIAP Inhibitor Embelin on TRAIL-Induced Apoptosis of Pancreatic Cancer Cells. *J Surg Res* 2007; 142: 281–286.

[76] Cortesi M, Zanoni M, Pirini F, et al. Pancreatic Cancer and Cellular Senescence: Tumor Microenvironment under the Spotlight. *Int J Mol Sci* 2021; 23: 254.

[77] AG Moir J, A White S, Mann J. Arrested development and the great escape – The role of cellular senescence in pancreatic cancer. *Int J Biochem Cell Biol* 2014; 57: 142–148.

[78] Jo H, Shim K, Jeoung D. The Potential of Senescence as a Target for Developing Anticancer Therapy. *Int J Mol Sci* 2023; 24: 3436.

[79] Lee S, Lee J-S. Cellular senescence: a promising strategy for cancer therapy. *BMB Rep*

2019; 52: 35–41.

[80] Hornsby PJ. Senescence As an Anticancer Mechanism. *J Clin Oncol* 2007; 25: 1852–1857.

[81] Yang K, Li X, Xie K. Senescence program and its reprogramming in pancreatic premalignancy. *Cell Death Dis* 2023; 14: 528.

[82] Jia L, Li H, Sun Y. Induction of p21-Dependent Senescence by an NAE Inhibitor, MLN4924, as a Mechanism of Growth Suppression. *Neoplasia* 2011; 13: 561–569.

[83] Warfel NA, El-Deiry WS. p21WAF1 and tumourigenesis. *Curr Opin Oncol* 2013; 25: 52-58.

[84] Abbas T, Dutta A. p21 in cancer: intricate networks and multiple activities. *Nat Rev Cancer* 2009; 9: 400–414.

[85] Wagner K-D, Wagner N. The Senescence Markers p16INK4A, p14ARF/p19ARF, and p21 in Organ Development and Homeostasis. *Cells* 2022; 11: 1966.

[86] Muñoz-Espín D, Serrano M. Cellular senescence: from physiology to pathology. *Nat Rev Mol Cell Biol* 2014; 15: 482–496.

[87] Jiang H, Wang G-T, Wang Z, Ma Q-Y, Ma Z-H. Resveratrol inhibits pancreatic cancer proliferation and metastasis by depleting senescent tumor-associated fibroblasts. *World J Gastrointest Oncol* 2024; 16: 3980–3993.

[88] Gillson J, Abd El-Aziz YS, Leck LYW, et al. Autophagy: A Key Player in Pancreatic Cancer Progression and a Potential Drug Target. *Cancers (Basel)* 2022; 14: 3528.

[89] Li J, Chen X, Kang R, Zeh H, Klionsky DJ, Tang D. Regulation and function of autophagy in pancreatic cancer. *Autophagy* 2021; 17: 3275–3296.

[90] Ma J, Xue H, He L, et al. The Role and Mechanism of Autophagy in Pancreatic Cancer: An Update Review. *Cancer Manag Res* 2021; Volume 13: 8231–8240.

[91] Mizushima N, Yoshimori T. How to Interpret LC3 Immunoblotting. *Autophagy* 2007; 3: 542–545.

[92] Tanida I. Autophagosome Formation and Molecular Mechanism of Autophagy. *Antioxid Redox Signal* 2011; 14: 2201–2214.

[93] Cao W, Li J, Yang K, Cao D. An overview of autophagy: Mechanism, regulation and research progress. *Bull Cancer* 2021; 108: 304–322.

[94] Toh PPC, Luo S, Menzies FM, Raskó T, Wanker EE, Rubinsztein DC. Myc inhibition impairs autophagosome formation. *Hum Mol Genet* 2013; 22: 5237–5248.

[95] Zang Y, Zhu L, Li T, et al. EI24 Suppresses Tumorigenesis in Pancreatic Cancer via Regulating c-Myc. *Gastroenterol Res Pract* 2018; 2018: 1–12.

[96] Yang S, Wang X, Contino G, et al. Pancreatic cancers require autophagy for tumor growth. *Genes Dev* 2011; 25: 717–729.

[97] Antonucci L, Fagman JB, Kim JY, et al. Basal autophagy maintains pancreatic acinar cell homeostasis and protein synthesis and prevents ER stress. *Proc Natl Acad Sci*; 112. Epub ahead of print 10 November 2015. DOI: 10.1073/pnas.1519384112.

[98] Rosenfeldt MT, O'Prey J, Morton JP, et al. p53 status determines the role of autophagy in pancreatic tumour development. *Nature* 2013; 504: 296–300.

[99] Hashimoto D, Bläuer M, Hirota M, Ikonen NH, Sand J, Laukkarinen J. Autophagy is needed for the growth of pancreatic adenocarcinoma and has a cytoprotective effect against anticancer drugs. *Eur J Cancer* 2014; 50: 1382–1390.

[100] Kang R, Zeh HJ, Lotze MT, Tang D. The Beclin 1 network regulates autophagy and apoptosis. *Cell Death Differ* 2011; 18: 571–580.

[101] Ranjan A, Iwakuma T. Non-Canonical Cell Death Induced by p53. *Int J Mol Sci* 2016; 17: 2068.

[102] Cui D, Qu R, Liu D, Xiong X, Liang T, Zhao Y. The Cross Talk Between p53 and mTOR Pathways in Response to Physiological and Genotoxic Stresses. *Front Cell Dev Biol* 2021; 9: 1–11.

[103] Badadani M. Autophagy Mechanism, Regulation, Functions, and Disorders. *ISRN Cell Biol* 2012; 2012: 1–11.

[104] Liao G, Gao B, Gao Y, Yang X, Cheng X, Ou Y. Phycocyanin Inhibits Tumorigenic Potential of Pancreatic Cancer Cells: Role of Apoptosis and Autophagy. *Sci Rep* 2016; 6: 34564.

[105] Joshi VB, Gutierrez Ruiz OL, Razidlo GL. The Cell Biology of Metastatic Invasion in Pancreatic Cancer: Updates and Mechanistic Insights. *Cancers (Basel)* 2023; 15: 2169.

[106] Beuran M, Negoi I, Paun S, et al. The epithelial to mesenchymal transition in pancreatic cancer: A systematic review. *Pancreatology* 2015; 15: 217–225.

[107] Yang J, Liu Y, Liu S. The role of epithelial-mesenchymal transition and autophagy in pancreatic ductal adenocarcinoma invasion. *Cell Death Dis* 2023; 14: 506.

[108] Loh C-Y, Chai J, Tang T, et al. The E-Cadherin and N-Cadherin Switch in Epithelial-to-Mesenchymal Transition: Signaling, Therapeutic Implications, and Challenges. *Cells* 2019; 8: 1118.

[109] Wang R, Yan Z. Cancer spreading patterns based on epithelial-mesenchymal plasticity. *Front Cell Dev Biol* 2024; 12: 1–11.

[110] Bousset L, Gil J. Targeting senescence as an anticancer therapy. *Mol Oncol* 2022; 16: 3855–3880.

[111] Cayo A, Segovia R, Venturini W, Moore-Carrasco R, Valenzuela C, Brown N. mTOR Activity and Autophagy in Senescent Cells, a Complex Partnership. *Int J Mol Sci* 2021; 22: 8149.

[112] Bryant KL, Stalnecker CA, Zeitouni D, et al. Combination of ERK and autophagy inhibition as a treatment approach for pancreatic cancer. *Nat Med* 2019; 25: 628–640.

[113] Gniazdowski M, Szmigiero L. Nitracrine and its congeners—An overview. *Gen Pharmacol Vasc Syst* 1995; 26: 473–481.

[114] Pawlak JW, Pawlak K, Konopa J. The mode of action of cytotoxic and antitumor 1-nitroacridines. II. In vivo enzyme-mediated covalent binding of a 1-nitroacridine derivative, ledakrin or nitracrine, with DNA and other macromolecules of mammalian or bacterial cells. *Chem Biol Interact* 1983; 43: 151–173.

[115] Augustin E, Moś-Rompa A, Nowak-Ziatyk D, Konopa J. Antitumor 1-nitroacridine derivative C-1748, induces apoptosis, necrosis or senescence in human colon carcinoma HCT8 and HT29 cells. *Biochem Pharmacol* 2010; 79: 1231–1241.

[116] Wiśniewska A, Niemira M, Jagiełło K, et al. Diminished toxicity of C-1748, 4-methyl-9-hydroxyethylamino-1-nitroacridine, compared with its demethyl analog, C-857, corresponds to its resistance to metabolism in HepG2 cells. *Biochem Pharmacol* 2012; 84: 30–42.

[117] Isambert N, Campone M, Bourbouloux E, et al. Evaluation of the safety of C-1311 (SYMADEX) administered in a phase 1 dose escalation trial as a weekly infusion for 3 consecutive weeks in patients with advanced solid tumours. *Eur J Cancer* 2010; 46: 729-734.

[118] Potega A, Dabrowska E, Niemira M, et al. The Imidazoacridinone Antitumor Drug, C-1311, Is Metabolized by Flavin Monooxygenases but Not by Cytochrome P450s. *Drug Metab Dispos* 2011; 39: 1423–1432.

[119] Konopa J, Horowska B, Paluszkiewicz EM, et al. Asymmetric Bis-acridines with antitumor activity and use thereof. Gdansk University of Technology. European Patent EP 3070078.

[120] Konopa J, Horowska B, Paluszkiewicz EM, et al. Asymmetric bis-acridines with antitumour activity and their uses. University of Technology. Cancadian Patent CA 2980084.

[121] Konopa J, Horowska B, Paluszkiewicz EM, et al. Asymmetric Bis-acridines with antitumor activity and use thereof. Gdansk University of Technology. U.S. Patent US 10202349 B2.

[122] Konopa J, Horowska B, Paluszkiewicz EM, et al. Asymmetric Bis-acridines with antitumour activity and their uses. Gdansk University of Technology. Japanese Patent 7226918.

[123] Paluszkiewicz E, Horowska B, Borowa-Mazgaj B, et al. Design, synthesis and high antitumor potential of new unsymmetrical bisacridine derivatives towards human solid tumors, specifically pancreatic cancers and their unique ability to stabilize DNA G-quadruplexes. *Eur J Med Chem* 2020; 204: 112599.

[124] Mieszkowska A, Nowicka AM, Kowalczyk A, et al. Metabolic Profiles of New Unsymmetrical Bisacridine Antitumor Agents in Electrochemical and Enzymatic Noncellular Systems and in Tumor Cells. *Pharmaceuticals* 2021; 14: 317.

[125] Laskowski T, Kosno M, Andrałojć W, et al. The interactions of monomeric acridines and unsymmetrical bisacridines (UAs) with DNA duplexes: an insight provided by NMR and MD studies. *Sci Rep* 2023; 13: 3431.

[126] Laskowski T, Kosno M, Andrałojć W, et al. The interactions of Pu22 G-quadruplex, derived from c-MYC promoter sequence, with antitumor acridine derivatives—An NMR/MD combined study. *Mol Ther Nucleic Acids* 2025; 36: 102513.

[127] Roxo C, Pasternak A. Switching off cancer – An overview of G-quadruplex and i-motif functional role in oncogene expression. *Bioorganic Med Chem Lett* 2025; 116: 130038.

[128] Pawłowska M, Kulesza J, Augustin E. c-Myc Protein Level Affected by Unsymmetrical Bisacridines Influences Apoptosis and Senescence Induced in HCT116 Colorectal and H460 Lung Cancer Cells. *Int J Mol Sci* 2022; 23: 3061.

[129] Potęga A, Paczkowski S, Paluszkiewicz E, Mazerska Z. Electrochemical simulation of metabolic reduction and conjugation reactions of unsymmetrical bisacridine antitumor agents, C-2028 and C-2053. *J Pharm Biomed Anal* 2021; 197: 113970.

[130] Pawłowska M, Kulesza J, Paluszkiewicz E, Augustin E, Mazerska Z. Unsymmetrical Bisacridines' Interactions with ABC Transporters and Their Cellular Impact on Colon LS 174T and Prostate DU 145 Cancer Cells. *Molecules* 2024; 29: 5582.

[131] Potęga A, Kosno M, Mazerska Z. Novel insights into conjugation of antitumor-active unsymmetrical bisacridine C-2028 with glutathione: Characteristics of non-enzymatic and glutathione S-transferase-mediated reactions. *J Pharm Anal* 2021; 11: 791–798.

[132] Kulesza J, Paluszkiewicz E, Augustin E. Cellular Effects of Selected Unsymmetrical Bisacridines on the Multicellular Tumor Spheroids of HCT116 Colon and A549 Lung Cancer Cells in Comparison to Monolayer Cultures. *Int J Mol Sci* 2023; 24: 15780.

[133] Kulesza J, Pawłowska M, Augustin E. The Influence of Antitumor Unsymmetrical Bisacridines on 3D Cancer Spheroids Growth and Viability. *Molecules* 2021; 26: 6262.

[134] Frackowiak JE, Kubica P, Kosno M, et al. Distinct cellular uptake patterns of two anticancer unsymmetrical bisacridines and their metabolic transformation in tumor cells. *J Pharm Biomed Anal* 2025; 252: 116493.

[135] Pilch J, Potęga A, Kowalik P, et al. In vitro biological evaluation of a novel folic acid-targeted receptor quantum dot−β−cyclodextrin carrier for C−2028 unsymmetrical bisacridine in the treatment of human lung and prostate cancers. *Pharmacol Reports* 2024; 76: 823–837.

[136] Pilch J, Matysiak-Brynda E, Kowalczyk A, et al. New Unsymmetrical Bisacridine Derivatives Noncovalently Attached to Quaternary Quantum Dots Improve Cancer

Therapy by Enhancing Cytotoxicity toward Cancer Cells and Protecting Normal Cells. *ACS Appl Mater Interfaces* 2020; 12: 17276–17289.

[137] Pilch J, Kowalik P, Bujak P, Nowicka AM, Augustin E. Quantum Dots as a Good Carriers of Unsymmetrical Bisacridines for Modulating Cellular Uptake and the Biological Response in Lung and Colon Cancer Cells. *Nanomaterials* 2021; 11: 462.

[138] Puls TJ, Tan X, Husain M, Whittington CF, Fishel ML, Voytik-Harbin SL. Development of a Novel 3D Tumor-tissue Invasion Model for High-throughput, High-content Phenotypic Drug Screening. *Sci Rep* 2018; 8: 13039.

[139] Vinci M, Gowan S, Boxall F, et al. Advances in establishment and analysis of three-dimensional tumor spheroid-based functional assays for target validation and drug evaluation. *BMC Biol* 2012; 10: 29.

[140] Tomás-Bort E, Kieler M, Sharma S, Candido JB, Loessner D. 3D approaches to model the tumor microenvironment of pancreatic cancer. *Theranostics* 2020; 10: 5074–5089.

[141] Pinto B, Henriques AC, Silva PMA, Bousbaa H. Three-Dimensional Spheroids as In Vitro Preclinical Models for Cancer Research. *Pharmaceutics* 2020; 12: 1186.

[142] Harrison RG. Observations on the living developing nerve fiber. *Anat Rec* 1907; 1: 116-128.

[143] Chen X, Tao Y, He M, et al. Co-delivery of autophagy inhibitor and gemcitabine using a pH-activatable core-shell nanobomb inhibits pancreatic cancer progression and metastasis. *Theranostics* 2021; 11: 8692–8705.

[144] Bouttier-Figueroa D, García-Valenzuela J, Cota-Leal M, Robles-Zepeda R, Sotelo-Lerma M. Preparation and characterization of antibacterial gels of galactomannan/ZnO nanocomposite in carbopol-based matrix using mesquite seeds as the biopolymer source. *Polym from Renew Resour* 2023; 14: 3–15.

[145] Longati P, Jia X, Eimer J, et al. 3D pancreatic carcinoma spheroids induce a matrix-rich, chemoresistant phenotype offering a better model for drug testing. *BMC Cancer* 2013; 13: 95.

[146] Friedrich J, Seidel C, Ebner R, Kunz-Schughart LA. Spheroid-based drug screen: considerations and practical approach. *Nat Protoc* 2009; 4: 309–324.

[147] Shichi Y, Gomi F, Sasaki N, Nonaka K, Arai T, Ishiwata T. Epithelial and Mesenchymal Features of Pancreatic Ductal Adenocarcinoma Cell Lines in Two- and Three-Dimensional Cultures. *J Pers Med* 2022; 12: 746.

[148] Matsuda Y, Ishiwata T, Kawamoto Y, Kawahara K, Tetsushi WP. Morphological and cytoskeletal changes of pancreatic cancer cells in three-dimensional spheroidal culture. 2010; 211–217.

[149] Sant S, Johnston PA. The production of 3D tumor spheroids for cancer drug discovery. *Drug Discov Today Technol* 2017; 23: 27–36.

[150] Xie B, Hänsel J, Mundorf V, et al. Pseudopterosin and O-Methyltylophorinidine Suppress Cell Growth in a 3D Spheroid Co-Culture Model of Pancreatic Ductal Adenocarcinoma. *Bioengineering* 2020; 7: 57.

[151] Lee S, Koo I, Hwang HJ, Lee DW. In Vitro three-dimensional (3D) cell culture tools for spheroid and organoid models. *SLAS Discov* 2023; 28: 119–137.

[152] Minami F, Sasaki N, Shichi Y, et al. Morphofunctional analysis of human pancreatic cancer cell lines in 2- and 3-dimensional cultures. *Sci Rep* 2021; 11: 6775.

[153] Singh SK, Abbas S, Saxena AK, Tiwari S, Sharma LK, Tiwari M. Critical Role of Three-Dimensional Tumorsphere Size on Experimental Outcome. *Biotechniques* 2020; 69: 333-338.

[154] Breslin S, O'Driscoll L. Three-dimensional cell culture: the missing link in drug discovery.

Drug Discov Today 2013; 18: 240–249.

[155] Yeon S, No DY, Lee S-H, et al. Application of Concave Microwells to Pancreatic Tumor Spheroids Enabling Anticancer Drug Evaluation in a Clinically Relevant Drug Resistance Model. *PLoS One* 2013; 8: e73345.

[156] Ware MJ, Colbert K, Keshishian V, et al. Generation of Homogenous Three-Dimensional Pancreatic Cancer Cell Spheroids Using an Improved Hanging Drop Technique. *Tissue Eng Part C Methods* 2016; 22: 312–321.

[157] Moreira L, Bakir B, Chatterji P, Dantes Z, Reichert M, Rustgi AK. Pancreas 3D Organoids: Current and Future Aspects as a Research Platform for Personalized Medicine in Pancreatic Cancer. *Cell Mol Gastroenterol Hepatol* 2018; 5: 289–298.

[158] Nelson SR, Zhang C, Roche S, et al. Modelling of pancreatic cancer biology: transcriptomic signature for 3D PDX-derived organoids and primary cell line organoid development. *Sci Rep* 2020; 10: 2778.

[159] Xu J, Pham MD, Corbo V, et al. Advancing pancreatic cancer research and therapeutics: the transformative role of organoid technology. *Exp Mol Med* 2025; 57: 50–58.

[160] Costa EC, Moreira AF, de Melo-Diogo D, Gaspar VM, Carvalho MP, Correia IJ. 3D tumor spheroids: an overview on the tools and techniques used for their analysis. *Biotechnol Adv* 2016; 34: 1427–1441.

[161] Abuwatfa WH, Pitt WG, Husseini GA. Scaffold-based 3D cell culture models in cancer research. *J Biomed Sci* 2024; 31: 7.

[162] Pednekar KP, Heinrich MA, van Baarlen J, Prakash J. Novel 3D μtissues Mimicking the Fibrotic Stroma in Pancreatic Cancer to Study Cellular Interactions and Stroma-Modulating Therapeutics. *Cancers (Basel)* 2021; 13: 5006.

[163] Chang C-Y, Lin C-C. Hydrogel Models with Stiffness Gradients for Interrogating Pancreatic Cancer Cell Fate. *Bioengineering* 2021; 8: 37.

[164] Fontoura JC, Viezzer C, dos Santos FG, et al. Comparison of 2D and 3D cell culture models for cell growth, gene expression and drug resistance. *Mater Sci Eng C* 2020; 107: 110264.

[165] Mollica H, Teo YJ, Tan ASM, et al. A 3D pancreatic tumor model to study T cell infiltration. *Biomater Sci* 2021; 9: 7420–7431.

[166] Jang S, Song J, Kim H, et al. Anti-Cancer Activity Profiling of Chemotherapeutic Agents in 3D Co-Cultures of Pancreatic Tumor Spheroids with Cancer-Associated Fibroblasts and Macrophages. *Cancers (Basel)* 2021; 13: 5955.

[167] Yang Z, Zhang Y, Tang T, et al. Transcriptome Profiling of Panc-1 Spheroid Cells with Pancreatic Cancer Stem Cells Properties Cultured by a Novel 3D Semi-Solid System. *Cell Physiol Biochem* 2018; 47: 2109–2125.

[168] Bielecka ZF, Maliszewska-Olejniczak K, Safir IJ, Szczylik C, Czarnecka AM. Three-dimensional cell culture model utilization in cancer stem cell research. *Biol Rev* 2017; 92: 1505–1520.

[169] Nunes AS, Barros AS, Costa EC, Moreira AF, Correia IJ. 3D tumor spheroids as in vitro models to mimic in vivo human solid tumors resistance to therapeutic drugs. *Biotechnol Bioeng* 2019; 116: 206–226.

[170] Zanoni M, Cortesi M, Zamagni A, Arienti C, Pignatta S, Tesei A. Modeling neoplastic disease with spheroids and organoids. *J Hematol Oncol* 2020; 13: 97.

[171] Zhang G, Liang Q, Wu Y, Wang Y. Insights on the differences between two- and three-dimensional culture systems in tumor models (Review). *Int J Mol Med* 2025; 56: 1-16.

[172] Zanoni M, Piccinini F, Arienti C, et al. 3D tumor spheroid models for in vitro therapeutic

screening: a systematic approach to enhance the biological relevance of data obtained. *Sci Rep* 2016; 6: 19103.

[173] Beutel AK, Schütte L, Scheible J, et al. A Prospective Feasibility Trial to Challenge Patient–Derived Pancreatic Cancer Organoids in Predicting Treatment Response. *Cancers (Basel)* 2021; 13: 2539.

[174] Jamshidi N, Jamshidi N, Modarresi Chahardehi A, Shams E, Chaleshi V. A promising breakthrough in pancreatic cancer research: The potential of spheroids as 3D models. *BioImpacts* 2024; 15: 30241.

LIST OF FIGURES

LIST OF TABLES